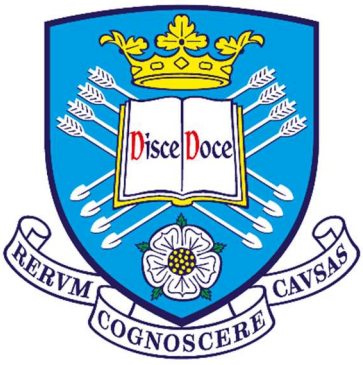

The University Of Sheffield.

Staphylococcus infection dynamics.

By

Rebecca Hodges, BSc.

A thesis submitted for the degree of Doctor of Philosophy

Department of Molecular Biology and Biotechnology, The University of Sheffield, Firth Court, Western Bank, Sheffield, S10 2TN

Summary

Staphylococcus aureus is a clinically significant human pathogen which poses an increasing healthcare threat due to the spread of antibiotic resistance. To better understand the process of *S. aureus* pathogenesis, a vertebrate model for infection, using zebrafish embryos, was previously pioneered at The University of Sheffield.

In this study I have utilised this systemic embryonic model of *S. aureus* infection in combination with a recently developed fluorescence microscopy technique – light sheet fluorescence microscopy, in order to investigate the real-time dynamics of *S. aureus* infection within a living host.

The first aim of this project was to develop methodology that enables the imaging of infected, living transgenic embryos, over extended time scales. Having established mounting and imaging parameters, infection progression was followed using fluorescent *S. aureus* reporter strains and fluorescently labelled host phagocytes.

The 4D imaging of these interactions identified macrophages as the host-niche in which bacterial expansion, followed by phagocyte escape, occurs. Furthermore, by using bacterial population studies it was confirmed that depletion of macrophages abolishes the immune bottleneck which proceeds clonal, population expansion of *S. aureus*.

When imaging embryos in the terminal stages of infection it was apparent that the large bacterial aggregates which form within the host, have biofilm-like characteristics. As such, the role of staphylococcal proteins involved in biofilm formation, during infection progression was investigated using fluorescent reporters for gene expression. It was determined that *S. aureus* nuclease is produced both inside of host phagocytes and later by bacteria associated with large aggregates. Nuclease was also identified as a novel virulence factor in the zebrafish embryo model of *S. aureus* infection.

Light sheet fluorescence microscopy has proven a useful tool to gain further insight into the temporal and spatial dynamics of *S. aureus* pathogenesis and to dissect real-time host-pathogen interactions on a cellular level.

Acknowledgements

Firstly, I would like to the Professor Simon Foster for the wonderful opportunity to carry out my PhD and all the support and guidance he has provided me with along this journey, and the encouragement to pursue the more bizaar ideas. For this I am forever grateful.

It was a pleasure to be welcomed into F18 by many, many lovely members of the lab, past and present, who have not only provided me with technical assistance but support, friendship and hilarity. Thank you for all the after work drinking that lubricated the more frustrating times and for listening to my moaning in the coffee room.

I am particularly grateful to Tomasz Prajsnar and Emma Boldock for the help with learning the zebrafish model and Robert Turner for his everyday brilliance and occupying the desk next to me as I think out loud. Some of this work was performed with Logan Bulock, from the University of Nebraska Medical Centre and I am grateful for his valuable insight.

Thank you to my absent friend Mark Cooke, who first had the hairbrained idea of using smURFP – it worked! I am sorry you didn't get to see it fluoresce in its bright pink glory, you are dearly missed.

I have met some incredible scientists who I am lucky to have made lifelong friends with, these women have set the bar very high, I hope I can pursue research with the same rigour and integrity. Thank you to these 'F-floor girlies', Victoria, Milena, Nicola, Kasia and Mina for wonderful adventures and accompanying me in consuming yet more gin. Hannah, thank you for the music, coffee and memorable nights.

Outside of research, the past few years have been some of the most difficult times of my life and I absolutely would not have been able to weather the storm and finish this work without the support of brilliant friends. Thank you to Hayley who can always sense my anxieties and endeavours to ease them. Thanks to Anne, Sally, Leanne and Fionnuala for always being on the end of the phone, you are the best friends anyone could wish for.

Special thanks to my lovely boyfriend James, who was my rock through the months of illness and kept me sane. I could not have got to this point without his love and support. I am especially grateful for all the times he patiently waited when my 'ten minutes' in the lab would routinely take hours. He has made me (and washed up) what must be a thousand cups of tea whilst I have been writing this thesis - I promise we will finally get a holiday.

Finally, thank you to my family, for your patience and understanding of my absence. My parents have provided me with endless love and support. I would not have got here without their encouragement and belief in my ability. They also funded my last four months in the lab when I did not receive sick pay and paid for my mortgage and food whilst writing up. This thesis literally would not exist if it wasn't for them. They did whatever it took to make sure I got to this point and I love them to pieces.

This work was funded by The University of Sheffield

Abbreviations

3D	Three dimensional
4D	Four dimensional
Ab	antibody
Agr	accessory gene regulator
AIP	auto-inducing peptide
AMPs	antimicrobial peptides
ATP	Adenosine tri-phosphate
bp	base pairs
BP	band pass
Bbp	bone sialo-binding protein
BiSAb	bi-specific antibody
C5aR1	C5a receptor 1
C	centigrade
CA	community associated
cas	CRISPR associated protein
CF	cystic fibrosis
CFU	clony forming units
CHIPs	chemotaxis inhibitory protein of staphylococcus
ClfA	clumping factor A
ClfB	clumping factor B
Cna	collagen-binding protein
Coa	Coagulase protein
CP5	capsular polysaccharide 5
CP8	capsular polysaccharide 8
CRISP	clustered regularly interspersed short palindromic repeats
CWA	cell wall anchored adhesin
DNA	deoxyribonucleic acid
dpf	days post fertilisation
Eap	extracellular adherence protein
ECM	extracellular matrix
eDNA	extracellular DNA
Efb	extracellular fibrinogen-binding protein
Ery	erythromycin
Fab	antigen binding fragment
Fc	constant region
FDA	Federal Drug Administration
FEP	fluorinated ethylene propylene
Fg	fibrinogen
fMLF	N-formylated tripeptide Nformylmethionyl-leucyl-phenylalanine
FnBPA	fibronectin binding protein A
FnBPB	fibronectin binding protein B
FOV	field of view
FPR1	formyl-peptide receptor
GB	gigabyte
GFP	Green Fluorescent Protein
GSK	Glaxo Smith Kline
h	hours
H2O2	hydrogen peroxide
HK	histidine kinase
Hla	α-toxin

HlgAB γ-haemolysin AB
HlgCD γ-haemolysin CD
HNP human neutrolphil peptide
HNP1 human neutrophil peptide 1
HNP2 human neutrophil peptide 2
HNP3 human neutrophil peptide 3
HOCl hypochlorous acid
hpf hours post-fertilisation
hpi hours post-infection
IAF-1 lymphocyte-function-associated antigen 1
ICAM-1 intracellular adhesion molecule-1
IE infective endocarditis
IM intra-muscular
IL interleukin
IsdA iron-regulated surface determinant protein A
IsdB iron-regulated surface determinant protein B
L Litre
LLO lysteriolisin O
LMP low melting point
LP long pass
LPS lipopolysaccharide
LSFM light sheet flourescence microscopy
LSM Laser scanning microscopy
LukAB leukocidin AB
LukED leukocidin ED
LWT London wild type
M molar
mAb monoclonal antibody
MaxIP maximum intensity projection
MIC minimum inhibitory concentration
mg milligrams
min minutes
ml milliliters
mm millimeters
MntC manganese transporter
MO morpholino antisense oligomers
MPO myeloperoxidase
MRSA methicillin resistant *S. aureus*
MSCRAMMs microbial surface components recognising adhesive matrix molecules
MSSA methicillin sensitive *S. aureus*
M-CSF macrophage colony stimulating factor
NA numerical aperture
NE neutrophil elastase
NEAT near iron transporter
NET neutrophil extracellular traps
NK Natural Killer
NLRs NOD-like receptors
nm nanometer
NSG non-obese diabetic/ severe combined immunodeficient mouse with null mutation in Il2R common gamma chain
NSPs neutrophil serine proteases
Nuc nuclease
OatA O-acetyltransferase
OD outer diameter

OD600 optical density at 600 nm
PAMPs pathogen associated molecular patterns
PBP2a penicillin binding protein
PCR polymerase chain reaction
PGRPs peptidoglycan recognition proteins
PRRs pattern recognition receptors
PSF point spread function
PSMs phenyl soluble modulins
PVL Panton-Valentine leukocidin
RAM random access memory
RAID redundant array of independent discs
ROI Region of interest
ROS reactive oxygen species
RT room temperature
sae *S. aureus* exoprotein expression
SAK staphylococcal kinase
SCIN staphylococcal complement inhibitor
ScpA staphopain A
sCMOS scientific complementary metal-oxide-semiconductor
SdrC serine-aspartate repeat protein C
SdrD serine-aspartate repeat protein D
SEB staphylococcal enterotoxin B
SELX staphylococcal enterotoxin-like toxin X
sGFP superfolder GFP
smURFP small ultra red fluorescent protein
SNR signal-to-noise ratio
SP short pass
SpA protein A
SPIM selective plane illumination microscopy
SPIN staphylococcal peroxide inhibitor
SSL13 staphylococcal superantigen like protein 13
SSL3 staphylococcal superantigen like protein 3
SSL5 staphylococcal superantigen like protein 5
SSS scalded skin syndrome
SSTIs skin and soft tissue infections
STRIVE *Staphylococcus aureus* surgical inpatient vaccine efficacy
T3SS type III secretion system
TB terabyte
TCS two-component regulatory systems
Tet tetracyline
TLRs Toll-like receptors
TNF- α tumour necrosis factor α
TNFR1 tumour necrosis factor receptor 1
TSB Tryptone Soya Broth
TSS Toxic Shock syndrome
TSST-1 toxic-shock syndrome toxin-1
UDP uridine diphosphate
VISA vancomycin intermediate-resistant *S. aureus*
VRE vancomycin resistant enterococci
VRSA vancomycin resistant strains
WT wildtype
µl microlitre
µm micrometer
° degree

Contents

List of Figures

List of Videos

	videos	Title
Chapter 1	Video 1	MaxIP timecourse of embryo with mCherry labelled neutrophils infected with SH1000-GFP'
	Video 2	Flythrough of embryo with mCherry labelled neutrophils infected with SH1000-GFP
	Video 3	rotating 3D reconstruction of mpeg:mCherry embryo infected with SH1000-GFP'
Chapter 2	Video 4	lyz mCherry SH1000 GFP naïve lesion formation
	video 5	rotating 3D reconstruction GFP lesion mCherry macrophages
	video 6	fmsGFP JE2 mCherry endocarditis like reconstruction
	video 7	Single slice timecourse SH1000-GFP infected endocardium
	Video 8	rotating 3d reconstruction of GFP lesion mCherry neutrophils
	Video 9	timecourse MaxIP fmsGFP infected with JE2 mCherry view2
	Video 10	timecourse MaxIP fms gfp JE2 mCherry view5
	Video 11	fmsGFP JE2 pMV158mCherry timelapse view 2 MaxIP
	Video 12	Biofilm like infection progression MaxIP
	Video 13	Biofilm like infection 3D rotation
	Video 14	dual labelled embryo JE2-mCherry 4 hpi onwards view 5 MaxIP
	Video 15	dual labelled embryo JE2 mCherry timecourse view 1_MaxIP
	Video 16	dual labelled embryo JE2-mCherry 4 hpi onwards view 5 subset t1-10 z340-460 MaxIP
	Video 17	rotating 3D render of dual labelled JE2 mCherry view 5 t1-10 z340-460
	Video 18	dual labelled JE2 mCherry 4hpi onwards view1 z450-650 MAXIP_cropped
	Video 19	dual labelled embryo infected with JE2 mCherry 4 hpi view 1 z450-650 MaxIP
	Video 20	dual labelled JE2-mCherry lesion t39 view 5 rotation

	Video 21	Short term timecourse of embryo infected with JE2-smURFP'.
Chapter 5	Video 22	Nacre embryo infected with JE2-mCherry pEM81'
	Video 23	flythrough of region containing non-lesion associated *S. aureus* within lyzC:mCherry embryo 24 hpi
	Video 24	3D reconstruction of large lesion expressing *nuc* within lyzC:mCherry embryo 24 hp
	Video 25	Large lesion with partial expression of *nuc* within lyzC:mCherry embryo 24 hpi
	Video 26	Expression of *nuc* in terminally infected, lyz:mCherry embryo
	Video 27	Lesion expressing *nuc* within Nacre embryo
	Video 28	MaxIP of dual labelled embryo infected with JE2-mCherry pCM20
	Video 29	Colocalisation analysis of *S. aureus* expressing *Nuc* within phagocytes'
	Video 30	- 3D rotation *nuc* expression within macrophage, timelapse subset FOV 6, t35-37
Supplementary	Supplementary video 1	lyz mCherry 6.3 x 104 SH1000-GFP
	Supplementary video 2	lyz mCherry 9.8 x 104 SH1000-GFP

List of tables

1 Introduction

1.1 *Staphylococcus aureus*

Staphylococcus aureus is a non-motile, gram-positive, oblate spheroid bacterium which replicates by binary fission in three perpendicular planes (Amako and Umeda, 1979), giving rise to its eponymous, three-dimensional clusters that resemble a 'bunch of grapes' - *staphlye* or 'berries' - *kokkus* in Greek and the distinctive golden colour of the bacteria gives rise to the name *aureus* (Kloos and Bannerman, 1994). It is one of 47 species within the *Staphylococcus* genus (which are described as facultative anaerobes) and is the most characterized within the genus, having been studied for over a century (Becker et al., 2014).

Like other staphylococcal species, *S. aureus* preferentially colonises the mammalian body, in particular the skin glands and mucous membranes (Archer, 1998). Whilst other staphylococci are capable of causing disease, *S. aureus* has evolved as a well-armed pathogen. Traditionally it was characterised by its coagulase protein (Coa) (Becker et al., 2014), which has the ability to clot blood plasma (Archer, 1998). Coagulase was previously believed to be unique to *S. aureus* within the genus and was used as a clinical indicator to discriminate between *S. aureus* infection and other staphylococci; however other coagulase positive staphylococci have been discovered more recently (Becker et al., 2014; Kloos and Bannerman, 1994).

As a facultative anaerobe, it can generate adenosine tri-phosphate (ATP) by fermentation in low oxygen environments. It grows optimally at temperatures 30-37 °C; however it has the ability to survive at temperatures from 6.5 – 46 °C and can withstand a wide range of pH (4.2 – 9.3)

1.2 Clinical significance of *S. aureus*

The anterior nares of around 20 % of the population are permanently colonised by *S. aureus* and another 60 % are transient carriers of the bacteria (Kluytmans et al., 1997) and although carriage can be harmless, it often precedes infection by this opportunistic pathogen (Huang and Platt, 2003).

S. aureus is the most common pathogen causative of nosocomial infections, colonising wound sites and in-dwelling devices such as catheters (Chatterjee et al., 2014; Kloos and Bannerman, 1994). Patients are often infected with a strain they were carrying prior to admission but colonised healthcare workers are also responsible for the spread the bacteria among patients (Huang and Platt, 2003; Lowy, 1998). *S. aureus* is causative of many forms of infection including (but not exclusively) scalded skin syndrome (SSS), cellulitis, impetigo, surgical wound infection and more seriously Toxic Shock syndrome (TSS), bacteremia, and acute endocarditis (Archer, 1998).

For a long time, *S. aureus* infections seemed to be acquired mostly in the hospital setting, however, more recently there have been emergence of community associated (CA) infections, which are now

occurring worldwide and are epidemic in the USA (Kobayashi and DeLeo, 2009). These community acquired strains are hypervirulent, commonly causing skin and soft tissue infections (SSTIs); however they are also capable of causing serious invasive infections such as fatal sepsis, nectrotising pneumonia, and necrotising faciitis (Kobayashi and DeLeo, 2009; Liu, 2009). CA infections often occur in people with pre-disposing risk-factors such as intravenous drug use, poor personal hygiene or diabetic foot ulcers (Dunyach-Remy et al., 2016; Kobayashi and DeLeo, 2009), but more worryingly there are an increasing number CA infections in healthy individuals that have not come into contact with healthcare and lack identifiable risk factors (David and Daum, 2010).

The life threatening TSS infections caused by the protein toxic-shock syndrome toxin-1 (TSST-1) (Dinges et al., 2000) were first reported in 1978, gaining attention in the 1980s with occurrence in healthy individuals, mostly concurrent with menstruation (Davis et al., 1980) but also TSS also occurs in post-operative patients, patients with respiratory infections and post-partum women (Zaghloul, 2015).

In both the hospital and community setting, 65-77 % of reported infections are the milder, SSTIs (Kobayashi and DeLeo, 2009). These can develop into far more serious infections as *S. aureus* has a propensity to gain access to the blood causing bacteremia, sepsis and spread to distant tissues (Archer, 1998; David and Daum, 2010; Kluytmans et al., 1997; Kobayashi and DeLeo, 2009).

1.2.1 Treatment of *S. aureus* infections

One of the first antibiotics, penicillin, was initially described by Alexander Fleming, subsequently purified and researched by Howard Florey and Ernst Chain (all three were awarded the Nobel prize in Physiology or Medicine in 1945 for their work), was first used in patients in 1942 and revolutionised the treatment of bacterial infections (Chain et al., 2005). Penicillin was widely used to combat *S. aureus* infection, but by the end of the same decade, most hospital isolates identified were resistant to penicillin (Wilson and Cockcroft, 1952). This resistance to killing by penicillin was conferred by the production of the enzyme β-lactamase which degrades penicillin by hydrolysing the β-lactam ring. As a result of resistance the semi-synthetic penicillins, such as methicillin, which were resistant to β-lactamase were developed. Soon after the introduction of these, *S. aureus* acquired resistance to methicillin (Barber, 1961). This new form of resistance was mediated via a novel penicillin binding protein (PBP2a) which has low-affinity for methicillin and therefore provides resistance to all available β-lactams (Hartman and Tomasz, 1984). PB2a is encoded by the *mecA* gene which is on a mobile genetic element, the SCC*mec* cassette (Katayama et al., 2000).

The emergence of *S. aureus* strains resistant to β-lactam antibiotics – termed Methicillin Resistant *Staphylococcus Aureus* (MRSA), in both the community and hospital settings has created an epidemic of infections which are very difficult to combat (Liu, 2009; Lowy, 2003; McCarthy et al.,

2015). This widespread resistance greatly increases the threat posed by staphyloccal infections, exacerbating the ability of a mild infection developing into a life-threatening illness.

A class of antibiotics, glycopeptides, which include the drug vancomycin have become the mainstay in combating MRSA infections. Vancomycin works by binding D-ala-D-ala residues involved in peptidoglycan synthesis, blocking cell wall production – this mechanism is unperturbed by production of both β-lactamase and PBP2a (Lowy, 2003). Strains more insensitive to vancomycin, termed Vancomycin Intermediate-resistant *S. Aureus* (VISA) were first identified in 1997, with many more reported since (Liu and Chambers, 2003). Vancomycin Resistant *S. Aureus* (VRSA) were first reported in the USA in 2002, with resistance acquired by a conjugal transfer of the vancomycin resistant enterococci (VRE) plasmid from *Enterococcus faecalis.* Among others, this plasmid contains the genes *vanA, vanH,* and *vanX* which are essential for the vancomycin resistant phenotype. Together VanA and VanH synthesise D-Ala-D-Lac and VanX is a D-D dipeptidase that hydrolyses the D-alanyl-D-alanine ester bond, preventing competition of D-Ala-D-Lac with the peptidoglycan precursor UDP-linked tripeptide. Incorporation of D-Ala-D-Lac into the peptidoglycan produces a cell wall whose synthesis is not susceptible to vancomycin (McGuinness et al., 2017).

The emergence of VRSA strains further escalates the severity that *S. aureus* poses as a 'super-bug', threatening a throwback to the pre-antibiotic era in terms of combating *S. aureus* infections.

1.2.2 Prevention of *S. aureus* infection

Mandatory surveillance of bacteraemia caused by MRSA since 2005 has revealed that screening and decolonising asymptomatic carriers of MRSA upon admission to hospital has resulted in the decrease in incidence of MRSA-caused bacteraemia in hospitals (Pearson et al., 2009). Public Health England have reported a 41 % reduction in the proportion of cases of bacteremia caused by MRSA from 2011/12 (11.3 %) – 2017/18 (6.6 %); this is the period in which reporting of bacteraemia caused by MSSA has also been compulsory. There has however been an increase in the total number of bacteraemia cases reported over this period, evidencing there has not been a reduction in incidence of bacteraemia caused by MSSA (Simor, 2011) (Public Health England, 2018). This is due to screening strategies which currently target resistant strains and patients are not routinely screened for carriage of sensitive strains (Wyllie et al., 2011). There are an increasing number of strategies for decolonisation of high-risk patients, carrying MSSA prior to elective surgery which have been attempted with varied success (Simor, 2011).

Due to the ever-increasing spread of resistance and rapid evolution of *S. aureus*, a vaccine against the pathogen would be very valuable, especially in high-risk groups, for example, prior to elective surgery. Currently there is no such vaccine available. The high plasticity of the *S. aureus* genome, its

ability to adapt to multiple hosts (Richardson et al., 2018), and the myriad of proteins it produces to survive within the host and subvert the immune response (Buchan et al., 2019) makes finding a vaccine target difficult. Although there are many successful vaccines targeting a single component of other pathogens such as well-conserved toxins and capsular polysaccharide (for example the tetanus toxoid and pneumococcal conjugate vaccines), attempts to confer immunity with vaccines targeting a single *S. aureus* antigen have all failed. The StaphVAX vaccine (a capsular polysaccharide conjugate) did reach phase III trials, and a 57 % decrease in bacteremia incidence was observed, with protection lasting 40 weeks post vaccination was observed, but it failed in a subsequent larger trial where no significant protection was found (Scully et al., 2014).

As a result of the failure of many single-antigen vaccines a multi-antigen approach is now being widely adopted. Several multi-antigen vaccine candidates have made it to phase II clinical trials (Giersing et al., 2016).

The Pfizer vaccine candidate, S4Ag, was the most advanced of these, reaching phase IIb trials after receiving fast-track approval from the FDA (Giersing et al., 2016) with its 4 antigen vaccine comprised of the adhesin clumping factor A (ClfA), manganese transporter (MntC), and the capsular polysaccharides 5 and 8 (CP5 and CP8). This aimed to elicit a broad humoral and cellular immune response targeting multiple virulence mechanism involved in establishing and maintaining infection (Anderson et al., 2012). However, it was announced in December 2018, that the '***ST****taphylococcus aureus* su**R**gical **I**npatient **V**accine **E**fficacy' (STRIVE) trial of the vaccine PF-06290510 in patients undergoing elective spinal fusion surgery, was discontinued due to futility - the low statistical probability of the study to meet its primary objectives (Pfizer investor press release, December 2018). A vaccine developed by Glaxo Smith Kline (GSK) contained 3 of the same antigens (ClfA, CP5 and CP8) in a candidate that contained 5 antigens; however this vaccine failed in phase I trials (Giersing et al., 2016). Other multi-antigens are being tested in earlier phases but many of these target toxins such as TSST-1, Panton-Valentine leukocidin (PVL) and staphylococcal enterotoxin (SEB) which are only present in a subset of strains (Scully et al., 2014).

A passive immunisation strategy, using monocolonal antibodies (mAb) raised against α hemolysin (Hla), MEDI4893, is currently undergoing phase II clinical trials looking at the safety, efficacy, and dosing in mechanically ventilated patients (who have a high-risk of contracting pneumonia) (ClinicalTrials.gov NCT02296320). The producer of the vaccine, MedImmune, have since reported increased efficacy using a combination of mAbs (MEDI4893 and H110 raised against ClfA) than with a bi-specific antibodies (BiSAbs) in murine models (Tkaczyk et al., 2017). This recent approach using multiple mAbs suggests that the efficacy of the MEDI4893 in phase II trials might not reach study objectives.

1.3 *Staphylococcal virulence determinants involved in host-binding and immune evasion*

S. aureus produces a vast repertoire of proteins, both membrane bound and secreted, which are involved in binding host proteins for colonisation and modulation of the host immune response.

1.3.1 The surface proteins of *S. aureus*

At the earliest stages of infection *S. aureus* must colonise the host. Attachment of the bacteria to host tissues via binding the extracellular matrix (ECM) is mediated by cell wall anchored adhesins (CWA). Among these are the microbial surface components recognising adhesive matrix molecules (MSCRAMMs) which often have two adjacent domains with IgG like folds (Deivanayagam et al., 2002) and a'dock, lock, and latch' model for binding of some of these surface proteins to their host substrates has been proposed (Ponnuraj et al., 2003). There is redundancy in the targets of MSCRAMMS with clumping factor A (ClfA), clumping factor B (ClfB) and bone sialo-binding protein (Bbp) all binding the plasma glycoprotein fibrinogen (Fg), two fibronectin binding proteins, fibronectin binding protein A & B (FnBPA & FnBPB) which also bind Fg, and two which bind desquamated epithelial cells, serine-aspartate repeat protein C & D (SdrC & SdrD) (Foster et al., 2014).

The MSCRAMM, collagen-binding protein (Cna), is involved in binding collagen rich tissues (Zong et al., 2005) such as the cornea (Rhem et al., 2000) and cartilage has a role in septic arthritis induced by *S. aureus* in a murine model (Xu et al., 2004). FnBPA promotes adherence to and internalisation by epithelial cells (Massey et al., 2001). However the region of the Cna protein responsible for adherence to keratinocytes is distinct from the fibronectin binding region (Edwards et al., 2011).

The main Fg binding protein, ClfA is a 96.4 kDa protein, a major virulence factor (O'Connell et al., 1998) and is found in 100 % of clinically isolated strains(Ghasemian et al., 2015). ClfA is involved in the process of agglutination, binding fibrin fibrils undergoing agglutination in the blood of the host. The N-terminal of ClfA contains a ~500 residue domain which binds the C-terminal of γ chain of Fg, preventing subsequent binding of additional fibrin subunits to the agglutinated fibrils (Geoghegan et al., 2010). Through this binding event, the bacteria are masked by the fibrils enabling evasion of phagocytosis within the host blood (Flick et al., 2013). ClfA protects *S. aureus* from murine macrophages- in a fibrinogen dependent process (Josefsson et al., 2001). Agglutination of these infectious thrombi in *S. aureus* sepsis is implicated in systemic dissemination in the host and is essential to its lethal outcome in mouse models (McAdow et al., 2011). ClfA is also essential in murine staphylococcal arthritis models (Palmqvist et al., 2005), and rat and rabbit models for endocarditis (Entenza et al., 2005; Siboo et al., 2001; Sullam et al., 1996). As a result of its vital role in infection and being localised on the cell wall of *S. aureus*, ClfA is an attractive vaccine candidate,

and both active and passive immunization with a combination of ClfA FnBPA & FnBPB is protective in mice (Arrecubieta et al., 2008). However, recent use of ClfA in the vaccine Veronate© failed in phase III testing (Schaffer and Lee, 2008).

In addition to MSCRAMMs, the near iron transporter (NEAT) motif family of CWA contains the proteins iron-regulated surface proteins A and B (IsdA & IsdB) which facilitate adhesion to desquamated epithelial (Clarke et al., 2006) and non-phagocytic cells (Zapotoczna et al., 2013) in addition to their roles in iron acquisition.Another adhesin, extracellular adherance protein (Eap) binds Fg, Fn, and prothrombin and promotes internalization to fibroblasts, reducing detectability by the host immune response contributing to persistence within the host (Haggar et al., 2003).

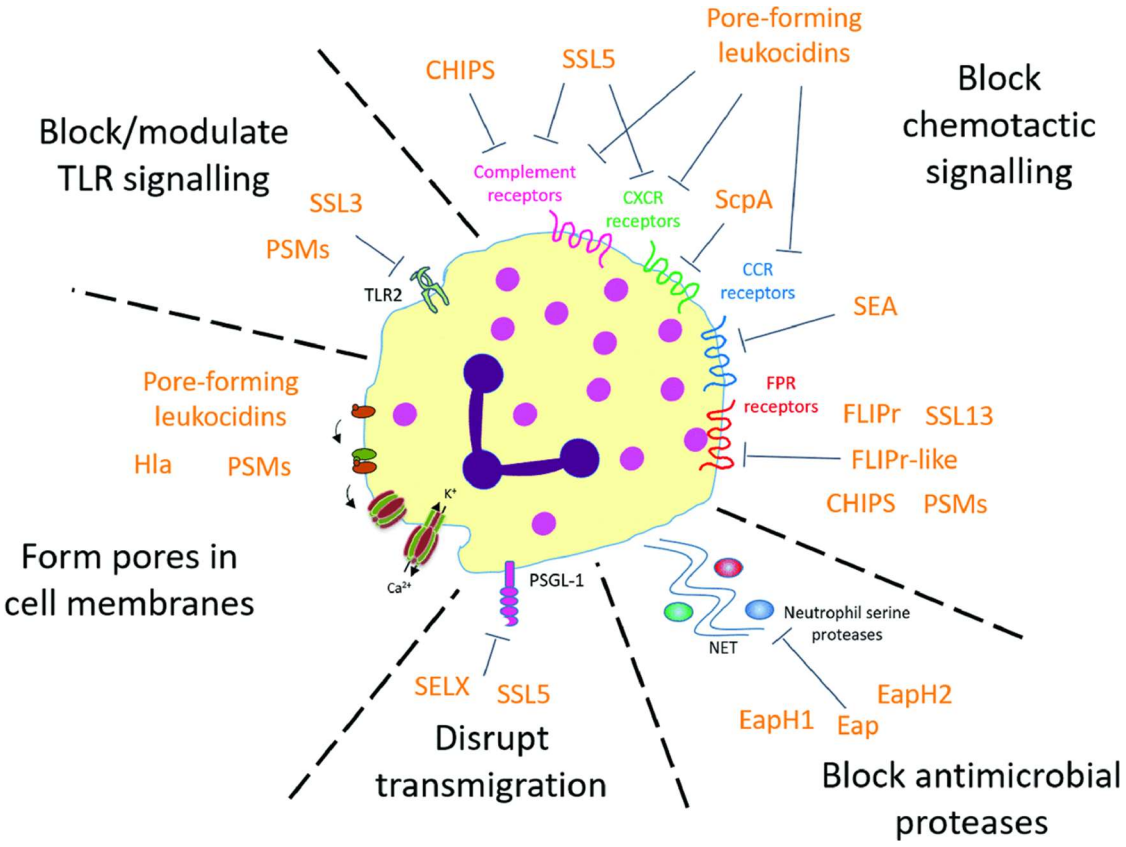

Figure 1.1 The secreted proteins of *S. aureus* and their roles in immune-evasion

Adapted from (Buchan et al., 2019). Schematic of a phagocytic cell demonstrating host-targets of *S. aureus* secreted virulence factors. Virulence factors are shown in orange: chemotaxis inhibitory protein of staphylococcus **CHIPs**, staphylococcal superantigen like protein 3, 5, 13 **SSL3**, **SSL5**, **SSL13**, staphylococcal kinase **SAK**, extracellular adhesion protein **Eap**, phenyl soluble modulins **PSMs**, α-toxin **Hla**, staphylococcal enterotoxin-like toxin X **SELX**, staphopain A **ScpA**

1.3.2 The secreted proteins of *S. aureus*

S. aureus has evolved to produce an arsenal of factors which interfere with the host immune response, many of these are secreted proteins working on different aspects of the innate immune response to the pathogen, (Figure 1.1). The first line of defense against infection are host barrier tissues, which produce antimicrobial peptides (AMPs) to combat invading pathogens, often via insertion into the plasma membrane bacteria. Staphylococcal kinase (SAK) is produced by *S. aureus* to inactivate one of the most abundant AMPs, α-defensin. SAK acts by directly binding and inactivating α-defensin, but also activates plasminogen – which degrades blood plasma proteins (Jin et al., 2004). Another defense against innate defences is the production of O-acetyltransferase (OatA) (Bera et al., 2005). OatA leads to a modification of the cell wall peptidoglycan, blocking activity of the host enzyme lysozyme (found in saliva, plasma and sweat) which acts by cleaving bonds between N-acetyl-muramic acid and N-acetylglucosamine in the peptidoglycan (Bera et al., 2005).

The complement pathways are biochemical cascades which are an integral part of the innate immune system, derived from more than 30 proteins present in the serum, tissue fluids and cell surfaces (Walport, 2001a). Complement is involved in clearing pathogens and the distinguishing between self and non-self targets during an immune response (Serruto et al., 2010). There are three types of complement pathway, classical, alternative and lectin pathways. The classical pathways is reliant on antibody recognition of a microbial target and suqbsequent binding of complement protein C1 (Walport, 2001b). The alternative pathway is continuously active at a basal level and relies upon host cell-surface proteins to inactivate components of the cascade. The lectin pathway is dependent on the recognition of specific patterns comprised of saccharides and related molecules. All three pathways converge upon the activation of the complement protein C3. The formation of membrane attack complex (MAC) – comprised of five complement proteins, results in the direct killing of gram negative bacteria by creating a pore in the bacterial membrane. However, gram positive bacteria are protected from formation of MAC and clearance of bacteria is reliant on phagocytosis stimulated by complement proteins C3b and C5a. Figure 1.2 depicts the three complement pathways and bacterial proteins that interfere with the cascade.

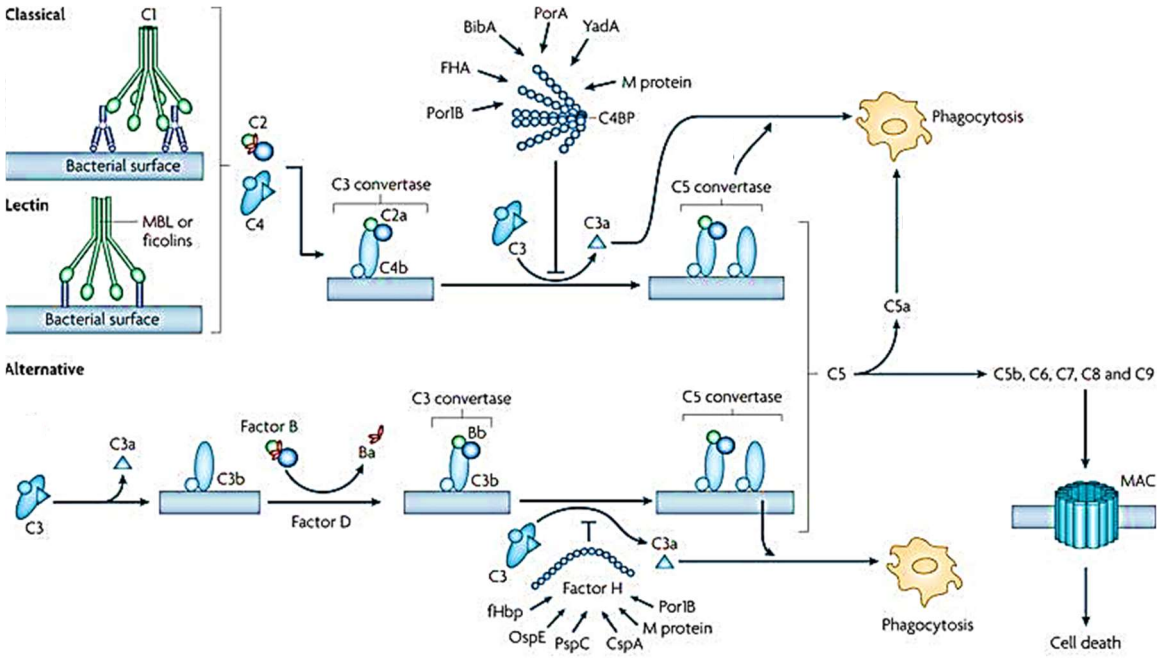

Figure 1.2 The complement pathways

Adapted from (Serruto et al., 2010). Activation of the complement cascade in response to pathogens. The classical and lectin pathways begin with humoral proteins binding bacterial antigens. The alternative pathway is constitutively active, but host cells prevent activation of bound **C3** through expression of Factor H. The complement protein **C3** is the pinnacle of the complement cascade and is activated by **C3** convertases **C3bBb** and **C4b2a**. It's activated form, **C3a** is a key mediator of phagocytosis. Additionally, complement **C5a** is also a pro-phagocytic signal of the cascade involved in the clearance of pathogens. The proteins **C5b**, **C6**, **C7**, **C8**, and **C9** for the membrane attack complex (**MAC**) which can directly kill gram negative bacteria by creating a pore in the bacterial cell membrane.

The pathogen also produces many proteins which disrupt the 'complement' cascade, one of these secretory products of *S. aureus* is Chemotaxis Inhibitory Protein of *Staphylococcus* (CHIPS) can bind receptors for C5a (C5aR1) (Postma et al., 2005) and formyl-peptide receptor (FPR1) on neutrophils (Haas et al., 2004). Two distinct regions of CHIPS bind these two receptors, blocking C5a and N-formylated tripeptide N-formylmethionyl-leucyl-phenylalanine (fMLF) binding C5aR1 and FPR1 respectively. Through this action CHIPS interferes with neutrophil chemotaxis and extravasion (Foster, 2005).

A key aspect of the complement system is C3, which is the crux of all three complement pathways (Serruto et al., 2010). This is cleaved by C3 convertase to form C3a (a potent chemoattractant) and C3b (involved in opsonisation, by covalently binding the cell wall of the pathogen and promoting phagocytosis) (Lambris et al., 2008). *S. aureus* interferes with C3 activity in a number of ways; by activating plasmin, SAK can degrade C3b. The bacteria produce extracellular fibrinogen-binding protein (Efb), which in addition to binding fibrinogen, binds a region of C3, preventing cleavage hence blocking the classical and alternative complement pathways, obstructing C3b deposition and also formation of C3 convertase (Lee et al., 2004). Besides this, Efb interferes with the adaptive immune response by preventing recognition of C3b by B-cells (Ricklin et al., 2008). The extracellular complement binding protein (Ecb) also disrupts opsonisation by binding C3b (Amdahl et al., 2013). A protein conserved by 90 % of *S. aureus* strains, staphylococcal complement inhibitor (SCIN) disrupts the complement cascade by binding to and stabilising the C3 convertases, C4b2a and C3bBb, thus disrupting all complement pathways. Through this activity, SCIN is probably the most potent modulator of the humoural immune response (Rooijakkers et al., 2005).

As well as its role in internalisation, Eap also targets intracellular adhesion molecule-1 (ICAM-1) on the surface of host endothelial cells. Through Eap binding ICAM-1 the intended ligand, lymphocyte-function-associated antigen (IFA-1), expressed on the surface of neutrophils, is blocked, preventing neutrophil adhesion, diapedesis, and extravasion (Haggar et al., 2004). Furthermore it inhibits the neutrophil serine proteases (NSPs) neutrophil elastase (NE), cathepsin G and proteinase 3, produced after phagocytosis to aid killing of internalised bacteria, by binding the catalytic clefts of the NSPs (Stapels et al., 2014).

Recently the protein 'Staphylococcal peroxide inhibitor' (SPIN) has been identified and characterised; it works by binding and inhibiting myeloperoxidase (MPO) (Jong et al., 2017). MPO is involved in the oxidative burst which occurs within neutrophils in response to intracellular bacteria, it catalyses the production of hypochlorous acid (HOCl) within the phagosome, from hydrogen peroxide (H_2O_2) and chloride ions. HOCl is the most potent oxidative product within the phagosome (Klebanoff et al., 2013). By occluding the active site of MPO, SPIN enables *S. aureus* to withstand the oxidative defense and survive within the neutrophil (Jong et al., 2017).

Protein A (SpA) is a 42 kDa protein produced by *S. aureus* that has been very well characterized; it can be both localized to the cell surface or secreted into the extracellular milieu (Lambris et al., 2008). Once secreted it can bind the antigen binding fragment (Fab) regions of the B-cell receptor, resulting in apoptosis of B-cells, hindering the adaptive immune response (Kobayashi and DeLeo, 2013). When associated with the bacterial cell surface, SpA binds the constant region (Fc) of an antibody (Ab), sequestering antibodies and inhibiting antibody binding to the hexameric complement component, C1q which stimulates the classical complement cascade (Lambris et al., 2008). More recently it has been shown that SpA also binds von Willebrand factor, promoting surface adhesion of *S. aureus* to the epithelium (Hartleib et al., 2000) and the tumour necrosis factor receptor 1 (TNFR1) of epithelial cells, resulting in the epithelium shedding the receptor and neutralising available tumour necrosis factor α (TNF- α) and it has been shown that SpA binding TNFR1 is essential for *S. aureus* induced pneumonia (Gómez et al., 2004).

A crucial part of the host innate-immune response is the activation of phagocytes after the recognition of pathogen associated molecular patterns (PAMPs) by pattern recognition receptors (PRRs). The two main classes of PRRs are the Toll-like receptors (TLRs) localized on the host cell surface and NOD-like receptors (NLRs) are cytosolic host receptors (Franchi et al., 2009; Kawai and Akira, 2010). Activation of PRRs leads to the production of cytokines (immune signaling proteins), chemokines (which recruit phagocytes) and stimulation of an inflammatory response. During this innate immune response, key cytokines CXCL1, CXCL2, CXCL7, and IL-8 are produced that all bind a target receptor CXCR2, a key chemotactic receptor found on the membrane of neutrophils (Hato and Dagher, 2015). *S. aureus* disrupts binding of these key immune modulators by production of, staphopain A (ScpA), a cysteine protease which cleaves the N-terminus of CXCR2 destroying the functionality of the receptor and abolishing neutrophilic response to CXCL1 and CXCL7 (Laarman et al., 2012). In addition, TLR2 (which is activated by both gram-positive and gram-negative lipoproteins) is also targeted by *S. aureus* by production of staphylococcal superantigen-like protein 3 (SSL3). SSL3 binds to the extracellular domain of TLR2, preventing heterodimerisation of TLR2/6 and TLR2/1 and as a consequence prevents the production of IL-8, disrupting neutrophil recruitment (Bardoel et al., 2012).

Another class of secreted staphylococcal proteins are the phenyl-soluble modulins (PSMs) which are 'surfactant toxins' (Peschel and Otto, 2013). These also indirectly target TLR2 by shedding lipoproteins from the bacterial membrane, leading to activation of downstream inflammatory pathways via production of TLR2 dependent chemokines (Hanzelmann et al., 2016). Although TLR2 plays an important role in clearing PSM producing *S. aureus* strains, high levels of PSMs are produced by highly pathogenic CA-MRSA strains and PSM production is essential for sepsis in murine models (Hanzelmann et al., 2016; Peschel and Otto, 2013). PSMs are unique to

staphylococci, however it has been shown that TLR2 activity in response to lipoprotein shedding of skin commensals *S. aureus* and *Staphylococcus epidermidis* (*S. epidermidis*) is ten times lower than TLR2 activity in response to lipoproteins of the non-commensal species *Staphylococcus carnosus* (*S. carnosus*) and this is due to the position of acylation of the long-chain fatty acids. The position of the acyl groups on the lipoproteins from *S. aureus* and *S. epidermidis* result in lipoproteins binding the TLR2/1 complex whereas the lipoproteins of *S. carnosus* binds the TLR2/6 complex. By binding TLR2/1 *S. aureus* and *S. epidermidis* lipoproteins silence innate and adaptive immune responses, suggesting immunomodulation by *S. aureus* that may underpin infection (Nguyen et al., 2017).

There are seven PSMs, all of which are produced by most strains of *S. aureus*, these are small peptides 20-45 αα in length, that have a cytolytic effect on leukocytes and erythrocytes (Peschel and Otto, 2013). Importantly these are cytolytic against human neutrophils (Surewaard et al., 2013; Wang et al., 2007), and unlike the bi-component toxins, PSMs do not have cell specificity (Cheung et al., 2012). Neutrophil killing by PSMs has been shown to occur subsequent to phagocytosis of the cells (Surewaard et al., 2013) and it is likely that the intracellular production of PSMs is triggered by the stringent response (Geiger et al., 2012). The ability to cause cytolysis of host cells is key to pathogenesis of *S. aureus* and deletion of the PSMs from the core genome of the hypervirulent CA-MRSA strains, USA300 and USA400, reduces cytolytic capacity to that of strain 252, a HA-MRSA, in a human neutrophil model (Wang et al., 2007).

The surfactant PSMs have likely evolved as a mechanism of creating channels within *S. aureus* biofilms, these channels give the biofilms their characteristic 'spongey' texture and provide access to required nutrients. The expression of PSMs in this instance is controlled by quorum-sensing in the post-exponential growth phase (Periasamy et al., 2012).

1.3.2.1 The pore-forming toxins of S. aureus

By secreting leukocytic toxins, *S. aureus* can trigger phagocyte cell death before bacterial killing has been accomplished. The mechanism of these toxins is to form a pore in the phagocyte membrane, causing leakage and inevitably lysis of cells. The alpha-toxin (also known as alpha-hemolysin, Hla) is the major cytotoxic agent produced, the protein forms a heptamer in the membrane, producing a β-barrel pore (Dalla Serra et al., 2005).

S. aureus also produces many bi-component leukotoxins, five of which are specific to human infection, Panton-Valentine leukocidin (PVL), leukocidin AB and ED (LukAB and LukED), and γ-haemolysin AB and CD (HlgAB and HlgCD)(Dalla Serra et al., 2005; Seilie and Wardenburg, 2017). The two subunits of the toxins are secreted separately, forming hexameric or heptameric complexes, producing pores in the leukocyte membrane (Kaneko et al., 1997). The most prominent of these bi-component leukotoxins is HlgAB, which is found in over 90 % of strains and can lyse

both erythrocytes and leukocytes. However, PVL is only found in around 3 % of strains isolated from nares of healthy individuals (Shukla et al., 2010), but is expressed in 77-100 % of CA-MRSA strains and is associated with the SCC*mec* cassette types IV and V, commonly found in CA-MRSA strains (Vandenesch et al., 2003). Presence of PVL correlates with severe contagious skin infection and severe pneumonia in healthy individuals (Foster, 2005).

LukAB is the most recently discovered bi-component toxin and is the most genetically distant from the other leukocidins (Ventura et al., 2010). It targets monocytes, macrophages, and dendritic cells (DuMont et al., 2011), and has been shown to cause extracellular killing of neutrophils (DuMont et al., 2013). There is cross-over in the roles of the different pore-forming toxins as LukED is also cytotoxic to dendritic cells, macrophages, and T-Cells, targeting the chemokine receptors CXCR1 and CXCR2 (Reyes-Robles et al., 2013).

Another defense against the immune response is the distinctive golden colour of *S. aureus,* which arises from production of staphyloxanthin, a carotenoid which works as an anti-oxidant to counteract oxidative stress encountered from reactive oxygen species (ROS) produced by the host immune response (Clauditz et al., 2006).

1.4 *Regulation of virulence determinant production*

Expression of *S. aureus* virulence factors are controlled by two-component regulatory systems (TCS) of which 16 have been identified within the genome and DNA binding proteins. These respond to environmental cues such as pH, CO_2 and bacterial density (Bronner et al., 2004a). The TCS are histidine-kinase complexes, localised in the cell-membrane, with an extra-cellular sensing domain and an intracellular response regulator.

1.4.1 Regulation of *S. aureus* exoprotein expression

The *S. aureus* exoprotein expression (*sae*) locus contains the co-transcribed *saeRS* TCS comprised of the sensor protein SaeS and the response regulator SaeR (Liu et al., 2016). SaeS consists of an N-terminal transmembrane domain followed by a 10 αα extracellular loop, which responds to environmental signals connected to a second transmembrane domain leading to an intracellular histidine kinase (HK) (Geiger et al., 2008). SaeR has a N-terminal receiver domain, which requires phosphorylation by the HK of SaeS. Phosphorylation of this domain is essential for SaeR binding target DNA; a 16 nucleotide consensus sequence which has been identified in 26 genes encoding exoproteins including the virulence factors Coa, Hla, emp, efb, SCIN, Eap, TSST-1 , FnbA/B, LukE/A, HlgC, Nuc, Sak, and Aur (Liu et al., 2016). Transcription of the sae operon (including the ancillary genes *saeP* & *saeQ*) is maximal in the post-exponential growth phase, however there is constitutive basal transcription of *saeRS* from a secondary promoter, producing enough SaeRS for sensing and responding to cognate signals (Jeong et al., 2011).

It has been shown that SaeRS is activated in response to molecules of the innate immune response. The antimicrobial peptides, human neutrophil peptide 1, 2, and 3 (HNP1-3, also known as α-defensins) are produced by neutrophils, found in the azurophilic granules, and are the main source of bacterial killing in the phagolysosome. HNP1-3 activate SaeRS at subinhibitory concentrations (Geiger et al., 2008) and unsurprisingly *saeRS* is activated within human neutrophils, however not all SaeR/S regulated virulence factors are upregulated in response to HNP1-3 (Zurek et al., 2014). Another stimulant of SaeRS is calprotectin, a member of the EF-hand calcium binding protein family, comprising 50 % of the neutrophilic cytosolic protein and is also found in high concentrations in abscesses, where it sequesters Zn and Mn, nutrient metal ions required for staphylococcal growth (Cho et al., 2015). Inhibitory concentrations of H_2O_2 (found within neutrophils, a constituent of ROS production) have also been shown to activate SaeRS (Geiger et al., 2008). It is not yet known how the differential expression of SaeRS controlled virulence factors is regulated.

1.4.2 The accessory genome regulator of *S. aureus*

A major regulator of *S. aureus* is the accessory gene regulator (Agr) which is involved in the regulation of gene expression in the post-exponential growth phase. This system is responsible for quorum sensing of *S. aureus*, which plays an important role in biofilm development, and the regulation and modulation of proteins involved in chronic infection (Boles and Horswill, 2008; Bronner et al., 2004b; Moormeier and Bayles, 2017a; Periasamy et al., 2012). *Agr* is both a transcriptional and translational regulator, a schematic of the activation of this regulatory system is shown in Figure 1.3. The *agr* locus contains two divergent promoters, P2 and P3, which direct expression of RNAII and RNAIII transcripts (Recsei et al., 1986). The first (RNAII) encodes proteins AgrB, AgrD, AgrC, and AgrA which are required for agr-mediated virulence factor regulation (Peng et al., 1988). AgrB is a membrane-associated protease which is involved in the digestion of AgrD to generate and secrete auto-inducing peptide (AIP), an octopeptide, quorum sensing molecule (Zhang et al., 2002). Accumulation of extracellular AIP leads to activation of AgrA and AgrC – a TCS. The binding of AIP to the transmembrane sensor kinase protein AgrC, causes homdimerisation of AgrC. Subsequently AgrC phosphorylates AgrA – the cytoplasmic response regulator Phosphorylation of AgrA leads to transcription of RNAIII which activates transcription of secreted proteins including Hla, Hlg, PVL, and TSST-1 and simultaneously represses surface bound virulence factors. (Dunman et al., 2001).

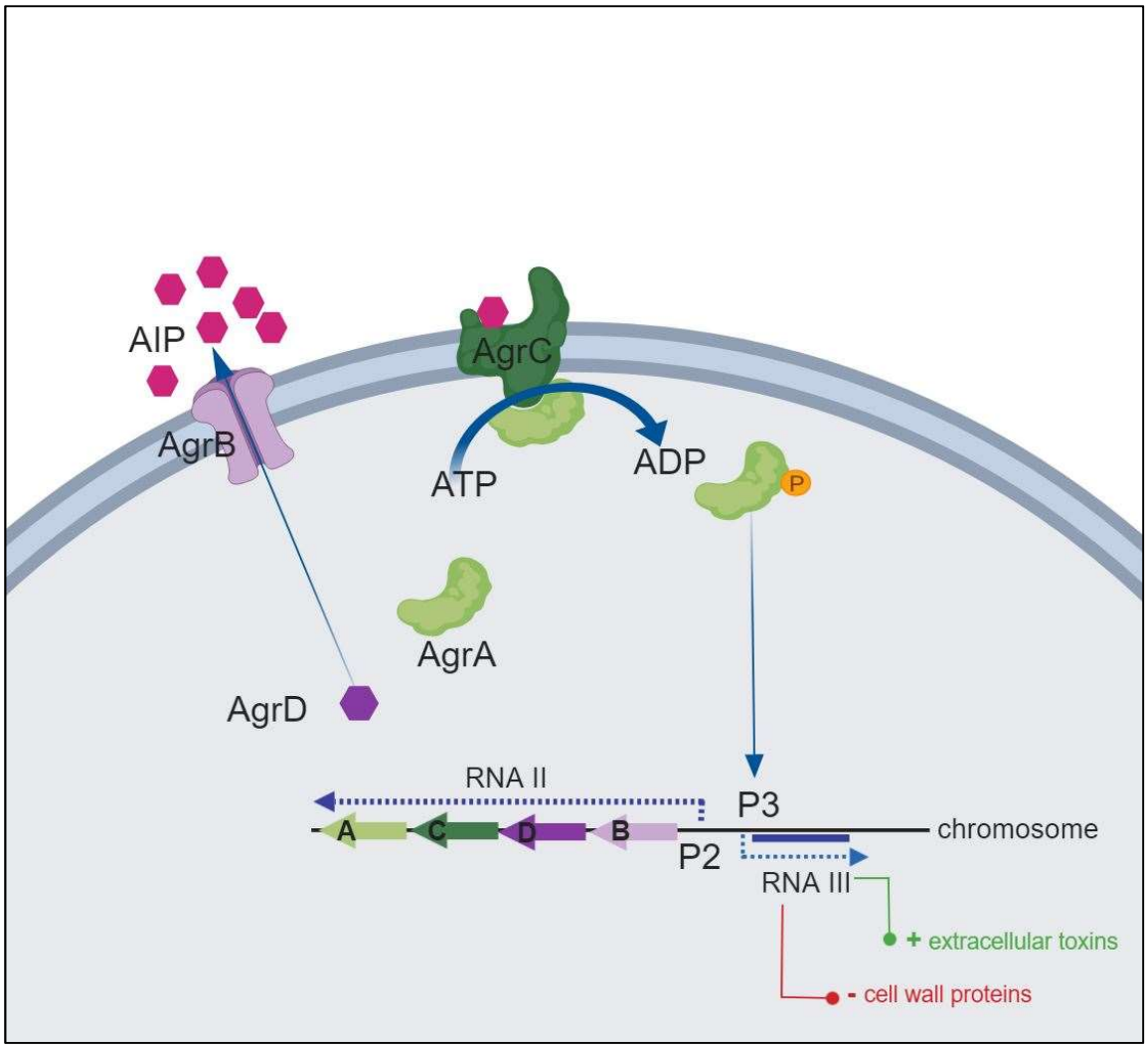

Figure 1.3 Schematic to show transcriptional and translational regulation by *agr*

The *agr* locus contains two divergent promoters **P2** and **P3**. Translation of **RNAII** results in the expression of proteins **AgrB**, **AgrD**, **AgrC,** and **AgrA.** The protein AgrD interacts with and is modified and secreted by AgrB, producing extracellular **AIP**. Binding of **AIP** to the extracellular sensor **AgrC**, leads to phosphorylation of the response regulator **AgrA**. Phosphorylation of **AgrA** results in transcription of the **P3** promoter, increasing production of extracellular toxins and decreasing production of cell wall associated proteins.

1.5 *Models of S. aureus infection*

1.5.1 *In vitro* infection models

As *S. aureus* has evolved to be especially good at infecting and surviving within humans, with proteins adapted specifically to subvert the human immune response, this makes modelling the infectious process difficult. *In vitro* and *ex vivo* models using human cell types such keratinocytes (Edwards et al., 2011; Kisich et al., 2007; Rhem et al., 2000), fibroblasts (Almirón et al., 2015; Kanangat et al., 2006), endothelial cells (Pöhlmann-Dietze et al., 2000) and even 3D primary co-culture models of the epidermis and underlying dermis (Popov et al., 2014) have been used to study colonization and infection. Whilst these are useful for investigating the interactions of *S. aureus* with the human ligands the bacteria have evolved specificity to, they are comprised of only one or two cell types and are not immune-competent and can only provide limited insight to the infectious process.

As well as epithelial cells, intact skin contains mast cells, dermal dendritic cells, macrophages, T and B cells and natural killer (NK) cells which are involved in the cutaenous immune response (Kupper and Fuhlbrigge, 2004). These are first line of defense against a pathogen, which cell culture models (comprised of a single cell type) lack. Isolation and/or primary culture of immune cell types, particularly neutrophils and macrophages are also regularly used to dissect the roles of individual *S. aureus* proteins during the infectious process and have identified bacterial components important for pathogenesis (DuMont et al., 2013; Haggar et al., 2004; Kaneko et al., 1997; Laarman et al., 2012; Ricklin et al., 2008; Scherr et al., 2015; Stapels et al., 2014; Surewaard et al., 2013). Here again, the use of these cells in isolation is not entirely physiologically relevant. Often results do not correlate with *in vivo* models and the procedure of isolating these cell types may perturb inherent function.

1.5.2 Invertebrate models of *S. aureus* infection

Manipulation of invertebrates is achieved more rapidly than vertebrates models and reverse genetic manipulation through techniques through crispr/cas9 provides a rapid target method of creating specific mutations, allowing elucidation of particular genes in disease progression (Tsai et al., 2016). However, the use of invertebrate models organisms for infection models is mainly limited to the innate immune response, but has the advantage of being more high-throughput than vertebrate models.

1.5.2.1 Caenorhabditis elegans

C*aenorhabditis elegans,* is an optically transparent nematode that is approximately 1 mm in size. *C. elegans* will feed off a bacterial lawn and this characteristic can be exploited as a route of inoculation for an infection model (Garsin et al., 2001). The model organism has been used to follow

infection with different well-characterised laboratory strains in addition to clinical isolates. Survival of L4 stage (the last larval stage of *C. elegans* development) *C. elegans* over the course of several days has been followed (Sifri et al., 2003). Upon ingestion, *S. aureus* colonises the digestive system of *C. elegans* and ~ 90 % are killed within 72 hours of infection. This model has been used to identify conserved aspects of *S. aureus* pathogenesis that are host-independent, the virulence regulators *sarA, agr*, and alternative sigma factor (σ_b), along with α- toxin and V8 serine protease have been identified as essential virulence determinants in this infection model (Sifri et al., 2003). An advantage of this model is the natural transparency of the organism, this can be exploited by microscopy and flurorescent bacteria can be followed within the host (Garsin et al., 2001). Another advantage is access to well characterized mutants, which have indicated that the conserved p38 mitogen-activated protein (MAP) kinase pathway – is involved in *C. elegans* defence against multiple pathogens, as a key response to *S. aureus* (Sifri et al., 2003).

1.5.2.2 Galleria mellonella

The larvae of *Galleria mellonella* have become a popular model for microbial infections. The life cycle of *G. mellonella* is short, they are inexpensive, do not require any special laboratory equipment and are not protected by Animals (Scientific Procedures) Act 1986 (ASPA) regulations and as such it is easy to maintain large numbers of the larvae to obtain statistically relevant data (Tsai et al., 2016). Their relatively large larval size makes for easy injection with the pathogen (García-Lara et al., 2005). Whilst *G. mellonella* are evolutionarily distant from mammals, they possess many similar components of the innate immune response including hemocytes (phagocytic cells) found in the hemolymph – analogous to vertebrate blood. As well as cellular components of innate immunity *G. mellonella* have some analogous components of the humoral response: opsonins, AMPs, (García-Lara et al., 2005; Tsai et al., 2016) and melanisation. Importantly they have peptidoglycan recognition proteins (PGRPs) (Tsai et al., 2016) and a phenomenon analogous to vertebrate nuclear extracellular trap (NET) formation occurs resulting from extracellular endogenous nucleic acids from oenocytoids (a subset of hemocytes) (Altincicek et al., 2008). The melanisation response is described as the 'synthesis and deposition of melanin to encapsulate pathogens at the wound site' and is analogous to abscess formation in vertebrates. This response is scored and used as a measure of virulence, along with survival of infection larvae (Tsai et al., 2016)

Unlike some other infection models, *G. mellonella* can be maintained at 37°c, which is human body temperature and the temperature *S. aureus* are routinely incubated in when cultured in the laboratory setting. The model has been used primarily to screen anti-staphylococcal compounds (García-Lara et al., 2005; Tsai et al., 2016).

1.5.2.3 Drosophila melanogaster

The fruit fly, *Drosophila melanogaster*, is a model organism that has been well genetically characterised and posseses an innate immune system similar to vertebrates. Their innate immune system has the ability to recognise peptidoglycan by TLRs (Leulier et al., 2003) and they have professional phagocytes, termed plasmocytes, that are analogous to mammalian monocytes, which engulf and destroy invading microbes (Leclerc and Reichhart, 2004). Like *G. mellonella* it also surrounds microbes in melanin and secretes AMPs into the haemolymph (Leclerc and Reichhart, 2004). *D. melanogaster* has been used to model *S. aureus* infection; bacteria are inoculated by pricking the thorax of the fruit fly with a needle dipped in bacterial suspension (Needham et al., 2004). Although this model is evolutionarily far removed from the human host, it was used to identify virulence determinants *pheP* and *perR* (Needham et al., 2004). PheP mutants were later also confirmed as attenuated in vertebrate models of *S. aureus* infection (Connolly, J., 2015).

1.5.3 Vertebrate models of infection

Vertebrate models of *S. aureus* infection benefit from both innate and adaptive immune systems, which can better mimic human infection than invertebrates or an *in vitro* models. However, the specificity of *S. aureus* adaptions as a human pathogen make challenges in modelling infection even in this higher model organisms.

1.5.3.1 Rabbit models of S. aureus infection

Rabbits are commonly used for infection of bone and tissue with *S. aureus*, they are practically useful for osteomyelitis models as bone size is larger than mouse, making precise surgical manipulations easier. Internal fixation models for both acute and chronic osteomyelitis are used, and the longer life span of the rabbit permits monitoring for up to 18 months (Reizner et al., 2014). They are used for modelling prothesis infection and testing the addition of anti-microbial polymers to prostheses and bone cements. A rabbit model of infective endocarditis (IE) has also been developed, as the physiology of the heart is similar to that of humans and bacterial vegetations on the heart have been shown to contain a similar number of bacteria as are isolated from patients (Spaulding et al., 2012a). Recently advances have been made on the widely adopted methodology, initially described by (Garrison and Freedman, 1970) this modifies the method and route of inoculation to better mimic the procedure experienced by cardiac patients (Wang et al., 2013). A rabbit model for pulmonary infection has been used, where a high dose of *S. aureus* administered by intrabronchial inoculation results in pulmonary illness and death (Strandberg et al., 2010). However immunisation using TSST-1 or staphylococcal enterotoxin B (SEB) protected rabbits from pneumonia in this lethal challenge model (Strandberg et al., 2010). This model demonstrated the inability to develop neutralising antibodies against the super antigen TSST-1, as previously observed in humans. This is manifested via immune dysfunction caused by the toxin, not the

inability of the host to recognise it as non-self. Immunisation with a combination of superantigens (including a mutant TSST-1 toxoid) confers the ability of vaccinated rabbits to withstand lethal challenge of *S. aureus* and protects against IE, pneumonia and sepsis (Spaulding et al., 2012b).

1.5.4 Murine models of *S. aureus* infection

The mouse is the primary animal used to model *S. aureus* infection and many different models exist to investigate the different types of staphylococcal infection. The mouse is a natural host of *S. aureus*, however these infections occur from mouse specific strains, primarily causing infection in preputial glands of male mice. Mice are not a natural host of human specific strains, which do not spread within a murine population and mice are less readily colonized by human strains than those of murine origin (Holtfreter et al., 2013). As a result, mice need higher inocula *of S. aureus* with human specific strains. Mouse models for sepsis, septic arthritis, pneumonia, blood borne metastatic abscess formation, peritonitis, endocarditis, and subcutaneous skin infection are routinely used (Kim et al., 2014).

1.5.4.1 Sepsis

Sepsis is commonly caused by *S. aureus* and is the result of an immune response to bacterial replication in the blood which often results in multiple organ failure and can be fatal (Kloos and Bannerman, 1994). To recapitulate this, mice are infected via the tail vein with a very high inoculum $5x\ 10^7$ – $5x\ 10^8$ CFU subsequently they develop septic shock with lethal outcome within 12 – 48 hours (Kim et al., 2014). Infected mice present with clinical signs of disease within 2-3 hours such as loss of appetite, diminished movement, ruffled fur, hunched posture and labored breathing (Cheng et al., 2009). In this model bacteria can be re-isolated from exsanguinated blood and are routinely found in all examined organs, whilst severe, this model has been used to identify key virulence determinants for staphylococcal sepsis (McAdow et al., 2011). This model was recently used to demonstrate that clonal expansion of bacteria –where only a few cells from the initial inoculum replicate leading to abscess formation (McVicker et al., 2014) is decreased when increased CFU are used in the inoculum (Pollitt et al., 2018). With higher infectious dose, the immune bottleneck responsible for the phenomenon, is bypassed and the host is simply overwhelmed. This decrease in survival is concurrent with increased bacterial burden in all recovered organs (Pollitt et al., 2018).

1.5.4.2 Septic arthritis

The route for administration of inoculum for the septic arthritis model is the same as in sepsis and the form of disease progression is determined by administering a lower dose, 7×10^6 – 2×10^7 CFU (Tarkowski et al., 2001). Bacteria disseminate to the synovial tissue and penetrate structures of the joint cavitiy, this is resultant in swollen and red joints and the animals exhibit joint stiffness. Interestingly although the route of adiminstration is the same, virulence factors identified in

disease progression of septic arthritis differ from those identified in sepsis models (Tarkowski et al., 2001).

1.5.4.3 Pneumonia

A murine pneumonia model has been developed in which the inoculum is delivered via a transnasal route to adult mice. This model is dose dependent and requires relatively high doses to cause disease with 4 x 10^8 CFU and 8 x 10^8 CFU causing 50 % and 90% mortality in 24 hours respectively (Wardenburg et al., 2007). A lower dose of 8 x 10^7 CFU results in no mortality, but animals display some symptoms of illness. The lungs of infected mice show disease pathology from 6 hours onwards, with infiltration of large number of immune cells and large staphylococcal foci are also found at this point (Wardenburg et al., 2007). This model exemplifies the dramatic effect small changes in dose can have on the outcome of the infection model and it is likely that the adaption of staphylococcal adhesion proteins to a human host is causative of the need for a high inoculum in this murine model (Kim et al., 2014).

1.5.4.4 Bacteraemia and metastatic abscess formation

There is a prevalence in bacteraemia and distal abscess formation in invasive staphylococcal disease in humans. This is modelled by systemic infection of the mouse by intravenous administration of the inoculum via the tail vein (Kim et al., 2014). Bacteraemia is achieved with doses of 1 x 10^6 – 1 x 10^7 CFU, *S. aureus* then exits the bloodstream and establish organ abscesses which can be found within the brain, lungs, liver, kidneys and heart (Cheng et al., 2009). These abscesses have a characteristic infiltration of immune cells, mostly neutrophils and are predominantly found on the kidneys (Kim et al., 2014). It has been shown that in addition to extracellular bacteria infiltrating host tissue, they are disseminated by neutrophils in the manner of a trojan horse (Gresham et al., 2000). Recently this model has revealed that neutrophils are also a mechanism of dissemination of *S. aureus* from these abscesses to other tissues (Pollitt et al., 2018) but that clonal expansion, occurs in macrophages prior to phagocyte escape. Whilst depletion of either neutrophils or macrophages results in decreased host survival, depletion of neutrophils does not abolish the immune bottleneck observed in this model (Pollitt et al., 2018).

1.5.4.5 Peritonitis

Patients with end-stage renal disease or those which receive peritoneal dialysis frequently develop peritonitis caused by *S. aureus.* To recapitulate this, mice are injected into the peritoneal cavity, to achieve disease a very high inoculum is needed, with doses of 5 x 10^8 and 6 x 10^9 CFU causing 50 % and 90 %. In this model there is formation of peritoneal abscesses, even in survivors of infection, but few staphylococci are found in the blood and metastatic abscess formation is rare in this model (Rauch et al., 2012). This model has been used to identify key host factors required for activation

and expansion of memory T-cells and therefore the requirements for a successful vaccination against *S. aureus* (Murphy et al., 2014).

1.5.4.6 Endocarditits

Infective endocarditis, usually associated with intra-vascular devices, is often caused by *S. aureus* in the nosocomial setting and the incidence of this is increasing (Federspiel et al., 2012). In addition to infection of post-operative patients, endocarditis commonly occurs in intr-venous drug users, caused by virulent CA-MRSA strains (David and Daum, 2010). To cause endocarditis in the mouse, valve trauma is produced by insertion of a catheter into the aortic valve via the left ceratoid artery. A day later the mouse is then infected intravenously with 1 x 10^6 CFU. Recovery of bacteria from the hearts of catheterised mice was 4 orders of magnitude greater then non-catheterised mice. This model is used to assess the efficacy of antibiotics on vegetative bacterial growths which occur on heart valves (Gibson et al., 2007).

1.5.4.7 Subcutaneous infection

S. aureus can cause skin infection in humans where the barrier of the skin has been compromised, such as a cut or graze. These infections can result in the production of purulent discharge from the infectious site (Kim et al., 2014), whilst these superficial infections are mild they can lead to life threatening infections previously described. To model these infections, subsequent to hair removal, 1 x 10^7 CFU is delivered by subcutaneous injection. Subcutaneous abscesses and regions of dermonecrosis can be measured to monitor infection progression (Bunce et al., 1992; Malachowa et al., 2013). More recently development of a model which mimics post-surgical infection that occurs in the hospital setting has been developed. This wound model involves a surgical incision to the thigh muscle, which is then sutured and inoculated with bacterial suspension. The skin is then sutured, and infection of mice is monitored. Excision of the muscle tissue provides insight into factors of the host response involved in pathogenesis and bacteria can be quantified by homongenisation (McLoughlin et al., 2006).

1.5.5 Humanised mouse models

As *S. aureus* has evolved to be particularly pathogenic to humans, many of the virulence factors have human specific ligands. As a result, attempts have been made to utilise humanised mice to better mimic staphylococcal infection. This was made possible by the recent development of the NSG mouse (non-obese diabetic/ severe combined immunodeficient mouse with null mutation in Il2R common gamma chain). These mice lack B, T, and NK cells, complement and possess defective myeloid cells, making them more susceptible to engraftment and better support human haemato-lymphopoiesis (the development of human adaptive immune response) (Ishikawa et al., 2005).

Humanisation of the mouse is achieved by transplanting human CD34+ stem cells into irradiated NSG pups (Lan et al., 2006).

This humanised mouse was first used for *S. aureus* infection by Knop et al., 2015 who administered a non-lethal dose via intraperitoneal injection. These humanised mice had significantly increased mortality than non-humanised controls and bacterial counts were higher in liver, spleen, kidney, lungs, and brain, demonstrating the ability of *S. aureus* to target human specific immune cells. In addition to this, there was evidence of T cell activation in the humanised mice (Knop et al., 2015). Subsequently, humanised mice have also been used in a subcutaneous skin infection model in which it was found that 10- 100 fold fewer bacteria were needed to cause analogous disease pathology in comparison with control mice and that humanised mice were more susceptible to PVL+ strains than control mice (Tseng et al., 2015). After respiratory infection of humanised mice, a 40-fold higher bacterial burden of the humanised mice in comparison to control mice was found (Prince et al., 2017). This pneumonia model also utilised additional knock-in of human *IL3* and *Csf2* improving reconstitution of macrophages. These mice had even higher bacterial burden than the standard NSG CD34+ mice. This study also demonstrated a role for the human-specific PVL, however no phenotype for the human-specific LukAB was found in this model (Prince et al., 2017).

All of these pioneering infection models have revealed increased susceptibility of humanised mice to *S. aureus* regardless of the method of inoculation. Further advancements in the humanisation of the murine immune response will improve the relevancy of these already promising developments in modeling *S. aureus* infection. These models could provide vital insight in vaccine trials, where there has currently been a lack of correlation between successful immunisation of mice and translation into human trials.

1.5.6 The use of zebrafish for modelling infection

Zebrafish (*Danio rerio*) is a small fresh-water fish (~4 cm in size) that has long been used for embryological and developmental studies, its use as a model organism provides an extensively characterised system which has more recently been exploited for vertebrate models of disease. The high capability of the zebrafish to reproduce and their small size (both as adults and larvae) make them suitable for high-throughput screening.

The publication of the entirety of the human genome in 2004 (International Human Genome Sequencing Consortium, 2004) has provided a reference for genome wide association studies (GWAS) and the ability to use whole genome sequencing (WGS) to identify molecular pathology of disease. Although the ability to identify genes *in silico* is a powerful tool, this has rapidly increased the number of genes, putatively causative of disease, in need of validation and mechanistic investigation. The zebrafish is being increasingly employed to research human pathogenesis in

favour of murine models (Liu et al., 2017), with zebrafish possessing homologs for 70% of the genes in the human genome (Howe et al., 2013). The advent of the CRISPR/Cas9 system has accelerated the ability to manipulate the zebrafish genome and provide targeted gene inactivation and overexpression (Chang et al., 2013).

Zebrafish possess leukocytes (including phagocytes) essential for the innate immune response, present from 25 hours post fertilisation (Lieschke et al., 2001). This model organism also has a well-developed complement system, functioning through classical, alternative, and lectin pathways, which play a role in pathogen and clearance (Boshra et al., 2006). Early embryos (up to 5 days post fertilisation) are incapable of independent feeding but are able to phagocytose pathogenic bacteria injected into the circulation, mounting an innate immune response and thus are capable of preventing overwhelming infections (Davis et al., 2002; Sar et al., 2003). As a result of these characteristics, it has become an attractive host for infection models since the initial use of it to study host response to native pathogen *Mycobacterium marinum* (Davis et al., 2002). It is being used as an infection model for an ever-increasing number of non-native pathogens. The advantages of the zebrafish embryo as an infection model, in comparison with human cell models and other vertebrate infection models, are briefly summarised in Table 1.1.

1.5.6.1 Zebrafish embryo models of infection with gram positive pathogens

Along with the zebrafish model for systemic *S. aureus* infection developed in Sheffield (Prajsnar et al., 2008) zebrafish embryos are being utilised as infection models for other gram-positive pathogens. *Listeria monocytogenes,* a food borne pathogen causative of meningitis in newborns, injected into the hindbrain of embryos 72 hpf provides a meningitis model for the pathogen and has identified the host protein GP96 (a protein of the endoplasmic reticulum) as protective against the pore-forming toxin, lysteriolisin O (LLO) which is involved in vacuole escape (Mesquita et al., 2017). Interestingly, in the model for *Streptococcus pyogenes,* intra-muscular (IM) injection results in massive muscle tissue necrosis, similar to the human necrotising fasciitis typical of *S. pyogenes* infection (Phelps and Neely, 2007).

Systemic infection of embryos with pathogenic *Enterococcus faecalis* is resultant in substantial tissue damage and host mortality (Prajsnar et al., 2013). Use of fluorescent mutants has demonstrated that the enterococcal polysaccharide antigen (*epa*) mutants are unable to evade phagocytosis unlike their WT counterparts. It has also demonstrated that the quorum sensing system, Fsr is an essential virulence determinant, but that *fsr* mutants replicate in embryos and that Fsr controls factors involved in later stages of infection (Prajsnar et al., 2013). The model has also been used to demonstrate that N-acetylglucosaminidase activity (AtlA) mutants, that form long chains, are also attenuated, likely due to an inability for the larger chains of cells to disseminate throughout the embryo (Salamaga et al., 2017).

1.5.6.2 Zebrafish embryo models of infection with gram negative pathogens

The zebrafish has been used as an infection model for the opportunistic pathogen *Pseudomonas aeruginosa*. This model requires a high inoculum as the bacteria is rapidly cleared by both macrophages and neutrophils (Clatworthy et al., 2009). The pathogen is primarily a threat to CF patients, where in the lungs it switches from planktonic growth to biofilm formation. The zebrafish model has shown that type III secretion system (T3SS) and the quorum sensing genes (*lasR* and *mvfR*) are essential for virulence (Clatworthy et al., 2009). Furthermore, the model has been used to identify roles for the LPS modifying SadC and WarA proteins, which modify the distribution of LPS O antigen. *P. aeruginosa sadC* and *warA* mutants are attenuated, as there is increased neutrophil recruitment in comparison with infection of embryos with WT (McCarthy et al., 2017). Embryos infected with either *sadC* or *warA* mutants had significantly higher levels of TNF-α in comparison to embryos infected with WT, suggesting that the modification of LPS has an immune-modulatory effect, aiding evasion of the host immune response (McCarthy et al., 2017).

Zebrafish embryos have also been used to study pathogenicity of the food-borne pathogen *Shigella flexneri*. Systemic infection of embryos with *S. flexneri* causes macrophage death and pathogenesis is again reliant on T3SS, as mutants are attenuated in this model (Mostowy et al., 2013). The model demonstrated that cytosolic *S. flexneri* are trapped by septins and targeted for autophagy (Mostowy et al., 2013), embryos depleted of the Sept15 (the zebrafish homologue of human Sept7) by injection of morpholino-modified antisense oligonucleotides (morpholinos) (which alter gene expression by binding host RNA targets) had increased mortality and bacterial burden when infected with WT in comparison with control embryos (Mazon-Moya et al., 2017). Live-imaging of this infection model has provided insight into the role of the cytoskeleton and its role in inflammation (Mazon-Moya et al., 2017; Mostowy et al., 2013).

1.5.7 Humanised zebrafish models

Recently zebrafish research has expanded into 'humanised' models, with the zebrafish genome being edited to provide expression of a human protein, rather than paralogs. This approach has been applied to pharmacokinetics, with expression of a human detoxification protein by the zebrafish liver, altering the metabolic profile of CYP3A4 targets, providing a more relevant drug screen (Poon et al., 2017).

Xenografts of patient T-cell acute lymphoblastic leukemia (T-ALL) into transgenic zebrafish which express humanised CXCL12 have been used as a preclinical, chemical genetic screen. This technique, which allows the engraftment of patient samples and test them with individual or combination chemotherapies, in a one-week time scale, could provide a pivotal tool in personalised medicine (Rajan et al., 2015). Humanisation of components involved in the immune response of the

host to infection was recently attempted, in order to improve the relevance of this infection model to *S. aureus* (Buchan, K. D., 2018).

1.6 *Intravital imaging of host-pathogen interactions*

1.6.1 Intravital imaging of zebrafish embryos

Intravital imaging techniques are one of the main benefits to the use of zebrafish as a model organism. The transparency of the embryos and the ability to fluorescently label cellular components and tissues such as macrophage specific *mpeg1* promoter (Ellett et al., 2011) and neutrophil specific *mpx* (Gray et al., 2011) and image these living specimens over long time scales makes them an attractive candidate for modelling infection. Not only can host components be labelled, but bacterial and fungal pathogens either dyed with fluorescent probes or genetically manipulated to produce fluorescent proteins can also be visualised (Bojarczuk et al., 2016; Gibson et al., 2017; McVicker et al., 2014; Ogryzko et al., 2019; Prajsnar et al., 2012; Willis et al., 2018). Not only can these cells be visualised by fluorescence microscopy, but rather elegantly, they can be photoactivated by lasers and simultaneously imaged (Brothers et al., 2013; Ellett et al., 2011; Isles, 2018). Conditionally activated fluorescent reporters such as indicators of oxidative stress or phagocytosis can also give insight to the infectious process (Tobin et al., 2012) and commercially available molecular probes, such as pH reactive dyes can also be used for live imaging of infected embryos (Serba, 2015).

Fluorescence stereomicroscopy has been used to visualise the localisation and migration of the larger host cells and bacterial cell population at low magnification, allowing for relatively simple and quick imaging of the host response to infection. This form of microscopy, imaging on the whole animal level, has been useful for the identification of reverse neutrophil migration (Ogryzko et al., 2019), bacterial abscess formation (Prajsnar et al., 2008), granulopoiesis (Willis et al., 2018), and dissemination of fungal pathogens (Gibson et al., 2017).

Confocal microscopy, obtaining higher resolution and higher magnification, has routinely been employed to investigate host pathogen interactions in more detail. This has enabled imaging of sub-cellular localisation of pathogens within the host such as co-localisation of *Mycobacterium marinum* with the autophagy marker, LC3 (van der Vaart et al., 2014), clonal expansion of *S. aureus* within neutrophils (Prajsnar et al., 2012), and septin cage entrapment of *S. flexinori* (Mostowy et al., 2013).

Spinning-disc confocal microscopy lowers the amount of laser exposure to the sample, reducing photo-toxicity to the living samples, enabling high resolution time course imaging. This methodology has been used to gain insight in infection progression and has aided identification of granuloma formation in *M. marinum* infection (Ogryzko et al., 2019), cryptococcal mass formation

Limitations of *in vitro* phagocyte challenge	Advantages of larval zebrafish model
Purification of immune cells can perturb function	Purification unnecessary
Media does not recapitulate tissue specific *in vivo* nutrients	*In vivo* nutrients
No soluble factors (e.g. opsonins, cytokines) from other cell types	Normal soluble components
No contact activation or inhibition by other cell types	Normal tissue environment
No effect of extracellular matrix interactions	Normal extracellular environment
Cannot monitor dissemination of infection	Tissue-to-tissue dissemination can be imaged
Limitations of *in vivo* mouse infection	**Advantages of larval zebrafish model**
Too large to examine infection host-wide at high resolution	Possible to image entire live fish
Opaque skin and organs limit fluorescent imaging below ~100 μm	Fish larvae are transparent
Elimination of macrophage function pleiotropic	Temporary macrophage ablation feasible
Very limited high-resolution, non-invasive imaging of pathogen or immune morphology	High-resolution, non-invasive imaging facile throughout the host

Table 1.1 Advantages of the use of embryonic zebrafish to study the interactions of pathogens with the host innate immune response.

Adapted from (Tobin et al., 2012). Comparison of zebrafish embryos with *in vitro* human cell culture and *in vivo* mouse infection models

resulting in vascular damage of the host (Gibson et al., 2017) and even the transfer of *S. aureus* from neutrophils to macrophages (Serba, 2015).

1.6.2 Intravital imaging of murine tissue

Imaging murine tissue has previously been limited to *ex vivo* imaging after fixation and or clearing samples for microscopy. A method for intravital imaging of mouse livers has recently been developed: this uses spinning-disc confocal microscopy which allows for time-course imaging of the host cells without photo-bleaching (Wong et al., 2011). Briefly, anesthetised mice are injected with fluorescently labelled antibodies and positioned laterally. A lateral incision from the costal margin to the midaxillary line is made, and tendons retaining the liver are severed in order to excise the liver. Blood vessels to the liver are carefully left intact to allow circulation of blood to the liver, the exposed liver is mounted on a slide and kept moist with saline (Wong et al., 2011). This intravital imaging technique has been used to demonstrate the intracellular survival of *S. aureus* within the tissue resident macrophages, Kupffer cells (Surewaard et al., 2016), and identify that augmentation of *S. aureus* by the peptidoglycan of human commensals also occurs within these Kupffer cells (Boldock et al., 2018).

Intra-vital imaging of the murine liver using two-photon confocal microscopy has recently been use to investigate the effect of LPS treatment on neutrophil activity on the liver and have manufactured a chamber specially designed for the incubation of the mouse whilst imaging the liver (Park et al., 2018). This method enables normal circulation of blood to and around the liver and this microscopy technique achieved a depth of up to 40 μm using a 20 x objective (Park et al., 2018).

In contrast with the non-invasive imaging of zebrafish embryos, these techniques are not compatible with monitoring for future timepoints, either by observation of survival or additional microscopy. It is an invasive method for single use and animals are sacrificed directly after imaging (Boldock et al., 2018; Park et al., 2018; Surewaard et al., 2016; Wong et al., 2011).

A recently developed microscopy technique, light sheet fluorescence microscopy (LSFM) can image very large depths within the zebrafish embryo and can achieve relatively high-resolution images, from low magnification objectives imaging a large field of view. The nature of this technique enables long-term time lapse imaging as the method has lowered phototoxicity to living specimens (Reynaud et al., 2014a).

1.7 *Aims of this study*

- To combine the unique zebrafish model of *S. aureus* infection with light sheet fluorescence microscopy to enable long term imaging of host-pathogen interactions in physiologically relevant conditions.
- Elucidate the temporal and spatial niche for bacterial expansion within the host.
- Investigate the real-time expression of bacterial virulence factors within a zebrafish host.

2 Methods

2.1 *Media*

Media were prepared using dH_2O and sterilised by autoclaving for 20 min at 121 °C and 15 psi.

2.1.1 Tryptic Soy Broth

Tryptic soy broth (Scientific Lab Supplies) 30 g/L

For tryptic soy agar (TSA) plates 1.5 % (w/v) bacteriological agar was added

2.1.2 LK broth

Tryptone 10 g L

Yeast extract 5 g/L

KCl 7 g/L

For LK bottom agar 1.5 % (w/v) bacteriological agar (VWR) was added.

For LK top agar 0.5 % (w/v) bacteriological agar (VWR) was added.

2.2 *Antibiotics*

Selective antibiotics were added to growth medium when necessary. Antibiotic stock solutions were prepared by dissolving antibiotic in appropriate solvent and filter sterilised (0.22 μm pore size) and stored at -20 °C. For use in liquid media antibiotics were added immediately prior to use, when used in agar plates molten agar was cooled to 55 °C before addition of antibiotics. All antibiotics used in this study are listed in Table 2.1.

Antibiotic	**Solvent**	**Stock conc. (mg ml^{-1})**	**Working conc. (μg ml^{-1})**
Kanamycin (Kan)	dH_2O	50	50
Chloramphenicol (Cm)	100% (v/v) EtOH	10	10
Erythromycin (Ery)	100% (v/v) EtOH	5	5
Lincomycin (Ln)	50% (v/v) EtOH	25	25
Neomycin (Neo)	dH_2O	50	50
Tetracycline (Tet)	100% (v/v) EtOH	5	5

Table 2.1 Antibiotic stock solutions and their concentrations

2.3 *Bacterial strains*

Bacterial strains used in this study are stored in Microbank© cryovials (Pro Lab Diagnostics) containing beads at -80 °C. These were cultured by streaking out onto TSA plates containing selective antibiotics when needed and incubated at 37 °C. Plates were stored short term at 4 °C, wrapped in Parafilm© (Bemis) to prevent plates drying out. For growth in liquid culture, bacteria were incubated at 37 °C with a volumetric ratio of 1:4 media to air, with 250 rpm shaking. All strains used in this study are listed in Table 2.2.

2.3.1 Bacterial culture

Unless otherwise stated, bacteria were cultured as follows: for liquid cultures a single colony was picked with a sterile loop and used to inoculate 10 ml of medium in a sterile 50 ml falcon tube and incubated 37 °C, with 250 rpm shaking. This overnight culture was used to inoculate 50 ml of fresh medium in a conical flask, to an OD_{600} of 0.05 and grown to exponential phase (OD_{600} 0.8 -1.2) at 37 °C on a rotary shaker at 250 rpm.

Strain number	**Relevant genotype**	**Selection marker**	**Source**
SJF4618	SH1000 PmalM1:GFP integrated at *geh* locus	Kan	Eric Pollitt
SJF4622	JE2 PmalM1:GFP integrated at *geh* locus	Kan	Eric Pollitt
SJF4631	SH1000 with PmalM1:mCherry integrated at *geh* locus supplemented with *lysA*::*ery lysA*+ cassette	Ery	(Pollitt et al., 2018)
SJF4634	JE2 with PmalM1:mCherry integrated at *geh* locus supplemented with *lysA*::*ery lysA*+ cassette	Ery	Eric Pollitt
SJF4622	SH1000 with PmalM1:mCherry integrated at *geh* locus	Tet	Eric Pollitt
SJF4625	JE2 with PmalM1:mCherry integrated at *geh* locus	Tet	Eric Pollitt
SJF4308	SH1000 with pMV158-mCherry plasmid	Tet	(Prajsnar et al., 2012)
SJF4302	JE2 with pMV158-mCherry plasmid	Tet	Tomasz Prajsnar
SJF5074	UAMS-1 pDM4 (*cidABC*:*GFP*, *lrgAB*:*dsRed*) dual *cid* and *lrg* reporter strain	Cm	(Moormeier et al., 2013)
SJF5075	UAMS-1 pCM20 (*nuc*::*gfp*), reporter strain for *nuc* expression	Ery	(Kiedrowski et al., 2011)
SJF5078	UAMS-1 pEM81 (*cidABC*:*gfp*), reporter strain for *cid* expression	Cm	(Moormeier et al., 2013)
SJF5079	UAMS-1 pEM80 (*lrgAB*:*gfp*), reporter strain for *lrgAB* expression	Cm	(Moormeier et al., 2013)
SJF5087	UAMS-1471 (Δ*nuc*) *nuc* mutant		(Kiedrowski et al., 2011)
NE1466	JE2 with Tn insertion in *cidR* (Tn::*cidR*)	Ery	(Fey et al., 2013)
NE1726	JE2 with Tn insertion in *lrgB* (Tn::*lrgB*)	Ery	(Fey et al., 2013)

RN4220	Restriction deficient transformation recipient strain		(Kreiswirth et al., 1983)
SJF5153	JE2-mCherry pCM20 (*nuc*:*gfp*), constitutively producing mCherry with GFP *nuc* reporter	Tet,Ery	This study
SJF5154	SH1000-mCherry pCM20 (*nuc:*gfp) constitutively producing mCherry with GFP *nuc* reporter	Tet, Ery	This study
SJF5152	JE2 pMV158-mCherry pEM81 (*cidABC*:*gfp*) constitutively producing mCherry with GFP *cidABC* reporter	Tet, Cm	This study
SJF5088	JE2 pMV158-mCherry pEM80 (l*rgAB*:*gfp*) constitutively producing mCherry with GFP *lrgAB*reporter	Tet, Cm	This study
SJF5091	JE2-mCherry pEM80 (*lrgAB*:*GFP*) with PmalM1:mCherry integrated at geh locus (constitutive mCherry production) with GFP *lrgAB* reporter	Tet, Cm	This study
SJF5092	JE2-mCherry pEM81 (*cidABC*: *GFP*) with PmalM1:mCherry integrated at geh locus (constitutive mCherry production) with GFP *cidABC* reporter	Tet, Cm	This study
SJF5155	SH1000 pMV158-smURFP constitutively producing smURFP	Tet	This study
SJF5156	JE2 pMV158-smURFP constitutively producing smURFP	Tet	This study

Table 2.2 Bacterial strains used in this study

2.4 *Plasmids*

All plasmids used in this study are listed in Table 2.3, plasmid DNA was isolated by GeneElute plasmid MidiPrep kit (method 2.9.7). Plasmids were designed using SnapGene.

Plasmid	Description	Selection marker	Source
pMV158-mCherry	Multicopy plasmid encoding fluorescent protein mCherry under the constitutive promoter PMal1	Tet	Tomasz Prajsnar
pMV158-GFP	Multicopy plasmid encoding GFP under the constitutive promoter PMal1	Cm	(Nieto and Espinosa, 2003)
pMV158-smURFP	Multicopy plasmid encoding smURFP under the constitutive promoter PMal1	Tet	This study
pCM20	GFP reporter for *nuc* expression	Ery	(Kiedrowski et al., 2011)
pDM4	Dual reporter for expression of *lrg* (dsRed) and *cid* (GFP)	Cm	(Moormeier et al., 2013)
pEM80	GFP reporter for *lrg* expression	Cm	(Moormeier et al., 2013)
pEM81	GFP reporter for *cid* expression	Cm	(Moormeier et al., 2013)

Table 2.3 Plasmids used in this study

2.5 *Buffers and solutions*

All buffers were made with dH_20 and if necessary autoclaved or filter sterilised. Buffers were stored at room temperatures unless stated otherwise.

2.5.1 Phosphate buffered saline (PBS)

NaCl	8 g l^{-1}
Na2HPO4	1.4 g l^{-1}
KCl	0.2 g l^{-1}
KH2PO4	0.2 g l^{-1}

2.5.2 Phage buffer

MgSO4	1 mM
CaCla2	4 µM
Tris-HCl pH 7.8	50 mM
NaCl	0.6 % (w/v)
Gelatin	0.1 % (w/v)

2.5.3 TAE (50 x)

Tris	242 g l^{-1}
Glacial acetic acid	5.7 % (w/v)
Na2EDTA pH 8.0	0.05 M

To produce a working TAE solution, the stock solution was diluted 1:49 dH_2O.

2.5.4 0.1 M Sodium phosphate buffer (pH 5.5)

Na2HPO4 (1.0 M)	93 ml
NaH2PO4 (1.0 M)	7 ml

2.5.5 50 mM Tris-HCl pH 7.5

Tris base 6.05 g l^{-1}

The pH was adjusted to 7.5 with HCl before autoclaving

2.5.6 20 mM Sodium acetate buffer

$C_2H_3NaO_2$ 1.64 g l^{-1}

The pH was adjusted to 4.5 with 100 % glacial acetic acid before to autoclaving

2.5.7 Ethanol 70 % (v/v)

EtOH 700 ml l^{-1}

dH_2O 300 ml l^{-1}

2.6 *Chemicals, compounds, and enzymes*

All chemicals and compounds used in this study were of analytical grade quality and were purchased from MilliporeSigma and Thermo Fisher Scientific unless stated otherwise. Restriction enzymes, polymerases, mastermixes and Gibson assembly mix were purchased from New England Biolabs.

Reagent	Stock concentration	Solvent
Lysostaphin	5 mg ml^{-1}	20 mM sodium acetate
CyGel Sustain	100 % (v/v)	
CaCl2	1 M	dH_2O
NaOH	1 M	dH_2O
EtBr	5 mg ml^{-1}	dH_2O
3-amino benzoic acid ester (Tricaine)	0.4 % (w/v)	20 mM Tris-HCl pH 7.0

2.7 *Centrifugation*

The following centrifuges were used to harvest samples:

Eppendorf microcentrifuge 5418, maximum speed of 16,783 RCF (14,000 rpm), capacity 24 x 1.5-2 ml

Sigma centrifuge 4K15C, maximum speed of 5525 RCF (5,100 rpm), maximum capacity of 16 x 50 ml.

Avanti High Speed J25I centrifuge, Beckman: JA-25.50 rotor, maximum speed of 75, 600 RCF (25,000 rpm) capacity up to 6 x 50 ml

Unless otherwise stated centrifugation was performed at RT.

2.8 *Determination of bacterial cell density*

2.8.1 Spectrophotometric measurement (OD_{600})

Optical density of bacterial culture was quantified by spectrophotometric measurements at 600 nm (OD_{600}). These measurements were taken using aJenway 6100 spectrophometer and Semi-micro PS cuvettes (Fisherbrand). If required, samples were diluted 1:10 in culture medium to keep measurements below OD_{600} = 1.0.

2.8.2 Direct cell counts (CFU ml^{-1})

The number of viable cells in liquid culture was estimated by direct cell counts. Bacterial samples were serial diluted 1:9 in PBS in triplicate and 10 ul samples of each dilution spotted onto TSA plates. Plates were incubated at 37 °C overnight and the number of colony forming units (CFU) per spot was determined and CFU ml^{-1} of culture estimated.

2.9 *Genetic manipulation of S. aureus*

2.9.1 Primer design

Primers used in this study were synthetic oligonucleotides (Eurofins) 25 - 50 bp in length based upon the DNA sequences of *S. aureus* strain USA300 FPR3757, plasmids, and encoding fluorescent proteins. Primer design for Gibson assembly was performed using NEBuilder Assembly Tool from https://nebuilder.neb.com. Lyophilised primers were resuspended in sterile milliQ and either stored as 100 µM stocks or as a working concentration of 10 µM, at -20 °C.

2.9.2 PCR amplification

Polymerase chain reaction (PCR) amplifications were performed using Phusion High Fidelity master mix (New England Biolabs). A final reaction volume of 50 µl contained:

Template DNA	50 – 100 ng
Forward primer (10 µM)	2.5 µl
Reverse primer (10 µM)	2.5 µl
Phusion High Fidelity master mix	25 µl
Sterile milliQ water	up to 50 µl

PCR amplification was carried out in Veriti Thermal Cycler (Applied Biosystems), the lid was preheated to 105 °C and the following conditions were used:

1 cycle	Initial denaturation	98 °C	30 s
30 cycles	Denaturation	98 °C	10 s
	Annealing	55-65 °C	10 s
	Extension	72 °C	15 s/kb
1 cycle	Final extension	72 °C	3-5 min

2.9.3 Gel extraction of DNA

DNA was separated by electrophoresis in 1 % (w/v) agarose in TAE gel containing 0.05 µg ml^{-1} ethidium bromide. The DNA band was visualised with a UV transilluminator and excised from the gel with a clean scalpel. The excised gel was weighed, and DNA was purified from the gel using QIAquick Gel Extraction Kit (QIAGEN) as per manufacturer's instructions.

2.9.4 PCR purification

DNA fragments from PCR reactions were purified with the QIAquick PCR purification kit as per the manufacturer's instructions.

2.9.5 Restriction endonuclease digestion

Restriction endonuclease enzymes were purchased from New England Biolabs, where possible 'high fidelity' restriction endonucleases were used. DNA was digested as per the manufacturer's

instructions, with buffers supplied by the manufacturer, using recommended enzyme concentrations. The reactions were incubated at 37 °C for 1 h, if there was further downstream manipulation of DNA fragments, these were purified as described in the Methods sections 2.9.3 and 2.9.4 .

2.9.6 Lysostaphin cell lysate preparation

A single colony was used to inoculate 50 ml of TSB (with appropriate antibiotic) in a 250 ml conical flask and incubated at 37 °C overnight. Cells were recovered by centrifugation at 3000 RCF for 10 min at 4 °C, washed in PBS and centrifuged as before. Supernatant was removed and the pellets weighed. The pellets were resuspended in PBS (20 ml per gram of cells) before adding 500 µg lysostaphin (10 mg ml^{-1}) per gram of cells. Cell suspensions were incubated with gentle agitation at 37 °C for 1-4 hours (depending on strain) until lysates had a gelatinous consistency.

2.9.7 Midi prep

Large scale plasmid purification of plasmid from *S. aureus* was performed using the 'GeneElute Plasmid MidiPrep Kit' (Sigma Aldrich). A single colony was used to inoculate 50 ml of TSB (with appropriate antibiotic) in a 250 ml conical flask and incubated at 37 °C, with shaking at 250 rpm overnight. Overnight cultures were recovered by centrifugation at 3000 RCF, for 10 mins at RT and the pellet resuspended in 'Resuspension buffer' at this point the 'lysostaphin digestion' (Method 2.9.6) was performed. From this juncture onwards the manufacturer's instructions were followed apart from one other deviation, incubation of column with milliQ at RT prior to elution was extended to 10 min and half the recommended volume was used for recovery of plasmid. Plasmid concentration was the determined by NanoDrop Lite.

2.9.8 Gibson Assembly

Inserts were obtained by PCR amplification (method 2.9.2), DNA vector backbone was prepared by MidiPrep (Method 2.9.7) followed by restriction endonuclease digestion (method 2.9.5) and purification (Methods 2.9.3 and 2.9.4). Assembly was then performed in a total volume of 10 µl with the following components:

Vector DNA	50ng
Insert DNA	3 fold excess of vector DNA
Gibson Assembly Master Mix (2x)	5 µl
milliQ water	up to 10 µl

The ligation was performed at 50 °C for 1 h, the product was then used to transform electrocompetent *S. aureus* (strain RN4220).

2.9.9 Preparation of electrocompetent cells

The *S. aureus* strain RN4220 was streaked on TSA and incubated at 37 °C overnight. A single colony was used to inoculate 400 ml of TSB, in a 2 L conical flask and cells were grown for 10 h, at 37 °C with shaking at 250 rpm. This culture was used to inoculate a fresh 400 ml of TSB, to an OD_{600} of 0.1, cells were incubated at 37 °C with shaking at 250 rpm for 1-2 h until an OD_{600} of 0.4-0.6 was reached. Cells were divided into 50 ml aliquots and recovered by centrifugation at 3000 RCF for 10 min at RT. Pellets were washed 3 times by resuspension in 25 ml sterile dH_2O and centrifugation at 3000 RCF at RT for 10 min. Pellets were resuspended in 20 ml 10 % (v/v) glycerol and centrifuged at 3000 RCF for 10 min at RT. The pellets were combined and resuspended in 10 ml 10 % (v/v) glycerol and incubated stationary at RT for 30 min. Cells were centrifuged at 3000 RCF for 10 min at RT, the pellet was resuspended in 500 µl 10 % (v/v) glycerol. 60 µl aliquots were transferred into micro-centrifuge tubes, snap frozen in liquid nitrogen and stored at -80°C.

2.9.10 Electroporation

A 60 µl aliquot of electrocompetent *S. aureus* was defrosted at RT, transferred to a 1 mm electroporation cuvette (Bio-Rad) and ~1 µg of plasmid DNA (a maximum of 10 µl) was added. A Gene Pulser Xcell electroporation (Bio-Rad) was used to carry out electroporation at 2.1 kV, 25 µF and 100 Ω. Cells were immediately recovered in 1 ml of TSB pre-warmed to 37°C, added to a 15 ml centrifuge tube and incubated for 3 h at 37 °C with shaking at 250 rpm. 200 µl aliquots were spread onto a TSA plates containing selective antibiotics and incubated at 37°C until colonies appeared (20 – 48 h).

2.9.11 Bacteriophage propagation

The *S. aureus* donor strain was grown overnight in selective media. 150 µl of overnight culture was combined with 5ml TSB, 5ml Phage Buffer and 100 µl phage lysate stock (Φ11 or Φ85), incubated at 25°C overnight until cleared. The lysate was filter sterilised (0.2µm) and stored at 4 °C.

2.9.12 Bacteriophage transduction

50ml of LK was inoculated with a single colony of the recipient *S. aureus* strain and incubated overnight 37 °C, 250 rpm. The overnight culture was centrifuged at RT, 3000 RCF for 10 min. The pellet was resuspended in 3 ml LK. 500 µl of *S. aureus* suspension was added to 1 ml of LK, 500 µl of phage lysate (from donor strain) and 10 µl of 1 M $CaCl_2$. The mixture was incubated statically at 37 °C for 25 min, followed by 15 min incubation at 37 °C, 250 rpm shaking. 1 ml of ice cold 0.02 M NaCit was added to the mixture and incubated on ice for 5 min, followed by centrifugation at 4 °C, 3000 RCF for 10 min. The pellet was resuspended in 1 ml 0.02 M NaCit and incubated on ice for 45-90 min, 200 µl aliquots were spread onto selective LK agar plates containing 0.05 % (w/v) sodium citrate and incubated at 37 °C for 24-48 hr. Colonies were picked and streaked on selective TSA plates to confirm resistance profile.

2.9.13 Agarose gel electrophoresis

1 % (w/v) agarose, with 0.5 µg/ml ethidium bromide in 1 x TAE buffer was prepared for separation of DNA samples. Prior to loading in wells of the gel, samples were mixed with 6 x DNA loading dye (Thermo Scientific). Gels were loaded into horizontal electrophoresis tanks (Bio-Rad) and submerged in 1 x TAE, samples were electrophoresed using 120 V, 400 mA for 30 – 44 min. Separated samples were visualised by UV transillumination at 260 nm and documented by the UVi Doc gel documentation system (UviTEC), GeneRuler 1 kb DNA ladder (Thermo Scientific) was used for approximation of size and concentration of DNA fragments.

2.10 *Zebrafish procedures*

2.10.1 Zebrafish husbandary

Adult zebrafish were housed in Home Office approved aquaria at the University of Sheffield and kept according to Home Office standards with a 14/10 hour light/dark cycle and maintained in a continuously re-circulating, closed system at 28 °C. After collection from the aquarium, eggs are kept in E3 with added methylene blue. Zebrafish embryos are not protected by Home Office regulations until < 5.2 dpf and all experiments were performed on this basis. All experiments that ended at < 5.2 dpf were disposed of in accordance to Home Office approved methods.

2.10.2 Zebrafish lines

All WT and transgenic zebrafish lines used in this study are listed in Table along with their use and origin

Zebrafish line	Use	Origin
London Wild Type (LWT)	WT	
Nacre	WT – no xanthophores	
Tg(*lyz.nfsB*:*mCherry*) SH260	mCherry labelled neutrophils	(Elks et al., 2011)
Tg(*mpx*:*gfp*)I114	GFP labelled neutrophils	(Renshaw et al., 2006)
Tg(*mpeg.mCherry* x CAAX)SH378	Macrophage specific mCherry labelled membranes	(Ellett et al., 2011)
Tg(c-*fms*:*gfp*)SH377	GFP labelled macrophages	(Dee et al., 2016)

Figure 2.1 Zebrafish lines used in this study

2.10.3 Zebrafish media

2.10.3.1 E3 medium (x 10)

NaCl	50 mM
KCl	1.7 mM
$CaCl_2$	3.3 mM
$MgSO_4$	3.3 mM

The 10 x E3 stock solution was diluted 1:9 with dH_2O to make a 1 x working solution, and methylene blue was added to a final concentration of 0.00005 % (w/v) to prevent fungal growth, prior to autoclaving.

2.10.3.2 Methylcellulose

E3 was prepared (Method 2.10.3.1) and after autoclaving cooling to 70 °C, 2.75 % (w/v) methylcellulose was added with stirring in an ice bath to facilitate solubilisation. After the solution clarified it was aliquoted into 20 ml syringes and stored at -20 °C. At least 24 h prior to use methylcellulose was defrosted at 28.3 °C and temporarily stored at this temperature.

2.10.4 Zebrafish anaesthesia

Zebrafish embryos were anaesthetised for experimental procedures with 3-amino benzoic acid ester (tricaine or MS322, Sigma) stock solution of 0.4 % (w/v) in 20mM tris-HCl (pH 7) stored at 4°C in dark conditions before diluting 1/20 to a working concentration of 0.02% (w/v) (200mg/L). Embryos were incubated in tricaine in E3 for at least 5 mins, covered to prevent exposure to light, until movement was no longer observed. After anaesthesia embryos were recovered in fresh E3 without tricaine.

2.10.5 Microinjection of *S. aureus*

Overnight cultures of *S. aureus* were prepared and subcultured in 50ml TSB inoculated to OD_{600} = 0.05 and incubated until the culture reached a density of OD_{600} = ~1. 40ml of culture was centrifuged at 3000 RCF at 4 °C, the supernatant discarded, and the pellet was washed twice in sterile PBS by centrifugation and resuspension. The final bacterial inoculum was kept on ice. Embryos were manually dechorionated 2 h prior to injection, 30 hpf embryos were anaesthetised and immobilised in 2.8 % (w/v) methylcellulose in E3. Bacterial suspension was loaded into a microinjection needle, made by heating and pulling glass capillary tubes (World Precision Instruments). The glass needle containing the inoculum was transferred to a Micromanipulator (WPI) and the inoculum dispensed by a pneumatic micropump (WPI, PV820). A dissection microscope (Leica, S6E) was used to visualise injections and 10mm/0.1mm Micrometer Scale (Pyser-SGI Ltd., PS1) used to calibrate the injection volume. 25-30 embryos were used per experimental group. After infection embryos were unmounted from methylcellulose and transferred to a petridish containg 25 ml E3 and incubated for 1-2 h at 28.3 °C. Embryos were then washed with E3 and individually transferred to wells of a 96-well plate.

2.10.6 Determination of embryo mortality subsequent to infection

To determine survival of embryos post infection, visual inspection of embryos was performed twice daily using a dissecting microscope (Leica), mortality of embryos was evidenced by cessation of heart beat and circulation. The number of deceased embryos at each timepoint was recorded and used to produce a Kaplen-Meier survival curve (Prism, GraphPad).

2.10.7 Determination of inoculating dose

During injection of zebrafish embryos, at the beginning and end of each group, 4 doses of the inoculum were injected into 1 ml of sterile PBS and incubated on ice. Subsequent to infection of embryos, 3 x 10 µl of the diluted dose were spotted onto TSA and dried before incubated at 37 °C overnight. CFU per spot were counted and average CFU used to calculate dose as follows:

$$Dose\ CFU = \frac{Av.colonies\ \times\ 100}{4}$$

2.10.8 Homogenisation of embryos for determination of bacterial burden

To determine the bacterial burden of individual embryos at any time post infection until 5.2 dpf, individual embryos were recovered in 200 µl of E3 and transferred to 500 µl cap tubes containing 1.4 mm ceramic beads (Peqlab). Embryos were homogenised by PreCellys 24-dual (Peqlab) and bacterial load of homogenates serially diluted and determined as described in Method 2.8.2.

2.10.9 Mounting embryos for microscopy (spinning disc/ airyscan)

Embryos were anesthetised before immersion in 0.8 % (w/v) low melting point (LMP) agarose in E3 with 0.02 % (v/v) tricaine, in a glass bottom culture dish (0.08-0.012 mm thickness), (embryos can be briefly manipulated/aligned before LMP agarose solidifies) E3 with 0.02 % (v/v) tricaine was added to maintain hydration of samples during microscopy.

2.10.10 Live imaging embryos by spinning disc confocal microscopy

An UltraVIEW VoX spinning disk confocal microscope (Perkin Elmer) and Velocity (Image Processing and Vision Company Ltd. UK) were used for image acquisition and processing. Images were acquired with a 20 x air lens (Nikon) or a 40x oil dipping lens (Nikon) using a 457-514 nm argon laser, 561nm sapphire laser and 642nm diode laser to excite fluorophores GFP, mCherry & Alexa Fluor 647nm respectively.

2.10.11 Mounting embryos in 0.8 % (w/v) agarose for lightsheet fluorescence microscopy

E3 was made up from 10 x E3 stock with sterile milliQ water and filtered (0.02 µm pore size); the solution was heated in the microwave to ~ 70 °C. Approximately 10 ml was added to a Falcon tube (50 ml) with pre-weighed LMP agarose (0.08 g) and mixed by vortexing. The solution was heated in the microwave in 10 s bursts (to avoid boiling over the solution and vortexed in between) to dissolve LMP agarose until homogenous. The solution was transferred to a pre-heated heatblock and incubated at 55 °C, when the LMP agarose in E3 had cooled to a temperature below 55 °C tricaine was added to give a final concentration of 0.02 % (v/v). Subsequent to infection, embryos were transferred to E3 (without methylene blue) containing 0.02 % (v/v) tricaine. The LMP agarose containing 0.02 % (v/v) tricaine was added to a glass dimple dish and embryos immersed into the LMP agarose using a glass Pasteur pipette. Under a dissecting microscope, a 1.1 mm glass capillary with plunger (Zeiss) was used to gently draw the embryos in LMP agarose containing 0.02 % (v/v) tricaine, head first into the capillary. The capillary was gently rotated as LMP agarose sets to keep the embryo in the centre of the capillary. Prior to imaging, once situated inside the Zeiss Z1 lightsheet microscope, the plunger is depressed to eject the embedded embryo into E3 within the imaging chamber.

2.10.12 Mounting embryos in CyGel within FEP tubing for lightsheet fluorescence microscopy

To prepare 1.1 mm FEP tubing (Adtech), straightened lengths were cut to 12 cm and sequentially sonicated for 10 min in 50 ml Falcon tubes containing sequentially 1M NaOH, 0.5 M NaOH, dH_2O, 70 % EtOH, dH_2O and stored in dH_2O.

E3 was heated and LMP agarose was added to prepare 2 % (w/v) LMP agarose in E3, agarose was cooled to 55 °C and tricaine was added to give a final concentration of 0.02 % (v/v) tricaine. The mixture was poured into a 35 mm petridish to a depth of 2 mm and left to set.

To prepare thermoflippable CyGel for microscopy, CygelSustain concentrate was incubated on ice and 180 µl transferred to a 500 µl reaction tube, 10 µl of 20 x E3 (double concentration of that used in Method 2.10.3.1) and 10 µl of stock tricaine solution added. Reagents were mixed by vortexing and incubated on ice, the glass dimple dish used for mounting embryos was also incubated on ice.

Subsequent to infection, embryos were transferred to E3 (without methylene blue) containing 0.02 % (v/v) tricaine. The mounting medium was transferred to the glass dimple dish and embryos were were transferred using a glass Pasteur pipette. A syringe with a blunt ended canula was inserted into the end of a length of FEP tubing, the FEP tubing was pushed into the petridish containing 2 % (w/v) LMP agarose E3 containing 0.02 % (v/v) tricaine and twisted. The syringe plunger was drawn up slightly as the FEP tubing was removed from the Petri dish so that a plug remains within the FEP. On the dissecting microscope, the FEP tubing was placed into the dimple dish and the syringe was used to draw up the embryo, tail first, in the mounting medium. Once the embryo was within the FEP tubing, another 2 % (w/v) LMP agarose plug was made, as before, beneath the head of the embryo. If a second embryo was to be mounted these steps were repeated. To release the canula from the tubing, a 21 gauge hypodermic needle was used to pierce holes just above the uppermost LMP agarose plug. Additional holes were made through the FEP tubing next to the agarose plugs, to allow diffusion of O_2 and tricaine from the imaging chamber. FEP tubes containing embryos were maintained in an upright position as the temperature of CyGel Sustain increases, it will form a micellar gel matrix at 21 °C.

2.10.13 Live imaging of embryos by lightsheet fluorescence microscopy

Prior to imaging the infection chamber was fitted to the Zeiss Z1 lightsheet fluorescence microscope. The imaging chamber was filled with 70 % (v/v) EtOH for at least 10 min then rinsed with dH_2O. The imaging chamber was then filled with E3 (without methylene blue) containing 0.02 % (v/v) tricaine which had been pre-warmed to 28.3 °C and this temperature was maintained by the peltier unit within the microscope.

The sample was placed in the sample holder and into the 360 ° imaging stage. The Zeiss Z1 microscope uses two light paths, either side of the sample, to illuminate a plane of the sample. The microscope has six laser lines for excitation, 405 nm, 445 nm, 488 nm, 561 nm, and 638 nm, a 20 x water dipping objective is perpendicular to the illumination light path for detection of fluorescent signal, which is transmitted to two sCMOS cameras.The filter set for simultaneous exicitation and detection using multiple laser lines is listed in Table 2.4. Routinely lasers 488 nm and 561 nm were used for excitation of GFP and mCherry respectively. Dual-sided imaging (using both left and right sided illumination) with pivot scan, was always performed. To enable long term imaging, low levels (0.8 – 2.0 %) of laser power were used. Acquisition is controlled by Zen Black software (Zeiss) and allows multiview acquisition – which can be performed at any angle, time courses and z-stacks to be imaged.

2.10.14 Reconstruction and analysis of lightsheet fluorescence microscopy data

Zen Black (Zeiss) was used to process data acquired by the Zeiss Z1 lightsheet fluorescence microscope. For image processing black was set at 200 grey levels to elimate background signal. The software was used for cropping and evaluating data and reconstructing 4D data into two dimensional images and videos.

ArivisVision 4D was used to reconstruct data in 3D and visualise the spatial location of *S. aureus* within embryos. These reconstructions could be followed through time and the software was also used to perform colocalisation analysis.

Filter set no	Beam splitter (wavelength nm)	Filter 1 (wavelength nm)	Filter 2 (wavelength nm)
1	SBS LP 490	SP 490	LP 505
2	SBS LP 510	BP 460-500	BP 525-565
3	SBS LP 560	SP 550	LP 585
4	SBS LP 580	BP 525-565	LP 585
5	SBS LP 640	BP 575-615	LP 660

Table 2.4 Filter set for Zeiss Z1

Filter sets in use in Zeiss Z1 short pass (SP), long pass (LP) and band pass (BP).

3 Developing a method for light sheet fluorescence microscopy of zebrafish embryos infected with *S. aureus*

3.1 *Introduction*

3.1.1 A systemic model for *S. aureus* infection in zebrafish embryos

Zebrafish have long been used for embryological and developmental studies, their use as a model organism provides an extensively characterised system which has more recently been exploited for vertebrate models of infection. The high capability of the zebrafish to reproduce and their small size (both as adults and larvae) make them suitable for high-throughput screening and the transparent nature of the fish makes them an excellent candidate for interrogating host-pathogen interactions by microscopy (Meijer and Spaink, 2011).

Zebrafish have both adaptive immunity and well developed innate immunity (Kasahara et al., 2004), with many toll-like receptors (TLRs). These have high homology to TLRs in other vertebrates including humans (Meijer et al., 2004), importantly TLR2 which binds peptidoglycan and lipoproteins of *S. aureus* cell wall (Dziarski and Gupta, 2005; Skerrett et al., 2017; Wolf and Underhill, 2018), which are upregulated during viral and bacterial infection (Meijer et al., 2004).

Additionally zebrafish possess other professional immune cells and signalling molecules; functional macrophages are present from 25 hours post fertilisation onwards, immature neutrophils from 18 hpf and differentiated neutrophils are present from 30 hpf (Lieschke et al., 2001). Many key cytokine subfamilies are conserved between zebrafish and mammals, however there has been diversification and expansion of some cytokine gene families in zebrafish, including a second lineage of interleukin (IL)-8 which is a crucial chemoattractant of neutrophils (Kolaczkowska and Kubes, 2013; van der Vaart et al., 2012).

By infecting zebrafish embryos with *S. aureus*, a non-native pathogen, the interaction between microbe and innate immunity in its entirety can be interrogated. Initial development of zebrafish adaptive immunity does not occur until 4 dpf and is not fully present until 4 weeks post fertilisation (Meijer and Spaink, 2011). The route of infection of bacteria is key to whether the host can withstand the infectious dose, for *S. aureus* the duct of Cuvier (circulation valley) is used as the site of injection, as if injected into the yolk sac the bacteria replicate quickly and overwhelm the host (Prajsnar et al., 2008). However yolk sac infection models have been used with other infections such as *Mycobacterium marinum*, and lends itself to automation, increasing throughput (Meijer and Spaink, 2011). By inoculating the bloodstream of the embryos, via the circulation valley, this model simulates how *S. aureus* enters mammalian blood causing bacteraemia. There are an increasing number of studies suggesting that phagocytes play a crucial role in the dissemination of *S. aureus*,

acting as a Trojan horse for the bacteria, which has evolved many mechanisms to evade host immune responses and is able to expand within the phagocyte (McVicker et al., 2014; Pollitt et al., 2018; Prajsnar et al., 2012; Thwaites and Gant, 2011) .

The ability of zebrafish host defences to withstand an infectious dose and in some cases control proliferation or clear infection when injected in the circulation valley with non-native pathogen allows the investigation of which components make bacteria pathogenic to an unknown host, as it has been demonstrated that bacteria with mutations in key virulence determinants are attenuated in this infection model (Prajsnar et al., 2008)

3.1.2 Zebrafish 'tool-kit'

In my study the interaction of bacteria and immune cells within the host is to be investigated. Both macrophages and neutrophils are able to phagocytose bacteria from the bloodstream and previous work has indicated that all bacteria in the circulation have been phagocytosed by 3 hpi (Prajsnar et al., 2012). The advent of transgenic zebrafish lines, with fluorescent proteins expressed under macrophage and neutrophil specific promoters, delivers the basis for intravital imaging.

The neutrophil specific myeloperoxidase (*mpx*) promoter drives GFP expression in the transgenic line *Tg*(*mpx*:GFP)^{i114} (Renshaw et al., 2006) which possesses fluorescent green neutrophils. Another transgenic reporter line *Tg(lyzC:nfsb.*mCherry*)*^{SH260},which uses the neutrophil specific lysozyme C gene with a bacterial nitroreductase (*nfsb*) fusion, drives mCherry expression (Elks et al., 2011; Prajsnar et al., 2012) . This produces mCherry labelled neutrophils, which can be ablated by incubation with the drug metronidazole (usually harmless) due to the neutrophil specific nitroreductase, which produces a cytotoxic metabolite of metronidazole (Curado et al., 2008).

More recently a macrophage specific promoter, *mpeg1* (expressed from 20 hpf onwards) was identified to create the transgenic macrophage reporter line *Tg*(*mpeg.mCherry* x CAAX)^{SH378} (Ellett et al., 2011), with red fluorescent macrophages. There is no co-expression of *mpx* and *mpeg1* so neutrophils and macrophages are labelled independently of each other in these two lines (Ellett et al., 2011). The gene *c-fms*, encoding a receptor for macrophage colony stimulating factor (M-CSF) (Ward and Lieschke) has been used to drive expression of GFP to provide an alternative macrophage specific fluorescence reporter (Dee et al., 2016).

As a model organism, the genome of the zebrafish has been well characterised and before the tools existed for efficient targeted mutagenesis such as CRISPR/cas systems, morpholino (MO) antisense oligomers were used as a method of gene knockdown in the zebrafish system (as well as other model organisms such as *Xenopus* and chick) and these remain effective tools for gene knockdown of essential genes in the female germ line (Stainier et al., 2017). Injected at the single cell stage, the single stranded oligomers bind complimentary RNA targets and disrupt gene function (rather than

the genetic sequence itself)(Timme-Laragy et al., 2012); morphant embryos can be used to help characterise the role of aspects of the host immune response when infected with *S. aureus* (Prajsnar et al., 2012).

3.1.3 Light sheet fluorescence microscopy

Prior to the invention of light sheet fluorescence microscopy (LSFM), imaging relatively large biological samples stained with, or expressing fluorophores was reliant on confocal and two-photon microscopy, both of which have a reasonable resolution and penetration of the sample. A confocal microscope discriminates against out-of-focus light by pinholing the detecting objective, increasing resolution in comparison with wide-field fluorescence microscopy. A limitation of this microscopic technique is that the increase in resolution gained by pinholing comes at the cost of decreased signal intensity, so exposure times have to be increased and are relatively long (Reynaud et al., 2008a). In addition to long exposure times, whilst very little out-of-focus light from outside of the focal plane is detected, the entire specimen is illuminated regardless of the depth of image that is acquired, so the damaging effects of the lasers (photo-toxicity and photo-bleaching) will affect the whole sample.

Further development of this technique by Stelzer and Lindek involved placing the detection objective at an angle (θ) to the illumination objective, reducing the amount of out-of-focus light to be discriminated against by the detection objective, and has been termed theta confocal microscopy. By reducing the amount of out-of-focus light, less light is needed for excitation of the fluorophores, reducing photo-toxicity and photo-bleaching. Like other confocal techniques this still relies on scanning across the region of interest with a laser and building up a stack of two-dimensional images (optical sectioning).

It was the further research into the theta principle, by Huisken and co-workers, using illumination orthogonal to detection, termed 'Selective planar illumination microscopy' (SPIM) that became the basis for LSFM (Huisken et al., 2004). The principle of SPIM is that focusing the excitation light using a cylindrical lens, produces a sheet of light that only illuminates the sample at the focal point; there is no out-of-focus light that reaches the perpendicular detection objective. By only exciting the plane being imaged, the amount of fluorophore excitations the entire sample receives as a 3D image is acquired is greatly reduced, as lasers are not bleaching fluorophores that are not simultaneously being imaged. As well as reducing photo-bleaching this reduces photo-toxicity and is therefore gentler on a living sample, both factors allow for repeated imaging over time. This improvement in photo-toxicity and photo-bleaching is essentially ratiometric to the size of the sample, the more z-slices acquired, the better the improvement in comparison to confocal microscopes for the same sample (Reynaud et al., 2008a). Resolution of SPIM is, like other fluorescent microscopic techniques (excluding super-resolution microscopy), determined by the

numerical aperture (NA) of the detection objective and the wavelength of detected light: this is known as the abbe limit (Heintzmann and Ficz, 2006).

Another advantage of the Zeiss Z1 microscope, developed from research output from Huisken's lab (Huisken et al., 2004; Selchow and Huisken, 2013) is that there is 360° rotation of the sample within the imaging chamber. As axial resolution (through the Z-stack) is always the lowest in comparison with x and y (acquired in the 2D image)(Reynaud et al., 2008b) the ability to rotate the sample and image the same area in another orientation, without worrying about photo-bleaching or photo-toxic effects, is incredibly powerful. The SPIM community have developed tools for image registration, fusing multiple angles to improve the resolution of the 3D reconstruction of the sample, being able to rotate a sample and image from another angle is especially useful in specimens which produce a high scatter (Pitrone et al., 2013).

The major caveat to this technique is the volume of data generated, orders of magnitude bigger than data generated by confocal microscopy. Typical experiments, imaging multiple fluorophores over time, generate files that are terabytes in size, which are streamed from the microscope to a computer during acquisition. The size of these files far exceeds available computer memory, because of this, it is challenging just to look at the data, before processing it (Reynaud et al., 2014a). Files of this size need to be stored on a redundant array of independent disks (RAID) and ideally network cables between acquisition computers, storage, and processing computers should have 10 Gbit capacity to enable the transfer of such large files. Processing this data can not be done on the computers available to most biologists - the best way to handle such data sets is by using parallel computing with powerful cluster computers. Some researchers minimise the size of the data set by deleting empty slices instantly and compressing black pixels (Eliceiri et al., 2012). More drastically, in some laboratories with the capacity to perform in-line processing, raw data is not stored at all, a risky strategy when using novel in-house software in a nascent technology, but it is often cheaper to repeat the experiment than store the bulky raw files. However, this is an ethically a grey area, as many journals and or funding bodies require that data is stored for a certain period of time; in Germany it is a legal requirement that raw data is stored for 10 years (Reynaud et al., 2014a). If requested by peers, it is unlikely that this processed data could be scrutinised or reconstructed by other techniques.

With many of the SPIM community using self-built microscopes and software, nearly all have individual file formats, and processing pipeline. There is a strong open source community for SPIM (Pitrone et al., 2013), sharing tools for reconstruction and analysis, however these are the products of applied computer science research, to use these tools biologists must learn programming languages (Reynaud et al., 2014a). Some plugins have been developed for FIJI, for the fusion of mutltiview images (Amat et al., 2014; Preibisch et al., 2010) and reconstruction of 3D stacks

(Schindelin et al., 2012). Whilst there are now commercially available light sheet microscopes, producing file formats that can be more readily shared between collaborators and the research community, there is a gap in standardised, commercial software that can handle the large files produced by light sheet microscopy. Perhaps the breadth of applications means that there is no 'one-size fits all' method for reconstruction and analysis (Reynaud et al., 2014b).

This microscopic technique was developed in an institute alongside developmental biologists (Huisken et al., 2004), as a result of this the Zeiss Z1 microscope has been optimised for imaging Medake (*Oryzias latipes*) and zebrafish, well used model organisms for developmental biology.

The sample is mounted and suspended in a chamber of medium, in the case of zebrafish this is E3 which is a very low concentration salt solution, meant to mimic the river-water native to zebrafish. The chamber also houses a Peltier unit, which allows incubation of the living sample at the correct temperature for development (Huisken et al., 2004; Selchow and Huisken, 2013), these conditions theoretically provide a physiologically relevant environment to follow the dynamics of *S. aureus* infection of a zebrafish host and should be representative of the established infection model.

3.2 *Chapter aims*

- To develop a mounting method and acquisition parameters that allow for long term imaging of zebrafish embryos infected with *S. aureus,* by a light sheet fluorescence microscope.
- To identify a means of reconstruction and analysis of the large data generated by this microscopic technique that provides spatial and temporal detail.

3.3 *Results*

3.3.1 Existing systemic infection model

The unique, systemic zebrafish model for systemic *S. aureus* infection, as described by Prajsnar et al., 2008 has been developed in Sheffield and has been previously used to identify bacterial components required for successful infection of the host. An *S. aureus* inoculum is administered via the circulation valley to embryos 30 hpf (Figure 3.1); survival of infected embryos is monitored up until 92 hpf.

Survival of infected embryos is dose dependent, Figure 3.2 shows that percentage survival of embryos decreases with increased dose of *S. aureus*. Infection with doses of 1500, 3855 and 8275 CFU resulting in 53 %, 23 % and 6 % survival at 92 hpi, respectively.

3.1 *Constitutive fluorescent strains*

Imaging *S. aureus* within the host requires brightly labelled fluorescent bacteria as dynamic imaging relies upon quick acquisition with low exposure times. Previously strains with GFP or mCherry encoded on a plasmid have been used (Serba, 2015) but more recently strains have been created with fluorescence encoded on the chromosome (Pollitt et al., 2018). This is better suited to long term imaging experiments as there is no risk that without antibiotic selection the bacteria will lose the plasmid encoding the fluorophore, so all bacteria within the host will be visualised at any stage during infection within the host.

The stable fusion strains have single copy genes encoding mCherry or GFP on the chromosome, integrated at the lipase locus using the backbone of pGM074 (Bottomley et al., 2014) a derivative of pKasBar (Wacnik, K., 2016) with either mCherry or GFP under the control of the pMal1 promoter (Nieto and Espinosa, 2003), from the plasmid pMV158-mCherry (S. Mesnage unpublished) which drives constitutive expression in *S. aureus*.

The fusion strains were constructed in four different strain backgrounds, with isogenic GFP and mCherry made in all backgrounds (Pollitt et al., 2018). The GFP strains have Kan as a selective marker and Tet was used as the marker for mCherry strains; however when recovered from mouse organs the mCherry strains showed affected tetracycline resistance, so were supplemented with an erythromycin resistance encoding cassette from strain SJF3673 (*lysA*::ery, lysA+) (Pollitt et al., 2018)

To characterise the strain, growth curves were carried out with SH1000-GFP strain in comparison to the parent strain, SH1000 WT, shown in Figure 3.3. SH1000-GFP follows the growth pattern of SH1000-WT.

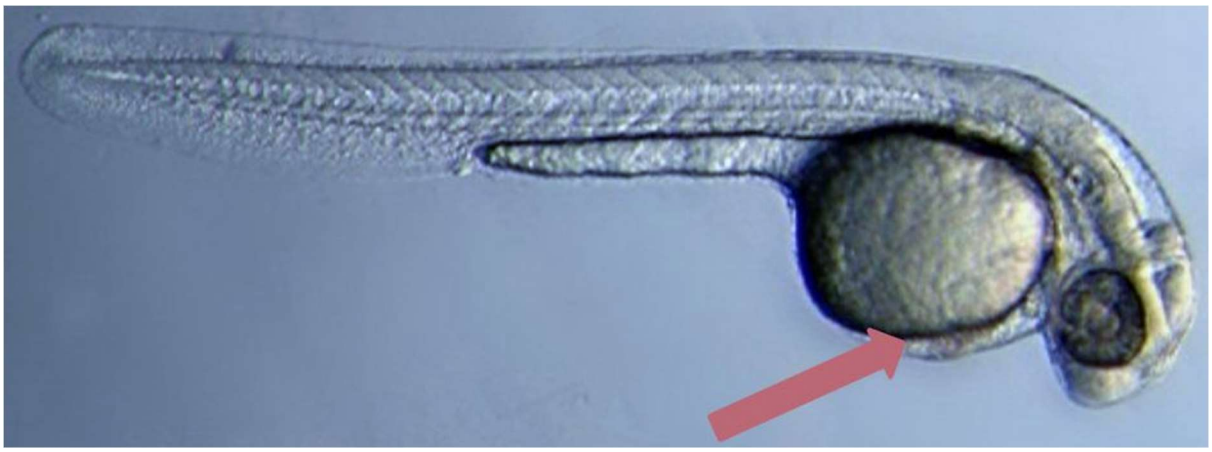

Figure 3.1 Zebrafish embryo 30 hpf

Micrograph of embryo acquired under dissecting mictoscope at 30 hpf. The site of infection, duct of Cuvier (or circulation valley) is indicated by red arrow.

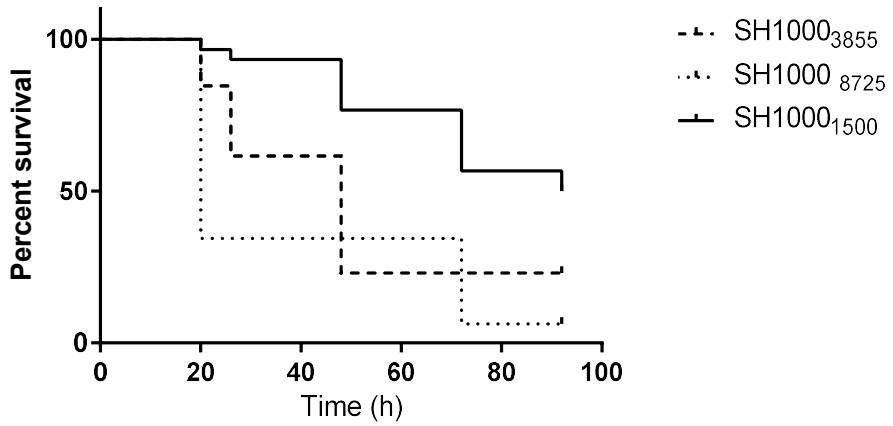

Figure 3.2 Survival of LWT embryos infected with SH1000 *S. aureus.*

LWT embryos were injected with different doses of SH1000: 1500CFU (n=30), 3855 CFU (n=31) & 8725 CFU (n=32). Survival at 92h was 50%, 23% & 6% respectively, percentage survival between groups are significantly different to each other, $P<0.0001$.

It is important that these fluorescent strains do not have altered pathogenicity when compared to their WT parents, so that the dynamics of infection when imaged are the same as previously published survival experiments. LWT embryos were infected via the circulation valley, 30 hpf with strains SH1000-GFP (SJF4618), SH1000-mCherry (SJF4631) and SH1000 WT (SJF861) and survival monitored for four days post infection. Results of this experiment (Figure 3.4) show no significant difference (P=0.658) in the survival rate of either SH1000-GFP or SH1000-mCherry in comparison to WT. With survival between 45-60 % for a dose of ~1500 CFU the infection dynamics are comparable to those previously observed (Prajsnar et al., 2008) therefore the addition of the fluorescence reporter does not affect pathogenicity of the bacteria in this systemic infection model, making them excellent candidates for long-term imaging of infection progression.

3.2 *Bacterial growth kinetics of SH1000-mCherry in vivo*

In order to confirm that the chromosomally encoded constitutive reporter strains replicate as per their WT parents *in vivo*, analysis of bacterial growth kinetics during infection was performed. As both the mCherry and GFP fluorescent protein reporters have similar virulence to WT (Figure 3.4), only bacterial kinetics of SH1000-mCherry *in vivo* was analysed. Embryos were infected 30 hpf with SH1000-mCherry ~1500 CFU. At regular timepoints five alive embryos and all dead embryos were collected, and homogenised, serial dilutions of samples were made and plated out for CFU enumeration (Figure 3.5a). After 26 hpi there is a divergence in host outcome which is concurrent with a difference in bacterial number recovered. Embryos that succumb to infection have between ~1.3 x10^5 - ~1 x10^7 CFU, in comparison to those that control infection where ~2x 10^3 CFU (the initial inoculum) or fewer bacteria are recovered per embryo, as the host clears infection. This matches previously observed *S. aureus* infection dynamics (Prajsnar et al., 2012) where there is an apparent 'population bottleneck' and bacterial expansion only occurs from a small number of the initial inoculum. The coinciding survival rate for this experiment is 25 % (Figure 3.5b). Whilst low for the dose of 2160 CFU, a proportion of the embryos that were collected alive at early timepoints of the experiment may have survived to the end, which would have increased the overall survival. As expected, SH1000-mCherry bacterial dynamics correspond with published SH1000 dynamics; this further confirms that the constitutive reporters are suitable for long term, real-time imaging of *S. aureus* infection within an embryo.

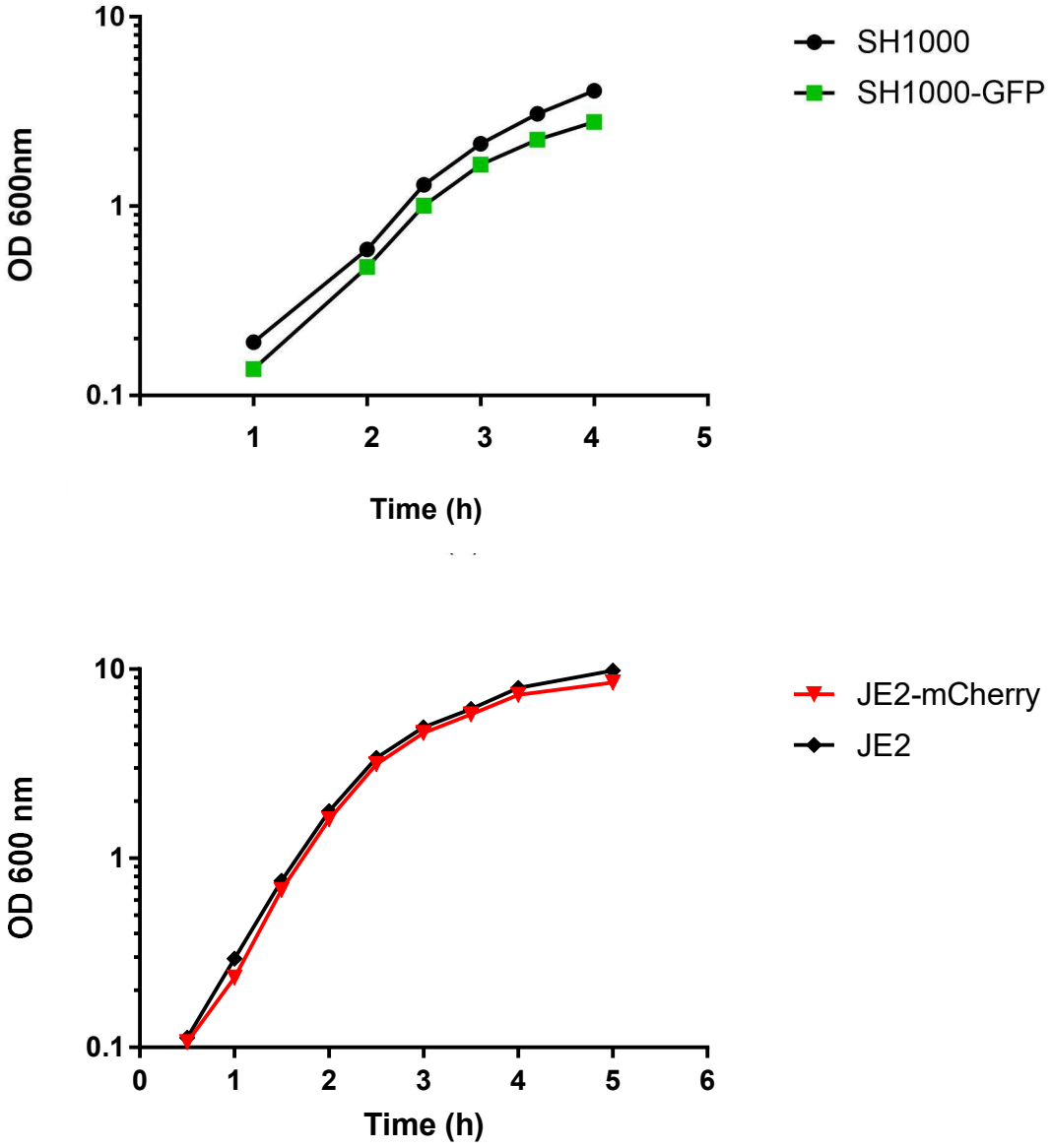

Figure 3.3 Comparison of growth of fluorescent reporter strains with WT parents

Growth of bacteria in liquid media was measured at regular timepoints by spectrophotometry (OD_{600} nm). A) growth of SH1000-GFP vs SH1000 B) growth of JE2-mCherry vs JE2

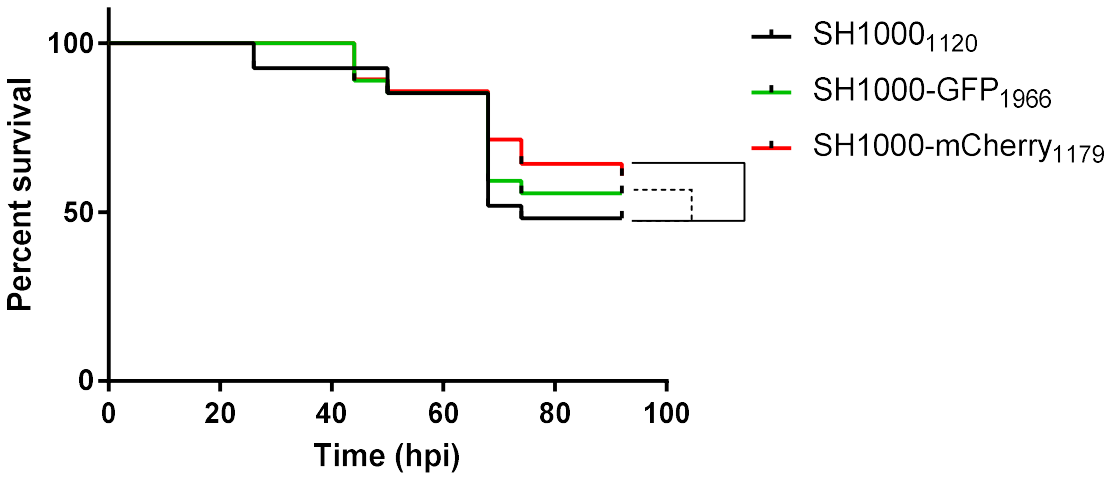

Figure 3.4 Survival of LWT embryos infected with SH1000 WT, SH1000-GFP & SH1000-mCherry

LWT embryos were infected with the chromosomally integrated, constitutively fluorescent, isogenic SH1000-GFP & SH1000-mCherry in comparison to SH1000 WT parental strain. Survival at 92 hpi was 55, 60 & 48 % respectively, there is NS difference in survival between SH1000-GFP and SH1000-mCherry and the parental strain, P = 0.627 and 0.363 respectively

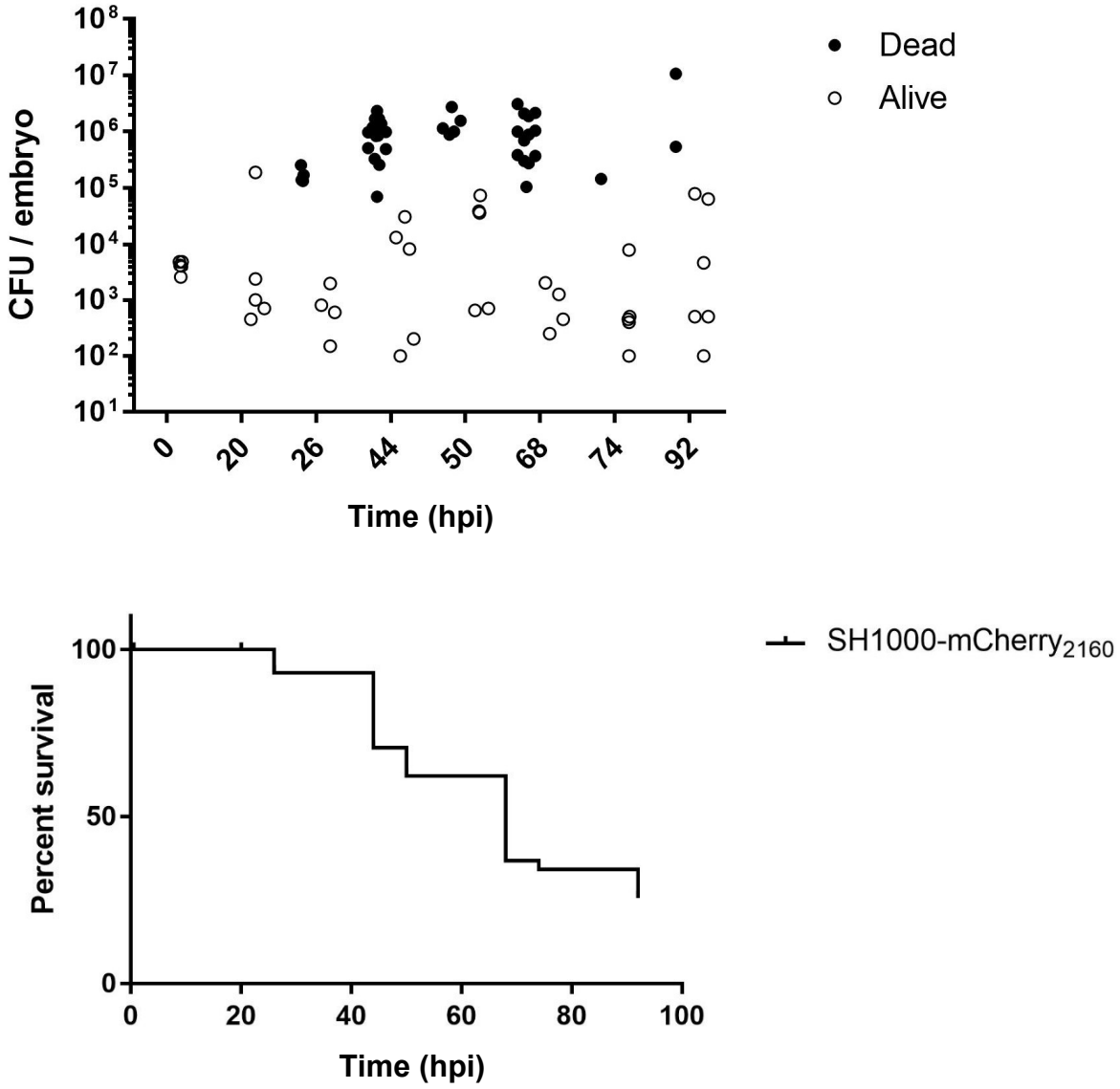

Figure 3.5 Bacterial growth kinetics of SH1000-mCherry in the LWT zebrafish host

A) Growth of *S. aureus* within LWT embryos. Zebrafish embryos were infected at 30 hpi with the strain SH1000-mCherry and at each timepoint 5 live and all dead embryos were collected and CFU per embryo was enumerated. **B)** corresponding embryo survival curve for bacterial growth kinetics.

3.3 *Standard mounting of embryos for LSFM*

The standard mounting protocol for zebrafish embryos for the Zeiss Z1 light sheet is to embed the sample in 0.8 % (w/v) LMP agarose in E3 with 0.02 % (v/v) tricaine, using a proprietary capillary with a plunger. Anesthetised embryos are transferred to 0.8 % (w/v) LMP agarose and drawn into the capillary, head first, via suction by pulling the plunger. Gentle rotation of the capillary whilst the agarose is setting keeps the embryo centred in the medium. When the agarose is set the capillary is put into the sample holder which is subsequently placed into the microscope. The plunger is depressed, ejecting the agarose into the imaging chamber containing E3.

3.4 *Acquisition zoom/multiple fields of view*

The detection lens on the Zeiss Z1 light sheet in the Wolfson Light Microscopy Facility (WLMF) is a 20 x water objective, with a numerical aperture (NA) of 1.0, which defines the limit of resolution (available 40x objective also has an NA =1.0 so would not increase resolution and only reduce the size of the ROI). Since the limit of detection of the Z1 is diffraction limited, the theoretical best resolution achieved is 254 nm, half the emission wavelength for GFP. The size of *S. aureus* is approximately 1 μm, so light sheet microscopy has the ability to resolve individual bacteria within the host, and theoretically to be able to differentiate between two bacteria. The objective has a 2x optical zoom, whilst this does not improve the resolution of the image, it designates the same number of pixels to an area half the size, giving the image more 'definition' with the ability to capture multiple ROI that can be 'stitched' together.

Figure 3.6 of a *Tg*(*lyzC.nfsb*:mCherry)^{SH260} infected with SH1000-GFP shows the same mCherry neutrophil containing GFP labelled bacteria A) imaged with 1x optical zoom, 20x objective, B) imaged with 2 x optical zoom 20 x objective (equivalent to 40 x) and C) imaged with 1 x optical zoom, 20 x objective with 2 x digital zoom after acquisition. Whilst there is more detail in the picture generated by the 20 x with 2 x zoom, there is no difference in the ability to see individual bacteria within the phagocyte. By comparison of Figure 3.6B and Figure 3.6C it is apparent that the digital zoom produces a less sharp image. Whilst reconstruction of data generated with the 2 x zoom will be higher quality, it would take twice as long to image the same volume and the data produced would double in size, making it more difficult to handle, so lower magnifications were used in this study.

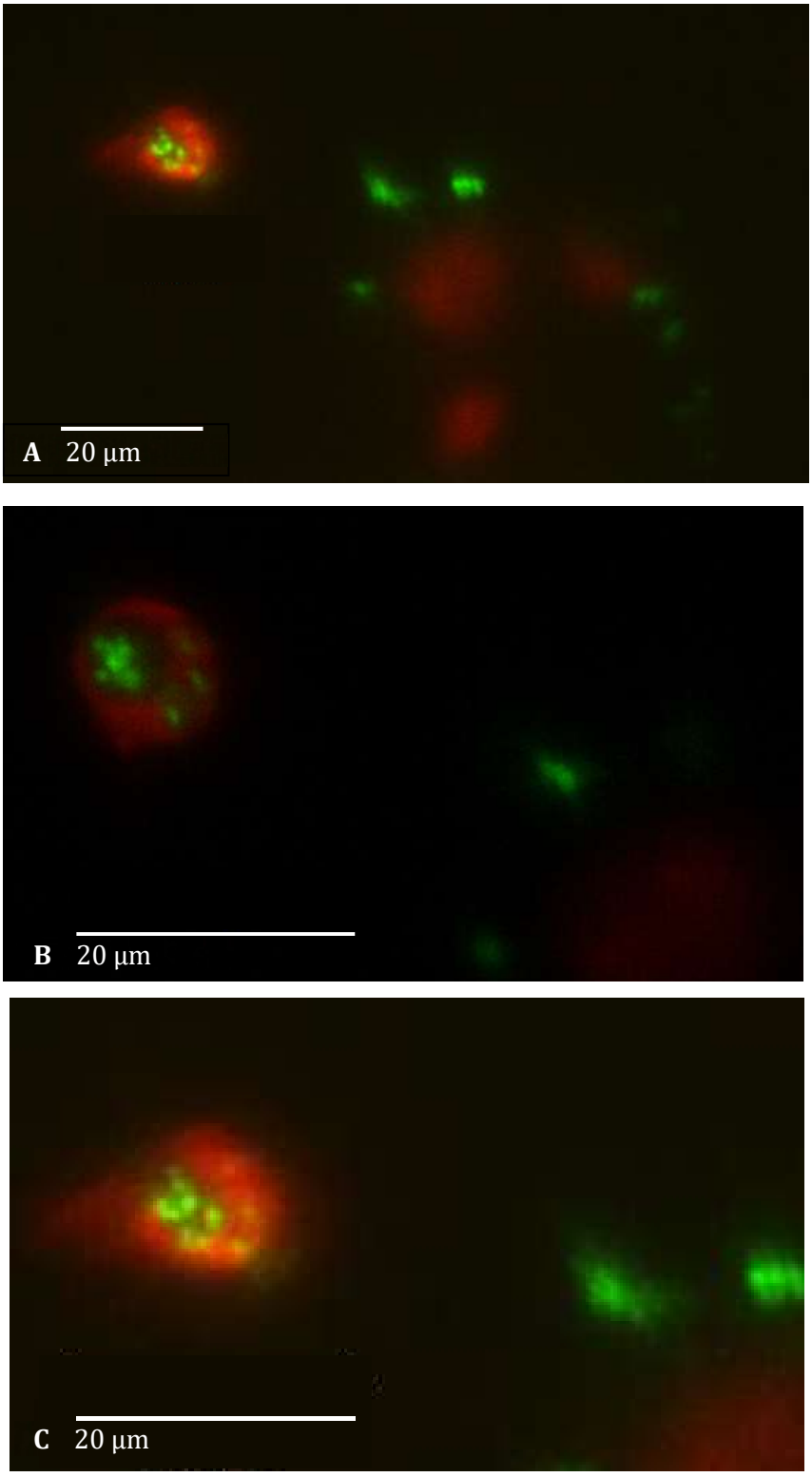

Figure 3.6 Comparison of 20 x magnification with 40 x magnification

Single slice, 1 µm of *Tg*(*lyz.nfsb*:mCherry)^{SH260} embryos with mCherry neutrophils, infected with SH1000-GFP, the same neutrophil was imaged consecutively with different magnifications acquired with **A)** 20 x (20 x objective, 1 x optical zoom) **B)** 40 x (20 x objective, 2 x optical zoom) **C)** 20 x (20 x objective, 2 x digital zoom post acquisition)

3.5 *Simultaneous excitation and detection of fluorophores*

Whilst trying to capture dynamic processes within a microscope, the speed of acquisition is paramount. As the model for *S. aureus* infection is systemic, the circulation valley is the ROI, and by its very nature there is movement of both host cells and bacteria by the circulation of blood, so optimising acquisition time is important. GFP & mCherry are the two fluorophores most widely used in the creation transgenic zebrafish lines with fluorescently labelled host cells and are also the fluorophores that have had the most success with their use in *S. aureus* strains. These fluorophores have a slight overlap in their emission and excitation spectra, shown in Figure 3.7, 575nm is the wavelength at which relative intensity switches over, from stronger GFP emission to mCherry. The quickest way to acquire data is by exciting and detecting both fluorophores at the same time, but this leaves potential for bleed-through (when the emission of one fluorophore is detected in the channel for the second fluorophore). Filter blocks enable this simultaneous excitation and detection of both fluorophores without overlap between channels. Filter blocks within the microscope combine three types of filter: excitation (to filter the light from the laser to the sample), barrier (to filter light from the sample to the detector) and dichroic beamsplitters (these direct the selected excitation wavelengths from the objective to the sample, wavelengths shorter than the designated wavelength reach the sample, longer wavelengths reach the barrier filter). Excitation filters are either short pass (SP) letting wavelengths lower than the 'cut-off' pass and blocking longer wavelengths, long pass (LP) blocking lower wavelengths and letting higher wavelengths pass or band pass (BP) which let a range of wavelengths through, blocking light shorter than the lower cut off and higher than the higher cut off.

3.5.1 Single track imaging

By using a single 'track' in Zen to image, both fluorophores are excited and detected simultaneously, the beam splitter and filter used to do this is shown in

Table 3.1. Whilst this filter set should allow for simultaneous imaging of GFP and mCherry, often there is bleed through between channels when setting up image acquisition; this is potentially due to a software error, as it does not always occur when repeating the same experiment. To prevent the occurrence of bleedthrough the same filter is used but with the two laser lines on separate imaging 'tracks'. Unfortunately, this increases imaging time, but the lasers can be switched with each frame in the stack, minimising physiological movement of fluorophores whilst capturing the stack.

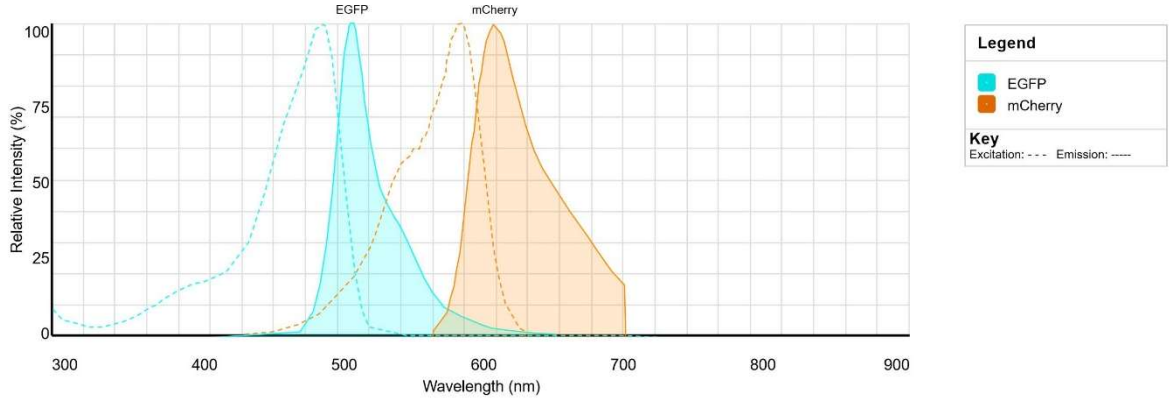

Figure 3.7 Excitation and Emission spectra for EGFP and mCherry

Excitation and emission spectra for EGFP and mCherry (ThermoFisher Fluorescence SpectraViewer), overlap in emission spectra is at 565 - 630 nm. Higher relative intensity at specified wavelengths switches from EGFP to mCherry at 575 nm, with 10 % relative intensity.

	Beam splitter	1st filter	2nd filter
Filter initially used	SBS LP560	SP 550 nm	LP 580 nm
New filter	SBS LP580	BP 525-565 nm	LP 585 nm

Table 3.1 Filter sets used for imaging GFP and mCherry

Filter sets with short pass (SP), long pass (LP) and band pass (BP), both should discriminate between emission in GFP and mCherry channels.

3.5.2 Single track imaging with a new filter set

During this study a new filter set for the Zeiss Z1 light sheet was acquired that includes a filter which has a dichromatic beamsplitter at 580 nm; this prevents the bleed-through previously experienced when trying to image GFP & mCherry on the same track, speeding up image acquisition. By simultaneously exciting and imaging both fluorophores, there is a reduction in temporal difference of sample physiology, increasing the precision of the localisation of fluorophores relative to each other. Additional ROI can be acquired for the same timepoint.

This filter provides the opportunity to image an additional far red fluorophore whilst only using two imaging 'tracks' without switching lasers as the excitation and emission spectra of GFP and far red does not have any overlap.

3.6 *Frequency of acquisition*

LSFM has been developed with the purpose of long-term imaging of live samples, for up to days at a time; it is possible to obtain 500-700 slices, with two fluorescence channels in ~2 minutes. Initially whilst trying to image the interaction of *S. aureus* within the host, capturing a timepoint of the ROI as fast as the microscope will allow, embryos were dying within the microscope. Laser levels were reduced from ~3-4 % to ~1-2 % laser power for 488 nm laser (excitation of GFP) and from ~6 % to ~2-3 % laser power for 561 nm laser (excitation of mCherry) to reduce the phototoxicity of the sample; however embryos with a low bacterial burden were still dying during imaging.

When imaging was reduced from as frequently as possible (~2 minutes) to every 5 minutes embryos still didn't survive overnight imaging. The incubation time between timepoints was increased to 20 minutes, which is less than the amount of time it takes *S. aureus* to replicate. After this reduction in imaging frequency embryos were able to withstand overnight imaging.

3.7 *Infectious dose that goes on to form a lesion*

As only 50 % of infected embryos succumb to infection when injected with a dose of 1500 CFU, the infectious dose was increased to 2000 CFU to increase the probability of the embryo selected for long-term imaging to succumb to infection. Whilst higher doses than this will increase the mortality of the embryos, Prajsnar and co-workers demonstrated that these higher doses do not result in lesion formation, but overwhelm the host immune response, resulting in embryos with 'cloudy' circulation valleys (Prajsnar et al., 2012). Furthermore, when the infectious dose is increased there is a loss of clonality, suggesting that bacteria do not pass through a 'immune bottleneck' but expand within the host with a lower proportion being phagocytosed.

3.8 *Acquisition field/ rotation to improve imaging quality*

Initial samples were imaged laterally, exemplified in Figure 3.8A, with autofluorescence from the yolk sac providing a spatial point of reference within the embryo; this lateral angle is the same orientation used for imaging on the Perkin Elmer spinning disk. Imaging the sample in this orientation is usually 600-700 slices 1µm in thickness. The deeper into the z-stack the more scatter there is of signal from the sample to the perpendicular detection camera, decreasing the focus of the light, producing a more blurred image. In addition to this, a large proportion of the ROI is taken up by space occupied by the yolk. By rotating the sample and imaging the embryo ventrally as shown in Figure 3.8C, with the first slices above the skin over the circulation valley, directly over the yolk, the number of slices in the stack is reduced. Therefore, shortening the light path and reducing the amount of tissue between slice and detection camera consequently improving the focus of the light detected from the sample. Not only is there improved focus, but the reduced thickness of the stack to ~200 slices 1µm in thickness reduces the amount of data produced making processing easier. This orientation also increases the amount of 'useful' data in each slice compared with the slices from the lateral plane, where the yolk occupies a large area of each slice. By imaging in this orientation there is a reduction in exposure time of the lasers to sample, concurrently further reducing photo-toxicity to the sample.

3.9 *Mounting multiple embyros in 0.8 % (w/v) LMP agarose*

As only 50 % of embryos infected with 1500 CFU succumb to infection, mounting multiple embryos within the lightsheet, during the same experiment, increases the likelihood of successfully imaging infection progression. Embryos do not need to be mounted in the same orientation, as the microscope has 360° rotation; however the two embryos need to be mounted within ~5 mm of each other to be able to image both samples. Whilst it is possible to mount two embryos with the 0.8 % (w/v) agarose, multiple attempts at long term imaging, resulted in loss of the lower embryo into the infection chamber, as the agarose in between the two embryos breaks, possibly due to the rotation and movement in Y axis. To image multiple embryos during the same experiment an alternative means of mounting was required.

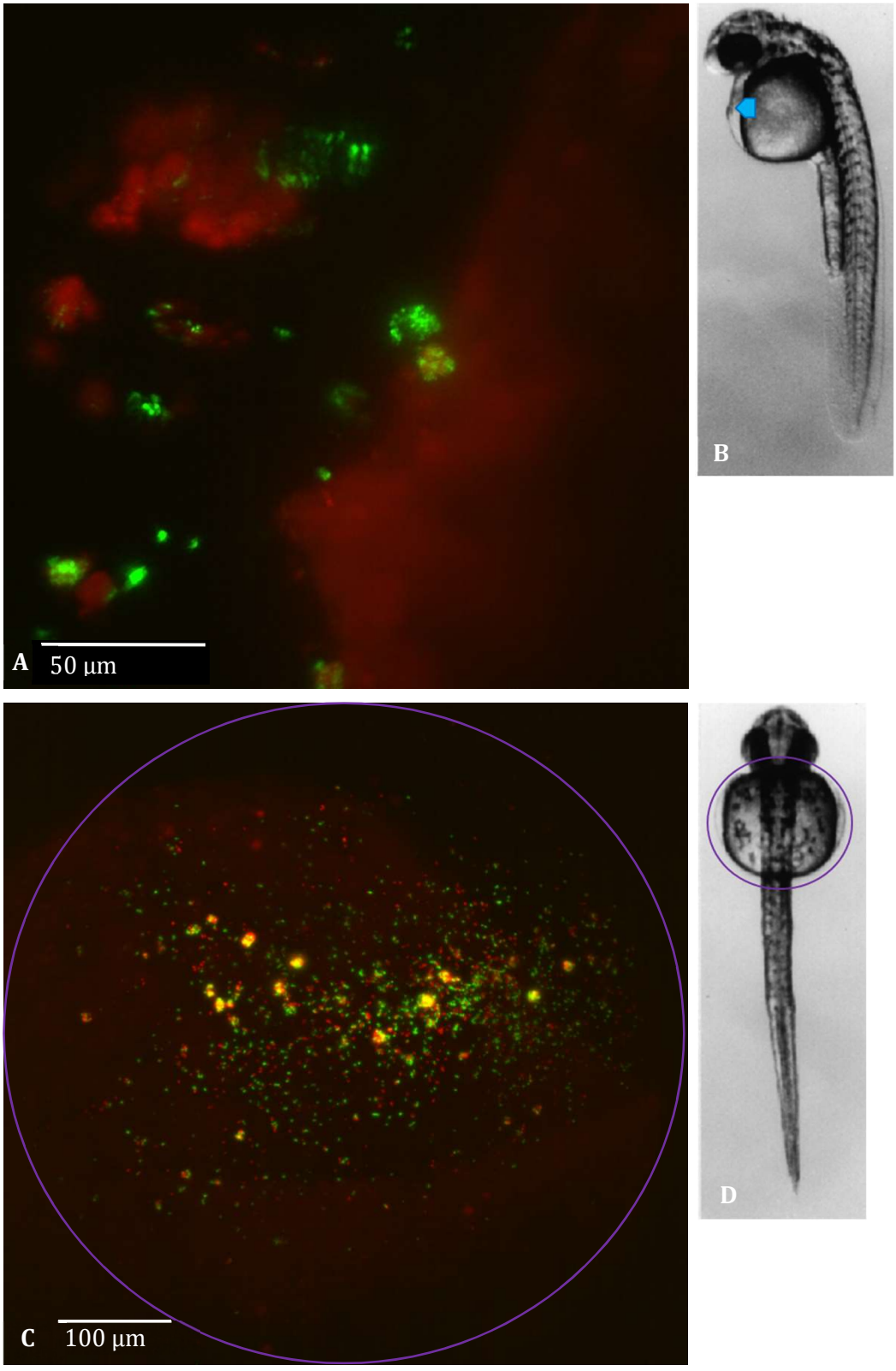

Figure 3.8 Imaging orientation of embryos

Orientation of embryos during image acquisition **A)** MaxIP of *Tg*(*lyz.nsfb*:mCherry)^{SH260} embryo infected with SH1000-GFP imaged laterally **B)** lateral orientation of an embryo 30 hpf, circulation valley indicated by blue arrow **C)** MaxIP of LWT infected with SH1000-GFP and SH1000-mCherry imaged ventrally **D)** ventral orientation of embryo 30 hpf, circulation valley circled in purpe. **B)** and **D)** adapted from (Nusslein-Volhard and Dahm, 2002).

3.10 *FEP tubing*

Whilst the 0.8 % (w/v) LMP agarose mounting method widely adopted for use with the Zeiss Z1 light sheet microscope provides a medium which gives both high imaging quality and good immobilisation of the sample, this concentration of agarose doe not allow for normal development of the zebrafish embryos. Ideally there should be normal development of the embryos during imaging, enabling infection progression comparable to the existing model of infection. A mounting method that enables adequate immobilisation but is simultaneously gentle on the embryo and does not constrain the sample and slow development is needed.

A method using fluorinated ethylene propylene (FEP) tubing to mount embryos has been published (Kaufmann et al., 2012). FEP tubing is most commonly used in HPLC machines, but it is well suited as a vessel for mounting zebrafish as it has a refractive index that is the same as water (1.338) so should not disrupt the light path from the sample to the detection camera.

3.10.1 Tubing diameter

FEP tubing is available in many sizes so two sizes of tubing with the same outer diameter of two sizes of the glass capillaries used for embedding in 0.8 % (w/v) agarose were tested (as these will fit perfectly into the sample holder without the need for adaptation), with an outer diameters (OD) of 1.1 mm and 1.9 mm. Both sizes of tubing had a wall thickness of 0.3 mm, as opposed to 0.5 mm in published methods, to further reduce any scatter of light from the sample. These were tested with E3 0.1 % (w/v) LMP agarose, tricaine 0.02 % (w/v), with a plug of 2 % (w/v) LMP agarose to contain the medium, as per Weber and collegues (Weber et al., 2014). The agarose allows for diffusion of oxygen and tricaine from media in the imaging chamber.

FEP tubing is prepped by sonicating for 10 minutes sequentially in 1M NaOH, 0.5NaOH, ddH_2O, 70 % (v/v) EtOH, ddH_2O.

12 cm of FEP tubing is pushed onto the end of a pipette tip and 3 % (w/v) methylcellulose in E3 is drawn through and rinsed with ddH_2O, this is to prevent the young embryos sticking to the walls of the FEP tubing. Anesthetised embryos in 0.1 % (w/v) LMP agarose are drawn into the tubing, whilst maintaining suction, the end of the FEP tube is pushed into a petri dish with a 2 mm layer of 2 % (w/v) LMP agarose and twisted to form a plug at the end of tube, depicted in Figure 3.9A. To test the viability of this method, mounted embryos are incubated in 40 ml E3 with 0.02 % (v/v) tricaine in a 50 ml centrifuge tube for 24 h. Mounted embryos were imaged immediately after mounting and after 24 h incubation using Apex Minigrab on the Leica dissecting microscope, using a graticule for scale as shown in Figure 3.10 and Figure 3.11. Embryos moved position during incubation in most of the FEP tubes, embryos mounted in the wider (1.9 mm OD) tubing moved most in 3 directions, and the embryos moved more across the width of the space they were

mounted in whereas embryos mounted in 1.1 mm inner diameter tubing moved mainly downwards towards the plug at the bottom of the tube.

3.10.2 Multilayer mounting of embryos in FEP tubing

Embryos mounted in a medium within FEP tubing have a structured casing, enabling the concurrent mounting of two embryos, (depicted in Figure 3.9B) without the loss of an embryo into the chamber as occurs when multiple embryos are mounted within 0.8% (w/v) agarose. This method is based upon work published by Kaufmann and collegues, increasing the number of embryos that can be imaged during an experiment (Kaufmann et al., 2012).

3.10.3 Diffusion holes

Uninfected, anesthetised embryos mounted in FEP tubing were dying whilst incubated. The published methods (Kaufmann et al., 2012; Weber et al., 2014) used as the basis in this study, claim to have normal development: it follows that the embryos should not die whilst mounted. There is reportedly sufficient diffusion of oxygen and tricaine through the agarose plugs from the surrounding E3; however to rule low concentrations of these out, four holes in a 'sieve like' manner were added to the FEP tubing, using a 21G hypodermic needle, in the area of the middle and top 2 % (w/v) agarose plugs (depicted in Figure 3.9C, D & E) in order to increase diffusion into the contained media.

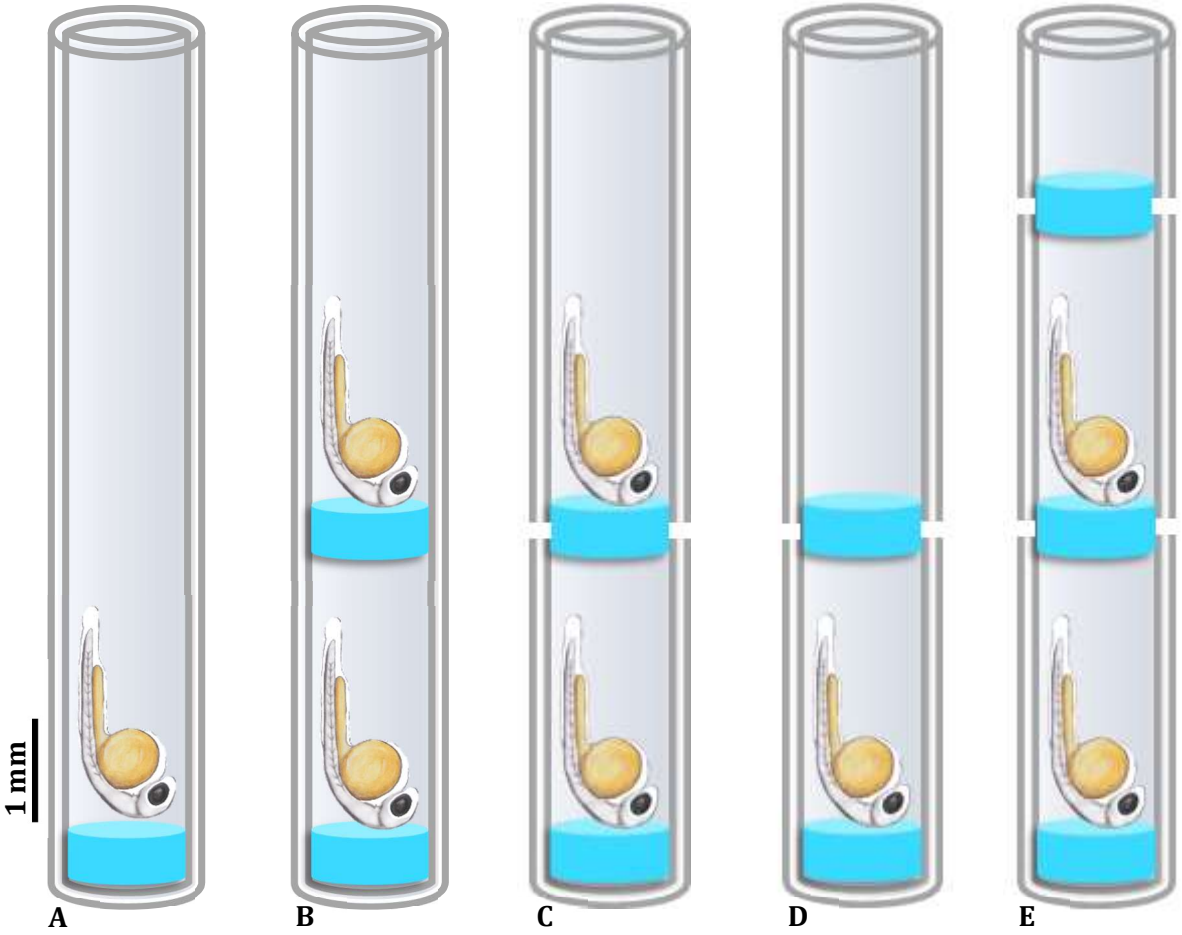

Figure 3.9 Schematic to illustrate different FEP mounting arrangements

A) FEP tubing with 2 % (w/v) LMP agarose plug **B)** multilayer mounting of two embryos in FEP tubing with 2 % (w/v) LMP agarose plug as per published method (Kauffman et al.,2012; Weber et al., 2014) **C)** addition of 'diffusion' holes in FEP tubing to area by middle 2 % (w/v) LMP agarose plug **D)** single embryo mounted in CyGel within FEP tubing with additional 2 % (w/v) agarose plug above embryo **E)** multilayer mounting of embryos within CyGel in FEP tubing, diffusion holes in middle and top 2 % (w/v) LMP agarose plugs

3.10.4 LMP agarose concentration

During repeated attempts at replicating the published method of mounting in FEP tubing in 0.1 % (w/v) LMP agarose, embryos always fell downwards towards the plug during incubation, suggesting that 0.1 % (w/v) LMP agarose did not give adequate immobilisation of the sample. Two alternative brands of LMP agarose were tested (Pierce and ThermoFisher) and embryos moved whilst mounted in these also. When left at room temperature, 0.1 % (w/v) LMP agarose inside a 1.5 ml centrifuge tube would set slightly over 48 hr but would lose any form when moved gently. When incubated at 28.3 °c the 0.1 % (w/v) LMP agarose does not set and remains the consistency of water.

After contacting authors to ascertain nuances in the published method were not being omitted and the method was being reconstructed correctly, no discrepancies were found. Following this, increasing concentrations of LMP agarose inside the FEP tubing were tested: 0.15% (w/v), 0.20% (w/v), 0.25% (w/v), 0.3% (w/v), 0.4% (w/v). Only the highest concentration, 0.4 % (w/v) LMP agarose immobilised the embryo.

Whilst the low LMP agarose concentrations do not immobilise the embryos, it also proved difficult to get the embryos to rest, head first, onto the agarose plug in the short time frame needed between infecting embryos and imaging.

NB After contacting the authors (Kaufmann et al., 2012; Weber et al., 2014) it transpired that the step of coating the inside of FEP tubing with 3 % (w/v) methylcellulose E3, is to prevent embryos from sticking to the walls of the FEP tubing. Since embryos are being imaged directly after infection, mounted in methylcellulose (as described in method 2.10.5), this step was subsequently omitted, as the embryos themselves are coated in methylcellulose.

3.10.5 Imaging embryos mounted in 0.4 % (w/v) LMP agarose within FEP tubing

Tg(*mpx:*GFP)^{i114} embryos were infected 30 hpf with SH1000-mCherry immediately after embryos were washed in E3 (without methyl blue) and mounted as previously described within FEP tubing, as per schematic Figure 3.9D, in 0.4 % (w/v) LMP agarose, head downwards with a 2 % (w/v) LMP agarose plug.

When setting up image acquisition using this mounting method, the image is less focused in comparison with 0.8 % (w/v) LMP agarose mounting. Automated and manual adjustment of light sheet thickness could not compensate for this, likely caused by an increase in scatter from the combination of FEP with 0.4 % (w/v) LMP agarose. Figure 3.12 shows individual z slices acquired from this experiment, panel A) acquired at top of the z-stack (less distance between fluorophore

and detection lens) individual bacteria within neutrophil (highlighted in blue) are indistinguishable. The focus of signal from the sample decreases as the depth of image acquisition increases, Figure 3.12B is from halfway through the z-stack, (45/100) and focus on neutrophils is poor. This combination of 0.4 % (w/v) LMP agarose within FEP tubing is not a suitable alternative to 0.8 % (w/v) LMP agarose mounting method as the required depth of focus for this study cannot be achieved.

3.11 *Cygel thermo-flippable immobilisation medium*

Cygel is a novel thermo-flippable compound that has a micellular formula, a gel developed as an immobilisation medium, an alternative to LMP agarose. Unlike most gelling reagents (such as agarose) commonly used whilst maintaining living cells, instead of heating a solution to liquify, which then cools to a semi-solid state, Cygel is liquid when cold and starts to gel when heated. The flipping point from liquid to solid is 21 °C, and as such would be a suitable matrix for immobilising an embryo incubated at 28.3 °C. Another benefit is that the solution is thermo-reversible, so can be cooled down to recover the sample without damage; whilst possible to recover an embryo from LMP agarose it is very difficult to do so without damaging it. The ability to remount embryos previously imaged, enables imaging of multiple embryos at multiple timepoints during the experiment, which could be incubated in normal conditions. Previous methods used by researchers (Serba, 2015) have involved leaving the samples mounted in an incubator between timepoints; not only does this have limited success when re-imaging (there is often movement of the original sample) but these embryos are constrained by relatively high percentages of agarose and do not develop normally.

Cygel has the same refractive index as water, so should not affect the focus of the light sheet and its micellular chemistry should not produce scatter of the light from the sample. The reagent comes readymade and can be mixed with buffers to provide the correct physiological environment for the sample; it needs to remain at concentrations of 80 % (v/v) and above for it to be able to gel, whilst it needs to immobilise the sample, a softer matrix to allow normal development is preferable.

To achieve the same salinity as 1 x E3, when in solution with Cygel and tricaine (but maintain a Cygel concentration of 80 % (v/v)) a 20 x E3 solution was made and different concentrations of Cygel were tested (Table 3.2), as molarity of the solution affects the flipping point. The lower concentrations of Cygel have a softer consistency, as expected; however when at a concentration of 75 % (v/v) there is no gelling of the formula at 28 °C. Although the flipping temperature is 23 °C there was thickening of the solutions at around RT, so for mounting experiments the solutions were kept on ice and the glass multi-well dish used for mounting was incubated on ice.

For each concentration apart from the non-gelling 75 % (v/v), 2 FEP tubes were prepared, each with two embryos mounted; these were incubated in 50ml reaction tubes, containing 40 ml E3 with 0.02 % (w/v) tricaine. Initially incubation was for 20 h and survival was monitored; after 26 h E3 in the reaction tubes was changed and fresh tricaine added in case of the anaesthetic wearing off.

Since the compound has the consistency of water when at 4 °C, by mounting the embryos in cooled medium, it was possible to draw the embryo into the FEP tubing. Vertical incubation, briefly on ice, allowed the head of the embryo to fall onto the agarose plug, shown in Figure 3.13 . As the sample moves quickly through the thin mounting medium and it thickens as it reaches temperatures above 21 °C, the embryo is sufficiently immobilised when incubated at 28 °C within the imaging chamber and does not continue to move downwards during image acquisition.

Cygel conc. (% (v/v))	Cygel (µl)	20 x E3 (µl)	Tricaine (µl)	ddH_2O (µl)	Gel matrix at 28 °c	Embryo survival 20h (%) n = 8	Embryo survival 44 h (%) n =8
75	150	10	10	30	×	-	-
80	160	10	10	20	✓	100	100
85	170	10	10	10	✓	100	75
90	190	10	10	0	✓	100	100

Table 3.2 Constiuents of mounting media for long term immobilisation of embryos in CyGel

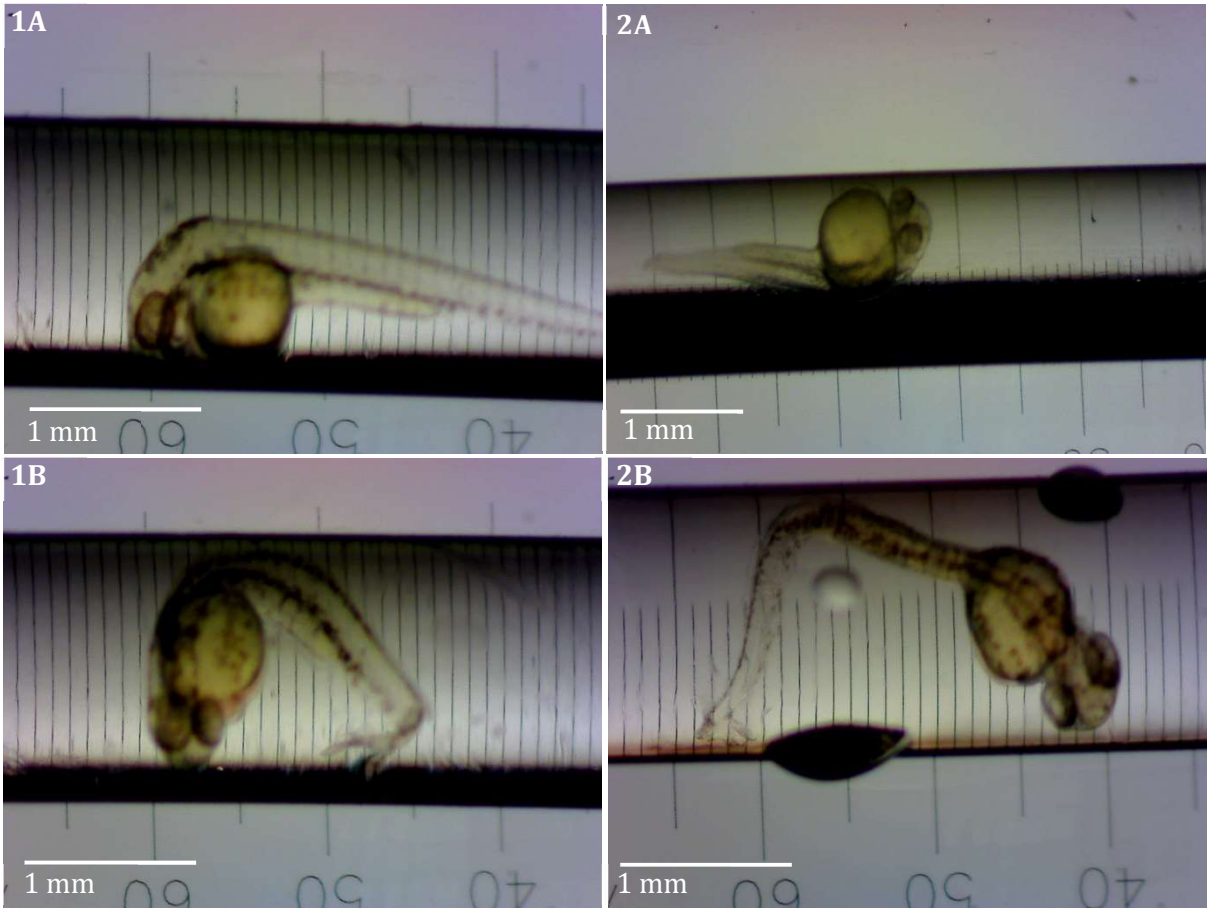

Figure 3.10 Images of embryos mounted in 0.1 % (w/v) LMP agarose within FEP tubing with OD 1.1 mm

Embryos (30 hpf) were mounted in 0.1 % (w/v) LMP agarose within FEP tubing with an OD of 1.1 mm, images 1A and 2A were taken directly after mounting. Images 1B and 2B (of the same two embryos), were taken after 24 h incubation of mounted embryos in E3 containing 0.04 % (w/v) tricaine. During incubation the position of embryos mounted within the FEP tubing.

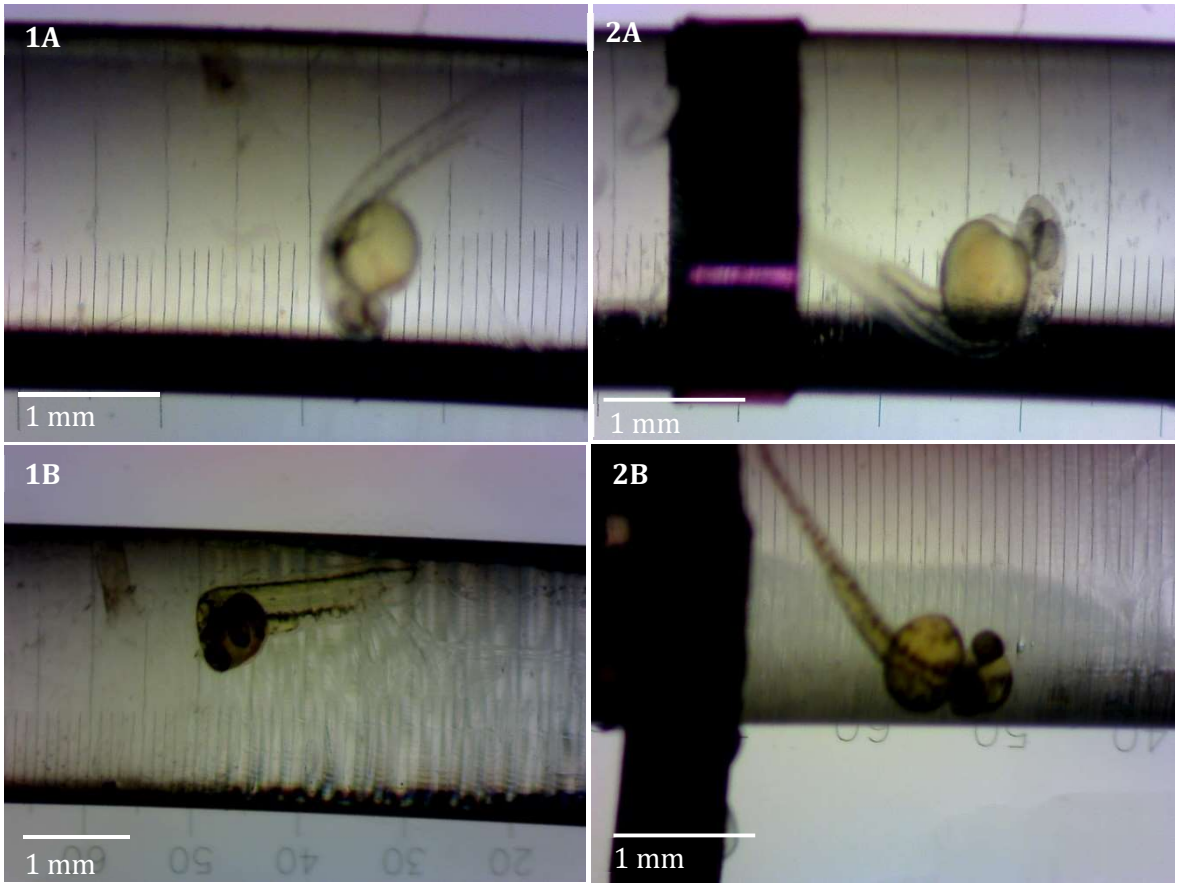

Figure 3.11 Images of embryos of mounted in 0.1 % (w/v) LMP agarose within FEP tubing with OD of 1.6 mm

Embryos (30 hpf) were mounted in 0.1 % (w/v) LMP agarose within FEP tubing with an OD of 1.6 mm, images 1A and 2A were taken directly after mounting. Images 1B and 2B (of the same two embryos), were taken after 24 h incubation of mounted embryos in E3 containing 0.04 % (w/v) tricaine. During incubation the position of embryos mounted within the FEP tubing.

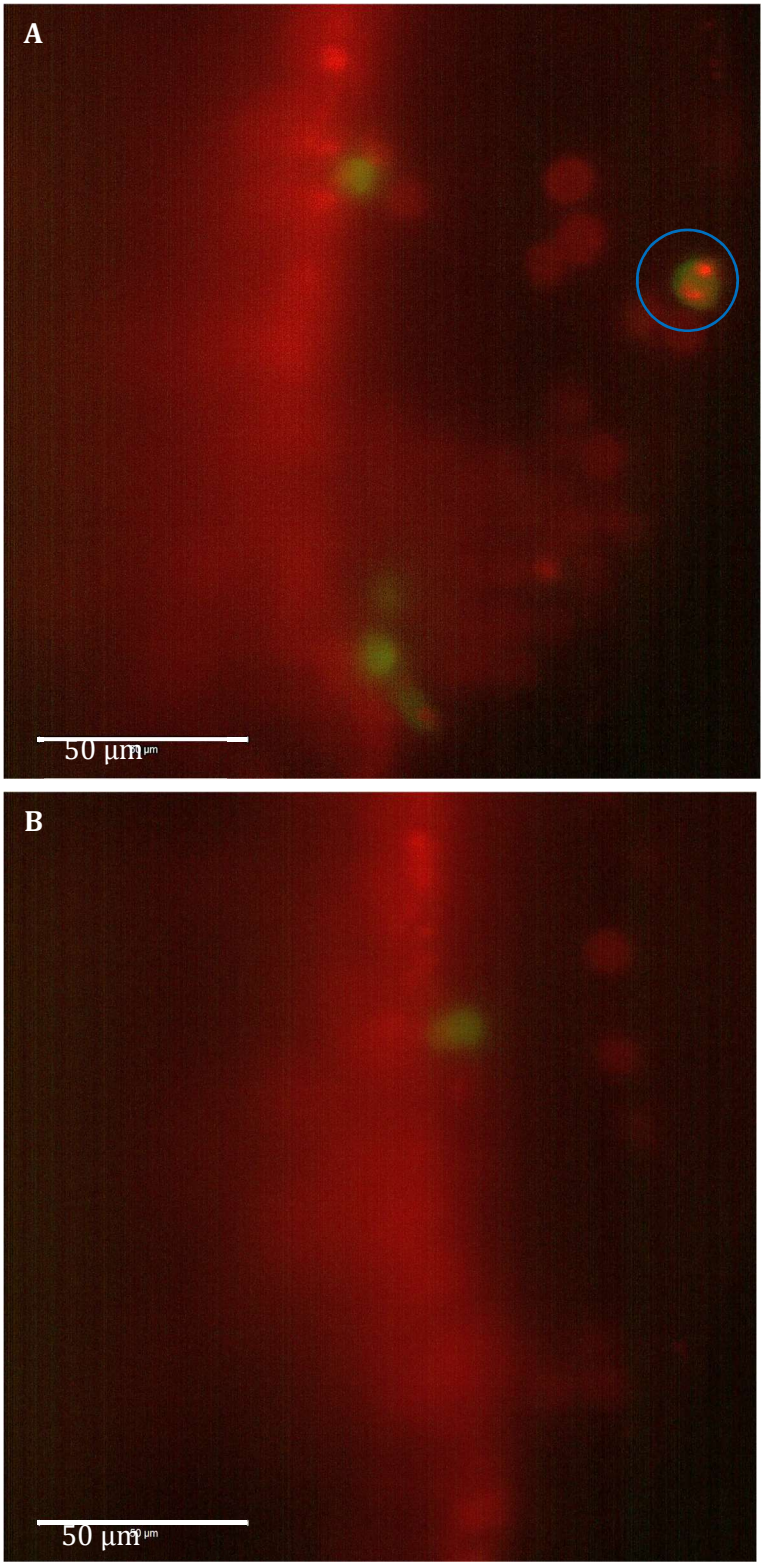

Figure 3.12 Imaging embryos in 0.4 % (w/v) LMP agarose within FEP tubing

Tg(*mpx*:GFP)^{I114} embryo infected with SH1000-mCherry, 1 hpi mounted in 0.4 % (w/v) LMP agarose within FEP tubing acquired with 20 x objective with 2 x optical zoom **A)** single slice (1 µm) from the top of the z stack (98/100), neutrophil (GFP) with intracellular bacteria (mCherry) circled in blue **B)** single slice (1 µm) from the middle of the z stack (45/100).

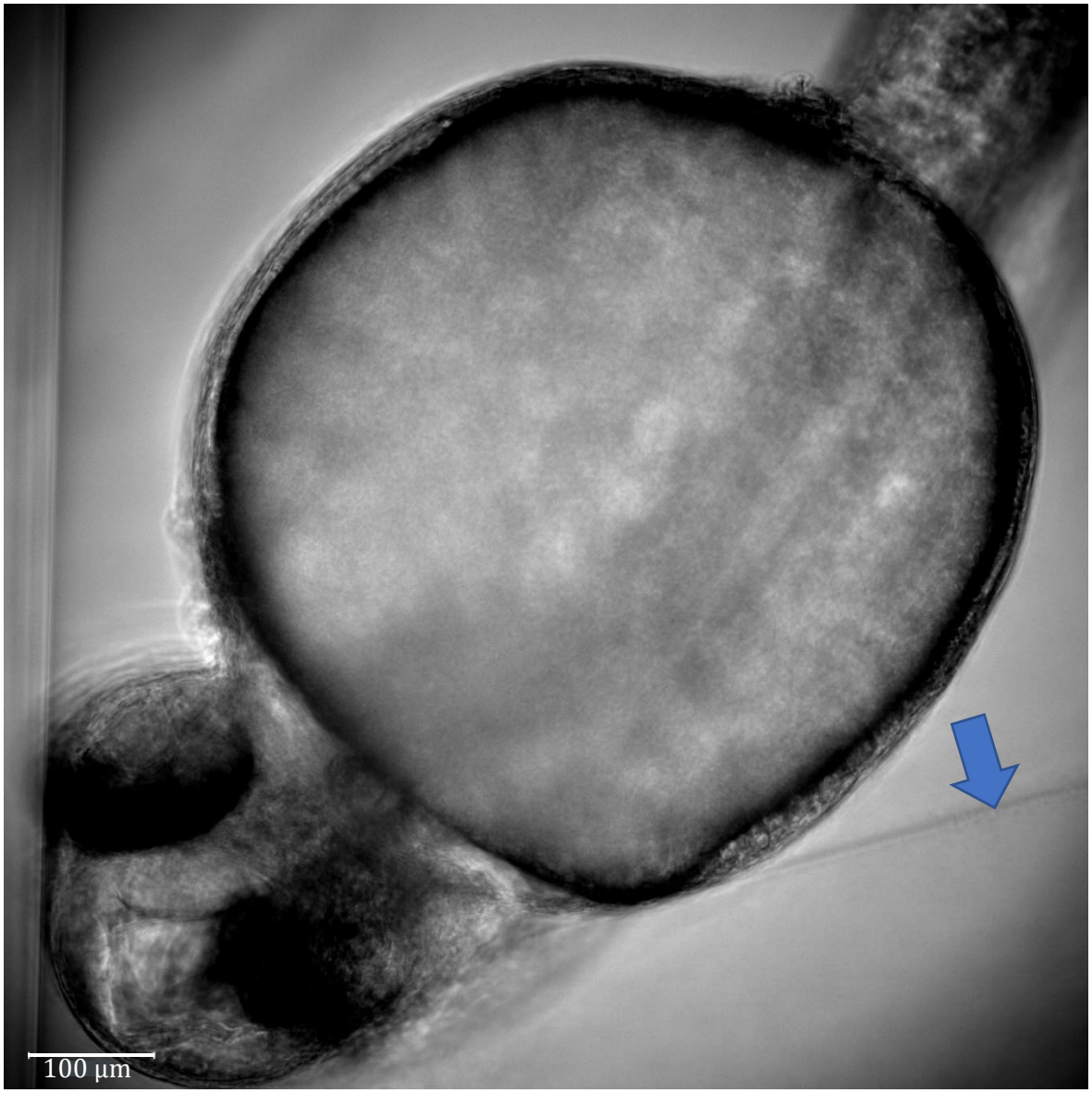

Figure 3.13 Embryo resting on LMP agarose plug

A *Tg*(lyzC.nsfb:mCherry)^{SH260} embryo 30 minutes post infection, mounted in CyGel, head downwards resting on 2 % (w/v)LMP agarose plug within FEP tubing. Blue arrow indicates top surface of plug.

3.12 *Tricaine*

Keeping embryos anesthetised during imaging is vital, not only so that the region of interest remains static, but also if the tricaine wears off whilst the embryo is mounted, it will cause stress and damage to the embryo. Long term exposure to tricaine has been implicated in slowing down the development of embryos and causing oedemas (Kaufmann et al., 2012). During light sheet experiments the sample is normally exposed to the same concentration of tricaine used to anesthetise before infection: stock solution is 0.4 % (w/v) before diluting 1/20 to a working concentration of 0.02 % (w/v) (200 mg/L).

If oedemas develop during the experiment, areas of the circulation are moved out of the ROI, beyond the imaging stack. Additional 'empty' planes in the z dimension are set up at the beginning of acquisition to allow for development of the embryo; however oedemas can double the z stack so important events can be missed.

Embryos with a low bacterial burden and oedemas have been recovered from the light sheet post imaging, as shown in Figure 3.14 in which an unmounted *Tg*(*mpx*:GFP)^{i114} embryo was examined by dissecting microscope after 18 h imaging. Figure 3.14A shows the oedema the fish has developed whilst mounted in the microscope, and panel B highlights an internal bleed associated with oedemas. From the LSFM time course, there are GFP neutrophils in the region of the bleed, the final timepoint is shown in Figure 3.14D. There are no visible bacteria either inside or outside of the phagocytes in this region, suggesting neutrophils are recruited to the injury rather than an infectious foci. It would not be representative to study the interaction of the immune system with bacteria whilst there are concurrent immunological events.

To investigate why oedemas were developing, a tricaine titration bathing experiment was performed. Embryos 30 hpi (n = 20 per group) were immersed in 250 µl of E3 with the following dilutions of tricaine: 1/20 (0.02 % w/v), 1/40 (0.01 % w/v), 1/60 (0.0066 % w/v) and 1/80 (0.005 % w/v) with E3 control and the number of embryos with oedemas at regular timepoints quantified. E3 was changed every 24 h, unless movement of the embryo was previously detected. Results in Figure 3.15 show that there is a decrease in oedema with decreasing tricaine concentrations. The standard 1/20 dilution used caused oedemas in 87.5 % of the embryos over 68 h, with oedemas observed from 26 h. All replicates of this experiment had lower occurrence of oedema then reported by Kaufmann et al., 2012, with oedemas initially occurring after relatively long periods of incubation (26 h). However, the dissecting microscope only provides 4 x magnification; the macroscopic determination of oedema formation might contribute to this lower incidence

At each timepoint embryos were checked for movement; the mirror on the dissecting microscope was turned quickly to 'flash' the embryos, which normally results in reactive movement. The 96

well-plate was also gently shaken to prompt movement. There were no visible movements from the 1/20 and 1/40 groups, however at 44 h & 68 h there was movement in 1/60 group. Movement in the control and 1/80 group was observed at all timepoints.

Whilst movement was first observed in the 1/60 & 1/80 dilution after 44 h incubation, embryos that were anesthetised in the standard 1/20 dilution and then mounted in 1/60 medium, with 1/60 dilution in the chamber; embryos moved whilst imaging was being set up. This occurred in both the 0.8 % (w/v) LMP agarose method & the CyGel FEP tubing method. A fresh stock of tricaine was tried with the same result.

A 1/40 dilution of tricaine was tried but showed inter-repeat variability; embryos initially remained still whilst mounted in this concentration, however sometimes embryos would move despite there being no difference in sample preparation. This is potentially due to batch variation in the tricaine stocks from the aquarium, as even stocks prepared by aquarium staff on the same day as experiments (suggesting no time for degradation of stocks) sometimes do not work at the 1/40 dilution.

To avoid movement of mounted samples, embryos were anesthetised in 1/20 and mounted in 1/20, with 1/40 dilution of the tricaine in the imaging chamber to maintain anaesthesia whilst imaging but reduce the chance of oedema forming.

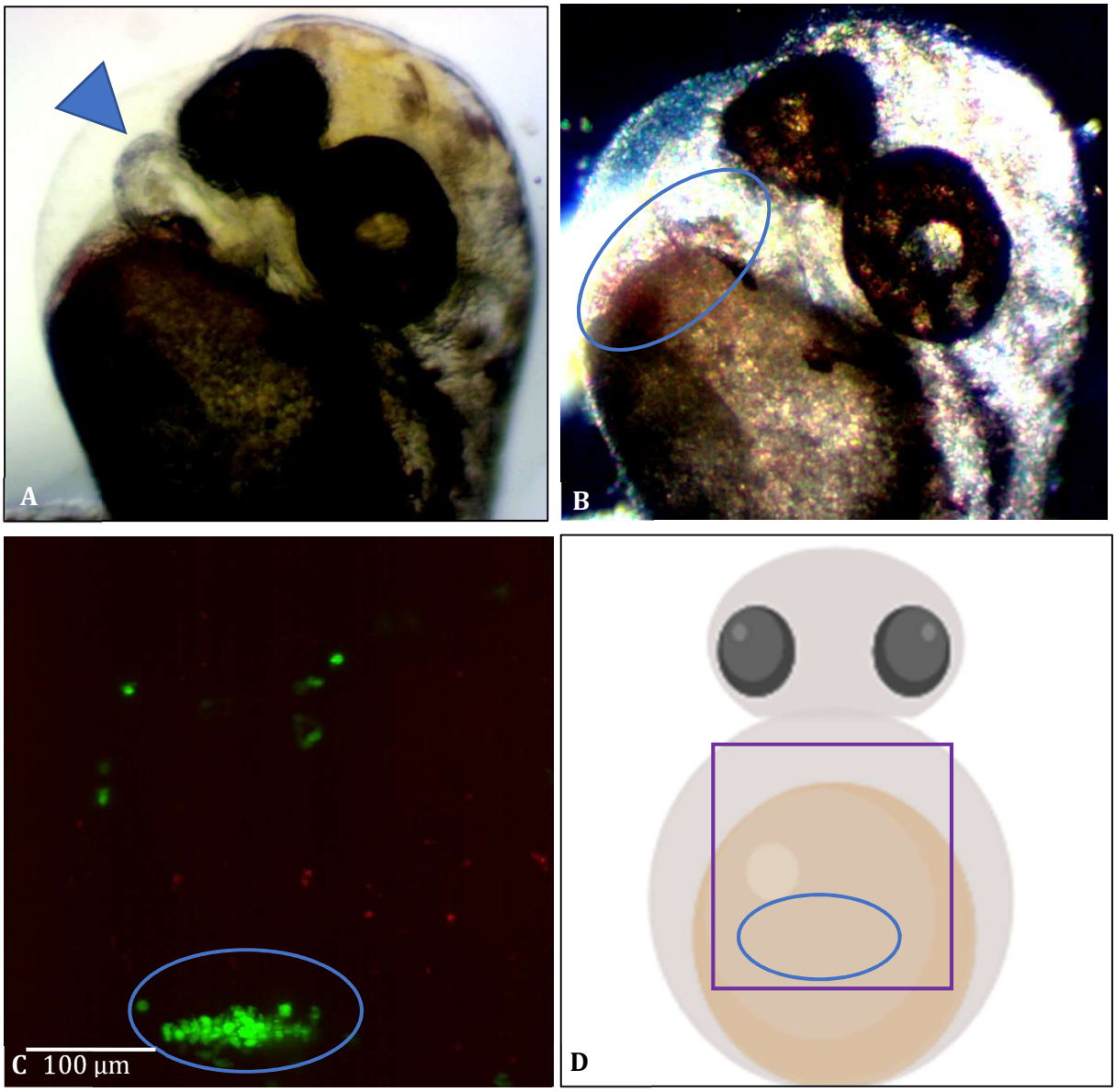

Figure 3.14 Embryo with oedema post LSFM timecourse

Panel **A**,**B** show *Tg*(*mpx*:GFP)^{i114} embryo (with GFP labelled neutrophils), unmounted post 18 h of LSFM imaging, **A)** Embryo on dissecting microscope, blue arrow indicating oedema **B)** mirrored light on dissecting microscope, internal bleed associated with oedema circled **C)** MaxIP of last timepoint from LSFM, *Tg*(*mpx*:GFP)^{i114} infected with SH1000-mCherry, GFP neutrophils in region of bleed circled. **D)** Schematic of embryo in ventral orientation with purple square for approximation of FOV and blue oval for approximation of bleed site.

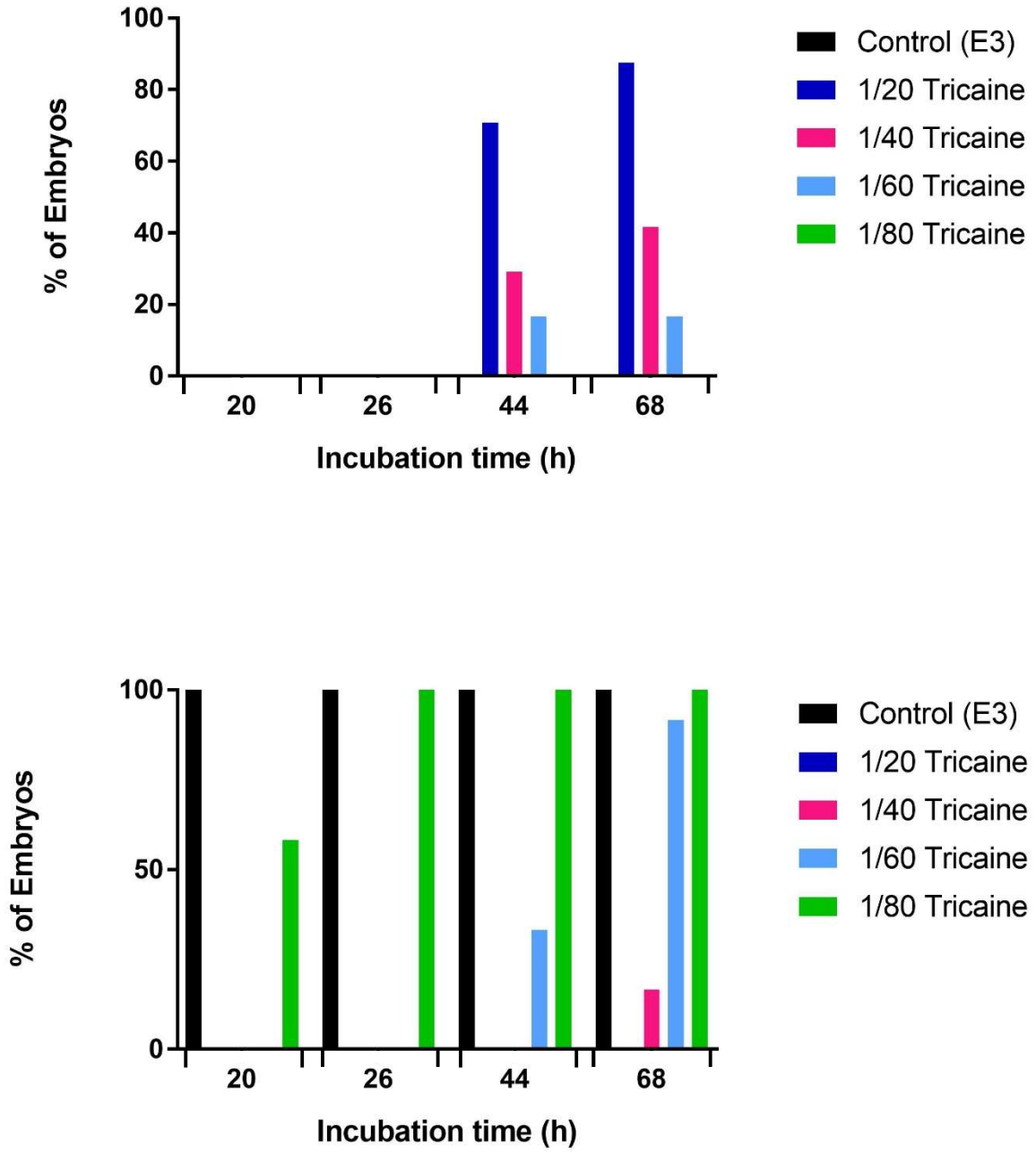

Figure 3.15 Effect of tricaine concentration on embryos

Embryos (n=24 per group) were immersed in 1/20, 1/40, 1/60 & 1/80 dilution of stock solution of tricaine 0.4 % (w/v) in E3, **A)** percentage of embryos with oedemas during incubation **B)** percentage of embryos moving during incubation in tricaine. During extended incubation some subjects died, percentages are adjusted accordingly.

If an embryo moves after mounting in the 0.8 % (w/v) LMP agarose that has set, there is disruption the texture of the medium, this 'lumpy' agarose disrupts the light path to or from the sample, degrading the clarity of the acquisition. Figure 3.16 shows a *Tg*(*mpx*:GFP x *mpeg*:mCherry.CAAX)^{I114,SH378} embryo (with GFP neutrophils and mCherry macrophages) infected with JE2-mCherry, first mounted and imaged directly after infection in 0.8 % (w/v) LMP agarose (Figure 3.16A) and the same ROI acquired with the same parameters after movement of the embryo (Figure 3.16B). Initially there was near-perfect resolution of individual bacteria both inside and outside the phagocyte, with low point spread function (PSF) shown inFigure 3.16A. This was obtained within the 1/40 dilution of tricaine in the chamber and 1/20 dilution used for injection and within the agarose. If there is movement of the sample, even if the concentration of tricaine is increased and the embryo no longer moves, there is no way of recovering the clarity of the image, even after realignment of the light sheet thickness.

Figure 3.16B shows the same slice and ROI of the embryo after movement disrupted the matrix of the set LMP agarose. After additional tricaine is added to the imaging chamber to anesthetise the sample, there is no clear resolution of either host macrophages and neutrophils or JE2-mCherry, even after manual re-alignment of the light sheet thickness. At this point a new sample needs mounting; in this instance the embryo was dissected out of the 0.8 % (w/v) LMP agarose and re-mounted into LMP agarose from the same batch. Light sheet alignment often needs re-adjusting for a new sample even for the same batch of embedding medium. After remounting the embryo and manual adjustment of light sheet thickness, resolution of bacteria and host cells was restored, as shown in Figure 3.17A. Orientation of the embryo after remounting and ROI for imaging is shown in the bright field image (Figure 3.17B).

3.13 *Data handling*

Imaging multiple fluorophores in 4D generates very large sized data sets, with a typical data set from a 24 h experiment exceeding 3 TB in size; this makes data handling difficult and requires a lot of computer processing power. The open SPIM community have developed some useful tools for cropping and compressing data sets, however the Zeiss Z1 light sheet produces a proprietary file type (.czi) incompatible with these open source tools. Not only is processing data difficult, but just moving the files and storing them is lengthy in itself. It is important to find a method of data processing that makes the data easier to handle and does not lose/hide important temporal/spatial events. The same data set has been used for comparative reconstruction.

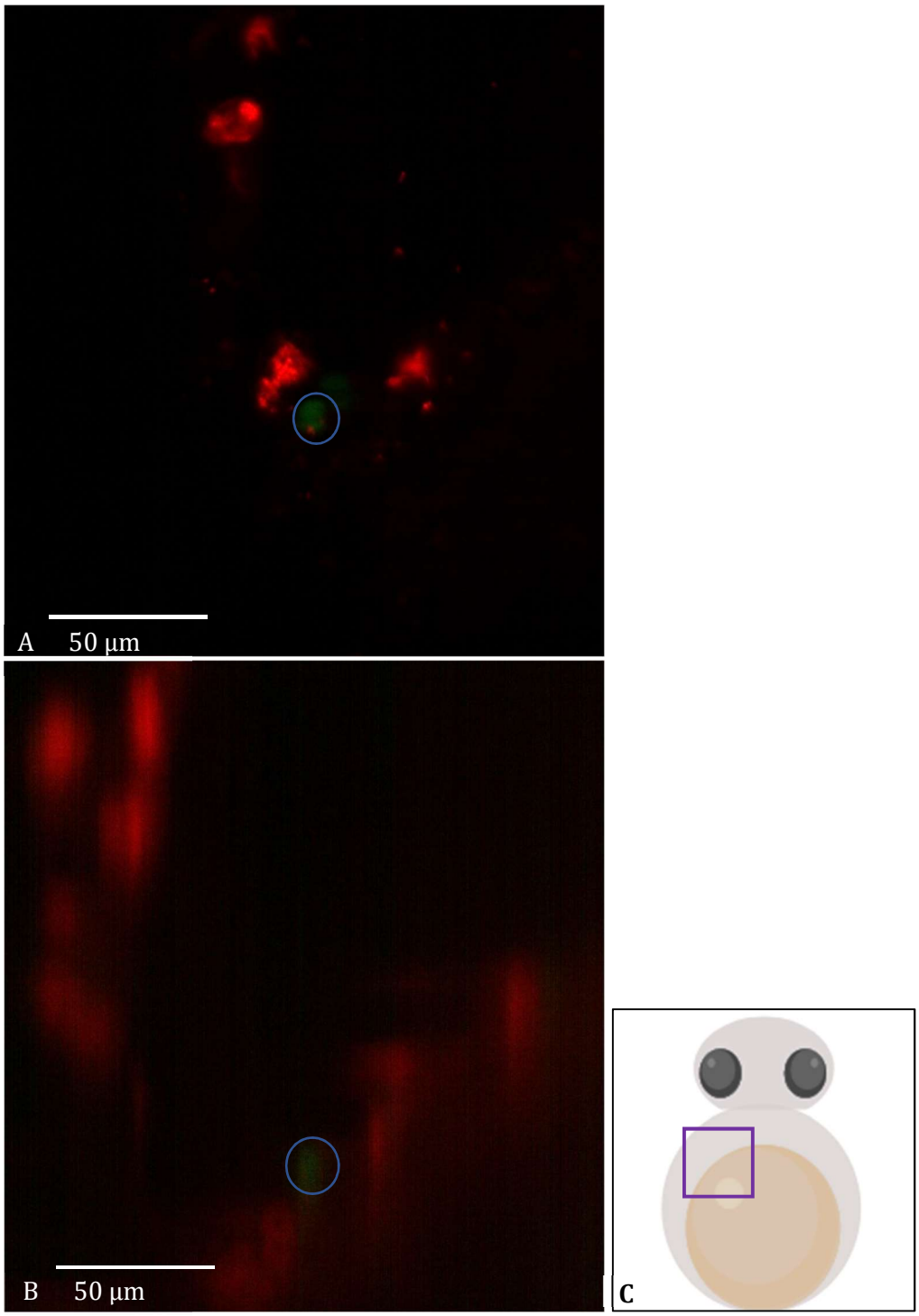

Figure 3.16 Resolution of light sheet prior and post movement in 0.8 % (w/v) LMP agarose

Tg(*mpx*:GFP x *mpeg*:mCherry.CAAX)^{I114,SH378} infected with JE2-mCherry mounted in 0.8 % (w/v)LMP agarose with 0.02 % v/v tricaine, incubated at 28 °C in E3 with 0.01 % v/v tricaine. **A)** 1 hpi, individual slice 0.7µm, 1.4 zoom, focused light sheet (light sheet thickness = 3.8 µm) resolves individual JE2-mCherry within both neutrophils (GFP) and macrophages (mCherry) and extracellular bacteria. **B)** 1.5 hpi, individual slice 0.7 µm, 1.4 zoom, non-focused light sheet (light sheet thickness = 3.8 µm) **C)** Schematic of embryo in ventral orientation with purple square for approximation of FOV

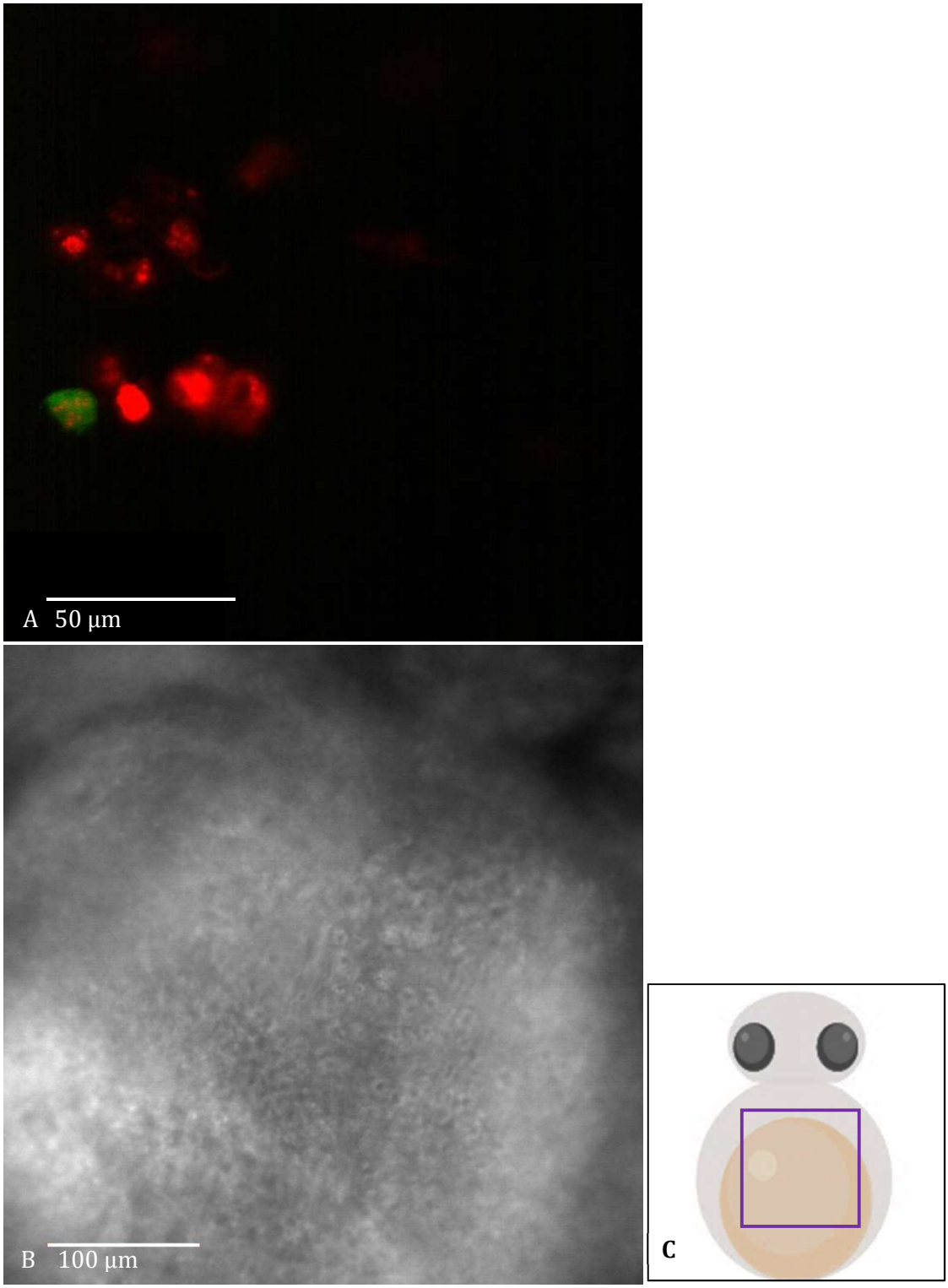

Figure 3.17 Resolution of light sheet of embryo remounted in 0.8 % (w/v) LMP agarose

Tg(*mpx*:GFP x *mpeg*:mCherry.CAAX)^{I114,SH378} infected with JE2-mCherry re-mounted in 0.8 % (w/v) LMP agarose with 0.02 % (v/v) tricaine, incubated at 28°c in E3 with 0.015 % v/v tricaine. **A)** 3 hpi, individual slice 0.7 µm, 1.4 x zoom, focused light sheet (light sheet thickness = 3.55 µm) resolves individual JE2-mCherry within both neutrophils (GFP) and macrophages (mCherry) **B)** 3 hpi, 1.1 x zoom, bright field of embryo orientation after re-mounting, focused on the circulation valley. **C)** Schematic of embryo in ventral orientation with purple square for approximation of FOV

3.13.1 Zen- Black edition

The proprietary Zeiss software Zen can be used to process data after acquisition, but this is an updated version of existing software; although tools within the package have been developed for handling LSFM data, the software struggles to handle the large files. During the course of this study, numerous software updates have undoubtedly made processing within Zen a less troublesome experience but still does not parallel the brilliance of the hardware.

3.13.1.1 Data cropping

Often 'empty' slices are obtained during the experiment, these images, acquired with a highly sensitive sCMOS camera are 16-bit images, capable of storing 65,535 (216) levels of colour, therefore storing 16-bit black is very bulky. To make data easier to manoeuvre, it would be prudent to remove these 'empty' slices. Zen does not contain a function to detect and/or remove all slices below a certain threshold, so this needs to be verified manually, throughout the data set, at every timepoint. For volumetric continuity, any slices removed need to be removed from all timepoints, so that data can be properly aligned and reconstructed. To crop these slices from the data set, a 'subset' must be created and rather than just deleting the specified images from the file, all the wanted slices in the data set are copied, this means a temporary near-doubling of data, before deleting the original file. Sometimes is not possible due to lack of space on local data drives needed for the processing.

3.13.1.2 Maximum intensity projection

A maximum intensity projection (maxIP) flattens the stack turning the brightest voxel in the ROI into a pixel, creating a single plane from hundreds of slices. This can be performed in ZEN and is relatively straightforward for a single timepoint (Figure 3.18); however, to follow infection over a long time scale, with imaging every 20 minutes, creating a video which comprises of maxIP over time can take over 14 h, often the software will crash during this process. These projections are a means of quickly determining whether events of interest occurred during the LSFM timecourse, producing files that are GB in size rather than TB. An example of this can be viewed in the **'Video 1- MaxIP timecourse of embryo with mCherry labelled neutrophils infected with SH1000-GFP'**

These are a useful overview to evaluate the experiment, however by flattening the stack, there can be misinterpretation of co-localisation. When GFP is within a mCherry labelled immune cell, the projection will give a yellow signal; there could be very bright GFP and mCherry, that occupy the

same pixel within the ROI but are axially distant. As well as this, when there is a foci of infection, it can be difficult to distinguish immune cells from each other.

3.13.1.3 'Fly-through' of z stack

After identifying timepoints of interest from a MaxIP, a video moving through all of the slices within the z-stack can be created, providing a more detailed insight to the spatial association between host cells and bacteria, whether the bacteria are intra- or extra-cellular. This can also distinguish between host phagocyte which appear close together in a MaxIP, if these cells are being recruited to a specific site or whether they are distance axially within the circulation. An example of this can be viewed in **'Video 2- Flythrough of embryo with mCherry labelled neutrophils infected with SH1000-GFP'**

3.13.2 Arivis

During this study a new software, Arivis 4D was launched. This software has been developed specifically for the handling of large microscopy data sets, like those produced by the Zeiss Z1 microscope. The capacity of software to open large file sizes is usually limited by the amount of available random-access memory (RAM) with 16GB RAM being the largest, widely available size of RAM on the market; it is likely this that causes the problems experienced using Zen. However, Arivis can open the large file formats, regardless of RAM available on the processing computer, after developing their 'Image core' format. This can store large files without redundancy, and can access arbitrary regions of the data set, across 4D, nearly instantaneously. This parallelisation of the data set allows for files that exceed the available RAM by 2 orders of magnitude to be opened and explored.

After converting files from the proprietary Zeiss format (.czi) to the Arivis 'Image core' format (.sis) data can automatically be opened in 3D; this provides rapid rendering of the data at individual timepoints which can be explored and freely rotated. These can be exported as videos, please view **'Video 3 – rotating 3D reconstruction of mpeg:mCherry embryo infected with SH1000-GFP'**.

These renders give good spatial insight to the data and readily show whether or not bacteria are inside or outside of the phagocytes. Arivis can be used to view the progression of the timecourse in 3D and to create videos of these reconstructions or produce a projection of 3D render into a 2D image, demonstrated in Figure 3.19.

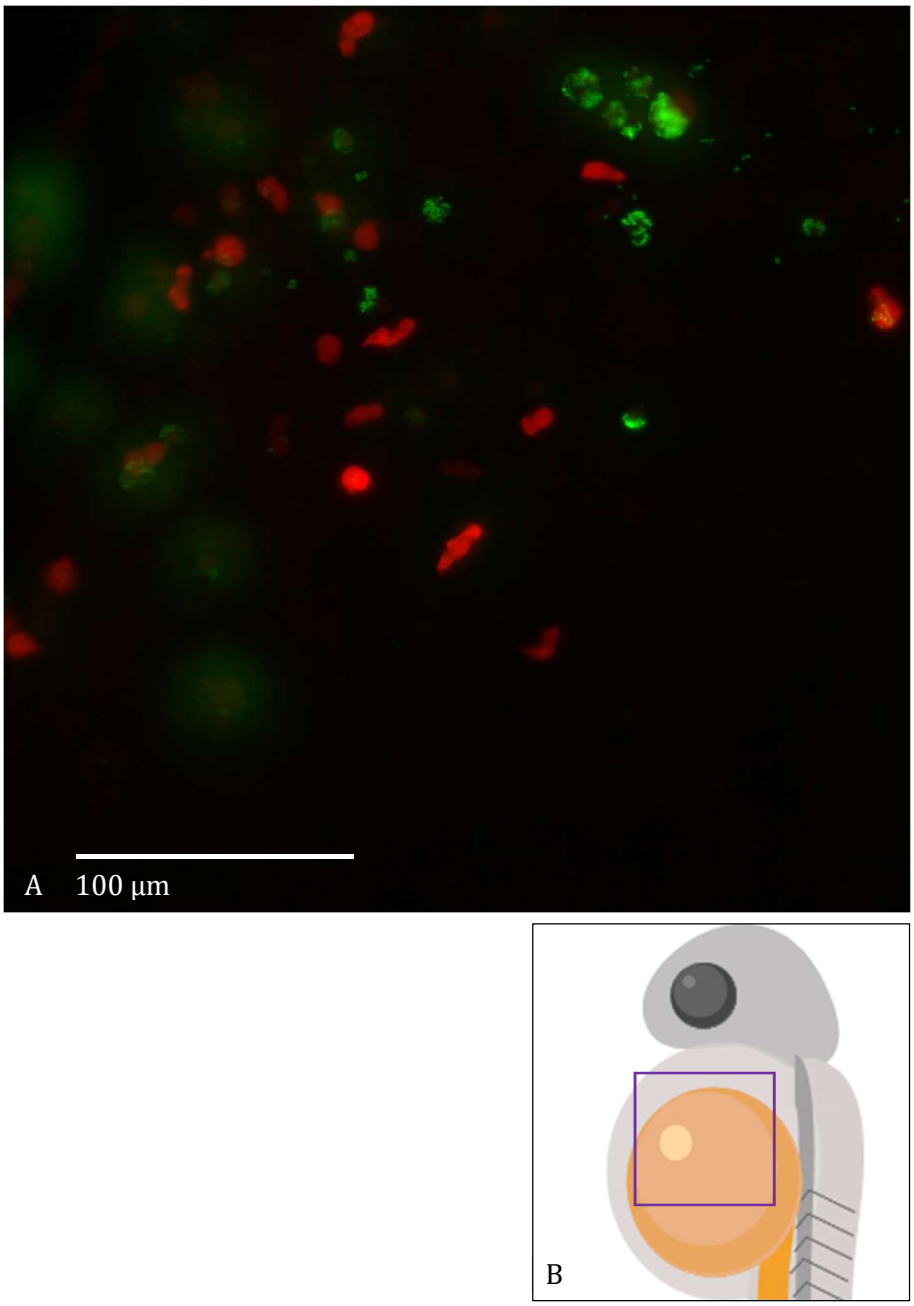

Figure 3.18 Maximum intensity projection, single timepoint

A)*Tg*(*lyz.nfsb*:mCherry)^{SH260} embryo (with mCherry labelled neutrophils)infected with SH1000-GFP, single timepoint at 2 hpi. MaxIP composed from 270 slices (1µm). **B)** Schematic of embryo in lateral orientation with purple square for approximation of FOV

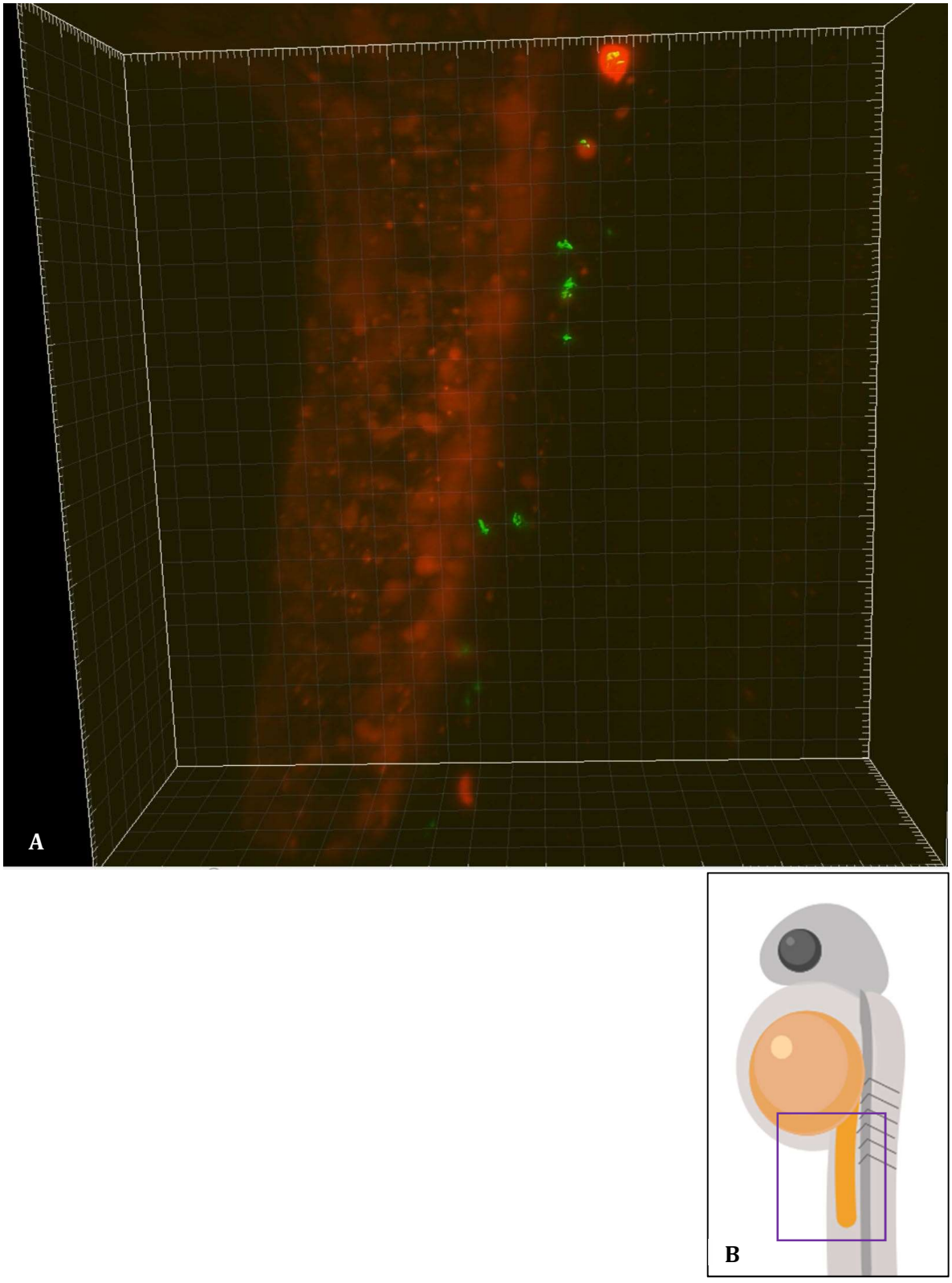

Figure 3.19 2D projection of 3D reconstruction created using Arivis 4D

A) *Tg*(*mpeg*:mCherry x CAAX)^{SH378} embryo (with mCherry labelled macrophages) infected with SH1000-GFP, imaged 4 hpi. 2D projection of 3D reconstruction created in Arivis 4D. Gridlines are 30 µm x 30 µm and minor gradations are 6 µm. **B)** Schematic of embryo in lateral orientation with purple rectangle for approximation of region of reconstruction.

3.14 *Discussion*

The established zebrafish model for *S. aureus* infection has been used to identify bacterial factors important for pathogenesis. Previous microscopic techniques have been used to image lesions within the host with low magnification lenses, and interaction of bacteria within the phagocyte with high aperture, high magnification (40 x and 62 x) lenses (Prajsnar et al., 2012; Serba, 2015). These are limited by the depth of penetration of the sample and the size of the FOV. LSFM provides an opportunity to use high aperture, low magnification lenses enabling high resolution image acquisition over large ROI. Lightsheet can penetrate the sample deeper than 500µm; however deeper imaging has a greater scatter of signal from the sample and reduces focus of the light to the detecting lens.

Another advantage of the Zeiss Z1 microscope over other imaging techniques is that the living sample can be incubated during imaging to provide conditions that should allow for the normal development of the host and infection progression. Although the microscope has been designed for the long-term imaging of living samples incubating in a chamber of medium, in practice the recommended protocols do not deliver the professed normal development of the sample. In this chapter many imaging parameters have been optimised and methods adjusted to deliver a protocol that can be used to image an infected embryo over long time scales.

Decreasing the laser power for acquisition, elongating the gap in between timepoints and changing the ROI, cumulatively has reduced phototoxicity to the embryo and resulting in imaging for over 24 h, that keeps the sample alive. In addition to the sample being able to withstand repeated imaging, a mounting technique that is gentler on the sample has been developed. The published FEP alternatives to 0.8 % (w/v) LMP agarose mounting did not work when replicated and a new method using a CyGel as an embedding matrix has been developed this should provide a matrix which can sustain the development of the embryo during imaging and enables getting the embryo into the correct position within the FEP tube in a short time after infection whereas other methods using 0.1-0.3 % (w/v) LMP agarose could not get the sample to rest on the agarose plug within an hour of infection, the sample would drift during acquisition. It is important to get the sample into the microscope as quickly as possible after infection to capture initial phagocytosis of bacteria within the host.

In addition to a mounting medium that allows for better development of the embryo in comparison with the 0.8 % (w/v) LMP agarose, the amount of tricaine used in long term imaging experiments has been reduced by 50 % to reduce the incidence of oedemas in mounted embryos. Although embryos infected with *S. aureus* often develop oedemas during survival experiments, it is important

that oedemas are not caused by other factors other than infection, altering the dynamics between host and bacteria.

Having established a protocol that can maintain an infected embryo during long term imaging, methods of reviewing and reconstructing data were explored. After acquisition data is initially cropped to eliminate extraneous data and this raw data is stored on a RAID. MaxIP are then created from data to provide an overview of the imaging outcome. Data is then cropped to highlight regions of interest and exported in video format. This cropped data can also then be converted into 4D using Arivis to gain spatial insight to the interaction between phagocytes and bacteria. A flowchart outling the process developed in this chapter is shown in Figure 3.20.

Development of these techniques has provided the basis for interrogating real time, host pathogen interactions, across four dimensions.

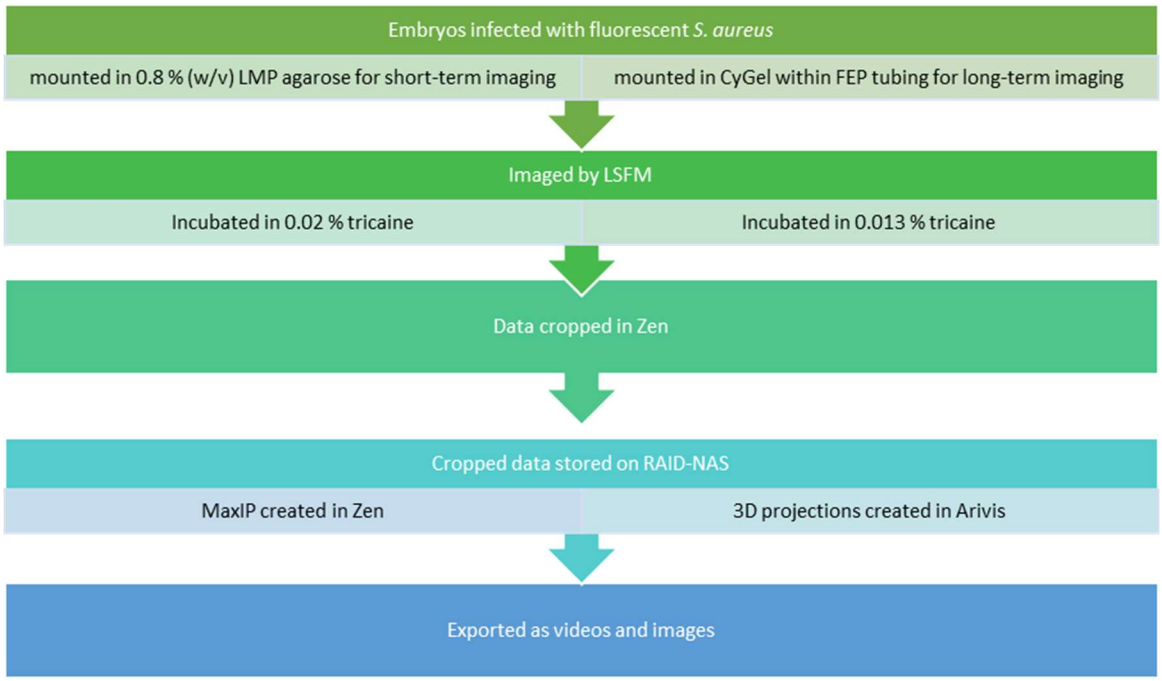

Figure 3.20 Process for imaging real-time interactions of *S. aureus* within a zebrafish embryo host by LSFM.

4 Dynamics of *S. aureus* infection of zebrafish embryos

4.1 *Introduction*

On infection of zebrafish embryos with *S. aureus*, of those that succumb to infection, previous work has demonstrated one third have clonal lesions (Prajsnar et al., 2012). By infecting with an inoculum of 1:1 isogenic strains carrying different fluorescent and antibiotic resistance markers Prajsnar et al. established that lesions are formed from only a few cells of the initial inoculum. These undergo population expansion within the host after passing through an immune "bottleneck". This bottleneck is found across different models *of S. aureus* infection; clonality has also been observed in murine models and is independent of bacterial strain (McVicker et al., 2014; Pollitt et al., 2018; Prajsnar et al., 2012). Moreover, successful bacteria which have overwhelmed the host subsequent to infection by a mixed inoculum are not genetically advantaged, as if isolates are used to infect more embryos as part of a mixed inoculum, they are not preferentially selected for (McVicker et al., 2014).

Immune bottlenecks have also been identified in *Salmonella enterica* (Grant et al., 2008) and *Streptococcus pneumoniae (S. pneumoniae)* (Manso et al., 2014). In the *S. pneumoniae* murine model of invasive disease a switch in distinct epigenetic profile is found when bacteria are reisolated from mice, whereas there was no detection of change of these epigenetic profiles in a murine nasopharyngeal colonisation model, suggesting the blood as the cause of this skew in profiles (Manso et al., 2014). Simultaneous systemic infection with isogenic *S. enterica* strains in a murine model have demonstrated that the bactericidal action by NADPH oxidase (required for generation of ROS by phagocytes) in the early stages of infection, is responsible for the change in ratio of isogenic strains reisolated in comparison with the inoculum. This indicates that phagocytes are the immunological bottleneck causing localised clonality in the *S. enterica* systemic model of murine infection (Grant et al., 2008).

Clonality has been observed within blood vessels of zebrafish systemically infected with *Cryptococcus neoformans (C. neoformans)*(Gibson et al., 2017). When infected with a mixed inoculum of fluorescently marked but otherwise isogenic strains, early formation of a single coloured cryptococcal mass within the vasculature of an embryo corresponded to overwhelming infection of the same strain. Multiple clonal cryptococcal masses of different isogenic strains were observed within different blood vessels of a single embryo; in these embryos a mixed strain overwhelming infection was observed. It has therefore been proposed that the spatial confinement of the small blood vessels trap individual *C. neoformans* which then develop clonal cryptococcal masses. These cryptococcal masses may lead to vascular damage and dissemination of the pathogen throughout the host (Gibson et al., 2017).

Macrophages are critical in the control of *C. neoformans* infection but a failure in macrophage response is not the only defect in embryos which succumb to infection. Intracellular proliferation of the pathogen within the phagocyte has been observed and are a source of increasing cryptococcal burden within the host. The *in vivo* properties of the cryptococcal cells affects the ability of macrophages to phagocytose the pathogen, with early response to systemic infection critical to the outcome of the host (Bojarczuk et al., 2016). In this systemic infection model both extracellular and intracellular factors are involved in the progression of cryptococcal infection (Bojarczuk et al., 2016; Gibson et al., 2017)

Previous research implicated neutrophils as the niche for *S. aureus* to expand within the host before a lesion if founded and overwhelming infection occurs in the zebrafish embryo model of systemic *S. aureus* infection (Prajsnar et al., 2012). Recently macrophages were identified as the niche for *S. aureus* expansion within a murine host (Pollitt et al., 2018); depletion of macrophages abolished the bottleneck seen in multiple infection models (McVicker et al., 2014; Pollitt et al., 2018; Prajsnar et al., 2012) and with it loss of clonal abscesses that arise from a mixed inoculum (Pollitt et al., 2018). Another study utilising the systemic zebrafish embryo model of *S. aureus* infection established that there is more intake of *S. aureus* into macrophages (which can contain over 100 bacteria) then there is into neutrophils, both as a percentage of the cell population and the number of bacteria phagocytosed per cell. The percentage of the neutrophil population that contains *S. aureus* decreases from ~60 % at 1-5 hpi to 20 % during later stages in infection (24-28 hpi); this is partly due to a 30 % increase in neutrophil population as the embryo develops but could also be due to intraphagocyte killing of *S. aureus* (Serba, 2015).

4.2 *Chapter aims*

- Imaging infected embryos directly following infection though to formation of lesion, utilising transgenic zebrafish lines with fluorescent phagocytes to investigate expansion of *S. aureus* in the host.
- Investigate the effect of macrophage depletion on clonal infection of the host and the role of macrophages as a possible niche for bacterial expansion.
- Create a new bacterial strain expressing a novel fluorophore complementary to GFP and mCherry enabling long term three colour imaging.

4.3 *Early embryo infection*

Tg(*lyzC.nsfb*:mCherry)^{SH260} embryos (with mCherry labelled neutrophils) were infected with SH1000-GFP 1 hpi and mounted in 0.8% (w/v) LMP agarose and imaged by LSFM every 15 minutes for 20 h. A MaxIP of this timecourse can be viewed in **'Video 4 – *lyz:mCherry* SH1000-GFP naïve lesion formation video'**. At the beginning of this experiment 1 hpi (Figure 4.1A), bacteria are present within the circulation of the embryo, prior to phagocytosis. Bacteria are initially phagocytosed by neutrophils (Figure 4.1B). As time progresses (5.5 – 14.5 hpi) neutrophils are recruited to a site with increasing GFP signal (Figure 4.1C). In Video 5, an increase in bacterial aggregates is concomitant with increasing number of circulating neutrophils. From 5.5 hpi onwards the GFP signal (from *S. aureus*) increases over time at this bacterial foci and neutrophils are observed collecting at this site within the host. When imaging is terminated at 21 hpi (Figure 4.1D) the bacteria are not within a labelled neutrophil. The increase in GFP signal from this region within the circulation is indicative of a small bacterial aggregate, that may have gone on to form a lesion within the host. It is also possible that these bacteria were within an unlabelled macrophage; in this case bacteria were either replicating within this immune cell or being passed from neutrophils to macrophages. This phenomenon has been observed in the zebrafish model for *S. aureus* infection previously (Serba, 2015), however as only neutrophils are labelled in the transgenic line used during this experiment it is not possible to definitively determine which of these 3 events has occurred.

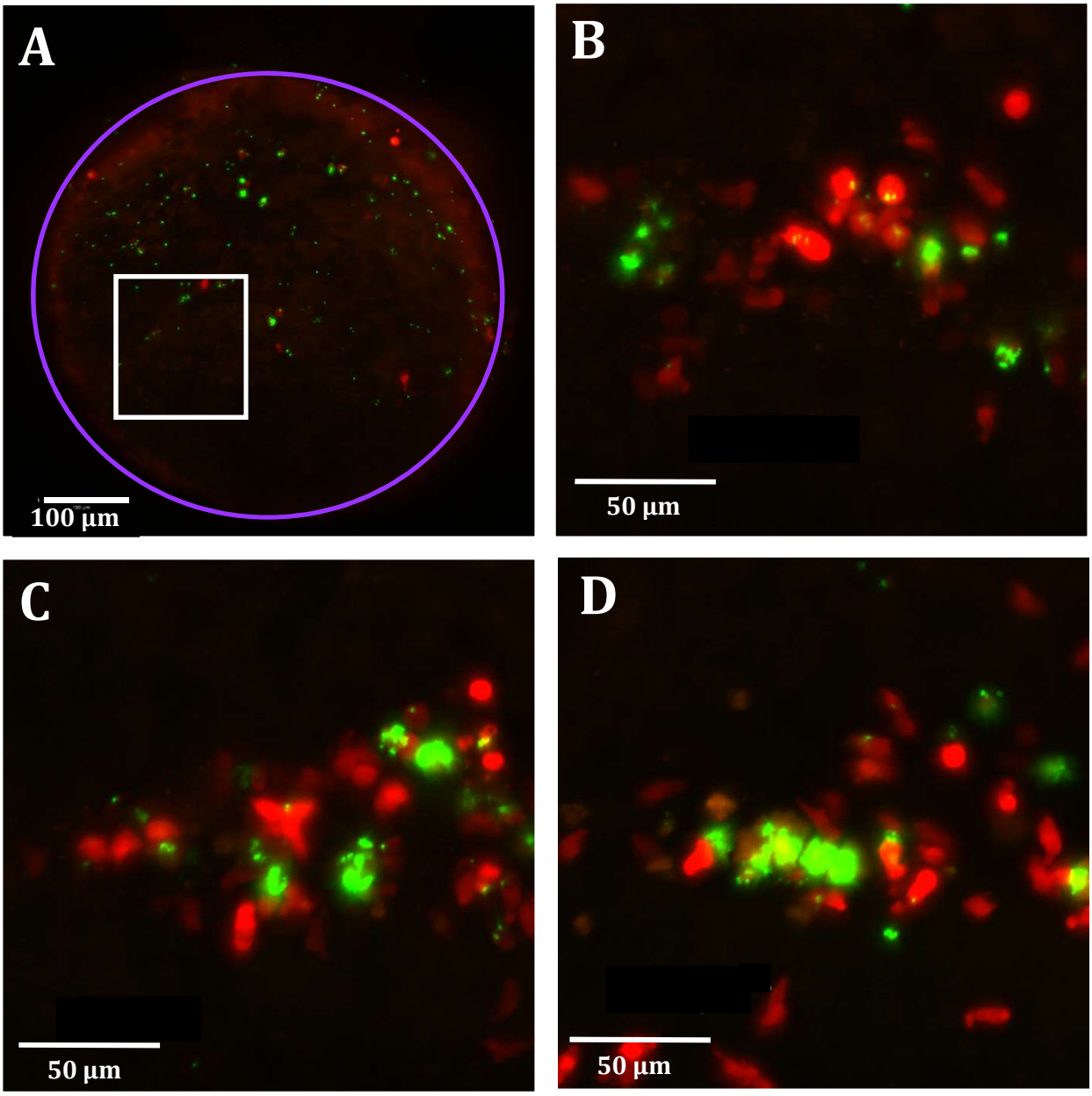

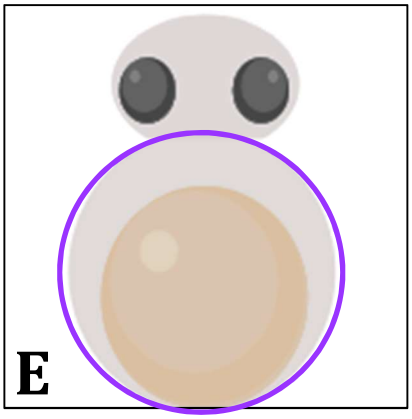

Figure 4.1 Early stages of infection

MaxIP of *Tg*(*lyz.nfsb*:mCherry)^{SH260} embryo (with mCherry labelled neutrophils) infected with SH1000-GFP **A)** whole FOV of circulation over yolk sac 1 hpi, extracellular bacteria visible within circulation, white box indicates ROI magnified in subsequent timepoints (B,C and D) **B)** 5.5 hpi bacteria are visible within neutrophils **C)** 14.5 hpi neutrophils are recruited to site of initial bacterial aggregation **D)** 21 hpi small extracellular bacterial aggregate not phagocytosed by neutrophils recruited to site **E)** schematic of embryo in ventral orientation

4.4 *Imaging of established infection highlighting macrophages*

Tg(*mpeg.*mCherry:CAAX)^{SH378} (mCherry labelled macrophages) embryos were infected with SH1000-GFP, and at 28 hpi embryos with visible lesions were imaged by LSFM. The topology of a typical lesion was reconstructed in 3D, a projection of this is shown in Figure 4.2. Within the circulation is a large lesion ~120 μm x ~150 μm and with mCherry macrophages on edge of the lesion. The same reconstruction rotating can be viewed in **'Video 5- rotating 3D reconstruction of GFP lesion'**. A large area of yellow co-localistion ~50 μm x ~50 μm, shows macrophages that contain a large number of bacteria, on the periphery of the lesion. Smaller aggregates that could be within unlabelled neutrophils are visible within the circulation, but there are also individual bacteria which can be resolved throughout the circulation as *S. aureus* disseminates throughout the host.

When trying to image embryos with formed lesions, embryos with bacteria spread over the endocardium of the heart have been observed; an example of this is shown in Figure 4.3, a *Tg*(*fms*:GFP)^{SH377} embryo (GFP macrophages) infected with JE2-mCherry. Multiple bacterial aggregates are within the oedema, above the circulation valley of the embryo which has been imaged; some of these could be within unlabelled neutrophils but some aggregates are larger than the expected size of neutrophils (> 15 μm). Individual bacteria can be resolved within the ROI and over the endocardium. Due to movement of the heart it is difficult to focus directly over the area; rapid continuous imaging (FOV images every 40s) allows for resolution of different volumes of the heart over successive timepoints. This movement causes nearby (or adherent) immune cells to become segmented, appearing as multiple cells. A video of 3D reconstruction of the movement of macrophages around the bacterial aggregates and infected endocardium can be viewed in **'Video 6 – fmsGFP JE2 mCherry endocarditis like reconstruction'**. Whilst movement over the heart artificially increases the number of macrophages in the ROI, segmentation co-localisation analysis performed in Arivis shows that 96% of macrophages in within the FOV contain JE2-mCherry.

After infection of *Tg*(*mpeg.*mCherry:CAAX)^{SH378} embryos (mCherry macropahges) infected with SH1000-GFP were mounted in 0.8 % (w/v) LMP agarose imaged 44 hpi by LSFM. A layer of SH1000-GFP covering the endocardium was observed, where individual bacteria can be resolved. To image movement of the heart with bacteria, a single slice (1 μm) was acquired continuously, as fast as acquisition would allow for 40 timepoints in 15 s. Figure 4.4 shows four successive timepoints (35-38) with individually resolved *S. aureus* and two macrophages. This quick timecourse can be viewed in '**Video 7 – Single slice timecourse SH1000-GFP infected endocardium'**.

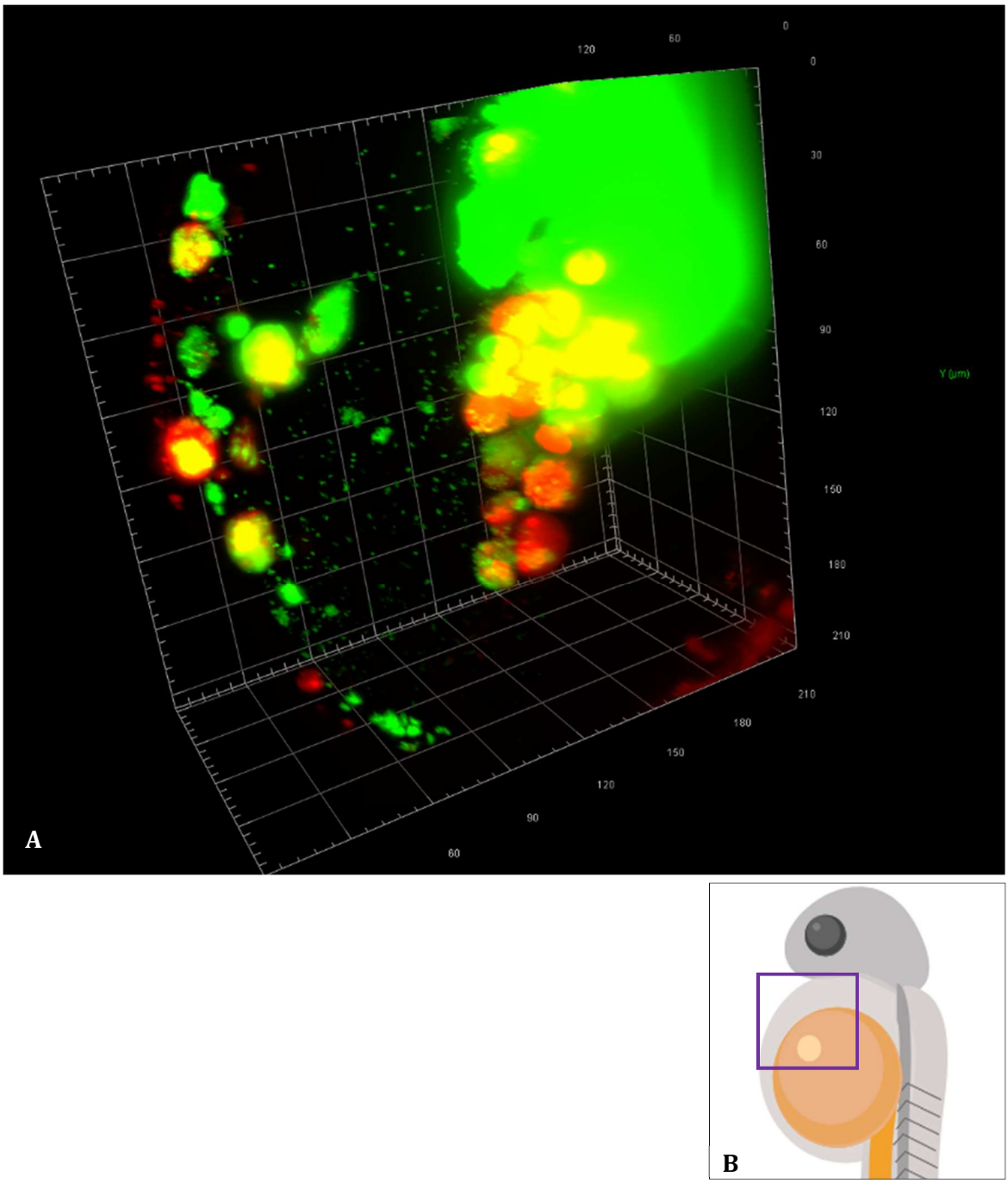

Figure 4.2 3D projection of GFP lesion within embryo with mCherry macrophages

A) *Tg*(*mpeg*.mCherry:CAAX)^{SH378} (embryo with mCherry labelled macrophages) infected with SH1000-GFP with large lesion was imaged 28 hpi by LSFM and reconstructed in 3D with Arivis Vision 4D. Gridlines are 30 µm x 30 µm, minor gradation are 6 µm. Macrophages are observed on the edge of the lesion and contain many bacteria. Individual bacteria which have disseminated from the lesion are also observed within the circulation. **B)** Schematic of embryo in lateral orientation, purple box for approximation of region of reconstruction.

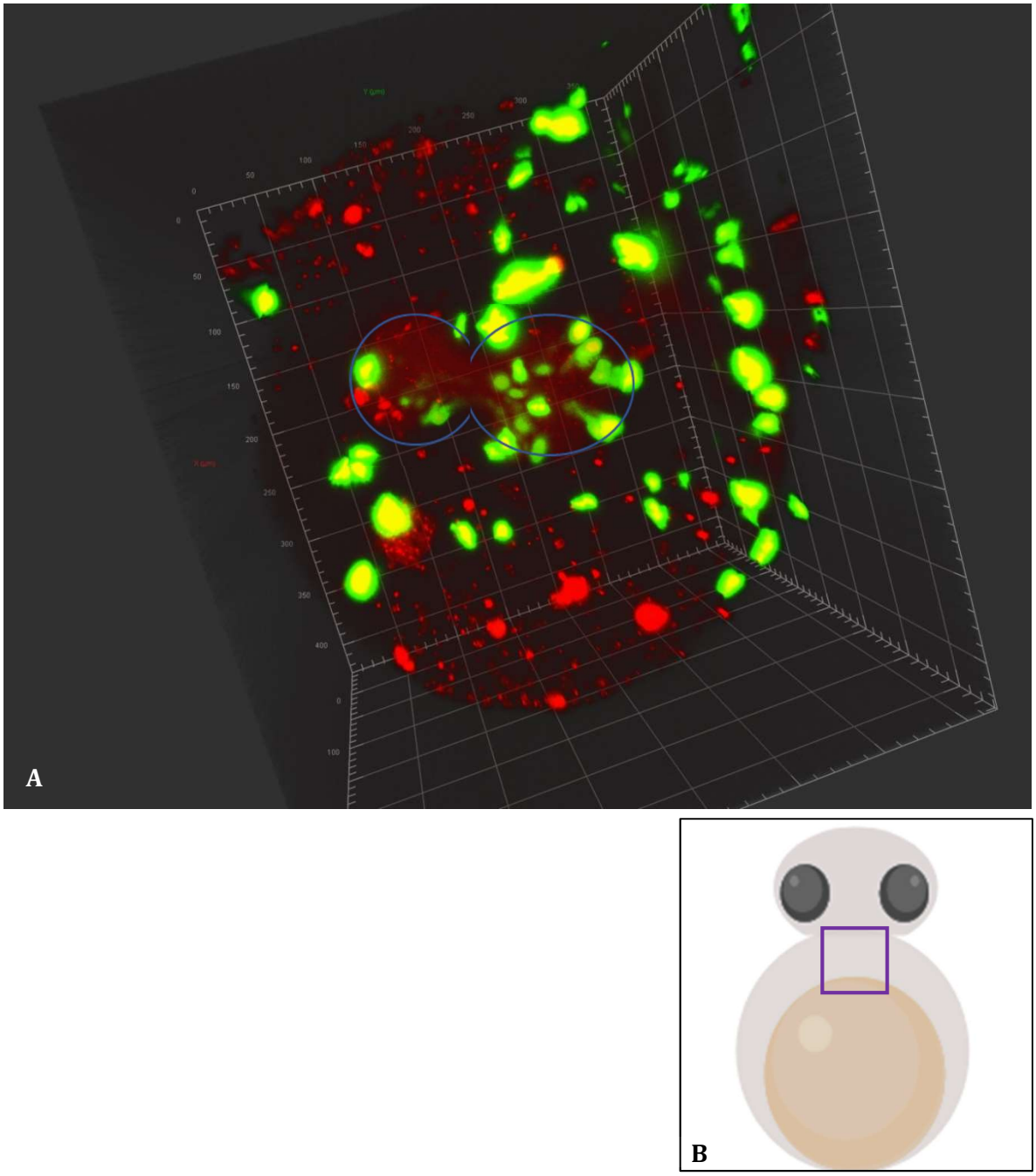

Figure 4.3 3D reconstruction of embryo with GFP macrophages infected with JE2-mCherry, with bacteria covering endocardium

A) *Tg*(*fms*:*GFP*)^{SH377} (GFP labelled macrophages) embryo infected with JE2-mCherry, was imaged 26 hpi by LSFM and reconstructed in 3D with Arivis Vision 4D. The region imaged is an oedema formed in the circulation. Blue ellipses highlight region of bi-valve heart, where bacteria are attached to the endocardium. Gridlines are 50 µm x 50 µm, minor gradations are 10 µm. **B)** Schematic of embryo in venteral orientation with purple box for approximation of region of reconstruction

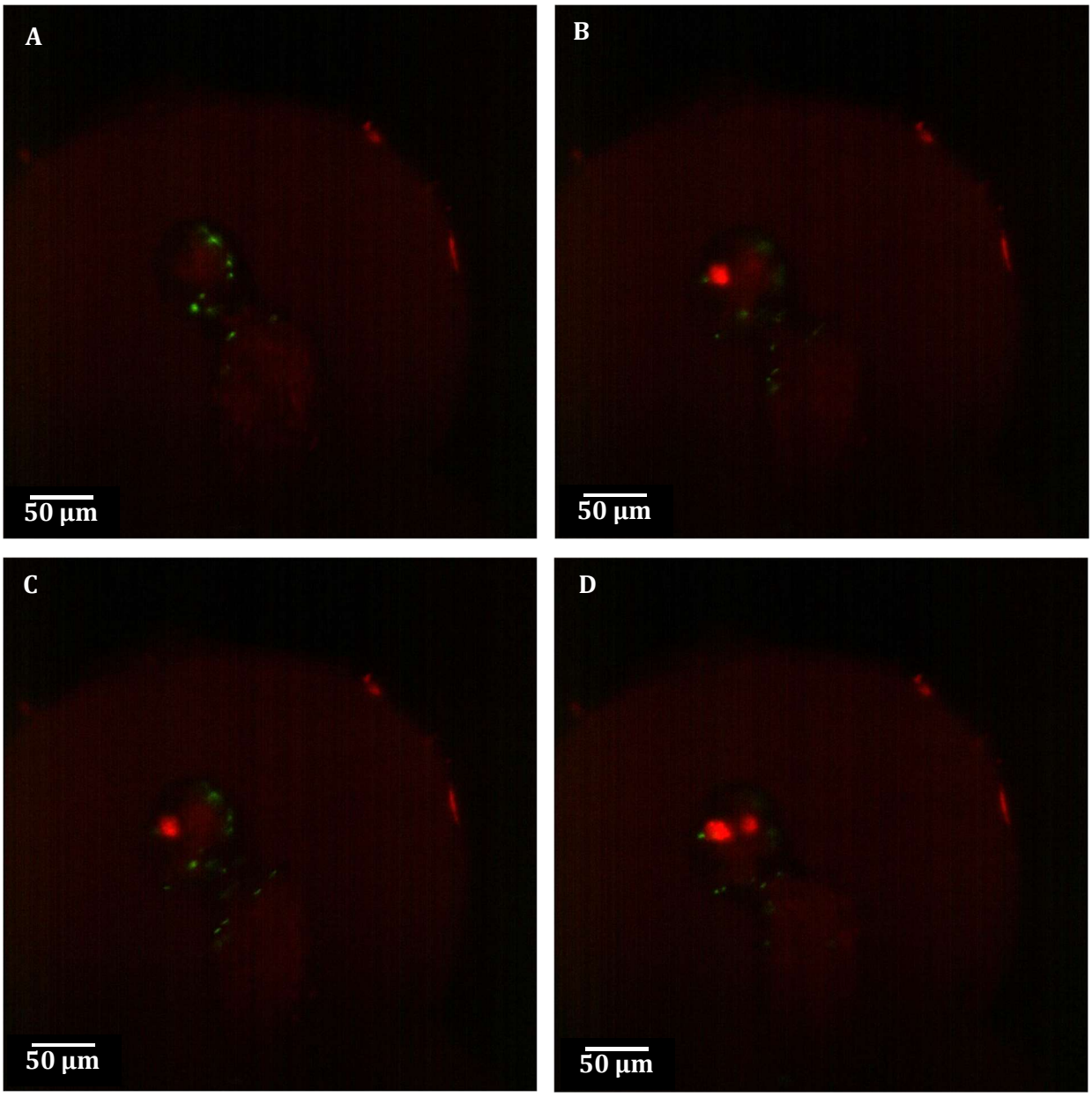

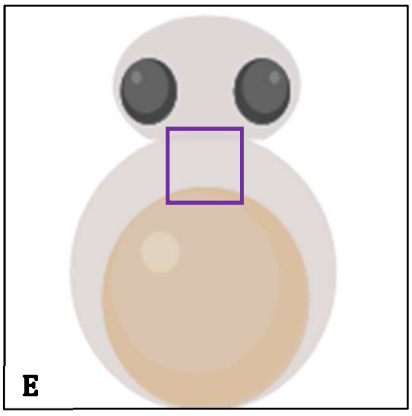

Figure 4.4 Single slice of infected endocardium

Individual slice (1µm) of *Tg*(*mpeg*.mCherry x CAAX)^{SH378} embryo (mCherry macrophages) infected with SH1000-GFP imaged by LSFM 44 hpi. Slice is centred on the heart inside of an oedema. Images were acquired as fast as possible, every 0.375 s for 15 s **A)** timepoint 35 (13.12 s) **B)** timepoint 36 (13.50 s) **C)** timepoint 37 (13.88 s) **D)** timepoint 38 (14.25 s). GFP *S. aureus* attached to the endocardium move in the FOV with the heartbeat. **E)** Schematic of embryo in venteral orientation with purple box for approximation of region of imaging

4.5 *Imaging of established infection highlighting labelled neutrophils*

Tg(*lyz.nfsb*:mCherry)^{SH260} (with mCherry labelled neutrophils) embryos with visible lesions were imaged 20 hpi. An embryo with a typical large lesion was reconstructed in 3D, and a projection the lesion topology of the lesion is shown in Figure 4.5. Within the circulation of this embryo is a large lesion ~250μm x ~200μm and mCherry neutrophils are present nearby. The same reconstruction rotating can be viewed in **'Video 8- rotating 3D reconstruction of GFP lesion mCherry neutrophils'**. There are 6 neutrophils near the lesion, with two that have internalised bacteria near an area of less dense bacteria. This embryo had a high bacterial burden of 2.8 x 10^7 CFU when enumerated after imaging. Focus of bacteria and neutrophils within this embryo is poor in comparison to other embryos with lower bacterial burden in this experiment imaged with comparable acquisition parameters, 3D reconstruction's of these can be viewed in **'Supplementary video 1 – lyz mCherry 6.3 x 10^4 SH1000-GFP'** and **'Supplementary video 2 - lyz mCherry 9.8 x 10^4 SH1000-GFP'.** It is often difficult to focus the lightsheet on embryos that have a high bacterial burden. It is possible that this is due to increased light scatter through the sample from bacteria within the embryo, much in the way that bacterial growth is measured by a spectrophotometer: as the bacteria become more dense in liquid culture, the scatter increases and a OD_{600} reading is calculated.

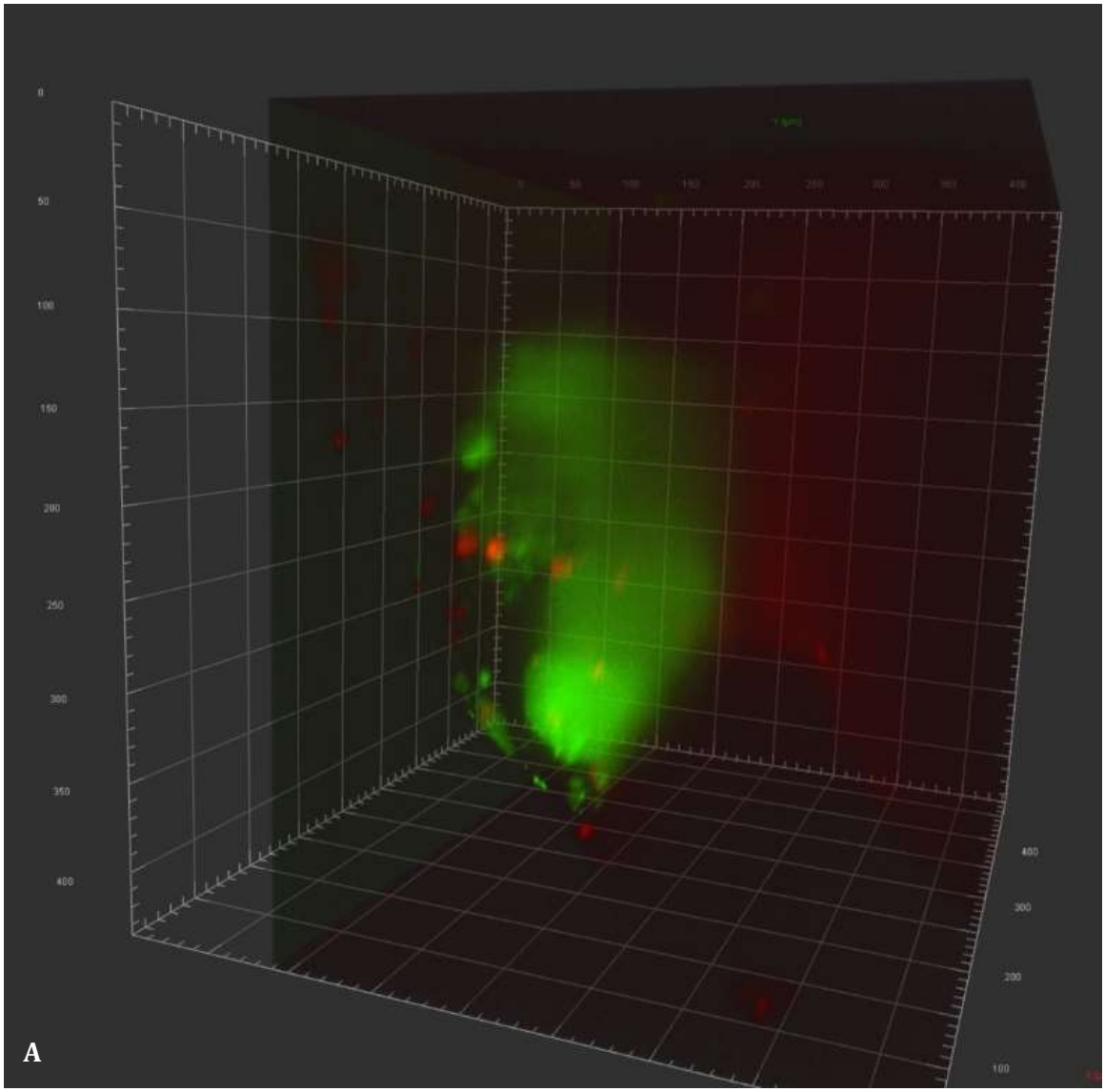

Figure 4.5 3D projection of GFP lesion within embryo mCherry neutrophils

A) *Tg*(*lyz.nfsb*:mCherry)^{SH260} embryo (with mCherry labelled neutrophils) infected with SH1000-GFP with lesion was imaged 20 hpi by LSFM and reconstructed in 3D with Arivis Vision 4D. Gridlines are 50 µm x 50 µm, minor gradations are 10 µm. **B)** Schematic of embryo in venteral orientation with purple box for approximation of region of reconstruction.

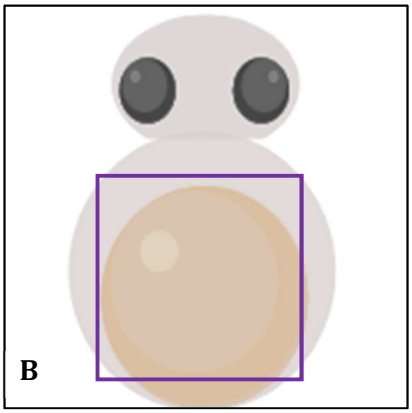

4.6 *Infection dynamics with labelled macrophages*

Tg(*fms*:GFP)^{SH377} embryos (with GFP labelled macrophages) were infected with 2050 CFU JE2-mCherry and mounted for LSFM imaging. After lightsheet adjustments imaging of 6 ROI began 1 hpi and the samples was imaged every 20 minutes. Initially individual bacteria are visible within the circulation. A MaxIP of the 4 FOV acquired ventrally (at the same imaging angle) over the circulation of the infected embryo 1 hpi is shown in Figure 4.6. During the timecourse, a lesion develops at the top of the circulation valley (FOV 2). MaxIP of this FOV in which the lesion develops is shown in **'Video 9– timecourse MaxIP fmsGFP infected with JE2-mCherry view 2'** the video captures 17 hr of imaging, (1-18 hpi). High scatter in this data set makes it more difficult to determine whether the bacteria that founded the lesion came from within a macrophage.

A second ROI acquired 40° rotation from this also captures the development of the JE2-mCherry lesion, MaxIP of this FOV can be viewed in **'Video 10 – timecourse MaxIP fmsGFP infected with JE2-mCherry view 5'**. In both angles over the ROI the initial volume of bacteria that develops into a lesion is not associated with GFP signal from macrophages . A MaxIP which shows the 4 FOV over the circulation, at the last timepoint of this timecourse is shown in Figure 4.7, by this point there are multiple large bacterial aggregates, whilst some of these may be within unlabelled neutrophils, most of these are too large to within a host cell, individual bacteria within the circulation are also visible, indicating infection has disseminated through the circulation. When an embryo has a high bacterial burden there is increased scatter of lights from the sample (as previously mentioned this is possibly a similar phenomenon to measuring bacterial density in a spectrophotometer) to the detection camera, all imaging channels, which is detrimental to focus. Another problem that arises during imaging is that as bacteria replicate exponentially when overwhelming infection occurs, there is increased signal in this imaging channel, which combined with scatter produces out of focus light in the detection plane. The putative site of initial bacterial expansion is shown in a split channel MaxIP (Figure 4.8), due to the high intensity from the mCherry (which sometimes obscures GFP in the MaxIP). A white circle highlights the area that proceeds to expand. There are no labelled macrophages in this region, the bacteria could be within an unlabelled neutrophil (although the size of the 4 aggregates are larger than average sized neutrophils) or they could have expanded from a macrophage either at an earlier timepoint or a region outside of the FOV.

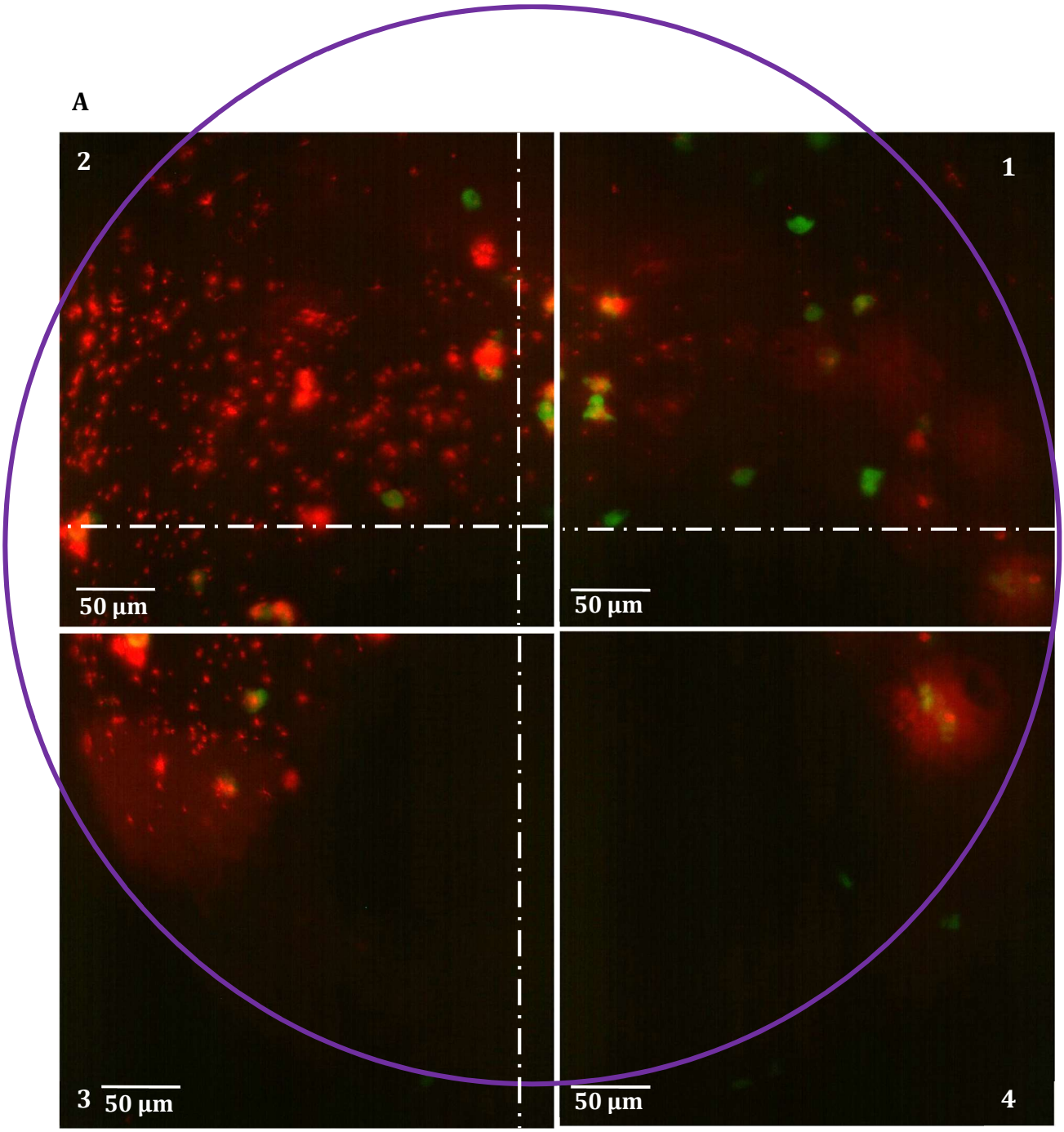

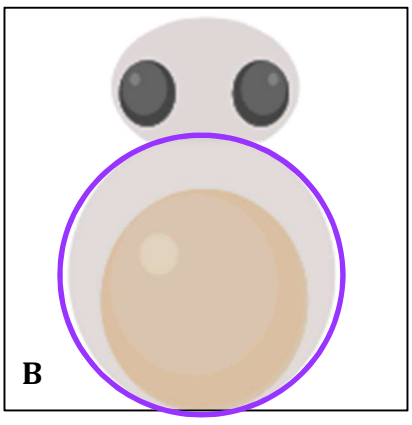

Figure 4.6 1 hpi MaxIP of four FOV over the circulation valley of embryo infected with JE2-mCherry

A) MaxIP of Tg(*fms:*GFP)^{SH377} embryo (with GFP labelled macrophages) infected with JE2-mCherry at 1 hpi. Overlapping FOV were acquired at the same imaging angle to cover the circulation valley (ROI circled in purple). Dashed line shows regions of overlap with adjacent FOV, order of FOV acquisition numbered in outer corner of each image. Individual bacteria can be observed in the circulation prior to phagocytosis **B)** Schematic of embryo in venteral orientation with purple circle for approximation of ROI

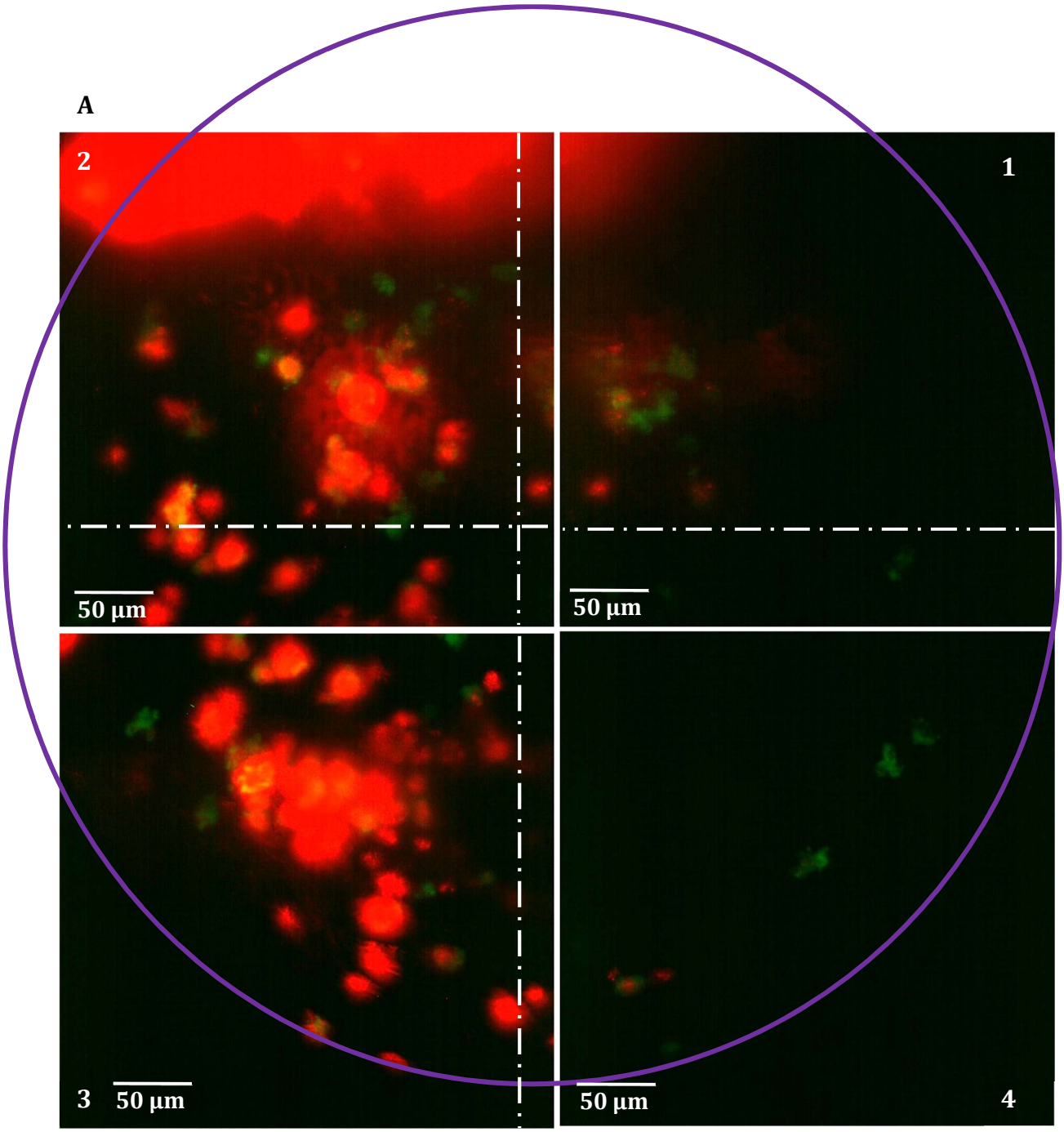

Figure 4.7 18 hpi MaxIP of four FOV over the circulation valley of embryo infected with JE2-mCherry

A) MaxIP of Tg(*fms:*GFP)^{SH377} embryo (with GFP macrophages) infected with JE2-mCherry at 18 hpi. Overlapping FOV were acquired at the same imaging angle to cover circulation valley (ROI circled in purple). Dashed line shows regions of overlap with adjacent FOV, order of FOV acquisition numbered in outer corner of each image. A large lesion can be observed in FOV 1 and a smaller aggregate associated with macrophages is within FOV 3 **B)** Schematic of embryo in venteral orientation with purple circle for approximation of ROI

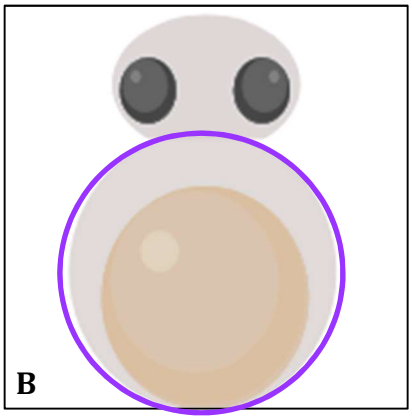

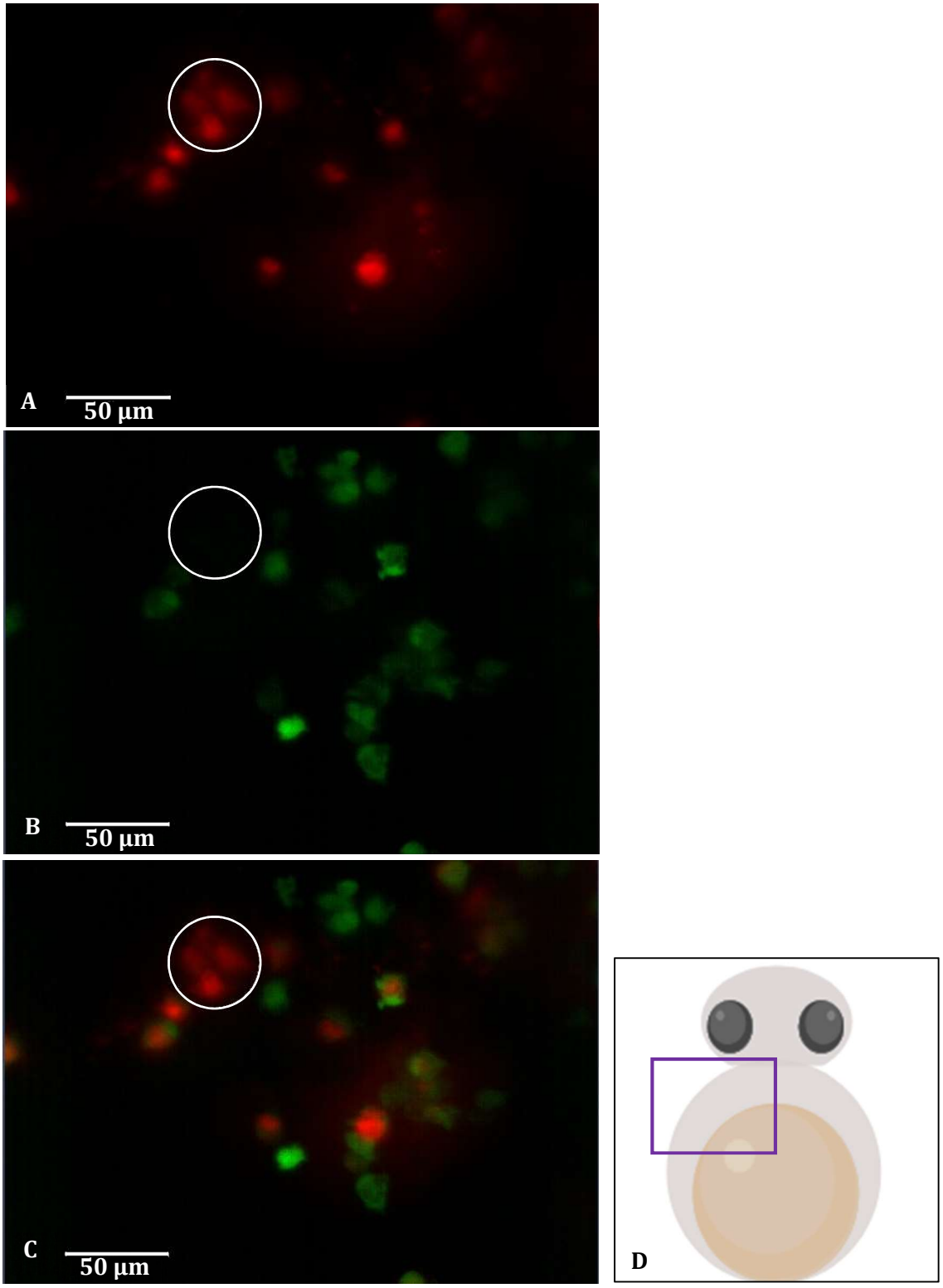

Figure 4.8 MaxIP of FOV 2 of embryo infected with JE2-mCherry

MaxIP of Tg(*fms:*GFP)^{SH377} embryo (with GFP macrophages) infected with JE2-mCherry at 9 hpi. **A)** GFP channel (macrophages) **B)** mCherry channel (JE2-mCherry) **C)** merge. White circle highlights the putative region of initial bacterial expansion. **D)** Schematic of embryo in venteral orientation with purple rectangle for approximation of FOV

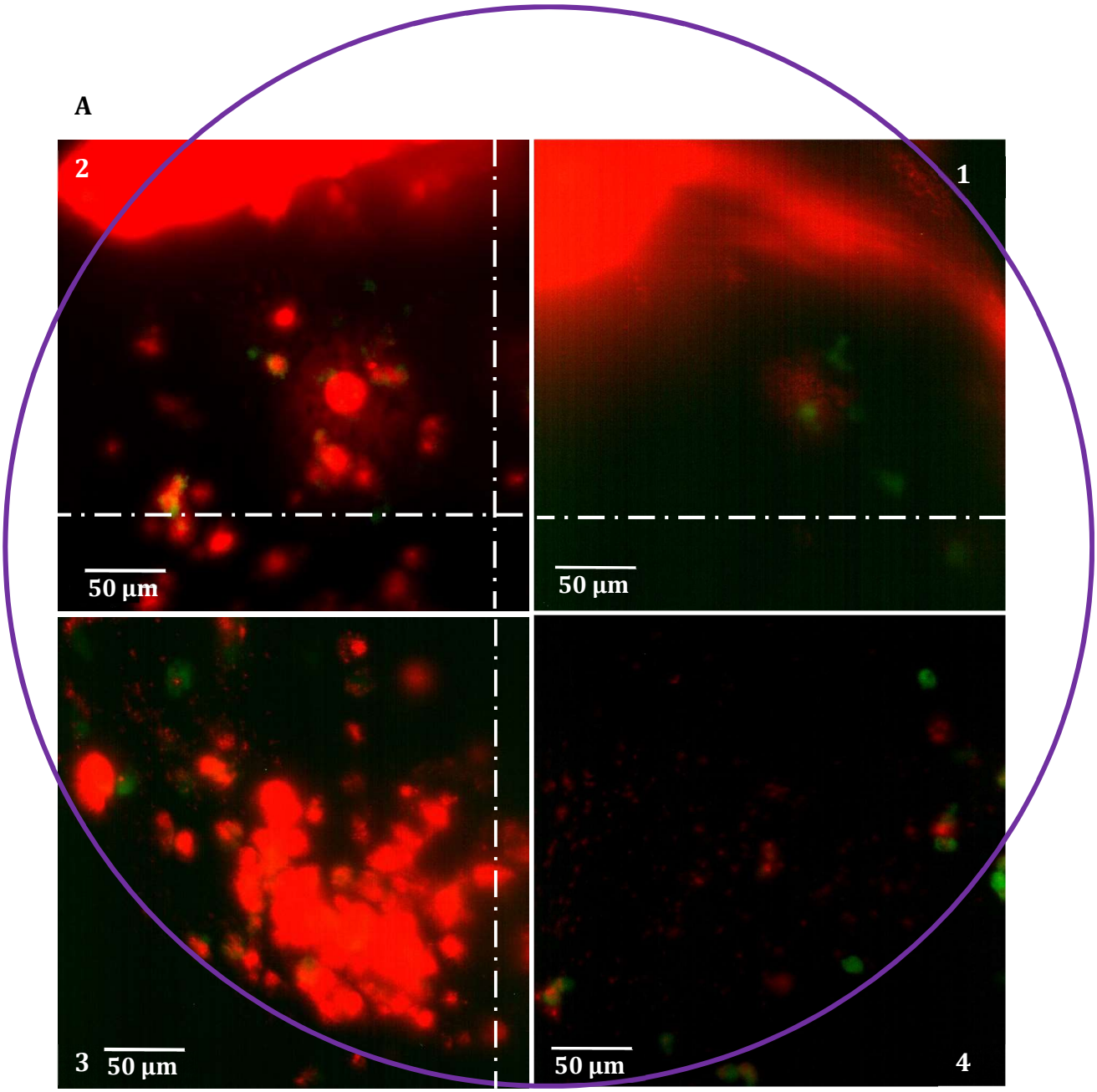

Figure 4.9 20 hpi MaxIP of four FOV over the circulation valley of embryo infected with JE2-mCherry

A) MaxIP of Tg(*fms:*GFP)^{SH377} embryo (with GFP macrophages) infected with JE2-mCherry at 20 hpi. Overlapping FOV were acquired at the same imaging angle to cover the circulation valley (ROI circled in purple). Dashed line shows regions of overlap with adjacent FOV, order of FOV acquisition numbered in outer corner of each image. A large lesion is visible at the top of the circulation valley in FOV **1** and **2** another smaller aggregate is also visible at the bottom of the circulation in FOV **3**. **B)** Schematic of embryo in venteral orientation with purple circle for approximation of ROI

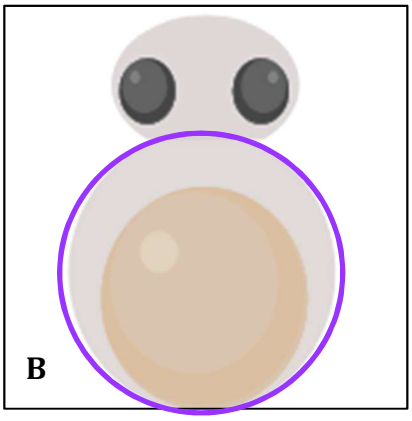

In another independent experiment *Tg*(*fms*:GFP)^{SH377} embryos (with GFP labelled macrophages) were infected with 2140 CFU JE2-mCherry and mounted for LSFM imaging. The timecourse experiment began 1 hpi and extracellular bacteria are visible within the circulation, MaxIP of four FOV over the circulation is shown in Figure 4.11. Two additional FOV were imaged at 42° rotation (FOV 2) from FOV 3 and 30° rotation (FOV 1) from FOV 4. A MaxIP of the timecourse in FOV 2 is shown in **'Video 11 – MaxIP timecourse of embryo with GFP macrophages infected with JE2-mCherry – endocarditis to overwhelming infection'** During the course of imaging initially bacteria are phagocytosed and then infection spreads over the endocardium (Figure 4.11A) and finally infection progresses through the circulation valley (Figure 4.11B). There were 3.1 x 10^6 CFU were recovered from this sample at 20 hpi when the timecourse was terminated.

At 7 hpi bacteria the mCherry signal becomes visible in the region of the heart (and as such is out of focus) a split channel MaxIP of FOV 2 at this time point is shown in Figure 4.12, (the area is circled in white). From this viewing angle it seems that there are no macrophages present and that this bacteria that are moving with the heart are outside of a phagocyte (possibly on the endocardium) or within unlabelled neutrophils. However, inspection of the same volume from FOV 3 has a macrophage with internal bacteria, split channel MaxIP shown in Figure 4.13. Whilst the two FOV are acquired instantaneously of one another, movement of the heart in this region will disrupt the position of nearby immune cells and it is not likely the heart would be imaged in the same position from one heartbeat to the next. The macrophage in this area in Figure 4.13 resembles the macrophage next to the circled area in Figure 4.12 and it is possible this macrophage was moved by the heart in between the FOVs being acquired. By 7.66 hpi bacteria are spreading over the endocardium a MaxIP of FOV 2 at this timepoint is shown in Figure 4.14. Although the mCherry signal from the region of the heat is blurred, there are only two small areas of GFP signal in this region and these could be from the same macrophage as the heartbeat multiplies & segments immune cells as previously described. When looking at FOV 3 (split channel MaxIP shown in Figure 4.15) at the same timepoint no macrophages are visible in the region of the heart. From this timepoint onwards the mCherry signal from *S. aureus* in the region of the heart increases. It is not possible to perform colocalization analysis on the timepoints at which bacteria are spread over the endocardium due to movement in the volume caused by the heart. However, from 8 hpi onwards the mCherry signal in this region increases rapidly and it is unlikely that bacteria occupying regions of this size could be within unlabelled neutrophils. As seen in in **'Video 11 – MaxIP timecourse of embryo with GFP macrophages infected with JE2-mCherry – endocarditis to overwhelming infection'** individual bacteria start to increase within the circulation from 9 hpi and multiple aggregates form within the circulation as infection disseminates.

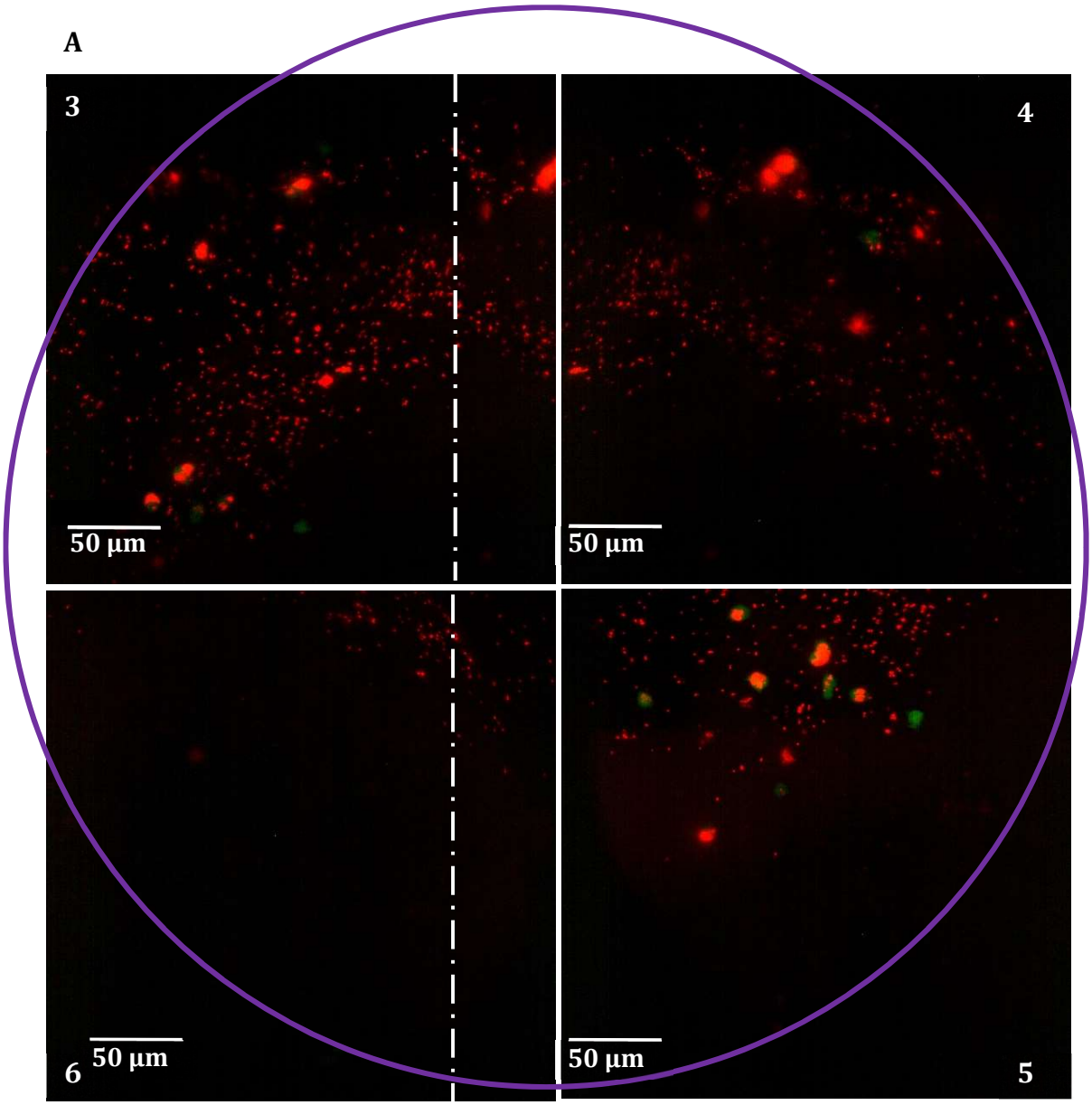

Figure 4.10 MaxIP of four FOV over circulation valley of embryo with GFP macrophages infected with JE2-mCherry

A) MaxIP of *Tg*(*fms:*GFP)^{SH377} embryo (with GFP macrophages) infected with JE2-mCherry at 1 hpi. Overlapping FOV were acquired at the same imaging angle to cover circulation valley (ROI circled in purple). Dashed line shows regions of overlap with adjacent FOV, order of FOV acquisition numbered in outer corner of each image. **B)** Schematic of embryo in venteral orientation with purple circle for approximation of ROI.

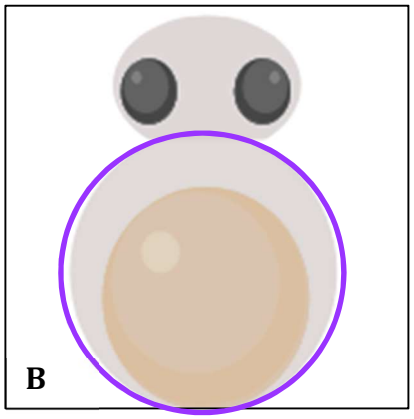

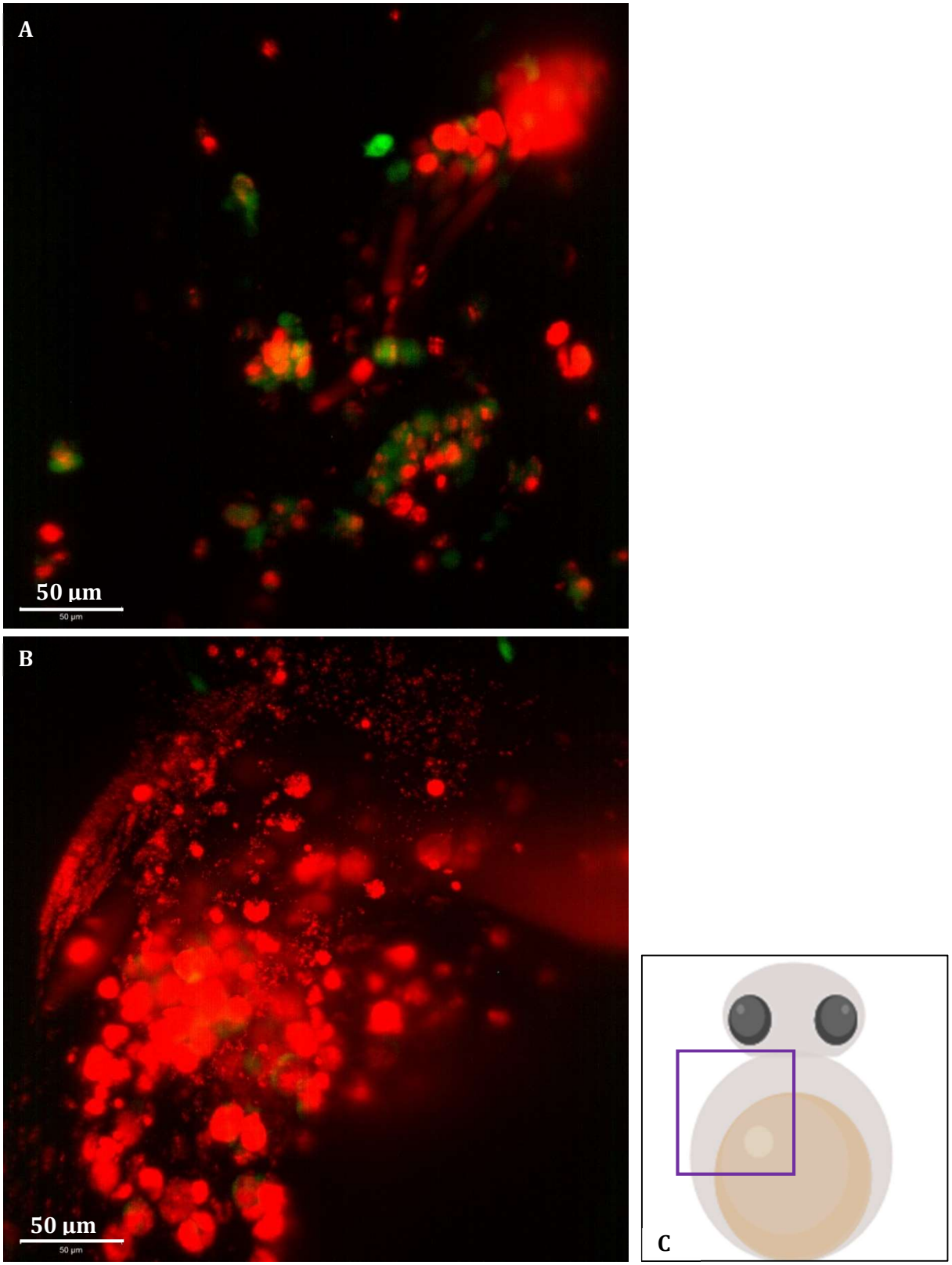

Figure 4.11 MaxIP of embryo with labelled macrophages infected with JE2-mCherry

A) MaxIP of Tg(*fms:*GFP)^{SH377} embryo (with GFP macrophages) infected with JE2-mCherry at A)11 hpi **B)** 20 hpi **C)** Schematic of embryo in venteral orientation with purple box for approximation of FOV

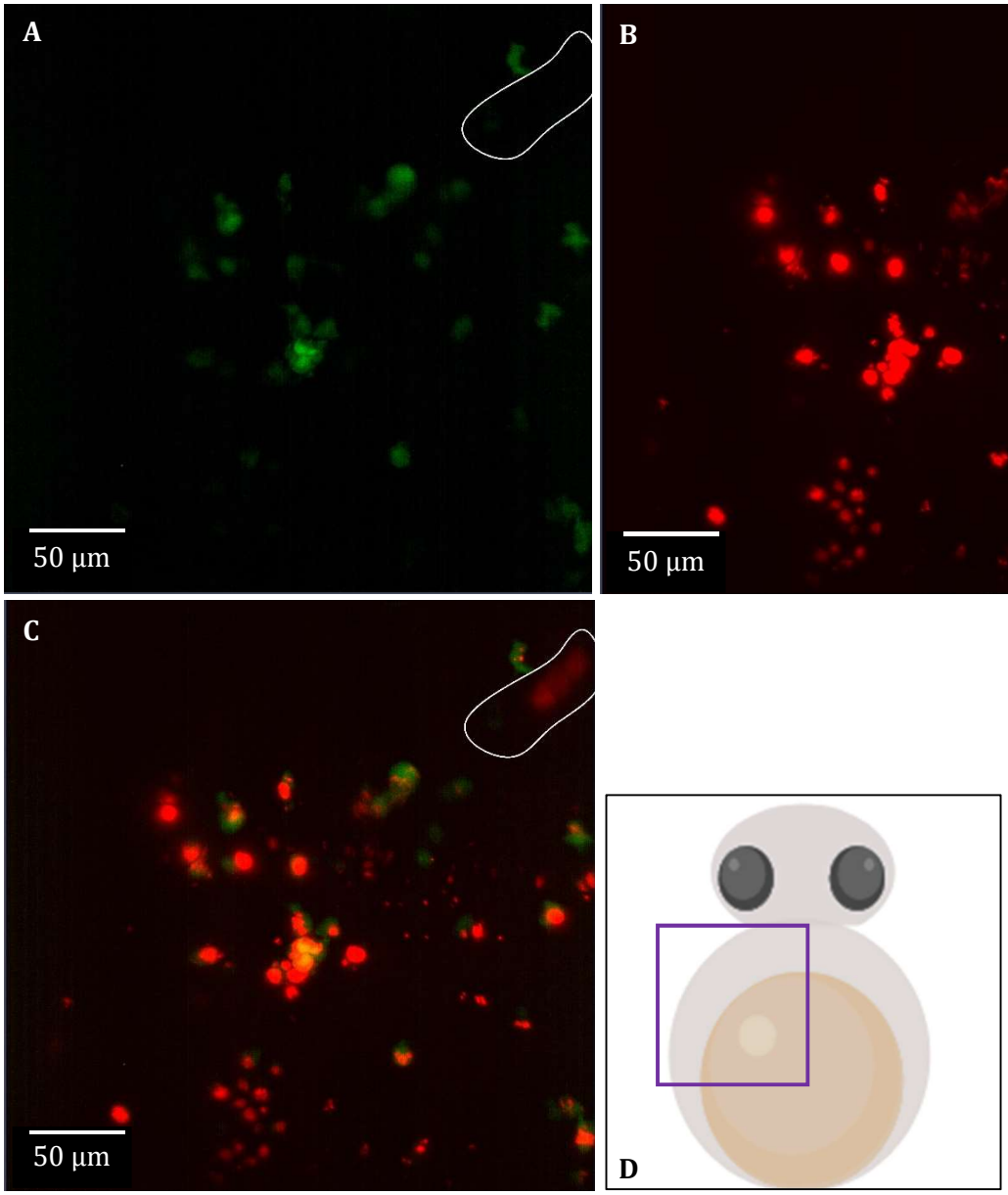

Figure 4.12 Split channel MaxIP of FOV 2 of embryo with GFP macrophages infected with JE2-mCherry 7 hpi

MaxIP of Tg(*fms:*GFP)^{SH377} embryo (with GFP macrophages) infected with JE2-mCherry at 7 hpi, FOV 2. **A)** GFP channel (macrophages) **B)** mCherry channel (JE2-mCherry) **C)** merge. White shape highlights region of heart. **D)** Schematic of embryo in venteral orientation with purple box for approximation of FOV

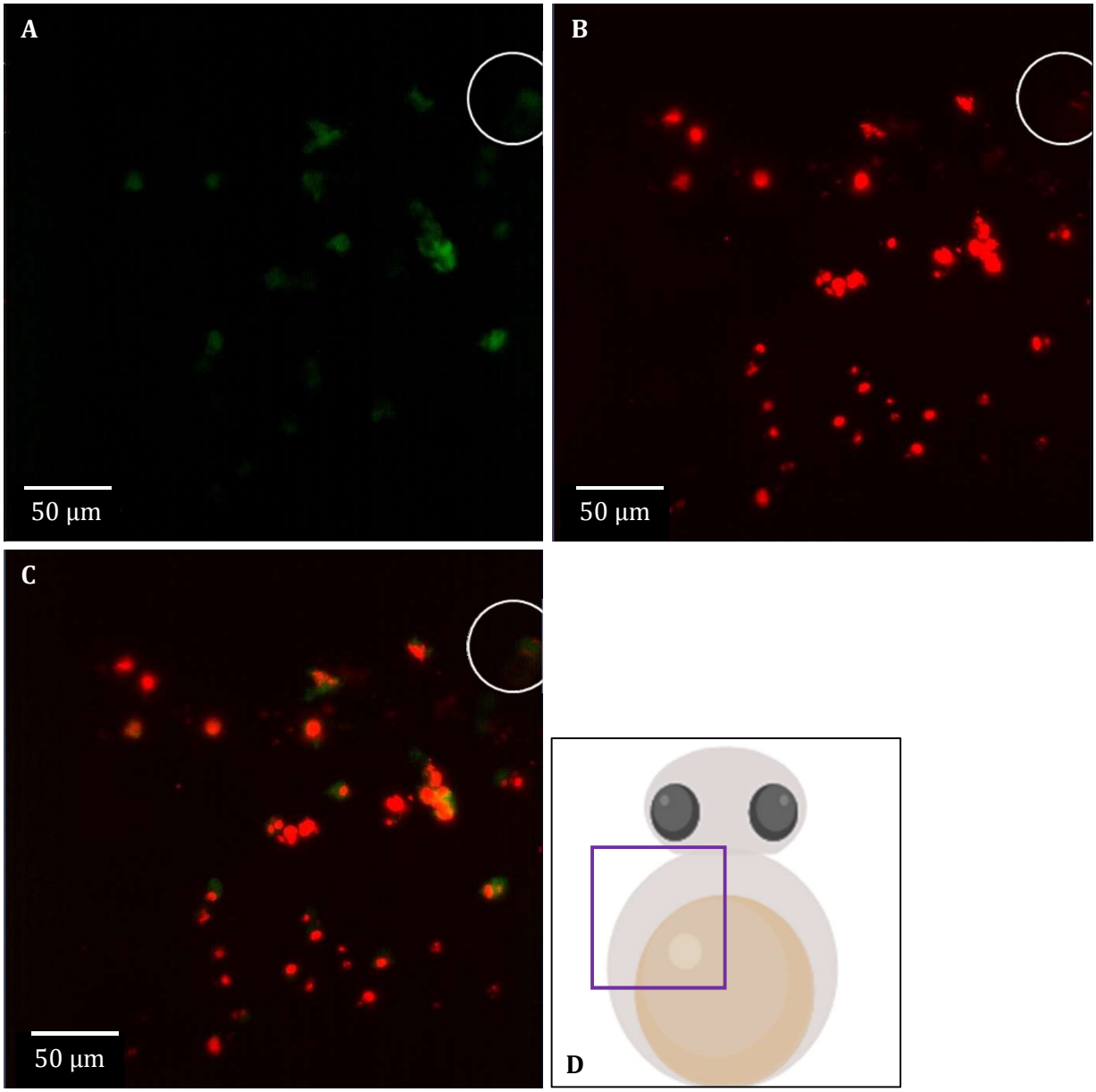

Figure 4.13 Split channel MaxIP of FOV 3 of embryo with GFP macrophages infected with JE2-mCherry 7 hpi

MaxIP of Tg(*fms:*GFP)^{SH377} embryo (with GFP macrophages) infected with JE2-mCherry at 7 hpi, FOV 3. **A)** GFP channel (macrophages) **B)** mCherry channel (JE2-mCherry) **C)** merge. White shape highlights region of heart. **D)** Schematic of embryo in venteral orientation with purple box for approximation of FOV

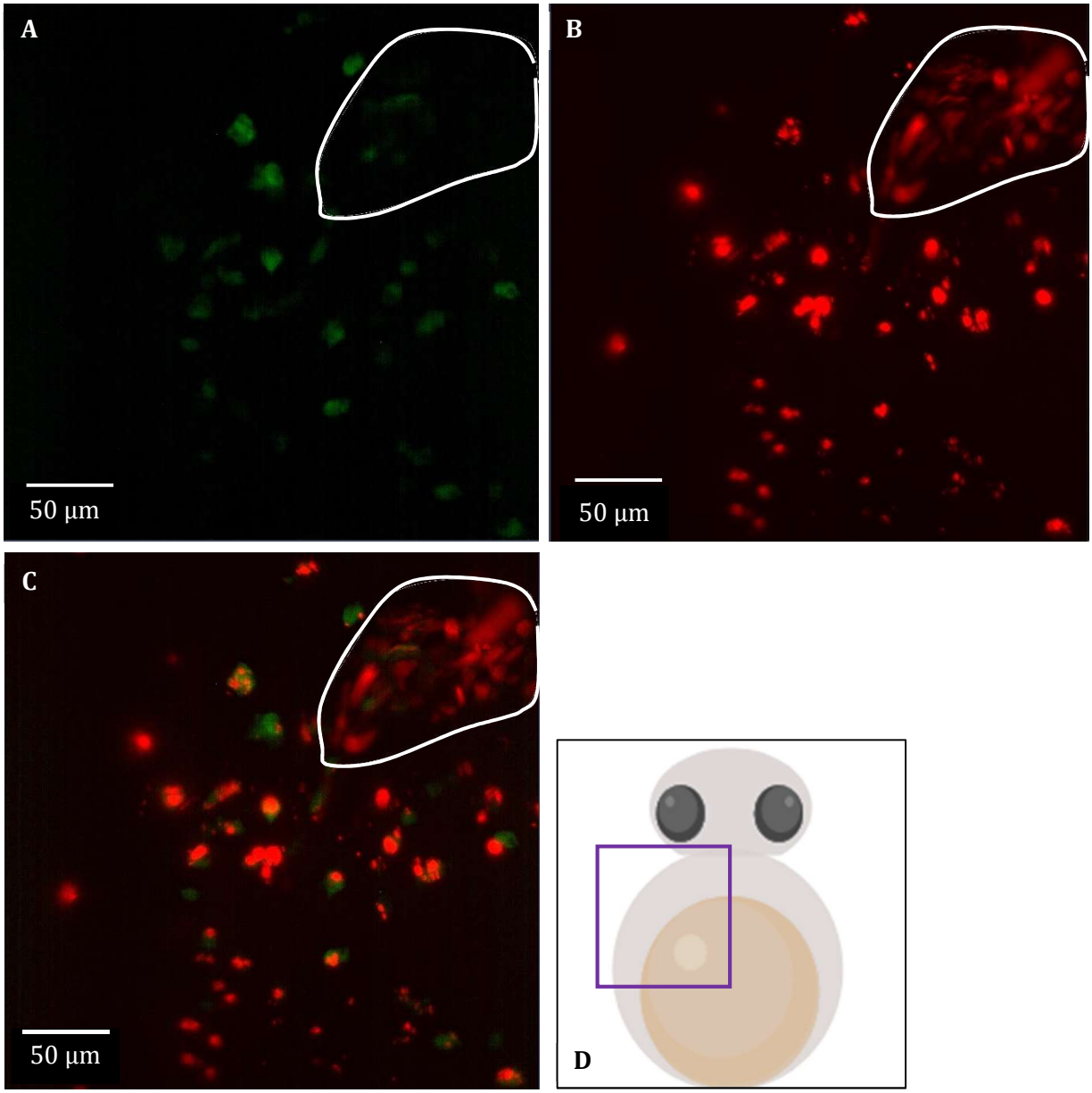

Figure 4.14 Split channel MaxIP of FOV 2 of embryo with GFP macrophages infected with JE2-mCherry 7.66 hpi

MaxIP of *Tg*(*fms:*GFP)^{SH377} embryo (with GFP macrophages) infected with JE2-mCherry at 7.66 hpi, FOV 2. **A)** GFP channel (macrophages) **B)** mCherry channel (JE2-mCherry) **C)** merge. White shape highlights region of heart. **D)** Schematic of embryo in venteral orientation with purple box for approximation of FOV

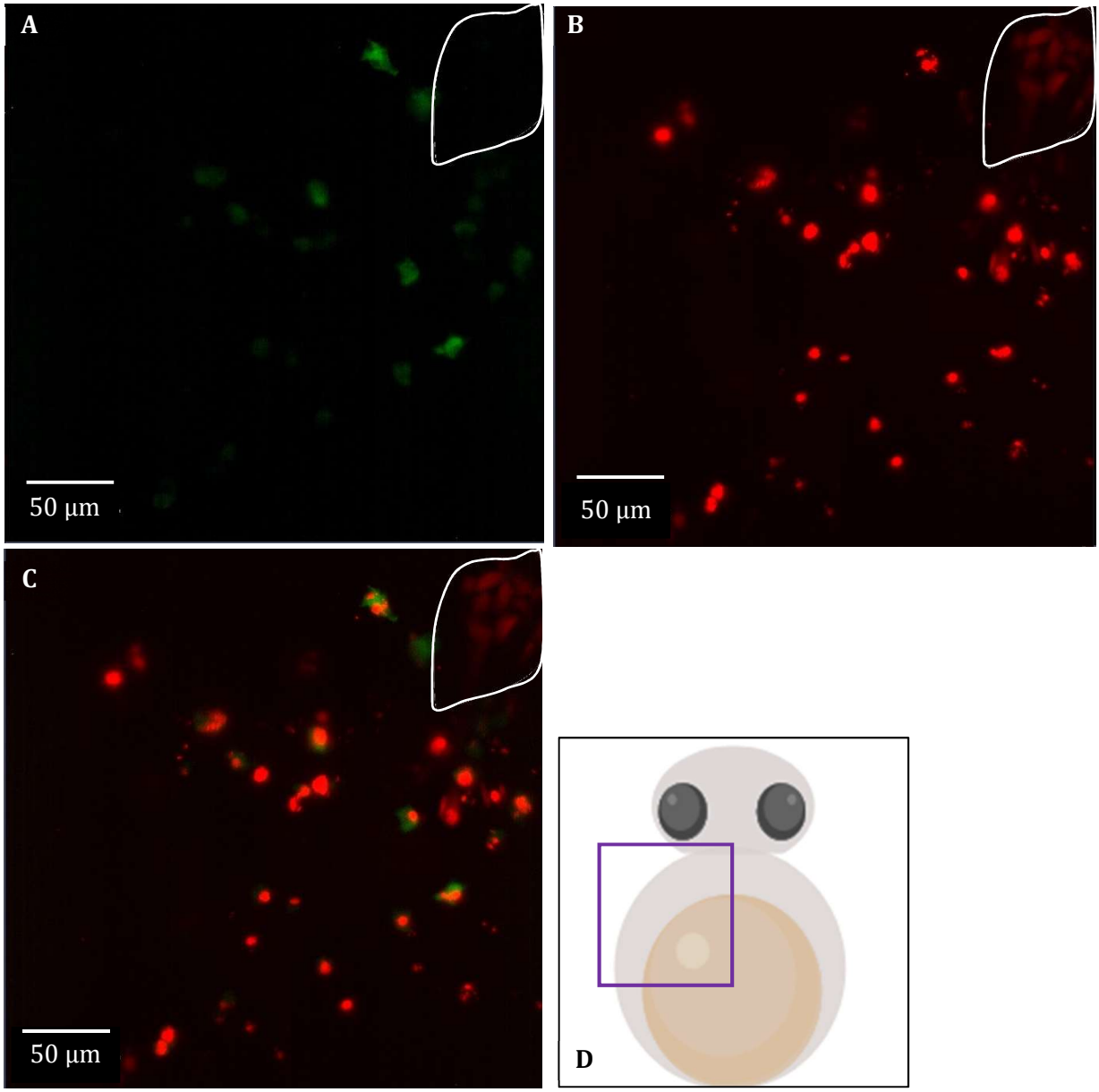

Figure 4.15 Split channel MaxIP of FOV 3 of embryo with GFP macrophages infected with JE2-mCherry 7.66 hpi

MaxIP of *Tg*(*fms:*GFP)^{SH377} embryo (with GFP macrophages) infected with JE2-mCherry at 7.66 hpi, FOV 3. **A)** GFP channel (macrophages) **B)** mCherry channel (JE2-mCherry) **C)** merge. White ellipses = region of heart. **D)** Schematic of embryo in venteral orientation with purple box for approximation of FOV

4.7 *Infection dynamics with labelled neutrophils*

Tg(*lyz*:nsfb.mCherry)^{SH260} embryos (with mCherry labelled neutrophils) were infected with 1600 CFU, SH1000-GFP and mounted for LSFM imaging. After initial set up of the microscope imaging began 2 hpi, the infected embryo was imaged every 15 minutes for 20 h. When recovered from the microscope the embryo had a slow heartbeat and was overwhelmed by infection, the embryo was homogenised and CFU enumerated. The infected embryo had a high bacterial burden of 1.6 x 10^6 CFU and was most likely at the terminal stages of infection.

A MaxIP of infection from the early stages (2 hpi) to endpoint 22 hpi is shown in **'Video 12 – Biofilm like infection progression MaxIP'**. Initially bacteria are still visible within the circulation before being phagocytosed, bacteria that are in small aggregates not inside labelled neutrophils are potentially within unlabelled macrophages. Progression of infection reveals a lesion that rapidly disseminates within the host, forming many large aggregates of bacteria within the circulation valley of the embryo. At 6 hpi the beginnings of this large lesion can be seen, this can be traced back to faint, diffuse GFP signal at 2.5 hpi (Figure 4.16A) there are no mCherry neutrophils in this region prior to initial bacterial spread, suggesting the bacteria could be within an unlabelled macrophage, or are in the circulation valley and have not been phagocytosed. At 3 hpi a neutrophil that does not contain any bacteria is near the region of initial bacterial spread (Figure 4.16B) however there are no neutrophils in this region at subsequent timepoints.

Strikingly within this embryo *S. aureus* has spread over the membrane of the yolk, covering it with a thin layer of bacteria, as well as thicker parts and multiple additional bacterial aggregates A 3D reconstruction of the infected embryo at 20 hpi this can be viewed in '**Video 13 – biofilm like infection 3D rotation'**. Figure 4.17 shows an individual slice (0.54µm in thickness) from the ROI at A) 22 hpi & B) 25 hpi bacteria that have spread over the membrane of the yolk can be individually resolved and there is an increase in the number of bacteria in this focal plane between these two timepoints.

Colocalisation analysis was performed on ROI at 2.5 & 20 hpi, a 3D rendering of the result of this is shown in Figure 4.18. This first identifies mCherry neutrophils by segmentation analysis (size >10µm) then identifies GFP labelled *S. aureus* by segmentation analysis (>2µm). Colocalisation identifies segments identified as *S. aureus* within identified neutrophils. These voxels are represented by yellow centroids in Figure 4.18. At 2.5 hpi, 48 % of identified neutrophils contain *S. aureus* compared with 16.6 % at 20 hpi (only one neutrophil in the FOV) when the embryo is heavily infected.

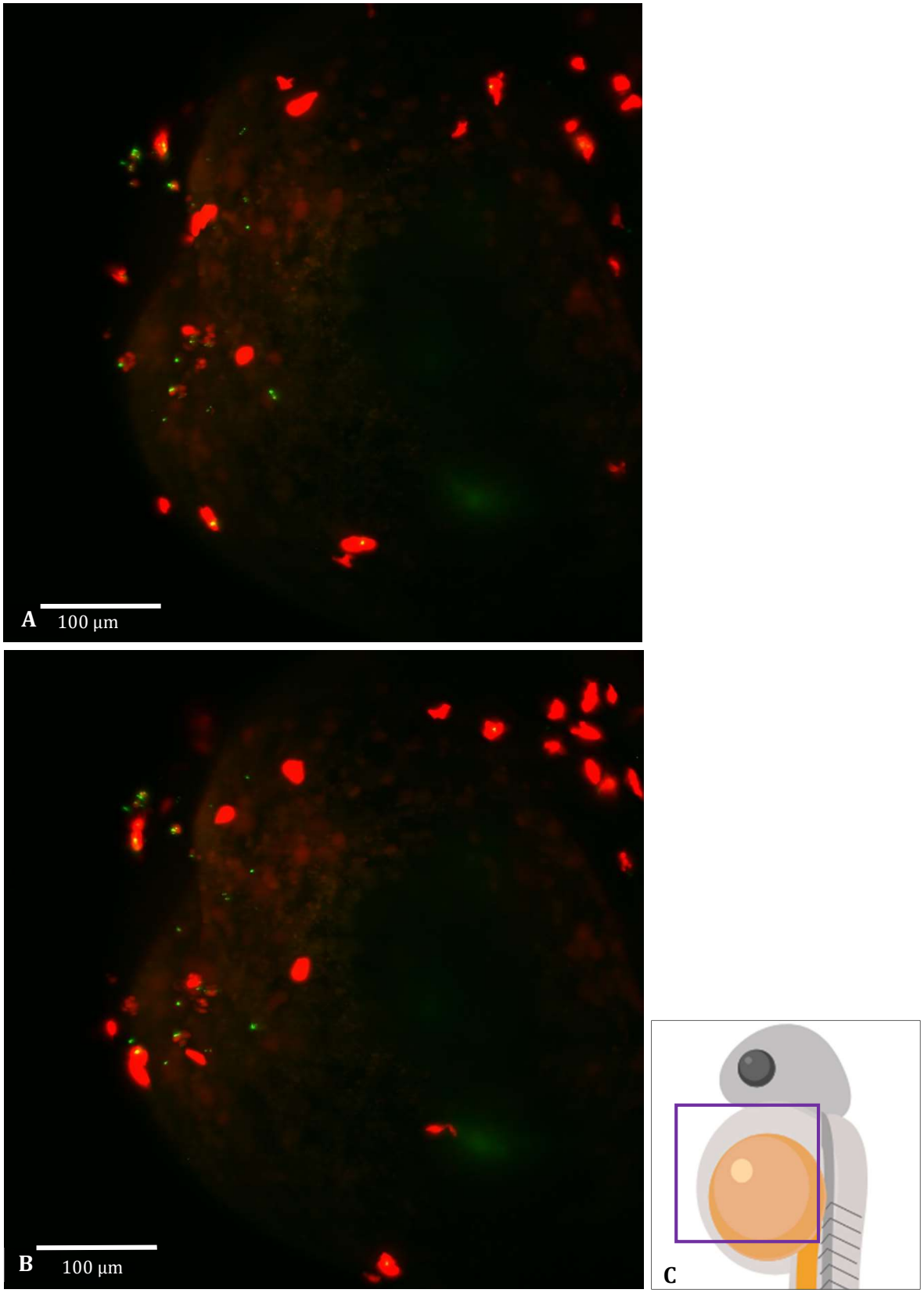

Figure 4.16 MaxIP of initial point of lesion formation

MaxIP of *Tg*(*lyzC*:mCherry)^{SH260} embryo (mCherry neutrophils) infected with SH1000-GFP, imaged by LSFM, at **A)** 3.5 hpi and **B)** 4 hpi **C)** Schematic of embryo in lateral orientation with purple box for approximation of FOV

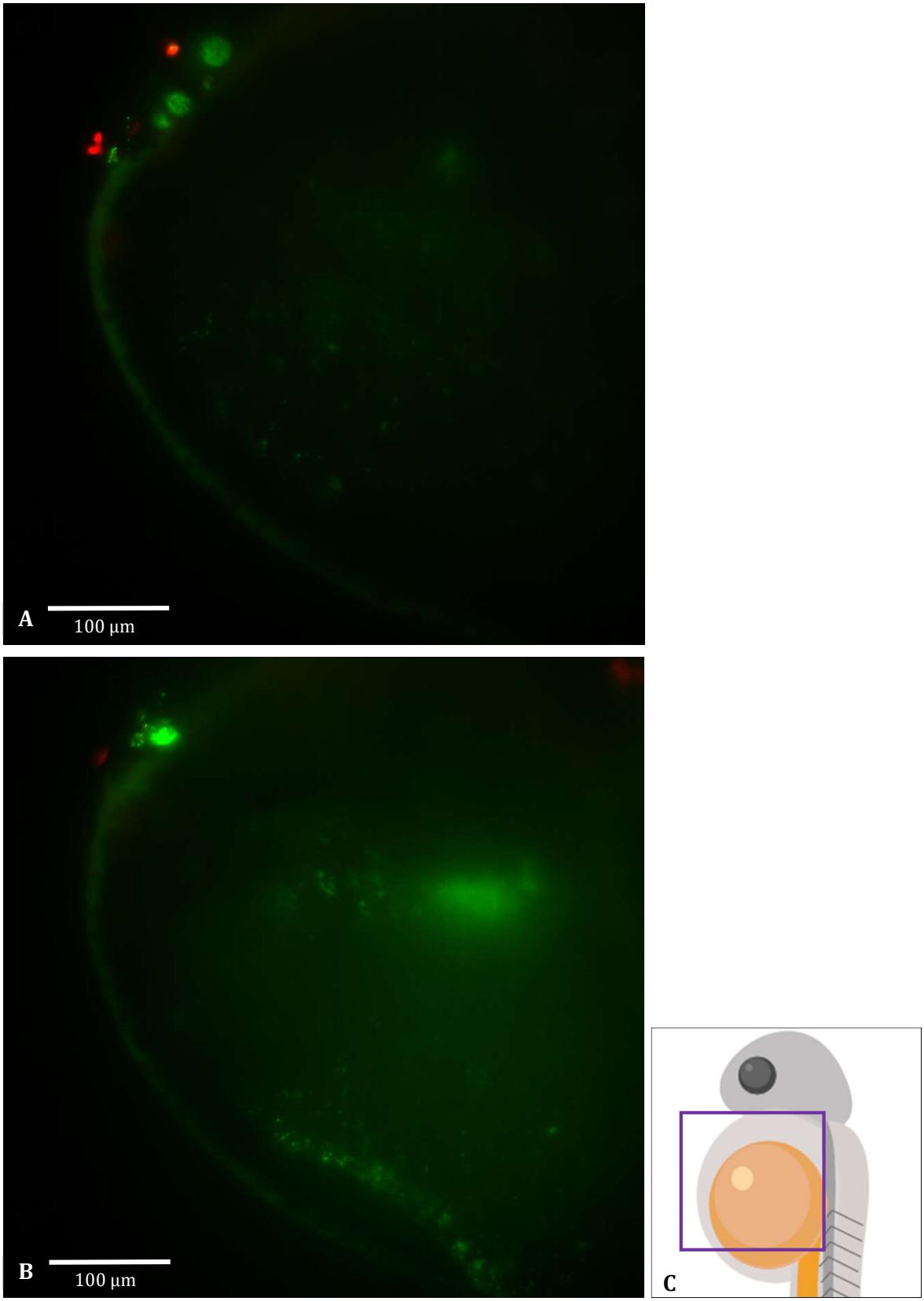

Figure 4.17 Individual slices from embryo infected with SH1000-GFP

Tg(*lyz*:mCherry)^{SH260} embryo infected with SH1000-GFP, imaged by LSFM, individual slice from Z-stack (1µm) acquired at same imaging depth at timepoints **A)** 22 hpi and **B)** 25 hpi **C)** Schematic of embryo in lateral orientation with purple box for approximation of FOV

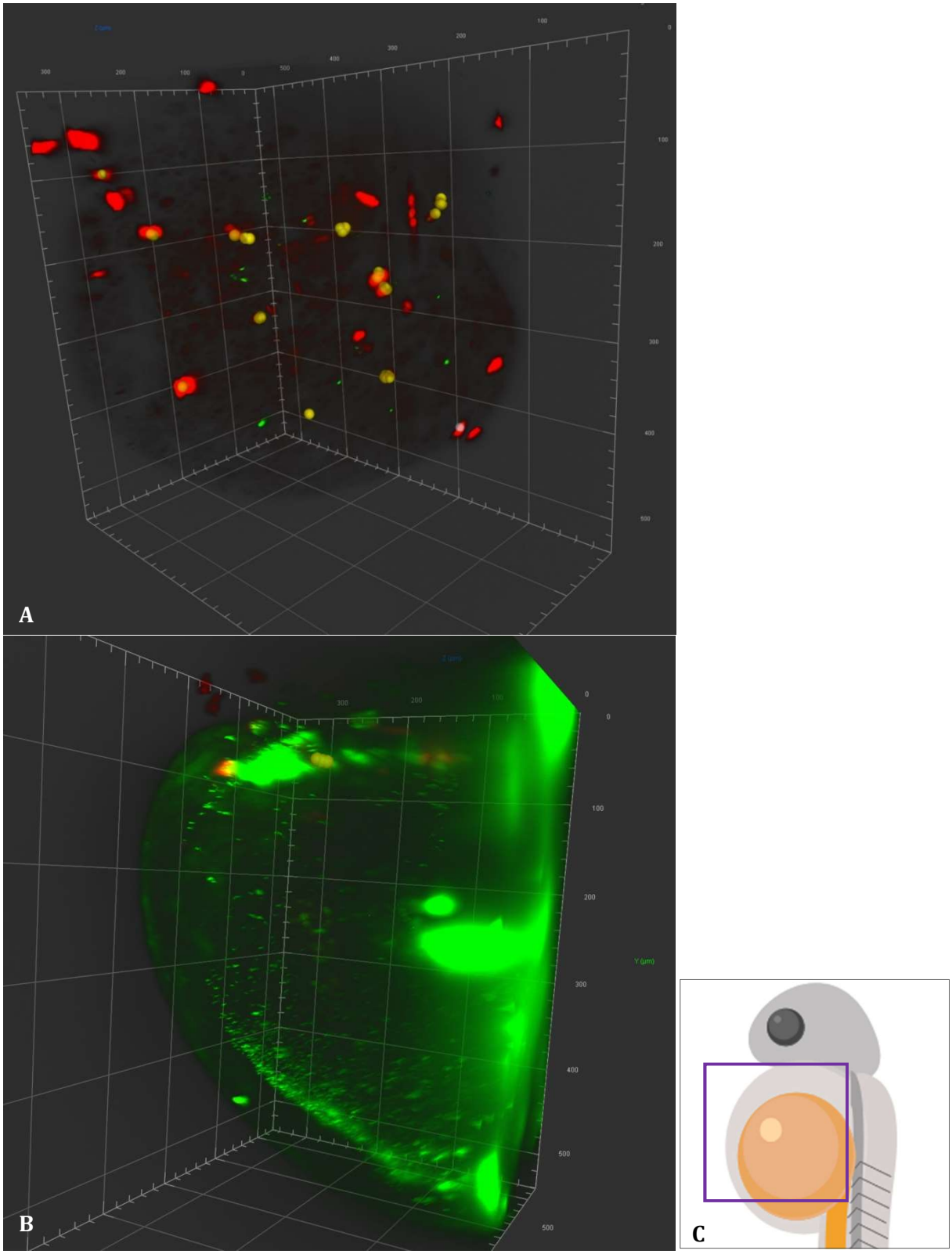

Figure 4.18 Colocalisation anaylsis of embryo infected with SH1000-GFP

3D reconstruction of *Tg*(*lys*:mCherry)^{SH260} (mCherry neutrophils) infected with SH1000-GFP. Colocalisation analysis of SH1000-GFP within mCherry labelled neutrophils was performed in Arivis 4D. Yellow centroids indicate voxel co localisation of GFP & mCherry. Gridlines are 100 µm x 100 µm and minor gradations are 20 µm **A)** 2.5 hpi B) 20 hpi **C)** Schematic of embryo in lateral orientation with purple square for approximation of region of reconstruction.

4.8 *Macrophage depletion*

During long-term imaging experiments following infection progression of *S. aureus* in embryos with labelled macrophages, expansion of bacteria from inside of a neutrophil have not been observed. Furthermore, when following dynamics in embryos with labelled macrophages, many macrophages are phagocytosing bacteria from early in the infectious process and frequently macrophages have a high bacterial load. As macrophages seem to be crucial for controlling systemic infection from initial inoculation and bacterial expansion occurring from 6 hpi onwards it is possible that macrophages are providing a niche for *S. aureus* to replicate within. To test this hypothesis and ascertain the role of macrophages on bacterial expansion embryos were depleted of macrophages prior to infection.

4.8.1 Effect of clodronate on *S. aureus* infection of zebrafish embryos

To elucidate whether macrophages are the niche in which *S. aureus* are expanding within the zebrafish host, LWT embryos were depleted of macrophages by injection with clodronate containing liposomes 24 hpf. Control embryos were injected with liposomes containing PBS. Both groups were infected with JE2-mCherry 30 hpf and survival monitored. Results are shown in Figure 4.19. As expected, survival of macrophage depleted embryos is significantly lower ($P = <0.0001$), with no survival of embryos in the clodronate treated group by 92 hpi.

4.8.2 Effect of macrophage depletion on clonal expansion of *S. aureus*

To investigate infection dynamics of *S. aureus* in a macrophage depleted host, clodronate treated embryos were infected with a mixed inoculum of two isogenic strains in a 1:1 ratio, with different antibiotic markers (Kan & Ery). All dead embryos were collected at regular timepoints and homogenised. Samples were plated out on both plain and selective media after serial dilution for enumeration. Total CFU count per embryo are shown in Figure 4.19B and there is no significant difference ($P = 0.5784$) in bacterial burden between the clodronate liposome treated and control PBS liposome groups. The proportions of strains recovered from macrophage depleted fish at the terminal point are shown in Figure 4.20, and proportions of strains recovered from control PBS treated fish at the terminal point are shown in Figure 4.21. In both macrophage depleted and control groups either of the isogenic strains can predominate, demonstrating there is no fitness benefit to either resistance marker.

For each sample the Shannon diversity index (H) (Equation 1) was calculated for the two isogenic strains and this was used to calculate population evenness, (E_H) (Equation 2) which defines how evenly matched different populations of organisms within a given environment (in this case the embryo) are. E_H of 1 is a balanced mixed population of the two isogenic strains and E_H of 0 means the entire population is comprised of a single strain. Without an immunological bottleneck, it would

be expected that species evenness from samples inoculated with 1:1 ratio of isogenic strains would have a E_H near 1.

$$H = \sum_{i=l}^{s} -(Pi * lnPi)$$

Equation 1 Shannon diversity index

H = Shannon diversity index, Pi = fraction of the entire population made up of species I, S = number of species encountered, Σ sum from species 1 to species S

$$E_H = H/lnS$$

Equation 2 Population evenness

E_H=Population evenness (Shannon equitability), H = Shannon diversity index, , S = number of species encountered

The distribution of population evenness over time is shown in Figure 4.22, linear regression of Figure 4.22A & B (clodronate treated and PBS control respectively) was performed: slope A) was not significantly non-zero (F = 0.116, P = 0.735) therefore there is no linear relationship between species evenness and hpi. Slope B) is significantly non-zero (F = 14.6, P = 0.0009) demonstrating a statistically significant correlation between time of death and decrease in E_H. The observed decrease in E_H shows an increased chance of a population being clonal over time and that these bacteria had likely passed through a population bottleneck. This is in concordance with the findings of Pollitt et al., (2018), who demonstrated a decrease in E_H (increase in clonality) over time in infected LWT embryos.

Comparison of distribution of species evenness between the clodronate treated & PBS control groups was performed by (non-parametric) Mann-Whitney test, the distributions are significantly different (P = 0.0023). This suggests macrophages are a potential immunological bottleneck for clonal expansion of *S. aureus* within the host, however clonal populations are observed in the clodronate treated group at 68 and 74 hpi, this could be due to an increase in macrophages over elapsed time since clodronate treatment, as has been quantified in the zebrafish infection model for *Cryptococcus neoformans* (Bojarczuk et al., 2016).

A previous study implicated neutrophils as the immunological bottleneck and found that there was a significant difference in the variance in ratios of two isogenic strains between groups of transgenic embryos ablated of either neutrophils or macrophages (Prajsnar et al., 2012). However, it is a possibility this could be due to less efficient depletion of the macrophages by metronidazole as opposed to using clodronate liposomes as the method of depletion. This study also infected neutrophil and macrophage depleted embryos at 54 hpf as opposed to 30 hpf usually used in the zebrafish model of *S. aureus* infection, and it is possible that by infecting embryos later in

development that professional immune cells present are more mature. Whilst survival of embryos depleted of macrophages was lower than survival of embryos depleted of neutrophils, there was ~40 % survival in this group (Prajsnar et al., 2012) compared with 0% survival of infected embryos depleted of macrophages by clodronate in this study (Figure 4.19A) . Furthermore the quantification of population variance was calculated as a ratio of the two isogenic strains; however this study utilised the more robust population evenness calculation adopted by Pollitt et al., 2018. As a metric, E_H is better suited for this analysis, because it is based upon *H*, the calculation of which is equally sensitive to both very rare and very abundant species within a sample (this is useful as samples in these experiments can be both evenly mixed or comprised predominantly of only one isogenic strain).

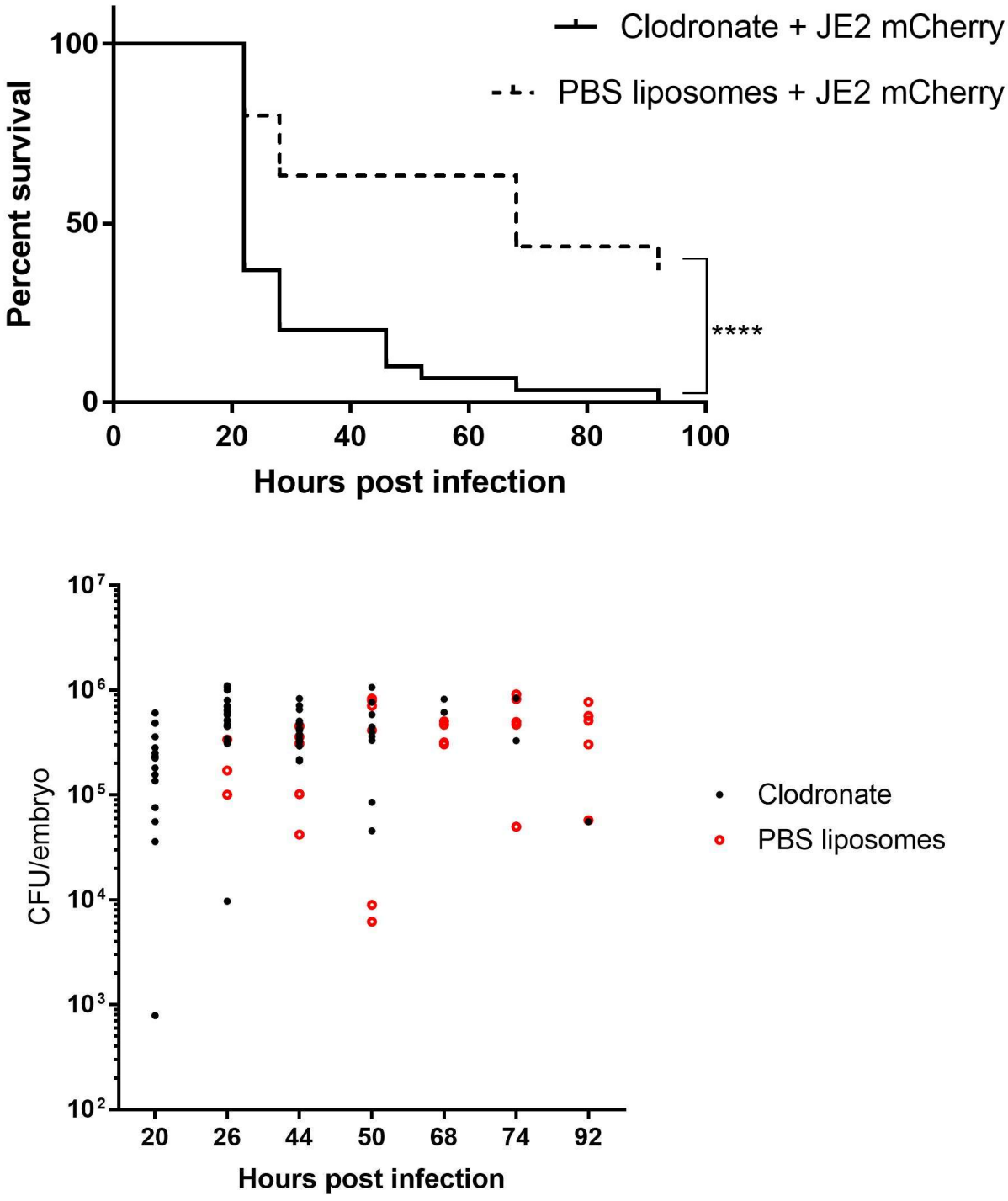

Figure 4.19 Bacterial dynamics of *S. aureus* within a macrophage depleted host

A) Survival of embryos depleted of macrophages by injection of clodronate liposomes prior to infection with JE2-mCherry. Mantel-Cox curve comparison P = 0.0001. **B)** CFU recovered from dead embryos after infection with mixed inoculum of isogenic strains, Mann-Whitney P = 0.578

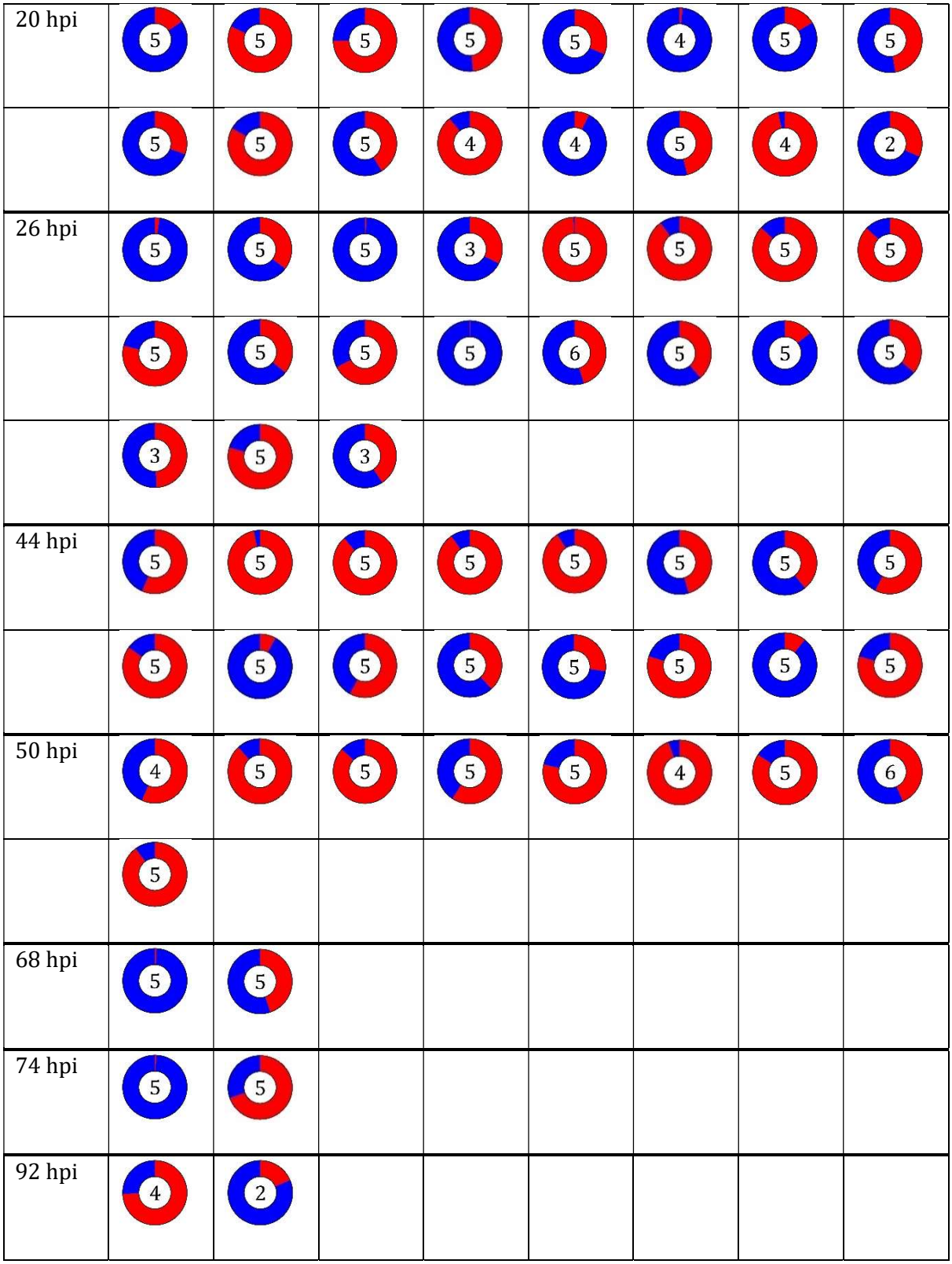

Figure 4.20 Proportions of isogenic strains recovered from macrophage depleted embryos

Embryos were treated with clodronate liposomes and infected with a 1:1 mixture of isogenic strains with Kan and Ery markers. Dead embryos were collected at regular timepoints and the proportion of bacteria recovered from individual embryos are shown in pie charts (with red and blue representing Kan and Ery respectively). The number inside each pie chart represents the log number of bacteria eg. 10^5 CFU = 5.

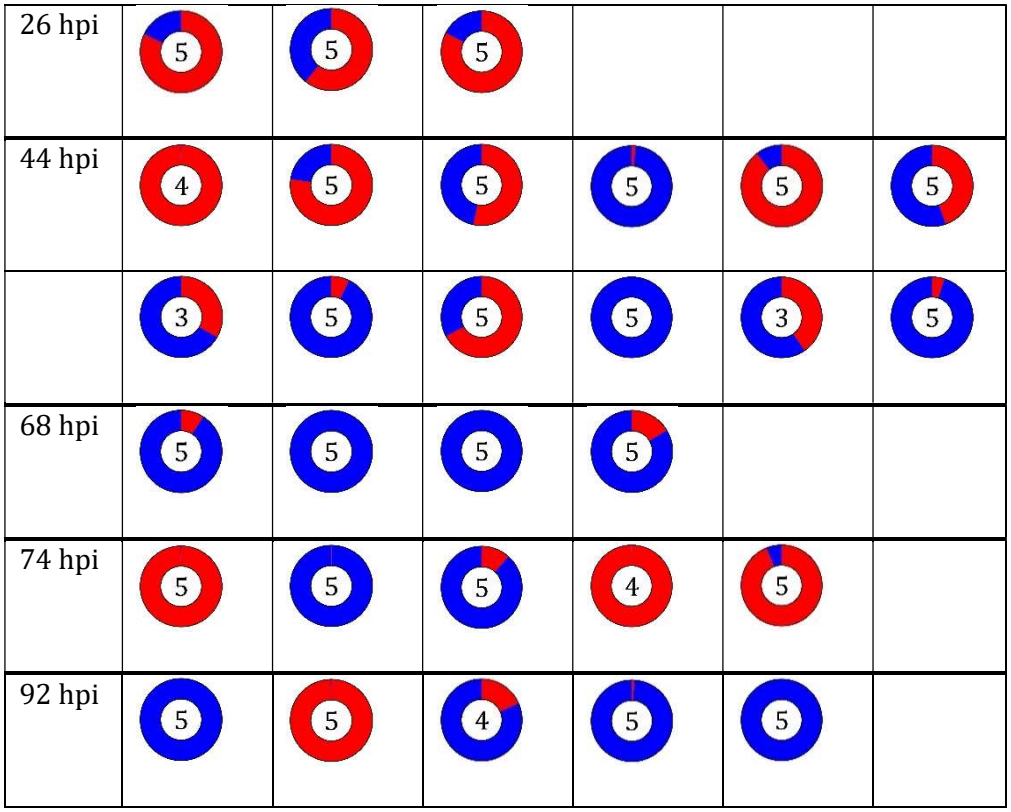

Figure 4.21 Proportion of isogenic strains recovered from control embryos

Embryos were treated with PBS liposomes and infected with a 1:1 mixture of isogenic strains with Kan and Ery markers. Dead embryos were collected at regular timepoints and the proportion of bacteria recovered from each embryo are shown in pie charts(with red and blue representing Kan and Ery respectively). The number inside each pie chart represents the log number of bacteria eg. 10^5 CFU = 5.

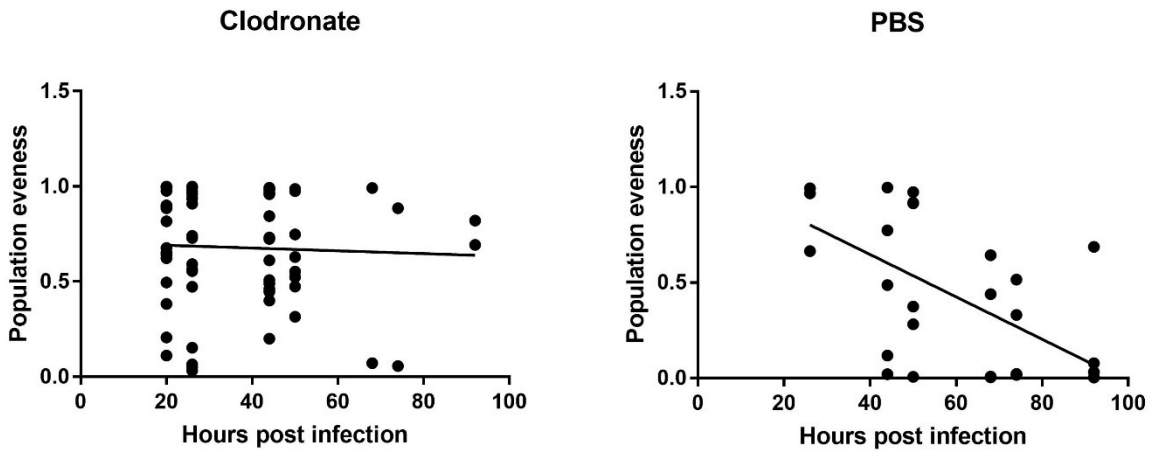

Figure 4.22 Population evenness of embryos infected with isogenic strains

Embryos were treated with clodronate or PBS liposomes and infected with a 1:1 mixture of isogenic strains with Kan and Ery markers. A) population evenness of clodronate treated embryos B) population evenness of PBS treated embryos. Line = mean linear regression. Linear regression: A) P=0.735, F= 0.1156, R^2=0.0018 B) P= 0.0009, F= 14.06, R^2=0.3425

4.9 *Following infection dynamics with labelled neutrophils and macrophages*

Tg(*mpx*:gfp)^{I114} and *Tg*(*mpeg*:mCherry x CAAX)^{SH378} were cross bred to produce *Tg*(*mpx*:gfp, *mpeg*:mCherry xCAAX)$^{I114, SH378}$ embryos. Embryos were screened after dechorionation at 24 hpf and embryos that were positive for both GFP neutrophils and mCherry macrophages were selected. At 30 hpf, embryos were infected with ~2000 CFU JE2-mCherry and mounted for LSFM. Although both the bacteria and macrophages are labelled with the same fluorophore (mCherry) the *Tg*(*mpeg:*mCherry x CAAX) $^{I114, SH378}$ labels the perforin-2 protein (encoded by *mpeg1*) which is an integral membrane component of the macrophage, as such it is possible to resolve bacteria within the macrophages even though they express the same fluorophore.

Initially imaging began whilst there were still extracellular bacteria, at 2.5 hpi and a MaxIP of the multiple FOV covering the circulation valley are shown in Figure 4.23. A timecourse imaging every 20 minutes was started from 4 hpi, a MaxIP of the multiple FOV covering the circulation at the beginning of the timecourse is shown in Figure 4.24. At the beginning of this timecourse experiment bacteria have been phagocytosed and are not visible within the circulation at 4 hpi. The JE2-mCherry used in this experiment produce a stronger signal when excited by 561nm laser and are clearly visible within the mCherry labelled macrophages of which only the membrane expresses the mCherry fluorophore, where labelling is not as strong.

During the experiment a lesion forms and is visible in multiple FOV from 6 hpi, a MaxIP of the time course can be viewed in **'Video 14- dual labelled embryo JE2-mCherry 4 hpi onwards view 5 MaxIP'** and the a MaxIP of the timecourse imaged 43° rotation can be viewed in **'Video 15 – dual labelled embryo JE2-mCherry 4 hpi onwards view 1 MaxIP'**.

The lesion seemingly originates from an area occupied by 3 macrophages (mCherry) and a neutrophil (GFP) all of which have internalised bacteria (mCherry); the macrophages in this area in particular have a high number of intracellular *S. aureus*. To clarify the origin of initial lesion formation, a MaxIP of 130 slices (83 μm thick) from the z-stack of FOV 5 was made for the first 10 time points and can be viewed in **'Video 16- dual labelled embryo JE2-mCherry 4 hpi onwards view 5 subset t1-10 z340-460 MaxIP'** at the 5th time point (5.66 hpi) a macrophage appears to lyse and at the 6th time point (6 hpi) extracellular bacteria are visible in the area. A 3D reconstruction of this volume was performed and the first 10 timepoints can be seen in '**Video 17 – rotating 3D render of dual labelled embryo JE2-mCherry 4 hpi onwards view 5 subset t1-10 z340-460 MaxIP'** this shows distinct macrophages with internalised bacteria at timepoints 1-4, at the 5th timepoint the signal in the same volume becomes diffuse, a 3D rendering of timepoints 3 (5 hpi) & 5 (5.66 hpi) are shown in Figure 4.25.

A MaxIP of 200 slices (128 μm thick) from the z-stack of FOV 1, 43° rotation of the same volume can be viewed in **'Video 18 - dual labelled embryo JE2-mCherry 4 hpi onwards view 1 subset z450-650 MaxIP'** this FOV has been cropped to center around formation of the lesion. This angle also shows that timepoint prior to the 5th timepoint bacteria in the region are all internalised, with intense bright mCherry signal coming from internalised bacteria within macrophages at timepoints 1-4. The 5th timepoint has diffuse mCherry in this ROI where previously a large macrophage with internalised JE2-mCherry occupied the area. A MaxIP of the same 200 slices (128 μm) for the whole FOV (1) can be viewed in '**Video 19- dual labelled embryo infected with JE2 mCherry 4 hpi view 1 z450-650 MaxIP'**

A 3D reconstruction of the lesion at 17 hpi from FOV 5 is shown in Figure 4.26 and video showing the interaction of the labelled phagocytes around the bacterial aggregate can be seen in '**Video 20- dual labelled JE2-mCherry lesion t39 view 5 rotation'.** Due to the macrophages and bacteria both being labelled with mCherry it was not possible to perform segmentation co-localistion analysis on this data set.

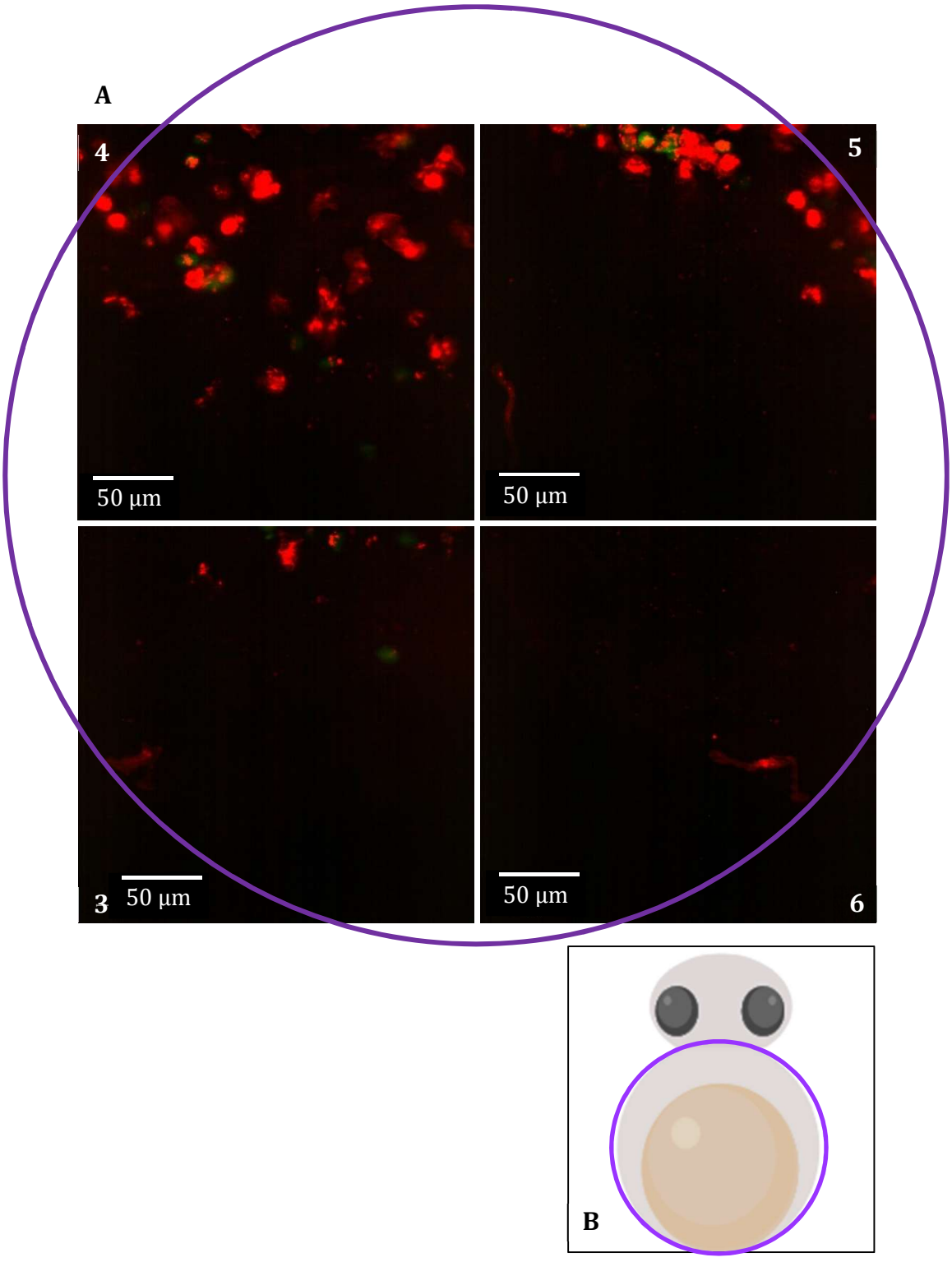

Figure 4.23MaxIP of dual labelled embryo infected with JE2-mCherry 2.5 hpi

A) MaxIP of *Tg*(*mpx*:GFP, *mpeg*:mCherry xCAAX)^{I114,SH378} embryo (with GFP neutrophils and mCherry macrophages) infected with JE2-mCherry imaged by LSFM at 2.5 hpi. FOV were acquired at the same imaging angle to cover the circulation valley (ROI circled in purple) order of FOV acquisition numbered in outer corner of each image. **B)** Schematic of embryo in ventral orientation with purple circle for approximation of ROI

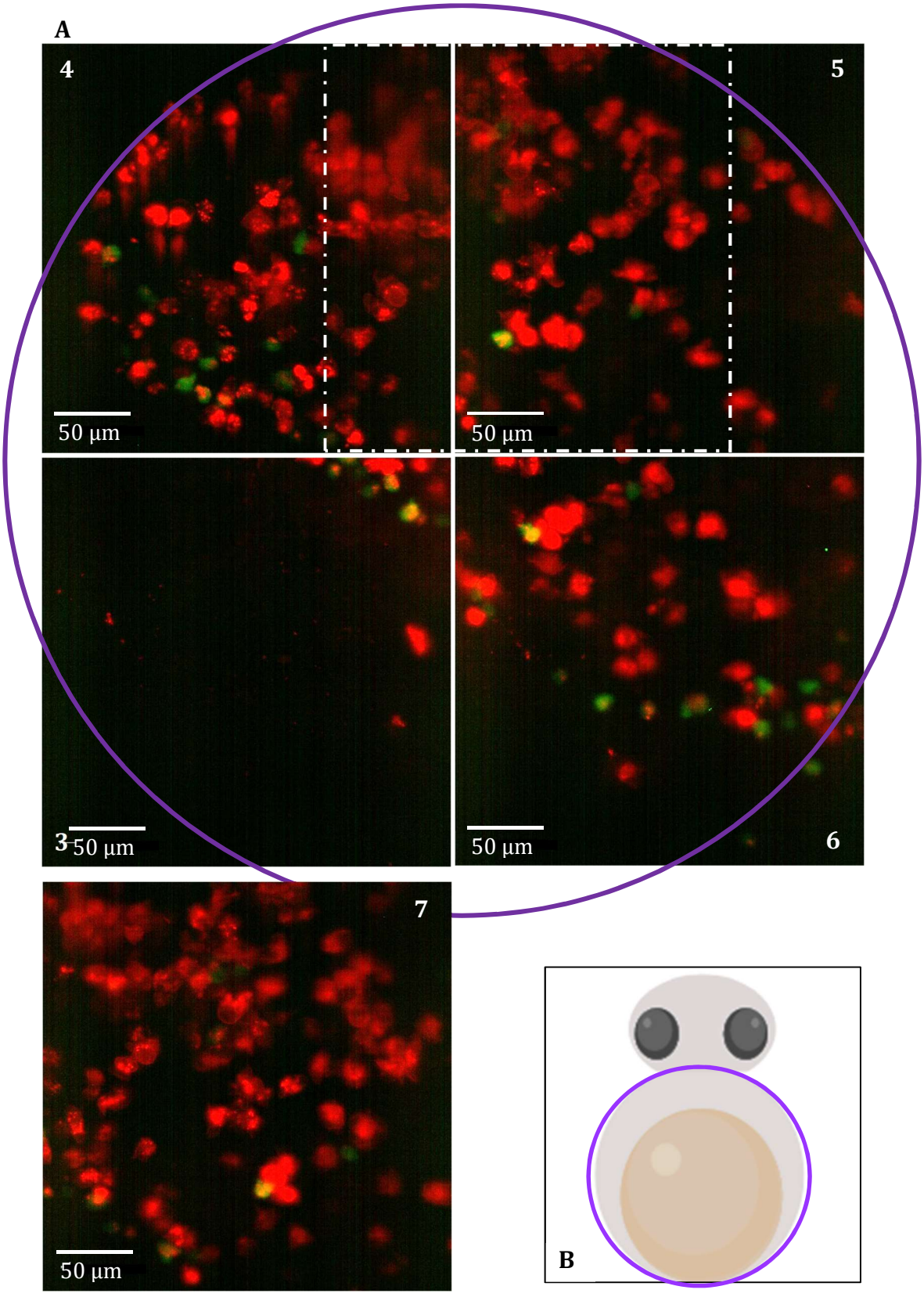

Figure 4.24 MaxIP of dual labelled embryo infected with JE2-mCherry 4 hpi

A) MaxIP of *Tg*(*mpx*:GFP, *mpeg*:mCherry xCAAX)^{I114,SH260} embryo (with GFP neutrophils and mCherry macrophages) infected with JE2-mCherry imaged by LSFM at 4 hpi. FOV were acquired at the same imaging angle to cover circulation valley (ROI circled in purple). Dashed outline shows region of overlap between FOV **4** and **5** which became FOV **7**, order of FOV acquisition numbered in outer corner of each image. **B)** schematic of embryo in ventral orientation with purple circle for approximation of ROI

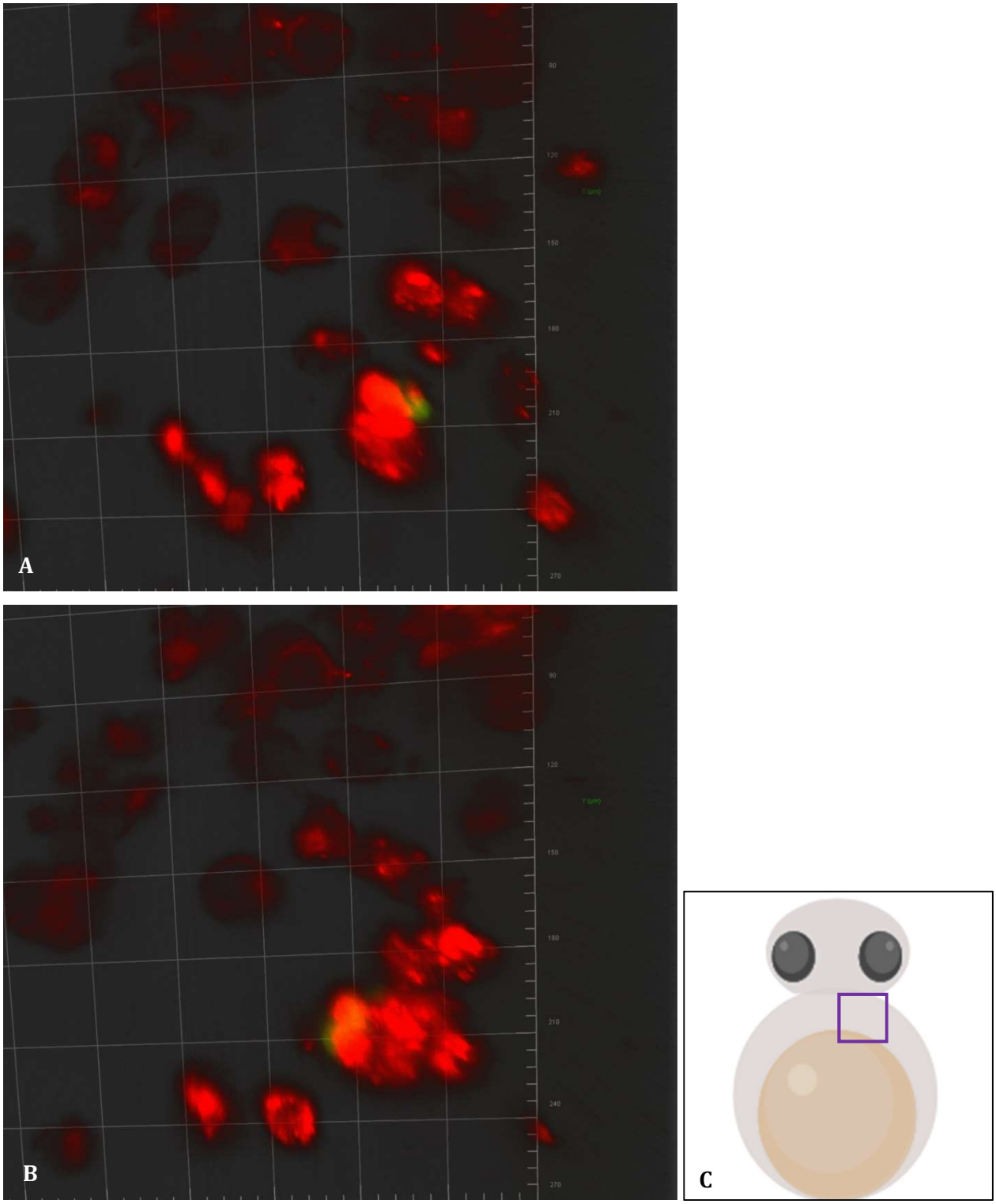

Figure 4.25 3D rendering of dual labelled embryo FOV 5

Subset of *Tg*(*mpx*:GFP, *mpeg*:mCherry xCAAX)^{I114,SH260} embryo (with GFP neutrophils and mCherry macrophages) FOV 5, 120 slices 0.64 µm thick (83 µm) was reconstructed in Arvivis **A**) ROI at 5 hpi **B**) ROI at 5.66 hpi. Gridlines are 30 x 30 µm, with 6 µm gradations **C**) Schematic of embryo in ventral orientation with purple box for approximation of reconstructed region. At 5.66 hpi (**B**) distinct punctate signal is observed in a diffuse area, previously occupied by a macrophage containing a high number of bacteria at 5 hpi (**A**).

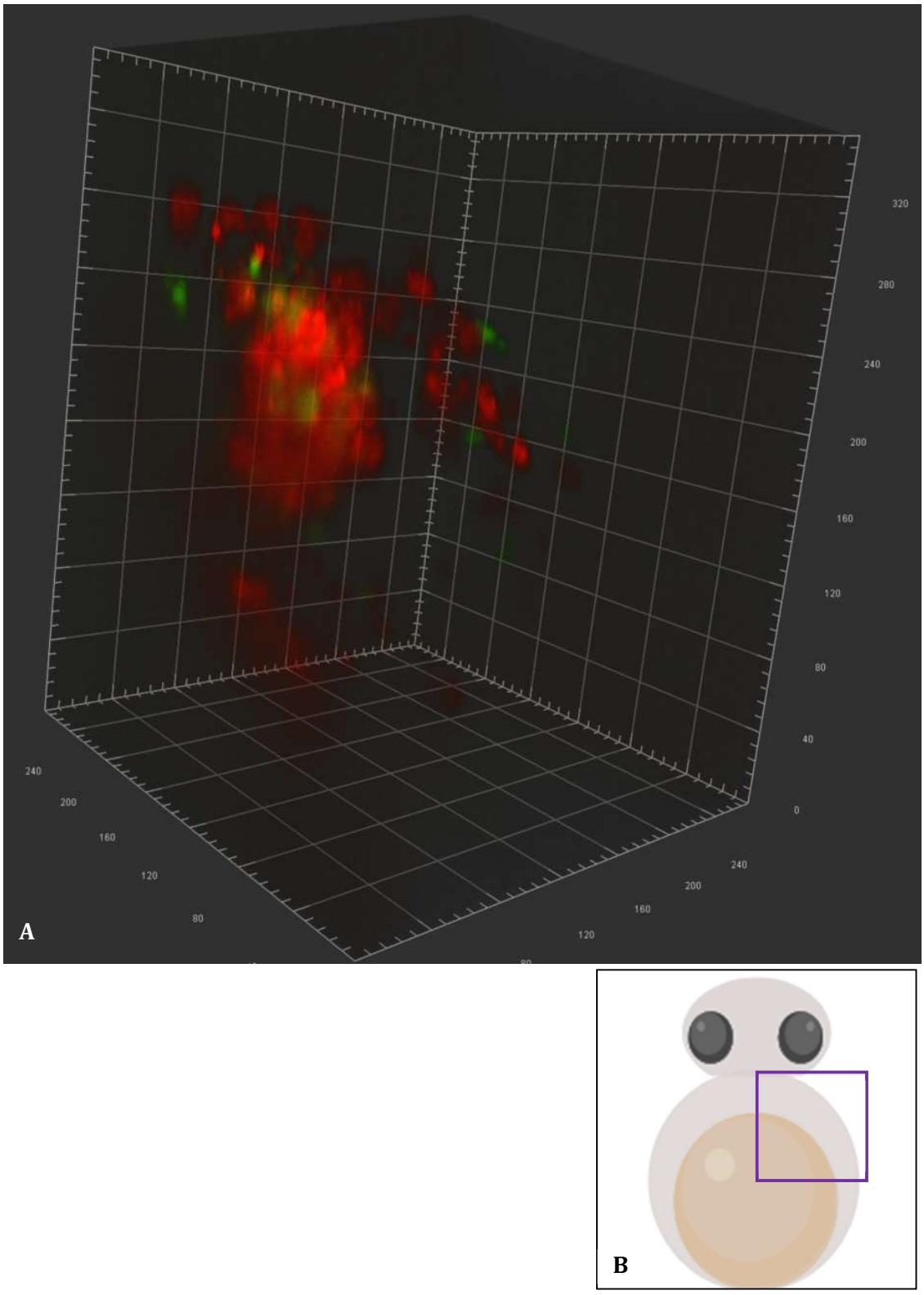

Figure 4.26 3D reconstruction of JE2-mCherry lesion within dual labelled embryo

A) 3D rendering of of *Tg*(*mpx*:GFP, *mpeg*:mCherry xCAAX)^{I114,SH260} embryo (with GFP neutrophils and mCherry macrophages) imaged by LSFM, FOV 5 at 17 hpi **B)** Schematic of embryo in ventral position with purple square for approximation of reconstruction.

4.10 *Development of smURFP as a reporter for labelling S. aureus during infection*

It is desirable to have another fluorophore, that could be expressed by *S. aureus*, complementary to GFP & mCherry to enable three colour imaging. Far-red (FR) and near infra-red (NIR) proteins are an attractive candidates as these wavelengths minimise light-scattering and absorbance by endogenous tissue, so there is reduced auto-fluorescence from living samples in the emission wavelengths of these channels (Jun et al., 2017). Previously, a method of staining *S. aureus* with Alexa fluor 647 succinimidyl ester was developed (Serba, 2015), which is useful for imaging *S. aureus* within embryos in the initial stages of infection, however this protocol stains the cell wall, so signal intensity is lost as the bacteria replicate within the host. It is therefore necessary to have a fluorophore genetically encoded for long term imaging.

A novel far red fluorescent protein has recently been developed (Rodriguez et al., 2016); this protein has been engineered without a chromophore: formation of these can be energetically costly to produce, take hours within the bacteria and produce ROS as a by-product. Instead the protein, small ultra-red fluorescent protein (smURFP) makes use of the native chromophore biliverdin (BV) and binds it covalently(Rodriguez et al., 2016). This reporter is the brightest FR protein created to date, (Luker et al., 2015; Rodriguez et al., 2016) with 96% molecular brightness relative to eGFP compared with 49% of mCardinal, previously the brightest FR fluorescent protein (Chu et al., 2014; Luker et al., 2015). smURFP has high photo-stability needed for long-term imaging, comparable to eGFP and higher than mCherry, tdTomato fluorescent proteins.

Developed for use in tissue culture and studies using animal models, without confirmed success in bacteria (although the protein has been engineered from light-harvesting phycobiliproteins of the cyanobacteria *Trichodesmium erythraeum*) smURFP was used as a candidate fluorophore for a constitutive far red marker in *S. aureus*.

4.10.1 Gibson assembly of pMV158-smURFP

The published sequence, GenBank: KX449134.1 was codon optimised for expression *by S. aureus* (appendix 8.1), and synthetic DNA was ordered. The plasmid pMV158-mCherry (Stephane Mesnage unpublished) was chosen for the plasmid backbone, the promoter controlling expression of the fluorophore is pMal1 promoter, which provides constitutive expression in *S. aureus*. The plasmid was isolated by midi-prep from strain SJF4308 and digested with NdeI & BglII to remove the fragment encoding mCherry, producing a linearised plasmid backbone of 6607 bp (Figure 4.27). Primers 'smURFP_forward' & 'smURFP_reverse' (Table 4.1) were designed for Gibson assembly and used to amplify both the linearised pMV158 & synthesised smURFP by PCR.

The two fragments were combined by Gibson assembly, the recombinant plasmid was purified by gel electrophoresis and the product was recovered by gel extraction, Figure 4.27 depicts the Gibson assembly and Figure 4.28 shows the plasmid map.

4.10.2 Creation of smURFP *S. aureus* strains

The resulting plasmid was transformed by electroporation into electro-competent *S. aureus* strain RN4220 and grown on Tet (5). Colonies containing resistance to Tet were isolated and the plasmid was moved by phage transduction by φ11 into the WT strains SH1000 & JE2. Colonies of both SH1000 & JE2 which grew on selective media after transduction were isolated, producing SH1000-smURFP & JE2-smURFP.

4.10.3 Confirmation of smURFP fluorescence

Isolated colonies were grown in selective media and *Tg*(*mpx*:GFP)^{i114} embryos (with GFP labelled neutrophils) were infected with either SH1000-pMV158smURFP or JE2-pMV158smURFP and mounted in 0.8 % (w/v) LMP agarose for imaging by LSFM. Both fluorophores were excited on the same imaging track, as they are spectrally distinct, using the usual filter set previously described in 3.5.2; the 638 nm laser was used to excite *S. aureus* expressing smURFP. The fluorophore was very bright, needing only 1.5 % laser power, 30 ms exposure time to produce 632 grey levels with low background levels, in comparison with 2.8 % laser, 30 ms exposure time to prodce 550 grey levels detected from the 488 nm (GFP) laser. Individual JE2-smURFP and SH1000 smURFP are visible within brightly labelled GFP neutrophils of the host (Figure 4.29).

4.10.4 Time-lapse imaging of smURFP in vivo

Timecourse imaging of *Tg*(*mpx*:GFP)^{i114} infected with JE2-pMV158smURFP by LSFM was set up overnight, from 2 hpi, imaging 6 FOV every 20 min to ensure that the novel fluorophore can undergo long-term imaging without photobleaching. Subsequent to overnight imaging, a second timecourse at 23 hpi, of a single FOV (containing some bacterial aggregates) was imaged continuously for 10 minutes, . A MaxIP of this can be seen in **'Video 21- Short term timecourse of embryo infected with JE2-smURFP'**.

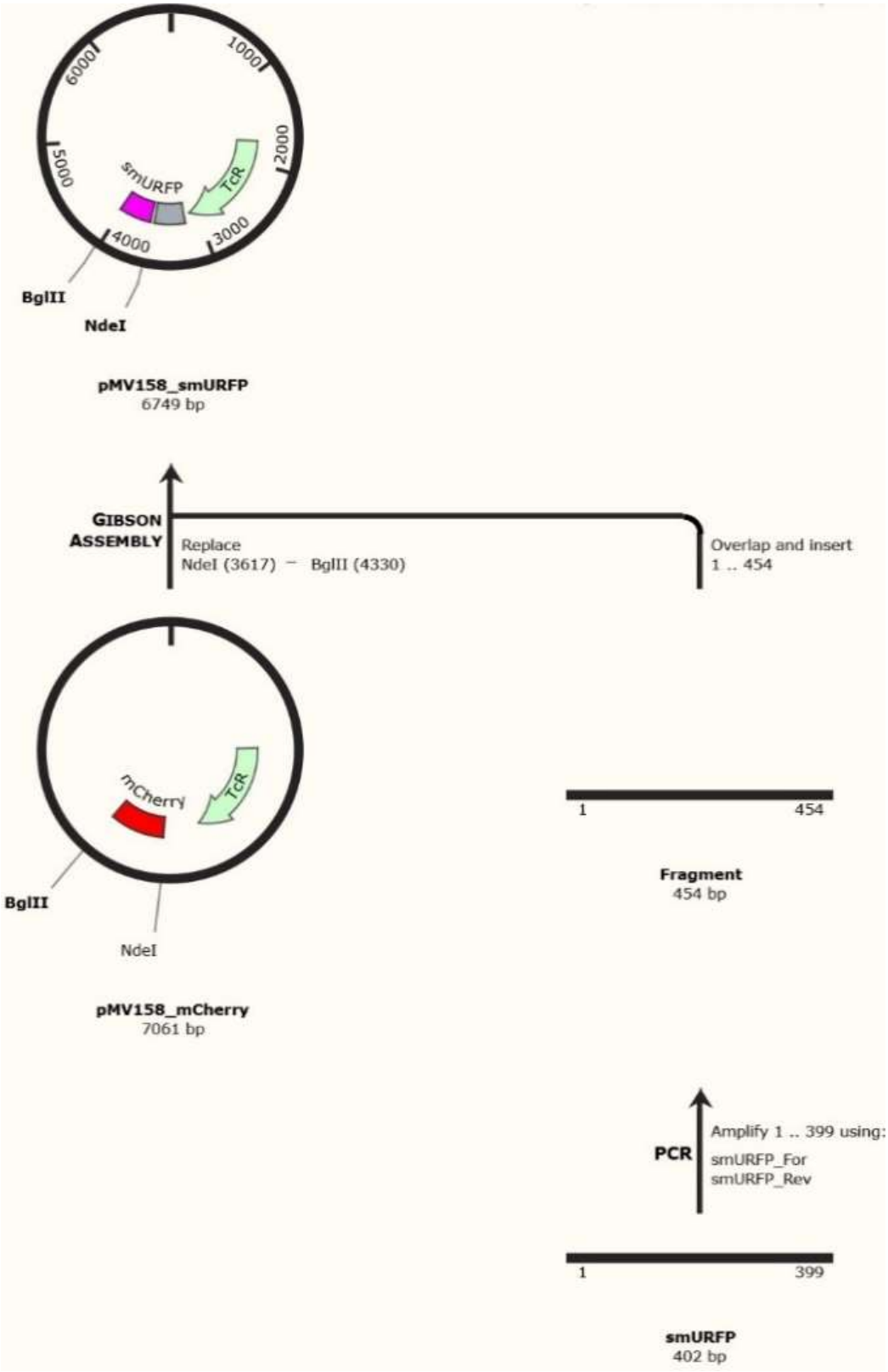

Figure 4.27 Plasmid design and assembly for pMV158_smURFP

Flowchart for Gibson assembly from pMV158_mCherry backbone and synthethesised smURFP fragment.

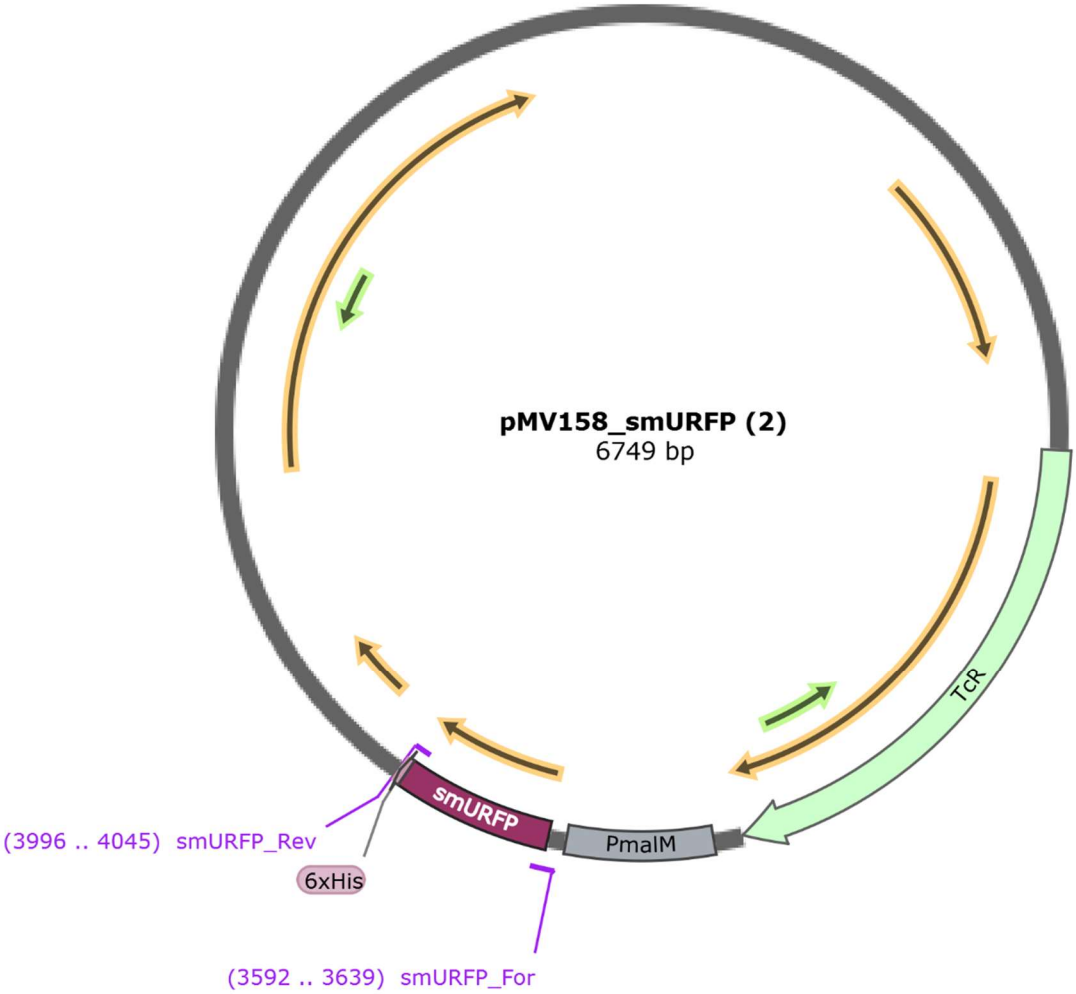

Figure 4.28 Plasmid map for pMV158-smURFP

Primer	Sequence
smURFP_forward	gattaactttataaggaggaaaaacatATGGCGAAAACATCAGAGCAG
smURFP_reverse	attaatgatgatgatgatgagatctAGACATAGCCTTTATGATATAG

Table 4.1 Primers used for Gibson Assembly of pMV158-smURFP

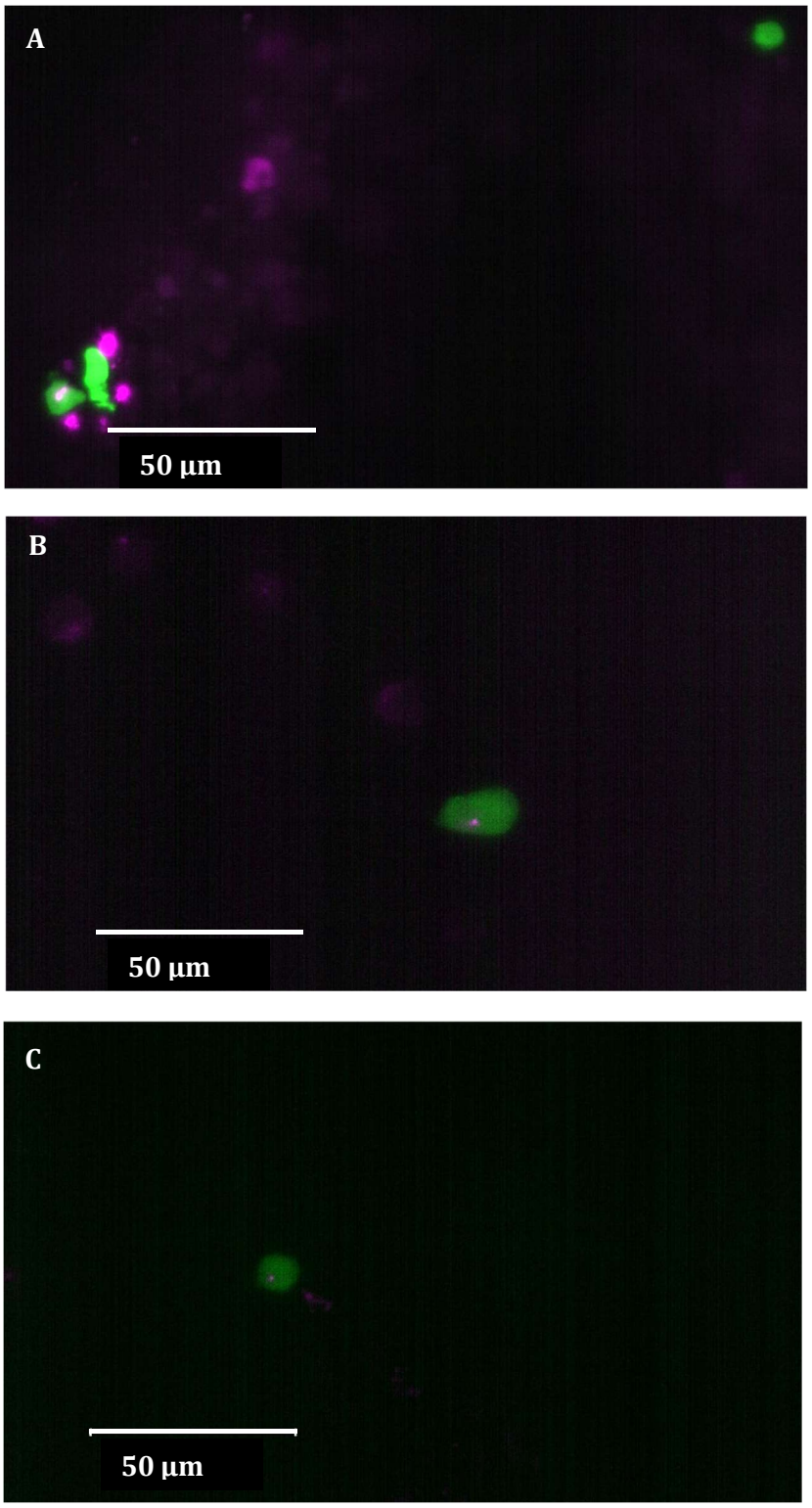

Figure 4.29 Individual *S. aureus* expressing smURFP resolved within a neutrophil

MaxIP *of Tg*(*mpx*:GFP)^{i114} embryos (GFP neutrophils) infected with either **A)** JE2-pMV158smURFP or **B)** SH1000-pMV158smURFP **C)** SH1000-pMV158smURFP imaged by LSFM at 2 hpi.

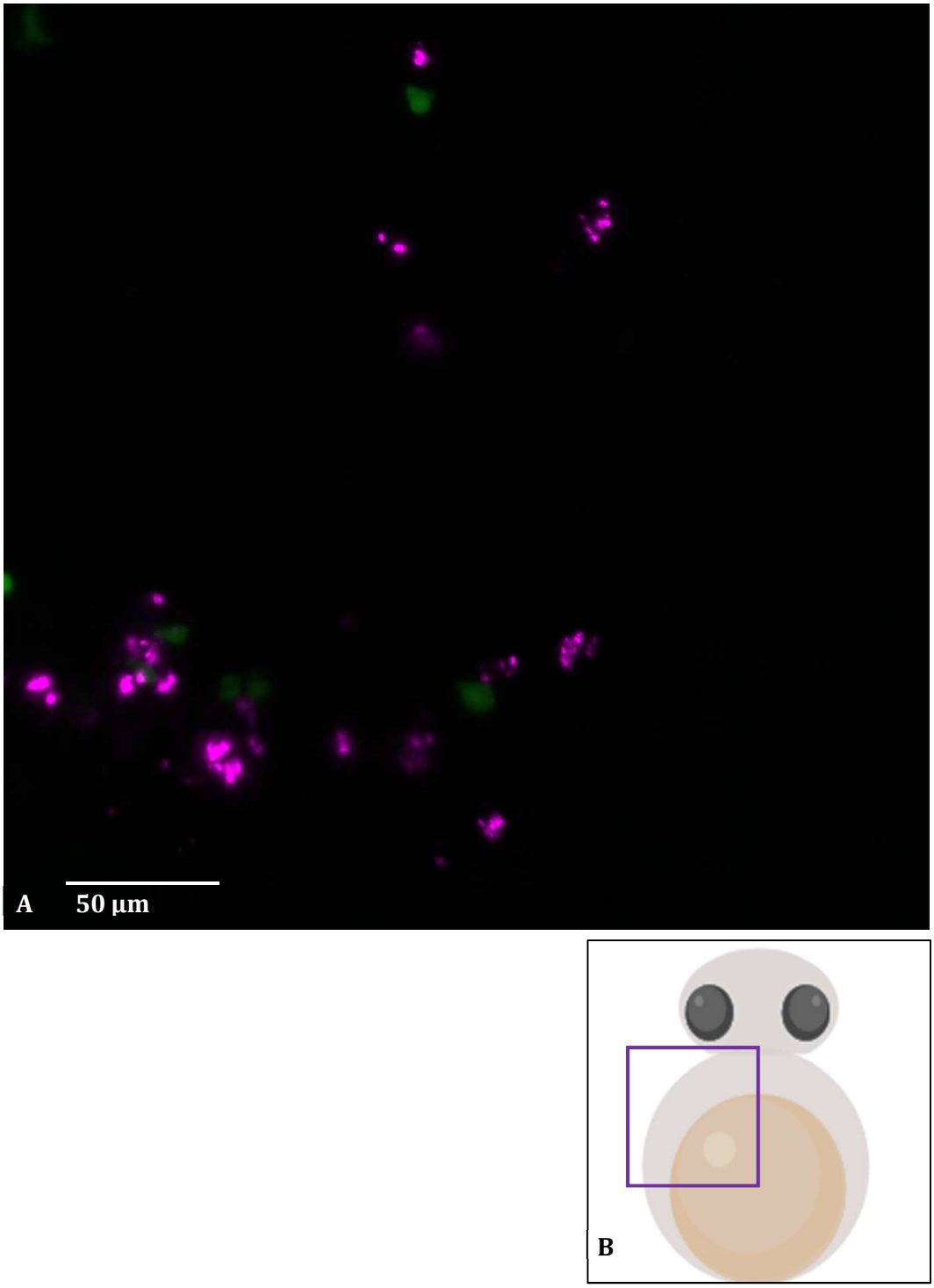

Figure 4.30 MaxIP of embryo infected with JE2-pMV158smURFP 22 hpi

A) MaxIP *of Tg*(*mpx*:GFP)^{i114} embryos (GFP neutrophils) infected with JE2-pMV158smURFP imaged by LSFM 22 hpi. **B)** Schematic of embryo in ventral orientation with purple box for approximation of FOV.

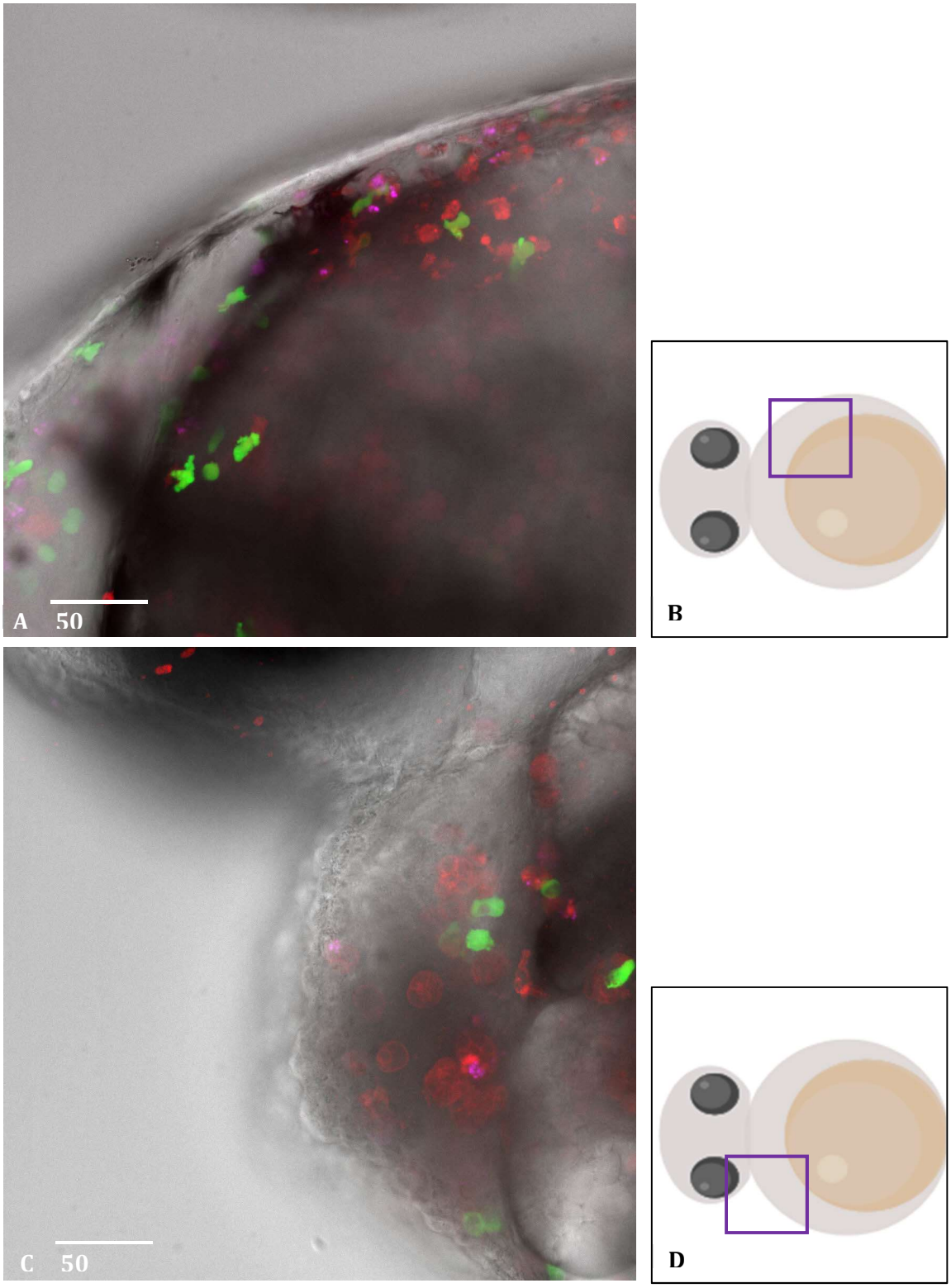

Figure 4.31 MaxIP of embryos infected with JE2-pMV158smURFP 20 hpi

A) and **C)** MaxIP of *Tg*(*mpx*:GFP, *mpeg:*mCherry x CAAX)$^{i114, SH260}$ (GFP neutrophils and mCherry macrophages) with brightfield image for orientation with the embryo. Distinct smURFP bacteria can be observed within the macrophages at 20 hpi. **B & D)** schematics of embryo in ventral orientation with purple squares for approximation of FOV for **A)** and **C)** respectively.

4.11 *Discussion*

In this chapter LSFM was used to investigate infection progression of *S. aureus* within a zebrafish host, utilising fluorescent bacteria and transgenic zebrafish lines. Whilst this technique has low throughput and therefore does not lend itself to statistical analysis when the event of lesion formation has occurred within the host, initial expansion events of bacteria can be traced back to around 6-8 hpi before subsequent lesion formation and overwhelming infection occurs.

Throughout this chapter it has been shown that there are trends of more signal from internalised bacteria in macrophages then in neutrophils and a higher proportion of the macrophage population have internalised bacteria; often many neutrophils contain no bacteria even when terminally infected. Although recent addition of analysis modules to Arivis4D can provide statistical analysis of this within the sample, comparison between samples is not possible due to differences in imaging volumes and length of timecourse experiments and is beyond the scope of this study.

When overwhelming infection has occurred during long-term imaging, bacteria have been observed to come from within a macrophage prior to expansion. The number of expansion events that have been captured by LSFM is low, but bacteria have not been observed to expand from within a labelled neutrophil, although more replicates would be needed to definitively prove that this does not occur.

To further investigate the dynamics of *S. aureus* infection and the role of macrophages in clonal expansion of bacteria within the host, clodronate liposomes were used to deplete macrophages. There was 0% survival of macrophage depleted embryos at 92 hpi, in comparison with 40-50% in control groups infected with the same inoculum. There was no difference in bacterial burden of terminally infected macrophage depleted embryos and control embryos. By infection with two isogenic strains the effect of macrophages on clonal expansion of *S. aureus* within the host was investigated. There is a decrease in species evenness between the two isogenic strains recovered from terminally infected control embryos as time post infection increases, however evenness of isogenic strains recovered from macrophage depleted embryos does not decrease overtime. The distribution of species evenness was significantly different (Mann-Whitney, $P = 0.0023$) between macrophage depleted and control groups. These data implicate macrophages as an immunological bottle neck which results in predominance of one isogenic strain that proceeds to overwhelm the host.

When overwhelming infection has occurred, *S. aureus* has a propensity to spread over membranes within the host, which has not previously been observed within this infection model. However, this observation is not surprising as *S. aureus* colonises human naso-pharynx (DeLeo et al., 2010) and has evolved to colonise tissue surfaces during infection. This is characteristic of many diseases

caused by the pathogen such as endocarditis, chronic wound infection and infection of lung epithelia in cystic fibrosis patients (Bhattacharya et al., 2015). Biofilms are also associated with these diseases and it is possible that these layers of *S. aureus* within the embryos and the lesions that form are biofilms forming *in vivo*.

To enable timelapse imaging with three fluorophores, a plasmid encoding a novel NIR fluorescent protein was designed and transduced into the WT strain JE2 & SH1000. The resulting JE2-pMV158smURFP & SH1000-pMV158smURFP strains fluoresce brightly when excited by a 638 nm laser and did not photobleach during overnight timelapse imaging; the bacteria are easily resolved within host immune cells. The NIR fluorescent protein smURFP does not have an electron accepting chromophore, designed for use in mammalian culture utilising native chromophores such as heme (Rodriguez et al., 2016). As a result of this it was possible that the fluorescent protein might not work when expressed by *S. aureus.* It is possible that staphyloxanthin, the carotenoid natively produced by *S. aureus,* performs the chromophore role as the structure (Pelz et al., 2005) is not dissimilar to the that of the native biliprotein produced by the cyano bacteria that the smURFP fluorescent protein was engineed from (Rodriguez et al., 2016).

Expression of smURFP by *S. aureus* on multicopy plasmid pMV158-smURFP was successful and the produced fluorophore is bright and does not photo-bleach during long -term imaging. As such it would be useful to have the NIR fluorophore as a single copy on the chromosome with expression under the control by the same promoter (PmalM) integrated at the lipase locus, the same as the chromosomal mCherry & GFP strains used in this study. A suicide plasmid using the pKASBAR vector system (Bottomley et al., 2014; Wacnik, K., 2016) has been designed and primers have been made for the production of this plasmid by Gibson assembly using the smURFP under control of PmalM from the plasmid pMV158-smURFP with plasmid backbone pGM074, the resulting plasmid is shown in Figure 4.32. Production of *S. aureus* strains with chromosomally encoded constitutively expressed NIR fluorophore would enable long term imaging of the *S. aureus* within a host with multiple cell types labelled with GFP and mCherry. The ability to image three fluorophores simultaneously over extended time scales would allow further insight into the dynamics of interaction between *S. aureus* and the zebrafish host. As the resultant strains would be isogenic to SH1000-GFP, SH1000-mCherry, JE2-GFP & JE2-mCherry, used in this study, experiments with a mixed inoculum and labelled host cells could be performed, to examine formation of clonal lesions within the host.

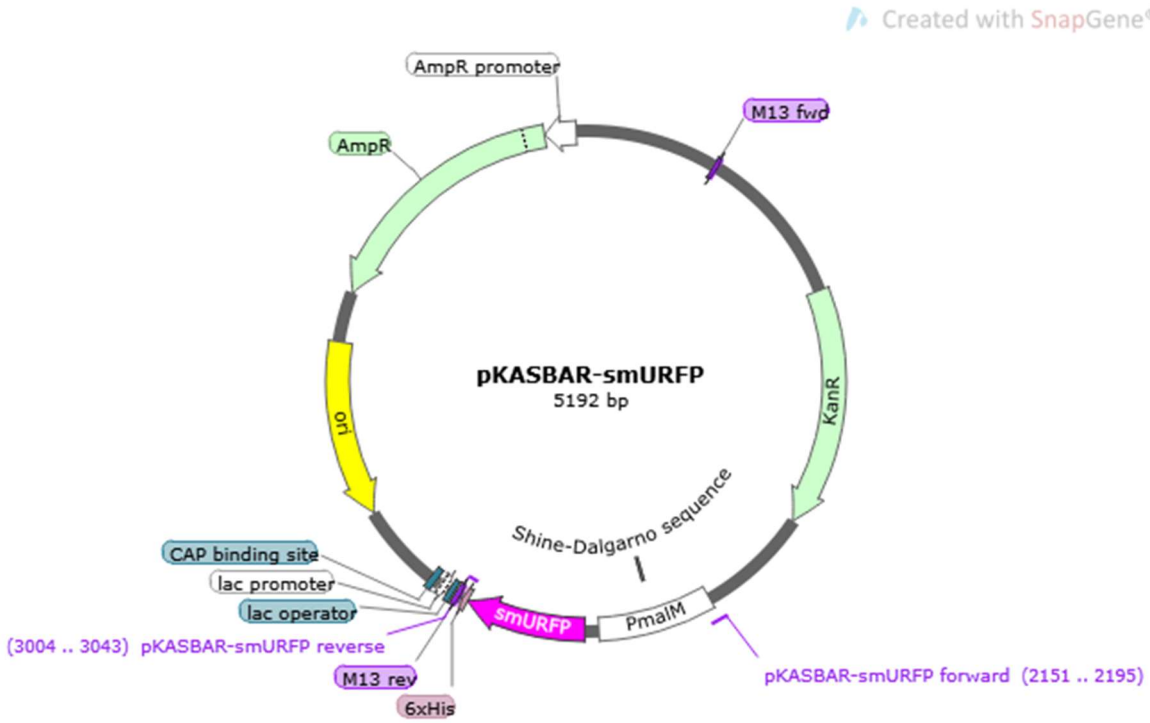

Figure 4.32 plasmid map for pKASBAR-smURFP

5 Evaluation of *S. aureus in vivo* lesions as biofilms

5.1 *Introduction*

Within the host *S. aureus* has the propensity to attach and persist on surfaces, these can be either biotic such as bone and heart valves (causing osteomyelitis and endocarditis respectively) or abiotic such as cathethers, bone prostheses and pacemakers (Barrett and Atkins, 2014; Chatterjee et al., 2014; Kiedrowski and Horswill, 2011; Lister and Horswill, 2014) and even facial fillers (which contain a hyaluronic acid matrix) used in aesthetic procedures (Dumitraşcu and Georgescu, 2013). Host components or synthetic material surfaces, are targeted by adhesins produced on the surface of *S. aureus.* Of these, the microbial surface components recognising adhesive matrix molecules (MSCRAMMs) mediate attachment to host components such as fibronectin, collagen and fibrinogen (Corrigan et al., 2007; Foster et al., 2014; Merino et al., 2009; O'Neill et al., 2008).

Once attached to a surface, *S. aureus* become embedded in an extracellular, polymeric matrix (ECM) comprised of both environmental factors and eDNA, polysaccharide and proteins secreted by the bacteria. These can cause chronic infections which are difficult to treat as the biofilm impedes the host immune response, such as phagocytosis by macrophages (Scherr et al., 2014). The bacteria within a biofilm have increased tolerance to antibiotics, resulting from their physiological status and lack of access, rather than acquired resistance (de la Fuente-Núñez et al., 2013). Due to their lowered susceptibility to antibiotics and host defences, biofilm associated infections are difficult to treat, often requiring removal of an implanted device or physical debridement of infected host tissue (Darouiche, 2004).

Biofilms are defined as "an aggregate of microorganisms in which cells are frequently embedded within a self-produced matrix of extracellular polymeric substance, adhere to each other and/or to a surface" (IUPAC definition). *S. aureus* which have adopted this sessile state, have a distinct phenotype and although the anoxic environment results in lower rates of metabolism and down-regulated cell division (Lewis, 2010) rather than being dormant, maturation of the biofilm is a highly regulated process (Moormeier and Bayles, 2017b). Previously accepted as a three-stage process 1) attachment 2) accumulation 3) detachment/dispersal, recent insights into the development of *S. aureus* has redefined it as a 5 stage developmental process shown in Figure 5.1. This new model for biofilm development consists of; 1) attachment 2) multiplication 3) exodus 4) multiplication 5) dispersal (Moormeier and Bayles, 2017b). It includes distinct characteristics of ECM during development (Kiedrowski et al., 2014; Moormeier et al., 2014; Otto, 2013; Schwartz et al., 2015) and differential gene expression controlled by numerous regulators including: Agr, SarA, SaeRS and σB (Archer et al., 2011; Beenken et al., 2010; Moormeier et al., 2014; Valle et al., 2003; Yarwood et al., 2004). The five stage biofilm process requires a series of components to be

differentially expressed to allow the appropriate temporal and spatial development. Study of these key mediators allow biofilm progression to be investigated and understood.

5.1.1 Nuclease

Nuclease (Nuc) is a *S. aureus* secreted protein which has robust DNase & RNase properties, working on both single and double stranded DNA (Cuatrecasas et al., 1967). It was one of the first enzymes to be investigated extensively with folding and structural studies. Production of this enzyme is conserved across both methicillin sensitive and MRSA strains (Kiedrowski et al., 2011) and as such can be used as a bio-marker for the direct detection of *S. aureus* in blood cultures (Lagacé-Wiens et al., 2007).

Nuc is responsible for the degradation of eDNA within the biofilm matrix and has been shown repeatedly to decrease cell density within the biofilm (Kiedrowski et al., 2011, 2014; Mann et al., 2009; Moormeier et al., 2014) Expression of nuclease in mature biofilms is putatively triggered by quorum sensing (Cheung et al., 2011) in response to cell density. In *S. aureus* the quorum-sensing system is controlled by Agr, a major-regulator of gene expression (Rutherford and Bassler, 2012). In addition to expression in mature biofilms, more recently Nuc has been shown to be responsible for a newly characterised stage of biofilm development 'the exodus' phase, where after confluence is reached, expression of Nuc by a subpopulation of bacteria results in the detachment of most of the biofilm population (Moormeier et al., 2014). Surprisingly expression of *nuc* at this stage is independent of regulation by Agr. Recently it has been shown that nuclease expression is under the control of the regulator SaeRS (Olson et al., 2013), a two-component regulatory system, controlling expression of many *S. aureus* virulence factors where no Nuc dependant exodus event occurs in an *saeRS* mutant (Moormeier et al., 2014).

Although Nuc was first identified in 1956 by Cunningham et al., (1956), only recently has the importance of the protein in pathogenesis been investigated. As such, Nuc has been described as a virulence factor involved in the evasion of host immune defences whilst establishing infection within the host (Berends et al., 2010; Olson et al., 2013). There is decreased bacterial burden in mice 8 hours post peritoneal infection (Olson et al., 2013) and increased clearance of *S. aureus* from the lung tissue of mice infected intranasally (Berends et al., 2010) when infected with a Δ*nuc* mutant. It has been proposed that the higher bacterial burden of mice infected with WT is due to the activity of nuclease in escaping neutrophil extracellular traps (NETs) (Berends et al., 2010), which are formed when activated neutrophils release a mixture of DNA, histones, proteases and

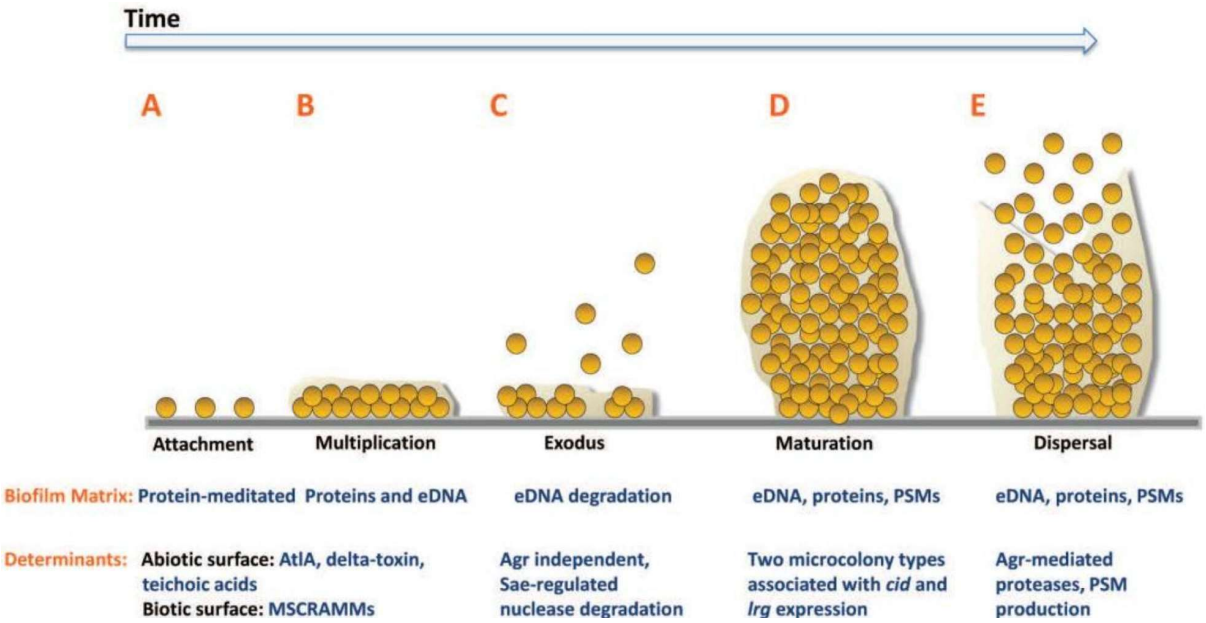

Figure 5.1 Stages of biofilm development – adapted from Moormeier and Bayles, 2017

S. aureus biofilm development a) attachment to surfaces via MSCRAMMs b) cells multiply within a proteinaceous matrix and eDNA c) when confluency is reached there is an exodus event and a sub-population of cells are released from the biofilm by degradation of eDNA d) three dimensional microcolonies form from cells that remain, during this stage there is rapid cell division e) Agr mediated quorum sensing initiates matrix modulation resulting in dispersal of cells via production of protease and PSMs

antimicrobial peptides (AMPs) (von Köckritz-Blickwede and Nizet, 2009). NET formation is a programmed cell death event distinct from apoptosis and necrosis, requiring the generation of ROS by NADPH oxidase (Fuchs et al., 2007). *S. aureus* has been shown to stimulate NET formation *in vitro* (Berends et al., 2010; Fuchs et al., 2007; von Köckritz-Blickwede and Nizet, 2009).

5.1.2 Cid

The *cid* operon consists of three genes, *cidA*, *cidB*, & *cidC* regulated by a LysR type transcriptional regulator, CidR. The *cidR* regulator responds to acetic acid accumulation in the growth media, a product of glucose metabolism (Rice et al., 2005). CidR positively regulates expression of *cidABC* and enhances murein hydrolase activity (Yang et al., 2005). The *cidA* gene encodes a putative holin protein, based on high similarity of the predicted secondary structure and homology (Brunskill and Bayles, 1996a). Fluorescent protein fusion and membrane fractionation studies have determined that CidA is a membrane bound protein (Ranjit et al., 2011). Mutation of the *cidA* gene has been shown to eliminate most murein hydrolase activity of *S. aureus* (Rice et al., 2003).

Recent studies have revealed CidC is a pyruvate oxidase, catalysing the removal of carboxylate from pyruvate forming acetate, contributing to the generation of acetic acid (Patton et al.) This activity of CidC, produces an environment which stimulates production of CidA and in turn, cell lysis. In contrast to the 'pro-death' actions of CidA & CidC, studies show that CidB is involved in sensing oxidative stress and *cidB* mutants are less sensitive to H_2O_2 (Windham et al., 2016).

5.1.3 Lrg

Expression of the *lrgAB* operon results in tower structures forming, during the 'maturation' stage of biofilm development, and it has been proposed that these structures arise due to a differential 'micro-niche' experienced within the biofilm (Moormeier et al., 2013). This follows as it has been shown that *lrgAB* expression is induced during overflow metabolism, occurring during growth on glucose in the presence of oxygen (Rice et al., 2005). The TCS LytSR regulates expression of *lrgAB* (Brunskill and Bayles, 1996a). This TCS was initially identified as a regulator of murein hydrolase activity and autolysis (Brunskill and Bayles, 1996b). More recently it has been proposed that activity of LytSR is mediated by it's sensing of acetyl phosphate (Sadykov and Bayles, 2012). Disruption of *lytS* abolishes expression of *lrgAB* within biofilms and concomitantly the rapid tower forming phenotype (Lehman et al., 2015).

LrgA is a hydrophobic membrane protein and based on its secondary structure and homology is a putative anti-holin (Brunskill and Bayles, 1996a). LrgA is thought to decrease murein hydrolase activity by binding CidA thus preventing homo-tetramers from forming a pore in the bacterial membrane (Ranjit et al., 2011). Disruption of the *lrgAB* operon results in increased biofilm adherence (Mann et al., 2009) and increased extracellular murein hydrolase activity (Groicher et al.,

2000). In addition to this the *lrgAB* mutant exhibits increased lysis, strengthening its proposed role as an inhibitor of cell death (Mann et al., 2009) and the mutation also enhances penicillin-induced killing suggesting that LrgAB contributes to antibiotic tolerance exhibited by biofilms (Groicher et al., 2000).

Disruption of *nuc*, *cidABC* and *lrgAB* operons alters the development and maturation of the biofilm. Together expression of these genes contributes to programmed cell death of a sub-population for the benefit of the rest of the population (Moormeier and Bayles, 2017b). There is a heterogeneity of expression profiles within the biofilm, corresponding to both spatial and metabolic variation *in vitro* (Moormeier et al., 2014). This plasticity allows the biofilm to adapt to a rapidly changing environment (Moormeier and Bayles, 2017b).

Whilst biofilms are commonly isolated from patients and of great clinical importance, most biofilm studies are performed *in vitro*, and lack host factors known to be involved in the process. By studying the expression of biofilm associated components within the living host their impact on the dynamic infection process can be investigated.

5.2 *Chapter aims*

- To investigate *in vivo* expression of components relevant to biofilm development in lesions formed in the zebrafish embryo model of *S. aureus* infection, using reporters for Nuc, Cid & Lrg production and different microscopic techniques to elucidate temporal and spatial production within biofilm-like lesions.
- Correlate biofilm component production with infection progression using transgenic zebrafish lines with labelled immune cells.

5.3 *Results*

5.4 *Expression of Cid and Lrg in vivo*

The *S. aureus* strain UAMS-1 pDM4 (*cid::GFP*, *lrg::DsRed*), a WT strain containing a plasmid with transcriptional reporters (promoter fusions) for both Cid and Lrg production (Moormeier et al., 2014) was initially used to test whether reporter expression was detectable within the host. LWT were infected with ~2000 CFU of UAMS-1 pDM4 and embryos with visible lesions were imaged from 26-31 hpi using the Perkin Elmer spinning disk microscope. Figure 5.1 shows an infected embryo with an already formed lesion, at 26 hpi was a small focus of DsREd, the (reporter for *lrg* expression). Over the 5 hours of timelapse, expression of *lrg* spreads within the lesion from this focus. There is GFP expression distinct from the lesion, at all timepoints during imaging, the distribution of GFP suggests that *S. aureus* expression *cid* are inside phagocytes.

5.4.1 Role of Cid & Lrg proteins in *S. aureus* pathogenesis *in vivo*

Strains from the Nebraska transposon mutant library (NTML) were used to determine the importance of proteins Cid and Lrg in infection progression of *S. aureus* within the host. The strains NE 1466 (JE2 Tn::*cidR*) and NE 1726 (JE2 Tn::*lrgB*) and the WT parent strain JE2, were injected into the circulation of Nacre WT embryos 30 hpf (Figure 5.3). There was no significant difference in survival of embryos infected with NE 1466 (JE2 Tn::*cidR*) (46.87 %) or NE 1726 (JE2 Tn::*lrgB*) (39.29 %) compared to JE2 (51.72 %) at 92 hpi , p = 0.89 and p = 0.26 (Mantel-Cox comparison) respectively, indicating that *cidR* and *lrgB* are not required for *S. aureus* pathogenesis. However, Cid and Lrg are both multi-component systems (CidABC and LrgAB) and recently it has been shown that as well as being regulated by CidR, *cidABC* is also repressed by the TCS SrrAB (Windham et al., 2016) so infection with triple and double mutants is necessary to fully determine whether the CidABC and LrgAB holin and anti-holin system have a role in *S. aureus* pathogenesis.

5.4.2 Construction of *cid* & *lrg* expression reporters in a constitutively fluorescent *S. aureus* background for *in vivo* imaging by microscopy

In order to gain temporal and spatial insight into expression of *cid* & *lrg in vivo* utilising fluorescence microscopy, single reporters for these proteins needed to be moved into a strain with a background constitutive fluorescence. The strains JE2 pMV158-mCherry (SJF 4403) & JE2-mCherry (SJF4625) which both have mCherry under the same promotor (pMal1) were compared on Nikon inverted Ti Dual camera microscope (LMF) and JE2 pMV158-mCherry was ~4x brighter (data not shown) so this strain was chosen as the background for the reporter strains.

Strains UAMS-1 pEM80 (*lrg::GFP*) & UAMS-1 pEM81 (*cid::DsRed*) (gift from Ken Bayles, UNMC) containing the reporter plasmids were resistant to both bacteriophages φ11 & φ85, so the plasmids

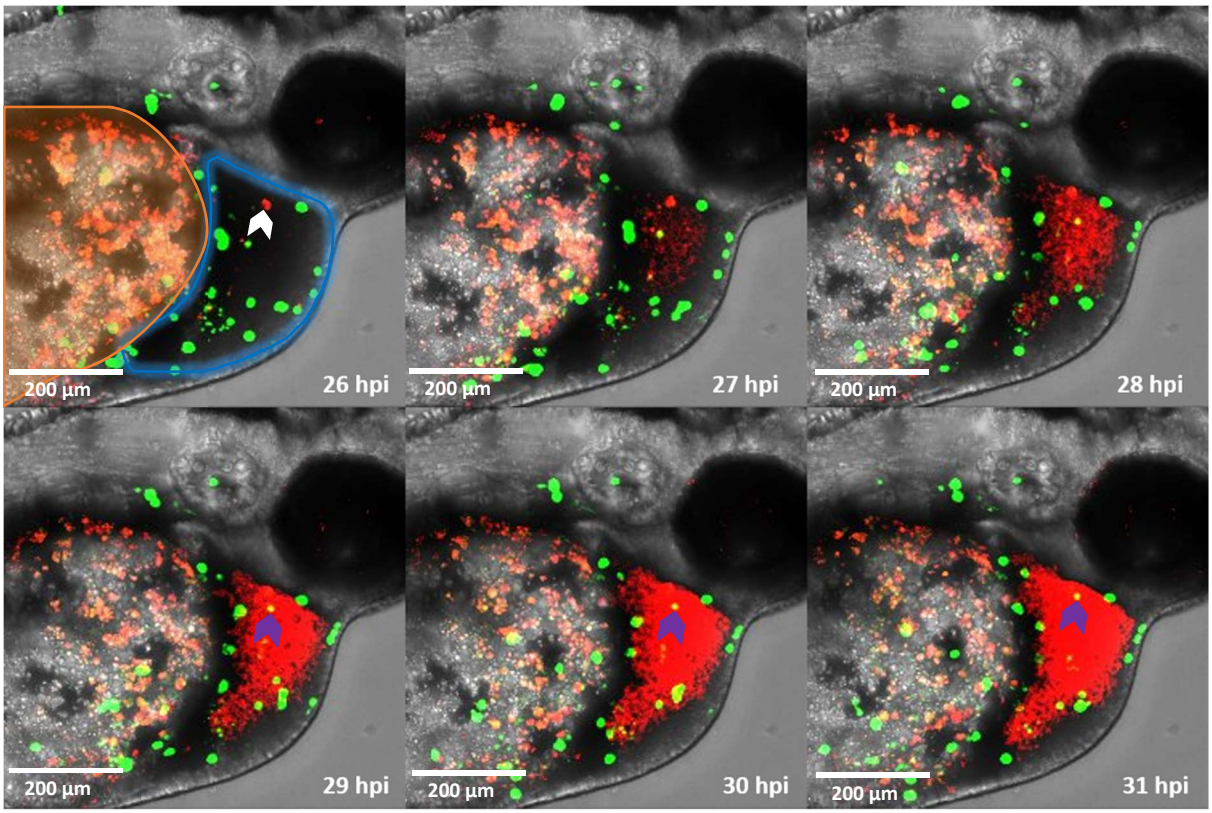

Figure 5.2 Expression of *cid* and *lrg* within *S. aureus* lesion

LWT embryo infected with UAMS-1 pDM4 (*cidABC::GFP, lrg::DsRed*) imaged 26-31 hpi, maximum intensity projection of fluorescence, with brightfield midstack. In the first panel (26 hpi) the region of auto-fluorescence from the yolk is highlighted in orange, the large lesion within the circulation is circled in blue. Scale bar = 200 µm. Expression of *lrg* (DsRed) begins at a focus within the already formed lesion (white arrow) and spreads over time throughout the lesion. Expression of *cid* (GFP) is seen above the lesion. From 29 hpi onwards, colocalisation of *cid* with *lrg* within the lesion is visible in yellow foci (indicated by purple arrowheads).

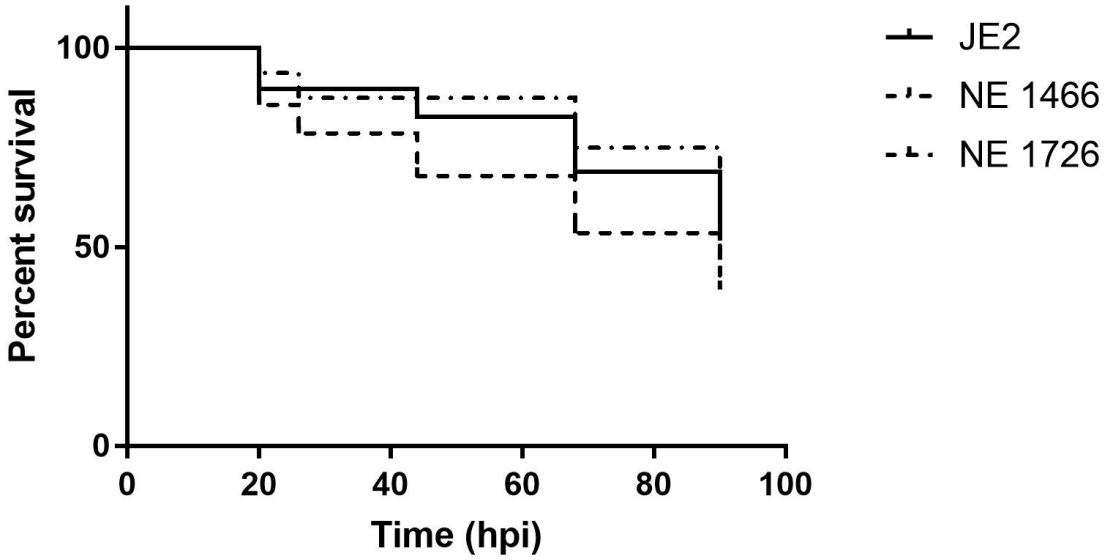

Figure 5.3 *In vivo* characterisation of strains NE 1466 (Tn::*cidR*), NE 1726 (Tn::*lrgB*) and JE2 in the zebrafish infection model

Survival curves for embryos infected with ~1500 CFU of JE2 (n=29), NE 1466 (Tn::*cidR*)(n=32) and NE 1726(Tn::*lrgB*)(n=28). There is no significant difference (Mantel-Cox comparison) in survival of embryos infected with NE 1466 and NE 1726 in comparison with JE2, P = 0.897 and 0.253 respectively.

pEM80 & pEM81 were isolated by midi prep following cell wall digestion by lysostaphin, to allow introduction into other *S. aureus* backgrounds.

The plasmid pEM80 is reporter for *lrgAB*, with production of sGFP under the control of the native *lrg* promoter, the plasmid backbone is based upon pCN51 (Charpentier et al., 2004). The reporter plasmid pEM81 is also based upon that same backbone with production of sGFP controlled by the native *cid* promoter.

Plasmids were subsequently transformed by electroporation into strain RN4220 and transformants were selected on LB containing chloramphenicol (20 μg/ml). Colonies resistant to Cm were selected and the plasmids were moved from RN4220 into JE2 pMV158-mCherry, SH1000 pMV158-mCherry, JE2 and SH1000 by transduction using φ11.

5.4.3 Expression of *cid in vivo*

Nacre embryos were infected with JE2 pMV158-mCherry pEM81 (*pMal1*::*mCherry*, *cid*::*GFP*)(N = 10) and mounted in a glass bottomed petri dish, in 0.8 % (w/v) LMP agarose 0.04 % (w/v) tricaine for spinning disc microscopy. Embryos were imaged from 1 hpi, where *S. aureus* is visible within unlabelled phagocytes (Figure 5.4). At this point all intracellular bacteria are expressing GFP, the reporter for *cid* expression. The same embryos were imaged again at 20 hpi, at this time some embryos had visible lesions within the circulation, shown in Figure 5.5; however these lesions did not fluoresce when excited by either 488 nm (GFP) or 631 nm (mCherry) lasers. Bacteria not associated with the lesion (inside phagocytes) at this timepoint are visible in the mCherry channel. As mCherry is constitutively expressed, all bacteria within an embryo should fluoresce in the mCherry channel. To determine why there was no signal from the lesions, all embryos with visible lesions were homogenised for total CFU counts on plain and selective media, selection of Tet and Cm was used to check for the presence of plasmids pMV158-mCherry and pEM81 (*cid::GFP*) respectively. All embryos had high bacterial burden ranging 3.3×10^5 - 2.5×10^6 CFU, but none of the embryos contained a bacterial population that had retained both of the plasmids, percentage of *S. aureus* recovered with Tet and Cm are shown in Figure 5.6. All samples contained both antibiotic markers within the population, whilst it seems that the reporter plasmid pEM81 was retained more, the group sizes from this experiment are not sufficient for statistical analysis. Since many bacteria recovered from embryos containing lesions were not resistant to Tet, this confirms that non-fluorescing lesions had lost the constitutively expressed plasmid, pMV158-mCherry. It is possible that bacteria within the host that have lost either plasmid would have a fitness benefit within the bacterial population, as they are likely able to replicate more rapidly as production of the fluorescent proteins would be energetically costly.

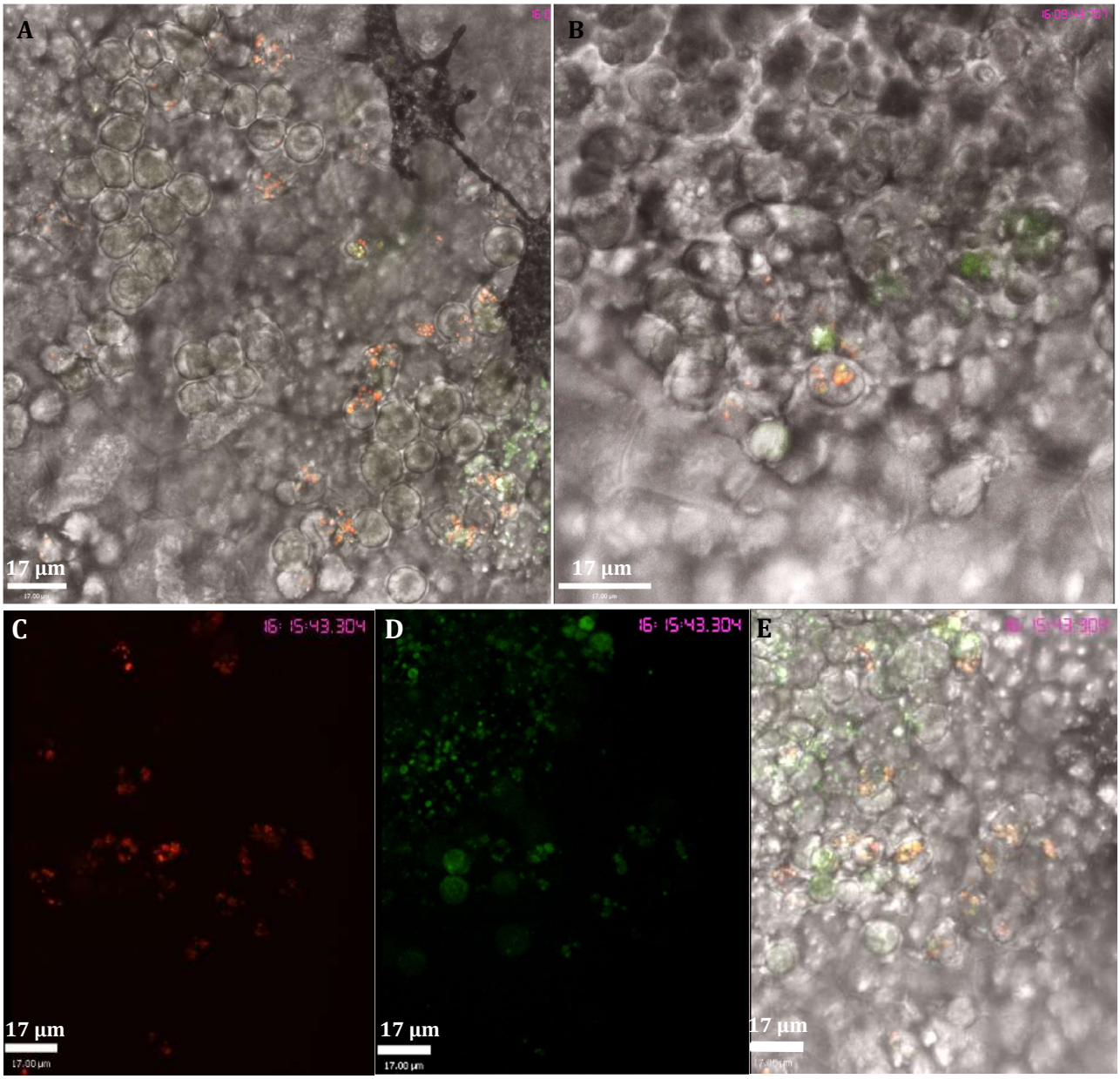

Figure 5.4 Expression of *cidABC* during early stages of *S. aureus* infection

Nacre (WT) embryos (no labelled host cells) infected with JE2-mCherry pMV158 pEM81(*cidABC*::*gfp*) were imaged 1 hpi. Extended focus projections (10-20 µm) **A)** & **B)** GFP, mCherry & brightfield composite, **C) D)** and **E)** are the same image showing **C)** mCherry **D)** GFP **E)** mCherry, GFP & brightfield composite. *S. aureus,* constitutively expressing mCherry are visible within phagocytes, bacteria are also visible in the GFP channel indicating expression of *cid* at this timepoint.

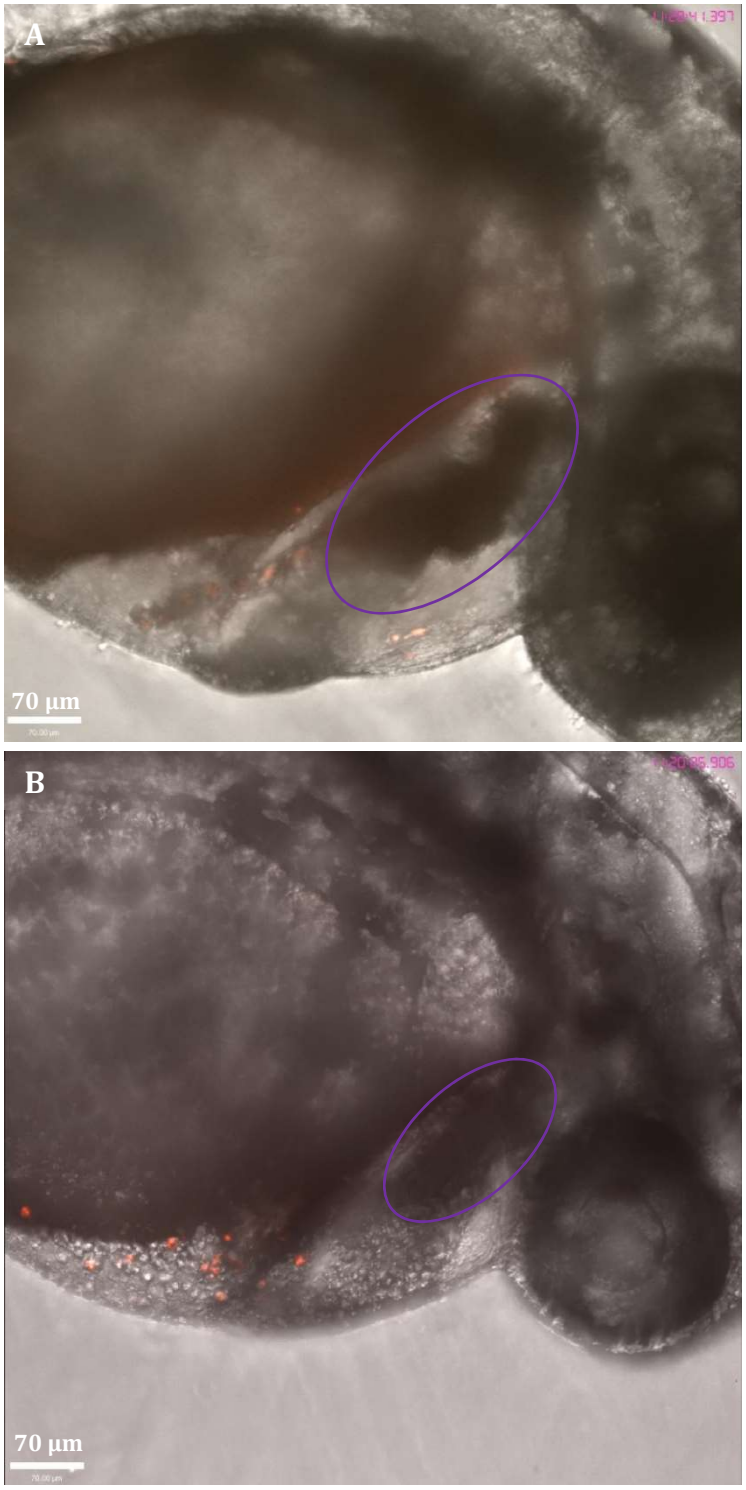

Figure 5.5 Expression of *cidABC* within Nacre embryos during late stage infection with *S. aureus*

Two Nacre (WT) embryos (no labelled host cells) **A)** and **B)** infected with JE2-mCherry pMV158 pEM81 (*cidABC*::*GFP*) (constitutively expressing mCherry, GFP expression controlled by native *cid* promoter) were imaged 20 hpi. Extended focus, z = (10-20 µm) Purple circle indicates large bacterial lesion within circulation valley.

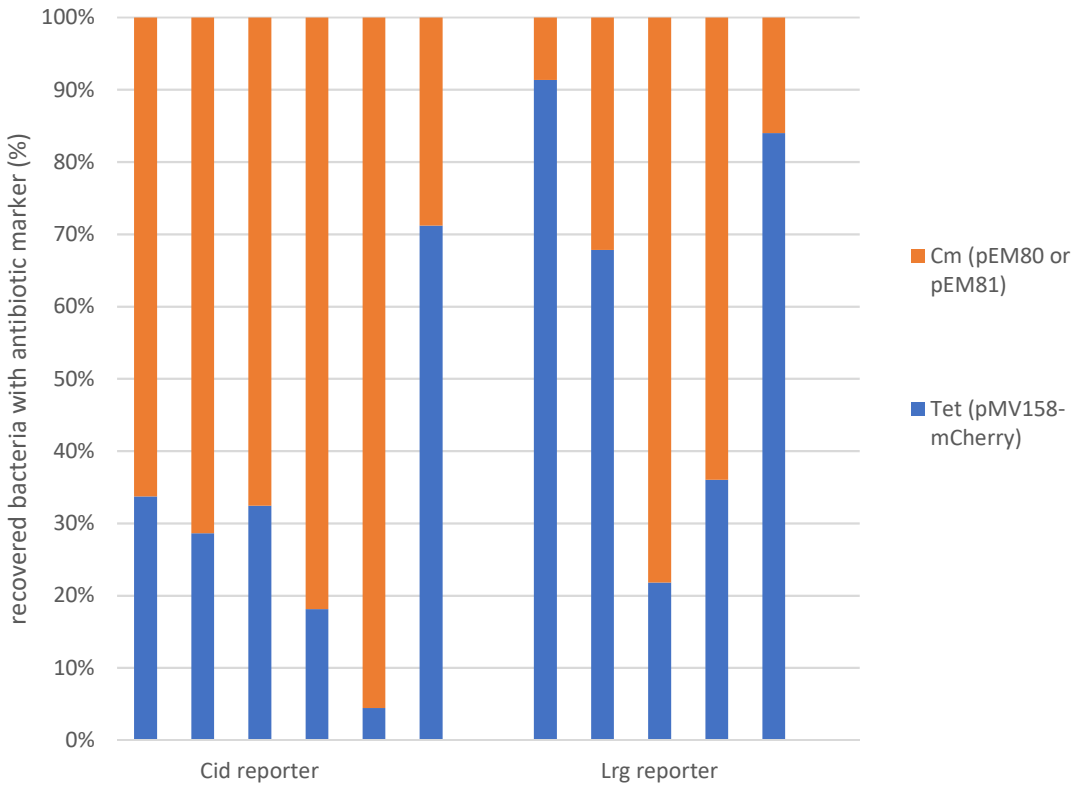

Figure 5.6 Proportion of antibiotic resistant bacteria recovered from embryos with visible lesions

All embryos from imaging experiment (Figure 5.5 and Figure 5.8) (Nacre infected with JE2 pMV158-mCherry pEM80 or JE2 pMV158-mCherry pEM81) with visible lesions were homogenised for bacterial enumeration. Percentage of bacterial population with resistance marker is shown for the two groups. Cid reporter: Cm marker = pEM81 plasmid, Tet = pMV158-mCherry
Lrg reporter: Cm marker = pEM80 plasmid, Tet = pMV158-mCherry

5.4.4 Expression of *lrg in vivo*

Nacre embryos were infected with JE2 pMV158-mCherry pEM80 (p*Mal1::mCherry*, *lrg::GFP*) (N = 10) and mounted in a glass bottomed petri dish, in 0.8 % (w/v) LMP agarose 0.04 % (w/v) tricaine for spinning disc microscopy. Embryos were imaged from 1 hpi, *S. aureus* constitutively expressing mCherry, are visible within unlabelled phagocytes shown in Figure 5.7, at this timepoint no production of GFP, the reporter for *lrg* expression, is visible. The same embryos were imaged 20 hpi, some had visible lesions within the circulation valley, however like the lesions within embryos infected with JE2 pMV158-mCherry pEM81 (p*Mal1::mCherry*, *cid::GFP*) (section 5.4.3), these large aggregates did not fluoresce when excited by a 631nm laser (mCherry). Some lesions had regions of GFP within the lesion, indicating expression of *lrg* by bacteria within the lesion. To determine why there was no mCherry signal from the lesions, all embryos with visible lesions were homogenised for total CFU counts on plain and selective media, Tet and Cm were used to check for the presence of plasmids pMV158-mCherry and pEM80 respectively. All embryos had high bacterial burden ranging 1.0×10^5 - 1.2×10^6 CFU, none of the embryos contained a bacterial population that had retained both of the plasmids, percentage of *S. aureus* recovered with Tet and Cm are shown in Figure 5.6. All samples had populations containing either resistance markers and neither pMV158-mCherry or pEM80 appear more dominant within the group of embryos that had formed lesions, however the group size (N =5) is was insufficient for statistical analysis. When the population percentages for all embryos with lesions are considered together (both groups infected with JE2 pMV158-mCherry pEM81 and JE2 pMV158-mCherry pEM80) there is no significant difference between proportion of the population that carries Tet (pMV158-mCherry) or Cm (cid/lrg reporter), Two-way ANOVA, $p = 0.544$.

To investigate plasmid retention of reporter strains groups of LWT embryos were infected with the strains JE2 pMV158-mCherry pEM80 or JE2 pMV158-mCherry pEM81, ~1500 CFU. Following infection, all embryos with visible lesions were collected (N =10 & N = 11 respectively), homogenised and plated on selective media for enumeration (data not shown). Two-way ANOVA found no statistical difference between the distribution proportions of pMV158-mCherry and pEM81 recovered ($p = 0.560$) and no statistical difference between the distribution proportions pMV158-mCherry and pEM80 recovered from the embryos ($p = 0.259$). Neither the reporter plasmids, or constitutive plasmids are more likely to be retained by the bacteria that overwhelm the embryo. It is evident that both plasmids cannot be tolerated by the same strain and the lack of antibiotic within the embryo during infection removes selective pressure.

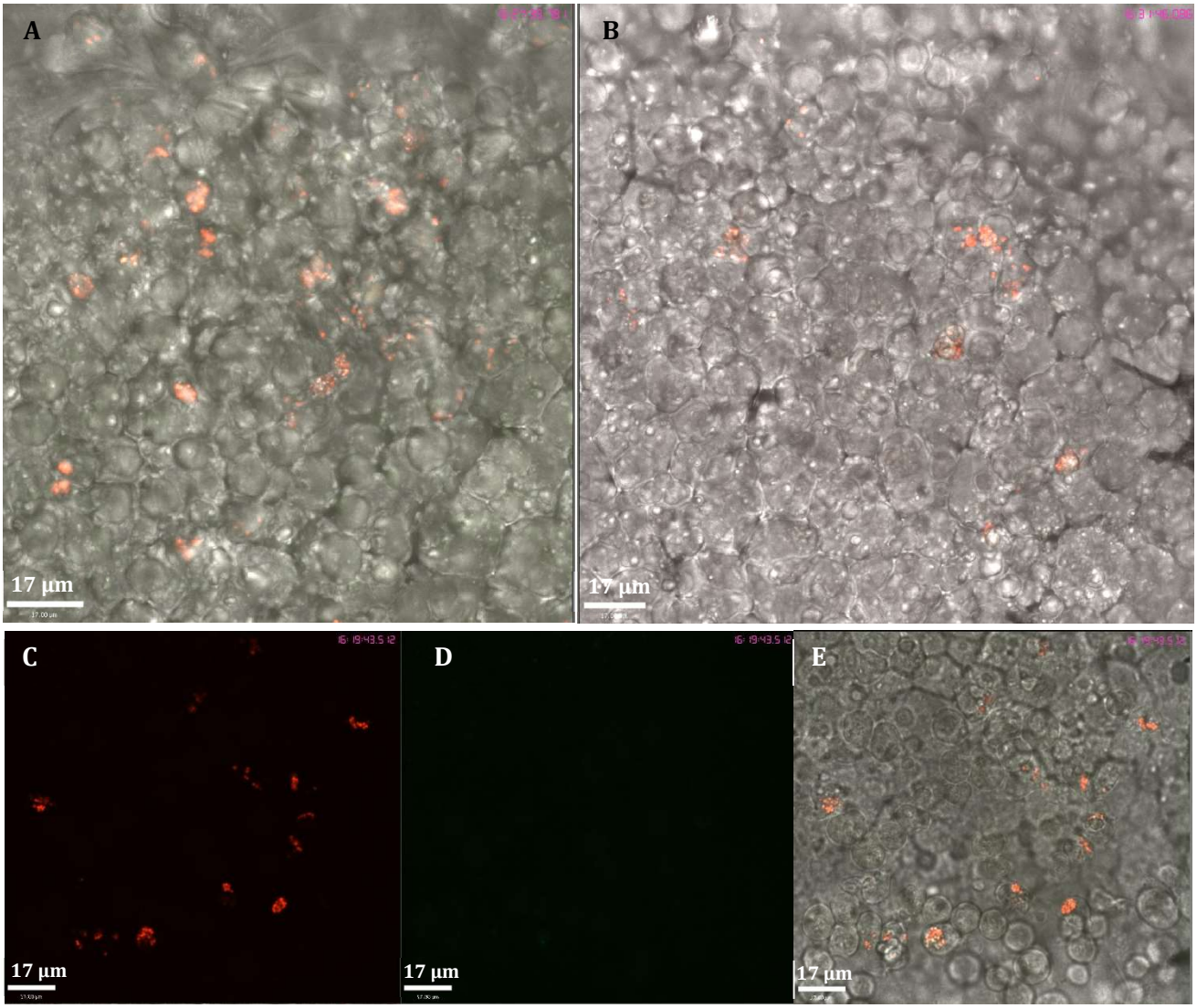

Figure 5.7 Expression of *lrgAB* during early stages of *S. aureus* infection

Nacre embryos infected with JE2 pMV158-mCherry pEM80 (*lrg*::*GFP*), imaged 1 hpi, extended focus projections (10-20 µm). **A)** & **B)** GFP, mCherry & brightfield composite, **C) D)** and **E)** are the same image showing **C)** mCherry **D)** GFP **E)** mCherry, GFP & brightfield composite. *S. aureus*, constitutively expressing mCherry are visible within cells, no signal was detected from bacteria in the GFP channel at this timepoint.

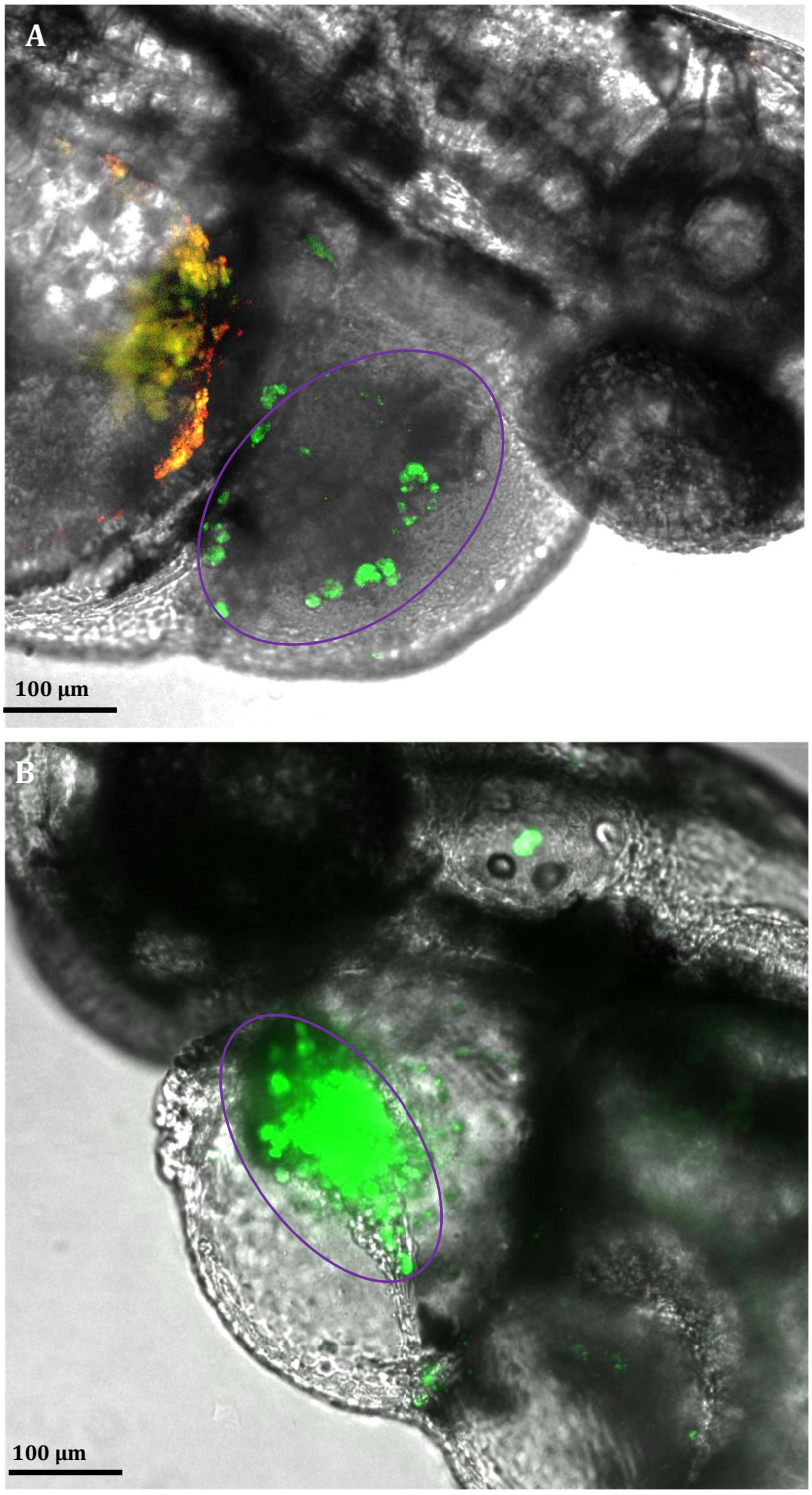

Figure 5.8 Expression of *lrg* within Nacre embryos during late stage infection with *S. aureus*

Two Nacre (WT) embryos (no labelled host cells) **A)** and **B)** infected with JE2-mCherry pMV158 pEM80 (*lrg*::*GFP*)(constitutively expressing mCherry, GFP expression controlled by native *lrg* promoter) were imaged 20 hpi. Extended focus, z = (10-20 µm) Purple circle indicates large bacterial lesion within circulation valley.

5.5 *Construction of cid & lrg reporters integrated in the chromosomal background*

To circumvent the problem with the constitutive expression of the background and the reporter from a plasmid, a chromosomally located fusion was used. Strains with mCherry under the control of the pMal1 promoter, integrated at the *geh* locus on the chromosome, as described by (Pollitt et al., 2018) were chosen as the strain background for the *cid* and *lrg* promoter fusions. The plasmids pEM80 and pEM81 were transferred by phage transduction into strains JE2-mCherry, SH1000-mCherry, JE2 & SH1000. Resultant colonies resistant to Cm were isolated and re-streaked onto media containing both Tet & Cm creating the strains JE2-mCherry pEM80, SH1000-mCherry pEM80, JE2 pEM80 & SH1000 pEM80, JE2-mCherry pEM81, SH1000-mCherry pEM81, JE2 pEM81 & SH1000 pEM81. Presence of plasmids pEM80 & pEM81 was confirmed by isolation by mini prep, followed by restriction digest by BamHI to linearise the plasmid and analysis by agarose gel showed a band of ~6400 bp from all samples (data not shown).

5.5.1 Comparison of pathogenesis of *cid* and *lrg* reporter strains with WT

To ensure that the addition of the reporter plasmids does not impact infection dynamics of *S. aureus* within a zebrafish embryo host, the strains JE2-mCherry pEM80 (GFP *cid* reporter), JE2-mCherry pEM81 (GFP *lrg* reporter) and JE2-mCherry were injected into the circulation valley of LWT embryos, 30 hpf (~1500 CFU) and survival was monitored, Figure 5.9. In all biological replicates, survival was slightly higher in groups infected with reporter strains, at 92 hpi survival was 39.3 %, 55.8% for reporter strains pEM80 and pEM81 respectively, in comparison with 36.7 % of the parental strain (Figure 5.9). There was no significant difference (Mantel-Cox curve comparison) between groups infected with JE2-mCherry pEM80 and JE2-mCherry pEM81 and the parental JE2-mCherry strain ($p = 0.75$, $p = 0.145$ respectively); this result indicates that imaging experiments performed to examine *cid* and *lrg* expression with these strains are representative of *in vivo* dynamics.

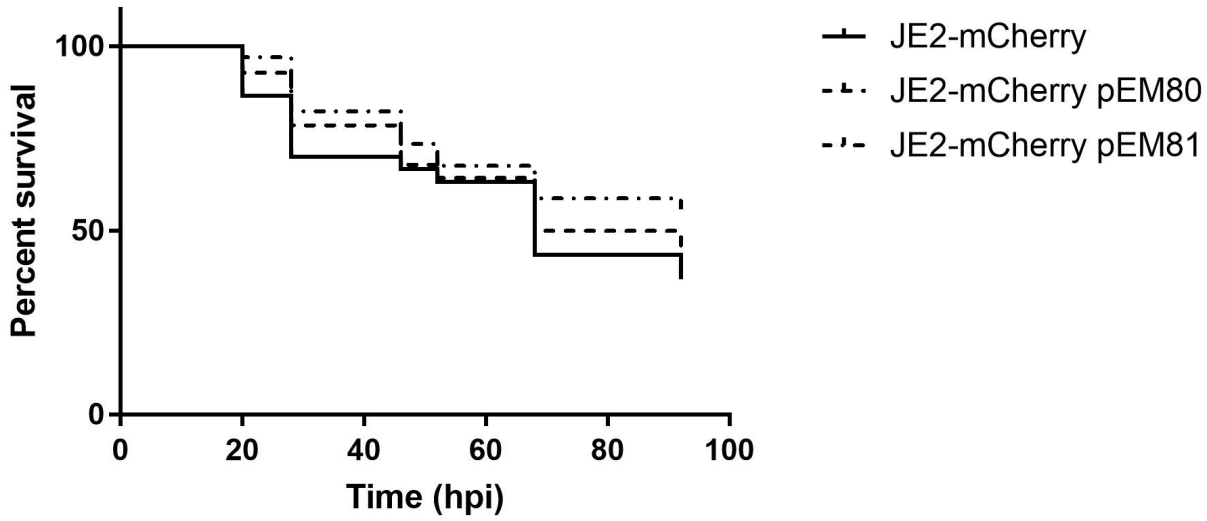

Figure 5.9 Infection of LWT with fluorescent reporter strains

Survival curves for LWT embryos infected with ~1500 CFU of JE2-mCherry (n=30), JE2-mCherry pEM80 (*lrg*::*GFP*) (n=28) and JE2-mCherry pEM81(*cid*::*GFP*) (n=34). There is no significant difference (Mantel-Cox comparison) in survival of embryos infected with JE2-mCherry pEM80 (*lrg*::*GFP*) and JE2-mCherry pEM81 (*cid*::*GFP*) in comparison with JE2 (p = 0.751, 0.145 respectively).

5.5.2 Expression of *cid* in lesions *in vivo*

Nacre embryos (N = 28) were infected 30 hpf with JE2-mCherry pEM81(*cid*::*GFP*), ~2000 CFU via the circulation valley. At 26 hpi embryos with visible lesions (N = 5) were mounted for microscopy in 0.8 % (w/v) LMP agarose in E3 containing 0.04 % (w/v) tricaine. Embryos were imaged by LSFM, demonstrating no GFP expression (from the *cid* reporter) in any of the samples imaged in this experiment, but as expected mCherry expression was found throughout all lesions. A 3D reconstruction of one of these embryos is shown in **'Video 22 – Nacre embryo infected with JE2-mCherry pEM81'.** When homogenised after imaging, all bacterial burdens (N=5, 1.1 – 1.8 x 10^5 CFU/embryo) were comparable when plated on plain and selective (Cm) media, indicating that the lack of GFP signal in this preliminary experiment was due to lack of expression of *cid* within the lesion, as opposed to loss of the reporter plasmid that was experienced with previous strains. Repeats using larger initial infection groups for single time point imaging may reveal expression of Cid within the lesion. Ideally long-term timelapse imaging of embryos with formed lesions by LSFM should provide more insight into real-time temporal expression of Cid within lesions *in vivo*.

5.5.3 Expression of *lrg* in lesions *in vivo*

Nacre Embryos (N = 24) were infected 30 hpf with JE2-mCherry pEM80, ~2000 CFU via the circulation valley. At 26 hpi embryos with visible lesions (N = 4) were mounted for microscopy in 0.8 % (w/v) LMP agarose in E3 containing 0.04 % (w/v) tricaine. Embryos were imaged by LSFM, and GFP expression was found in all large lesions (>50 μm) at this timepoint. A MaxIP is shown in Figure 5.10, where most of the lesion within the circulation valley is expressing GFP, the reporter for *lrg* expression, at this single timepoint. All lesions expressed the constitutive mCherry throughout. Subsequent to imaging, all embryos were homogenised and bacterial burdens (N = 4, 0.9 – 1.9 x 10^5 CFU/ embryo) were comparable when plated on plain and selective media (Cm), demonstrating that the plasmid (pEM80) is stable in the background of JE2-mCherry. Repeats of this preliminary experiment, with larger initial infection groups (more lesions at this timepoint) and may provide more insight into the topological expression of Lrg within the lesion. Time-lapse imaging from an earlier timepoint (20 hpi) might provide information about temporal control of Lrg expression within lesions.

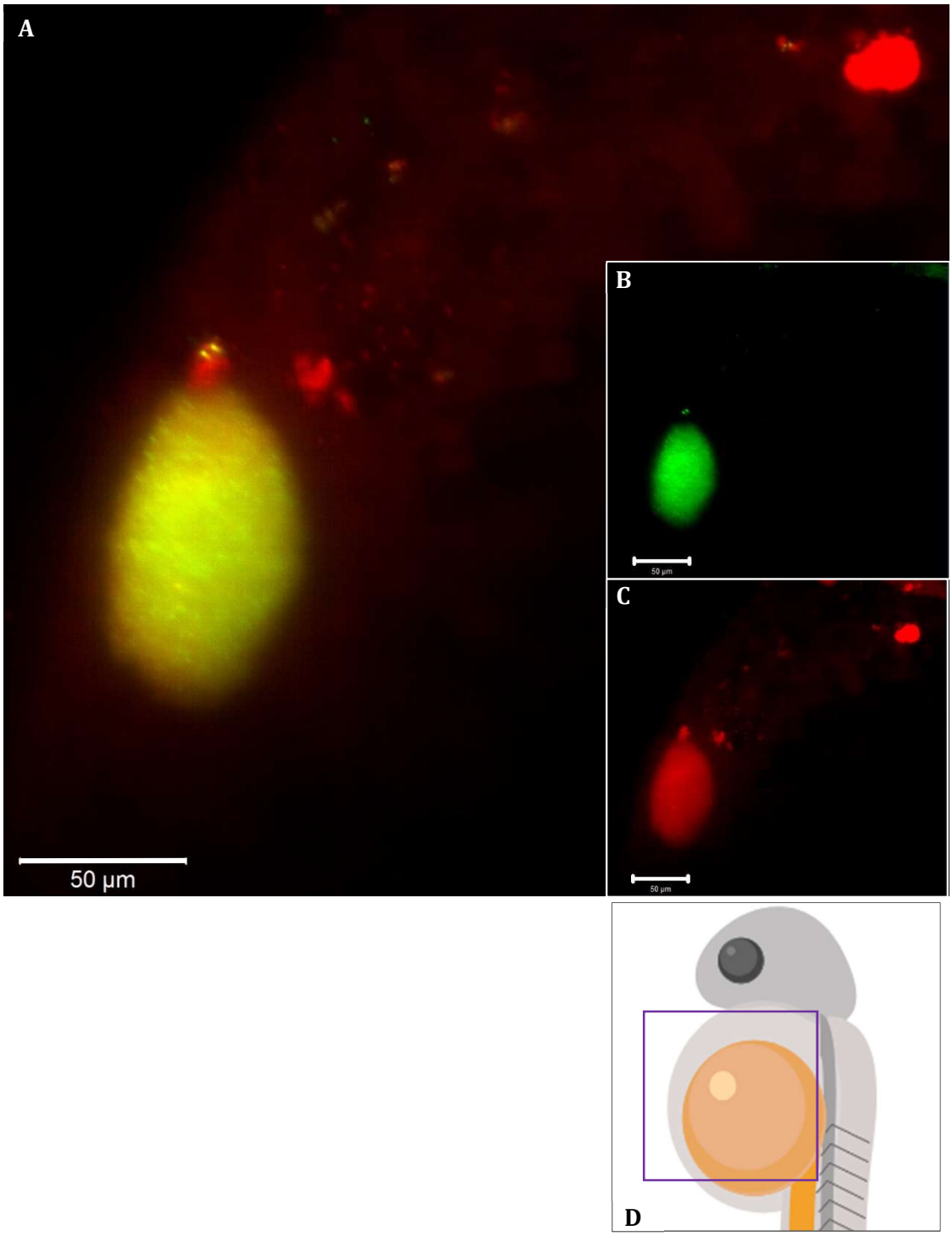

Figure 5.10 Expression of *lrg* within a lesion *in vivo*

A) MaxIP of Nacre embryo (no labelled immune cells) infected with JE2-mCherry pEM80 (*lrg*::*GFP*) (constitutive expression of mCherry, GFP *lrg* reporter) imaged by LSFM 26 hpi. Circulation of embryo was imaged laterally. A lesion ~100 x ~50 um is visible within the circulation, GFP signal is visible throughout most of the lesion showing expression of *lrg* at this timepoint, with two distinct foci of expression also at the top of the lesion. A smaller secondary lesion, not expressing GFP is also visible at the top of the circulation. **B)** schematic of embryo in laterral orientation, purple square for approximation of FOV. Scale = 50 µm.

5.6 *Role of Nuc in S. aureus pathogenesis in vivo*

To determine whether the *nuc* reporter plasmid pCM20 (*nuc*::*GFP*) affects pathogenesis UAMS-1 pCM20 (*nuc*::GFP) and its parent UAMS-1 were injected (~2000 CFU) into the zebrafish circulation valley 30 hpf. UAMS-1 pCM20 (*nuc::GFP*)had virulence comparable to the parent strain UAMS-1 (Figure 5.11). For comparison the Nuc mutant UAMS-1 Δ*nuc* was also injected into the zebrafish and was significantly attenuated compared to the parent strain ($p = 0.0014$) indicating that expression of *nuc* is important for infection progression (Figure 5.11).

5.6.1 Construction of a *nuc* reporter in a constitutively fluorescent background

The strain UAMS-1 pCM20 contains a reporter plasmid for Nuc, with sGFP under the native promoter for Nuc as described in Kiedrowski et al., 2011. In order to visualise the bacteria irrespective of *nuc* expression within a fluorescence microscope the plasmid required transferral to a strain with constitutive fluorescence from a contrasting fluorophore. After the problems encountered with the plasmid incompatibility of pEM80 and pEM81 promoter fusions with the constitutive pMV158-mCherry strains, JE2-mCherry (mCherry encoded on the chromosome at *geh* locus) was chosen as the background. As previously described (section 3.1), the chromosomal JE2-mCherry strain (SJF 4625) had shown affected Tet resistance when recovered from a murine infection model so had been supplemented with an Ery resistance cassette (strain SJF 4634)

As erythromycin is the resistance marker for pCM20 (*nuc*::*GFP*) plasmid, the previous SH1000-mCherry & JE2-mCherry strains (SJF 4622, SJF4625) with affected tetracycline resistance were used as the parental strain.

SH1000-mCherry (SJF4622) and JE2-mCherry (SJF4625) were streaked out from -80 °C stocks on TSB containing no antibiotics and Tet 2.5 μg/ml, 5 μg/ml, 10 μg/ml, both strains grew on all concentrations of Tet and colonies were comparable to plain TSB (data not shown). These strains were also streaked out on Ery 2.5 μg/ml, 5 μg/ml, 10 μg/ml; neither SJF4622 or SJF4625 grew on any concentration of Ery, as expected. Both SJF4622 and SJF4625 grow a yield similar to WT when cultured overnight in a working concentration of Tet. Presence of the fluorophore was confirmed by excitation by 561 nm laser in Z1 light sheet microscope.

When recovered from infected embryos CFU counts on Tet (5 μg/ml) were comparable to plain media. As both strains grew on double working concentration of Tet and reach an expected density overnight, it seems neither has 'affected' resistance and both have a working copy of mCherry, rendering them suitable as the background for the Nuc reporter.

Attempts to propagate bacteriophage φ11 or φ89 on UAMS-1 pCM20 were unsuccessful; an overnight culture of the strain was digested with lysostaphin prior to plasmid purification by Midi-

prep. The plasmid was transformed by electroporation into electrocompetent RN4220 and grown on erythromycin. Colonies resistant to erythromycin were selected and the plasmid was transferred by phage transduction with φ11 into the strains JE2-mCherry (SJF 4625), SH1000-mCherry (4625), JE2 & SH1000, creating the strains JE2-mCherry pCM20 (*nuc*::*GFP*), SH1000-mCherry pCM20 (*nuc*::*GFP*), JE2 pCM20 (*nuc*::*GFP*), and SH1000 pCM20 (*nuc*::*GFP*).

5.7 *Expression of nuc in vivo*

5.7.1 Expression of *nuc* in lesions

To investigate whether lesions that form within embryos express *nuc*, *Tg*(*lyzC*:mCherry)^{SH260} (with mCherry labelled neutrophils) were infected with JE2-mCherry pCM20 (constitutively labelled mCherry, GFP Nuc reporter). Embryos with established lesions were mounted in 0.8% (w/v) LMP agarose and imaged by LSFM 24-28 hpi. At this point of infection all established lesions (>50 μm) express *nuc*. Figure 5.12 is a projection of a 3D reconstruction of a large lesion expressing *nuc*, *S. aureus* has disseminated, and extracellular bacteria are visible within the circulation of the embryo, the rectangle highlights a volume of bacteria, not expressing *nuc* are visible within the circulation, some of these 'aggregates' could be inside labelled neutrophils. A fly-through of this region, showing individual bacteria can be viewed in in **'Video 23 -flythrough of region containing non-lesion associated *S. aureus* within lyz:mCherry embryo 24 hpi'**. A rotating 3D reconstruction of this can be viewed in **'Video 24 - 3D reconstruction of large lesion expressing *nuc* within lyz:mCherry embryo 24 hpi'**. Reconstruction of an embryo 24 hpi with a large lesion is shown in Figure 5.13, a region of the lesion ~32 x 24 μm expressing Nuc at the edge of the lesion, spanning the depth of the lesion. A 3D reconstruction centred on this region can be viewed in **'Video 25 – Large lesion with partial expression of *nuc* within lyz:mCherry embryo 24 hpi'.**

To understand how *nuc* expression occurs over time, time lapse imaging of an embryo with large lesion (~200 x 200 x 280 μm), from 26 hpi was performed by LSFM. A 3D reconstruction of the first timepoint is shown in Figure 5.14 and a video showing a rotating 3D reconstruction as time progresses can be viewed in **'Video 26- Expression of *nuc* in terminally infected, lyz:mCherry embryo'**. There is an increase in GFP signal from the lesion as time progresses, between 2.66 - 3 hours into imaging (29 hpi), the circulation valley ruptures as infection overwhelms the embryo. As well as large areas of *nuc* expression throughout the lesion, there is expression of *nuc* in bacteria not associated with the lesion, not inside a labelled neutrophil.

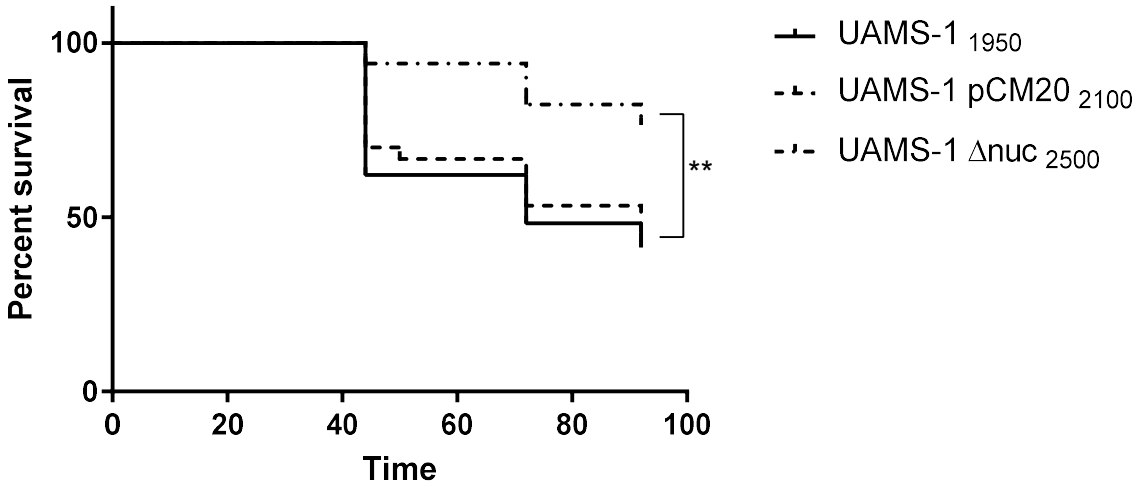

Figure 5.11 *In vivo* characterisation of Nuc mutant and Nuc reporter strains in zebrafish infection model

Survival curves for UAMS-1 (n=29), UAMS-1 pCM20 (n=30) and UAMS-1 Δnuc (n=34), UAMS-1 Δnuc is significantly attenuated in comparison with WT (** $p<0.005$ bonferroni corrected) whereas UAMS-1 pCM20 shows no difference in virulence in comparison with WT.

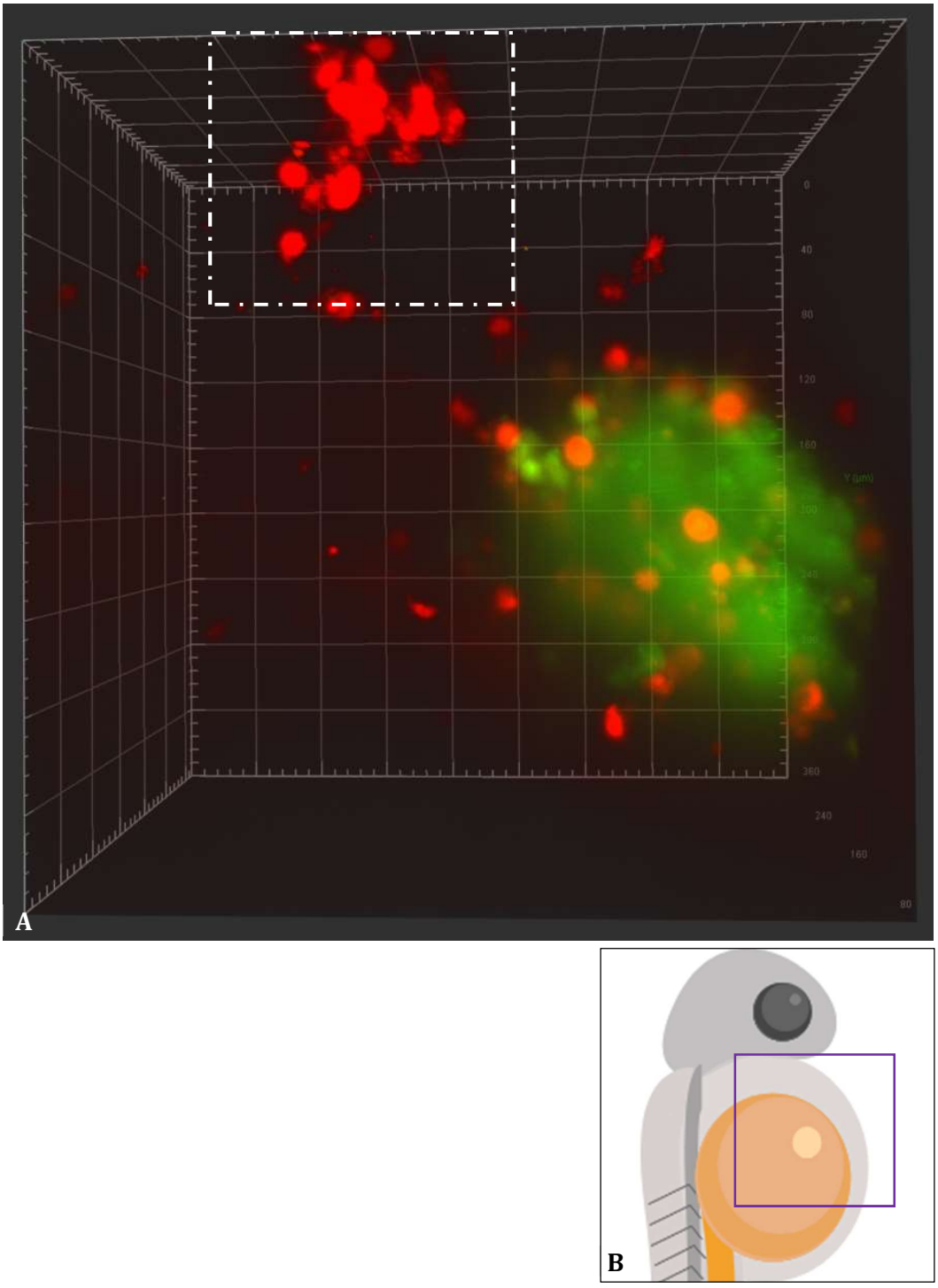

Figure 5.12 Lesion expressing *nuc* within Lyz:mCherry embryo

A) *Tg*(*lyz*:mCherry)^{SH260} embryo (mCherry neutrophils) infected with JE2-mCherry pCM20 (*nuc*::*gfp*) (constitutive expression of mCherry, GFP *nuc* reporter) imaged by LSFM 26 hpi, reconstructed in Arrivis 4D. Dashed rectangle shows area of extracellular bacteria not associated with lesion. Grid squares = 40 x 40 µm, minor gradations = 10 µm. **B) S**chematic of embryo in lateral orientation, purple square for approximation of reconstruction.

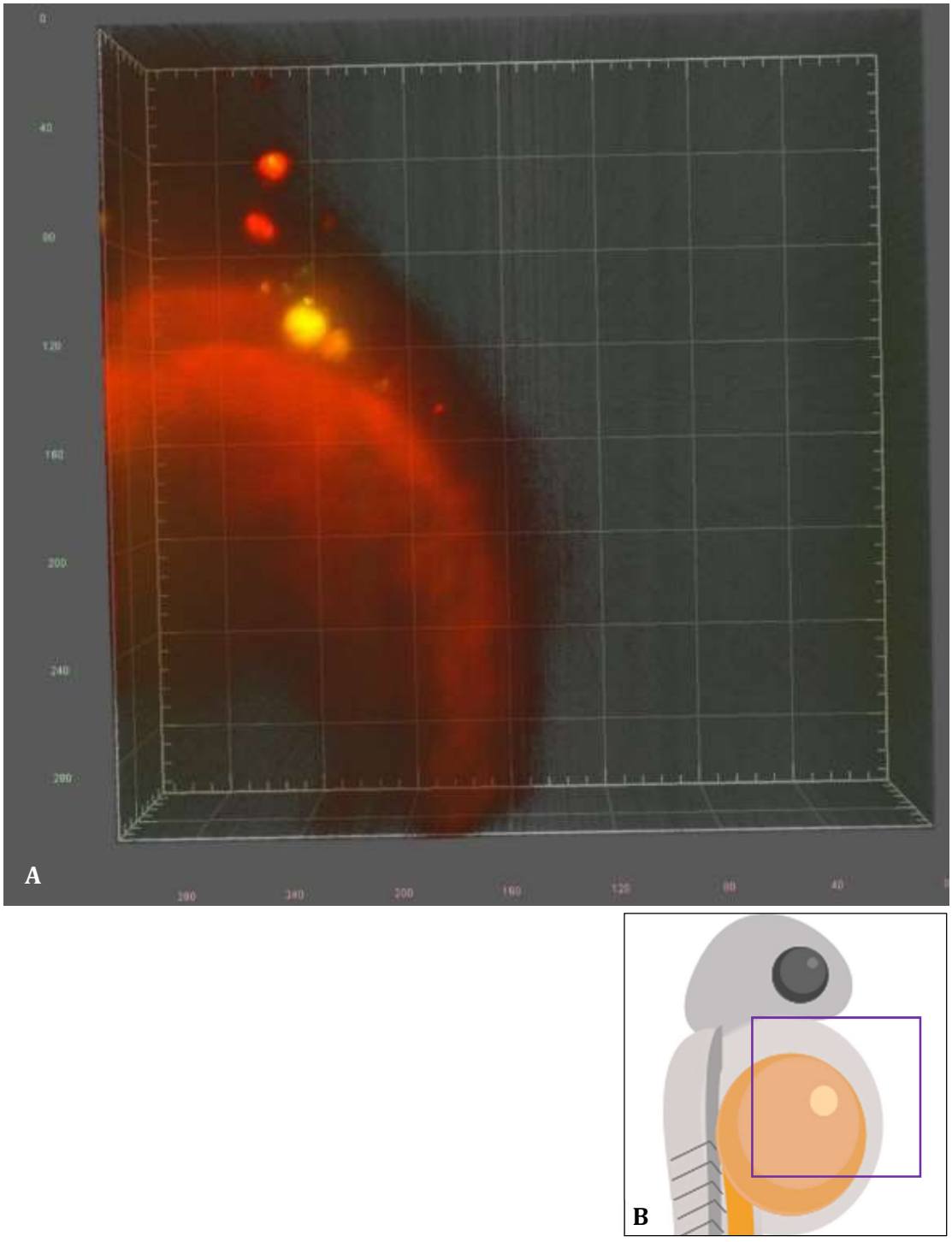

Figure 5.13 Lesion expressing *nuc* within embryo

A)3D projection of *Tg*(*lyz*:mCherry)^{SH260} embryo (mCherry neutrophils) infected with JE2-mCherry pCM20 (*nuc*::*GFP*) (constitutive expression of mCherry, GFP *nuc* reporter) imaged by LSFM 24 hpi, reconstructed in Arrivis 4D. Grid squares = 40 x 40 µm, minor gradations = 10 µm. Large lesion is visible within the circulation valley of the embryo, with a small region of *nuc* expression at one edge **B)** Schematic of embryo in laterral oriention, purple square for approximation of reconstruction.

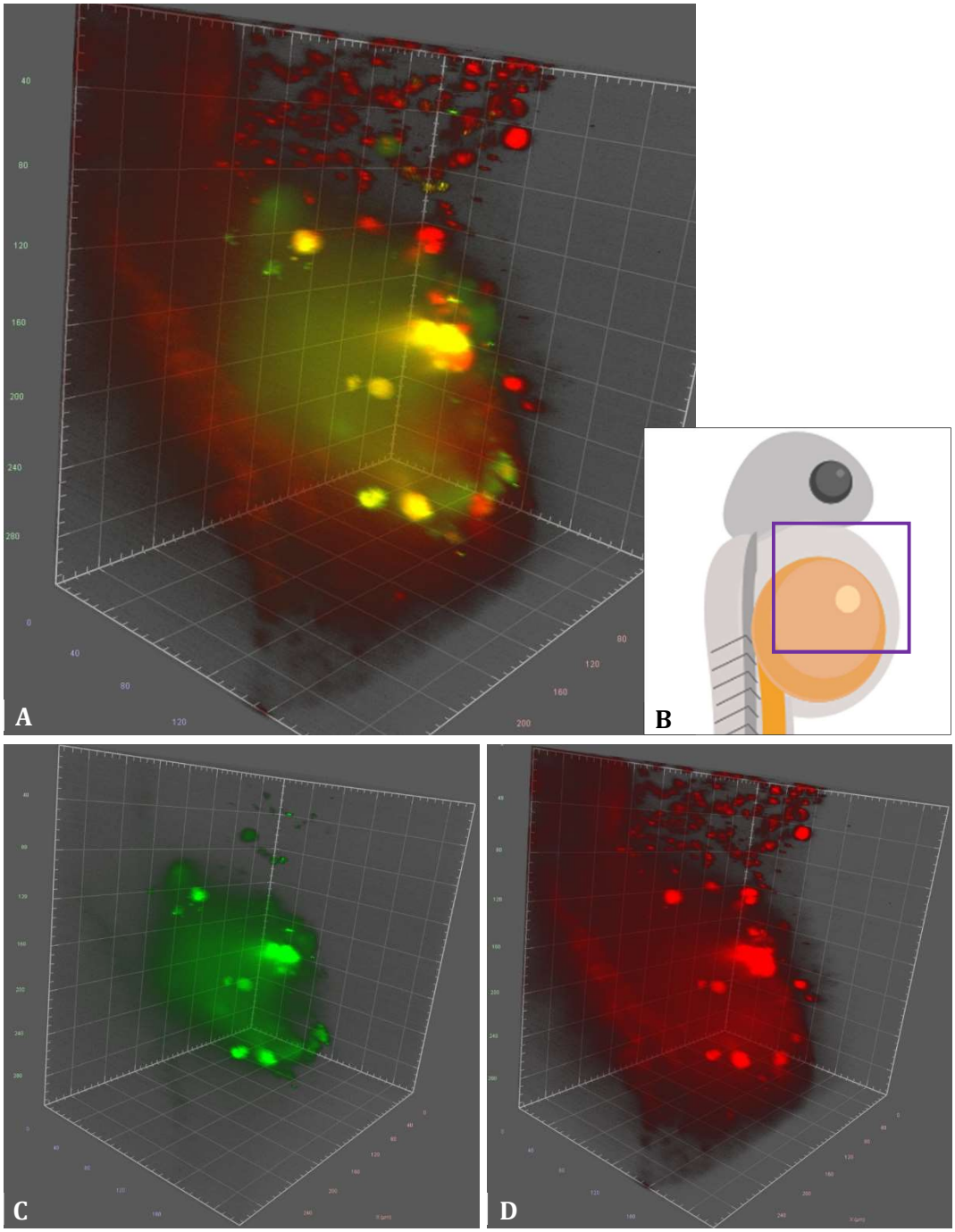

Figure 5.14 3D reconstruction of large lesion within embryo

A) 3D projection of *Tg*(*lyz*:mCherry)^{SH260} embryo (mCherry neutrophils) infected with JE2-mCherry pCM20 (*nuc*::*GFP*) (constitutive expression of mCherry, GFP *nuc* reporter) imaged by LSFM 24 hpi, reconstructed in Arrivis 4D. Grid squares = 40 x 40 µm, minor gradations = 10 µm. Large lesion is visible within the circulation valley of the embryo, with a small region of *nuc* expression at one edge **B)** Schematic to show orientation of embryo, with purple rectangle representing area of reconstruction **C)** GFP channel showing areas of *nuc* expression **D)** mCherry channel showing all bacteria within the lesion.

Individual, extracellular disseminated bacteria, not expressing *nuc* are also visible within the circulation of the embryo.

To gain a more detailed insight of expression of *nuc* by *S. aureus* within a lesion, Nacre (WT) embryos, infected with JE2-mCherry pCM20 were imaged with Zeiss LSM 880 AiryScan microscope at 26 hpi. AiryScan microscopy does not pinhole light like a standard confocal microscope, instead it utilises a concentric, hexagonal, detector array, thus increasing the SNR. The acquired 'Airy disc' is processed by Zen, producing deconvolution, super-resolution images within a living sample (Huff, 2015). Figure 5.15 shows *S. aureus* from the lesion within the circulation of the embryo, the majority of these bacteria are expressing *nuc*. The resolution reveals individual bacteria in this image. To track *nuc* expression of individual cells within a lesion, time lapse imaging of Nacre (WT) embryos with visible lesions 26 hpi was performed. Figure 5.16 shows a 3D reconstruction of a typical lesion at 26 hpi from this experiment, a rotating reconstruction can viewed viewed in **'Video 27 – Lesion expressing *nuc* within Nacre embryo'**. This exemplifies the differential production of the Nuc protein by the population; however, bacteria deeper within the lesion produce lower fluorescence due to more scatter of fluorescent signal, as there is a longer lightpath through tissue to the dectector. Imaging to a depth of 100 μm by this method of microscopy over time bleaches the sample, even using low levels of laser power (488 nm: 0.5 % laser power, 561 nm: 1.0 % laser power). Figure 5.17 shows the timelapse of this volume (timepoints 2-5), with the decrease in fluorescence signal from bacteria within the lesion over time. Although this microscopic technique can give localisation of *nuc* expression within a lesion on a per bacteria basis, it is not suited to following expression of the reporters within embryos over time.

5.7.2 Temporal and spatial localisation of *nuc* expression during infection

To investigate whether *nuc* is expressed during the infectious process, dual labelled *Tg*(*mpx*:GFP, *mpeg*:mCherry CAAX) $^{I114, SH378}$ embryos (GFP neutrophils, mCherry macrophages) were infected with JE2-mCherry pCM20 (*nuc::GFP*) and imaged from 1 hpi by LSFM. A MaxIP of the first timepoint is shown in Figure 5.18, there are extracellular bacteria visible in the circulation and inside both labelled macrophages and neutrophils. A MaxIP of the infection timecourse (FOV 6) can be viewed in **'Video 28 – MaxIP of dual labelled embryo infected with JE2-mCherry pCM20'**. Expression of Nuc by phagocytosed bacteria is visible from 9 hpi inside both neutrophils (Figure 5.19) and macrophages (Figure 5.20) but only by a small proportion of the phagocytosed bacteria. As both phagocytes and *S. aureus* are both labelled with both GFP and mCherry, it is difficult to determine whether Nuc is being expressed within neutrophils (although bacteria expressing *nuc* are brighter than the GFP expressed in the cytosol of the neutrophil).

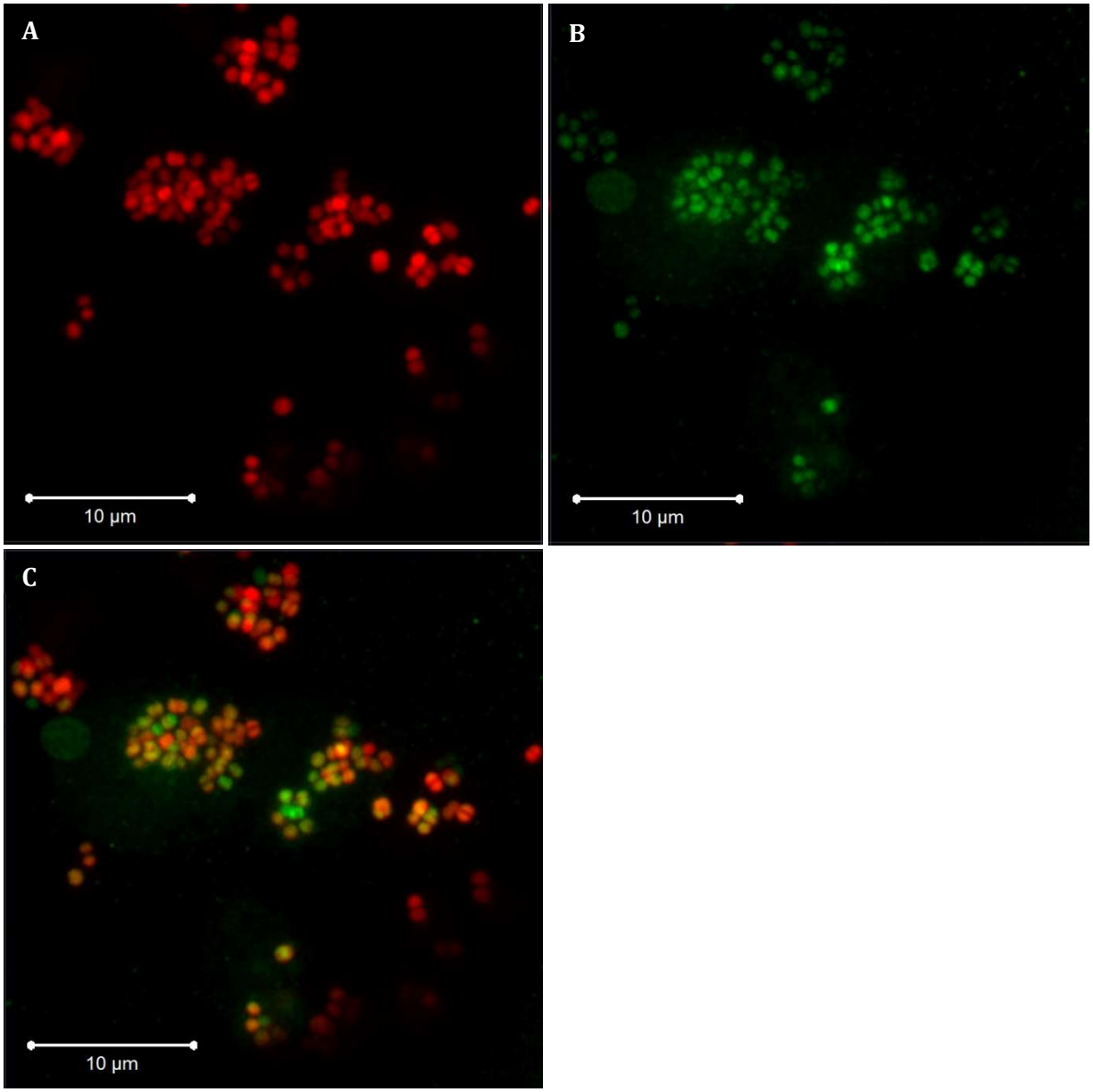

Figure 5.15 MaxIP *S. aureus* expressing *nuc* within a lesion

MaxIP (8µm) of Nacre WT (no labelled phagocytes) infected with JE2-mCherry pCM20 (*nuc*::*GFP*) (constitutive expression of mCherry, GFP *nuc* reporter), 26 hpi with lesion within circulation **A)** mCherry (all *S. aureus*) **B)** GFP (Nuc expressing *S. aureus*) **C)** merge. There is differential expression of *nuc* by bacteria within the same lesion and evidence of bacterial replication in the lesion as unlabelled septa between individual bacteria.

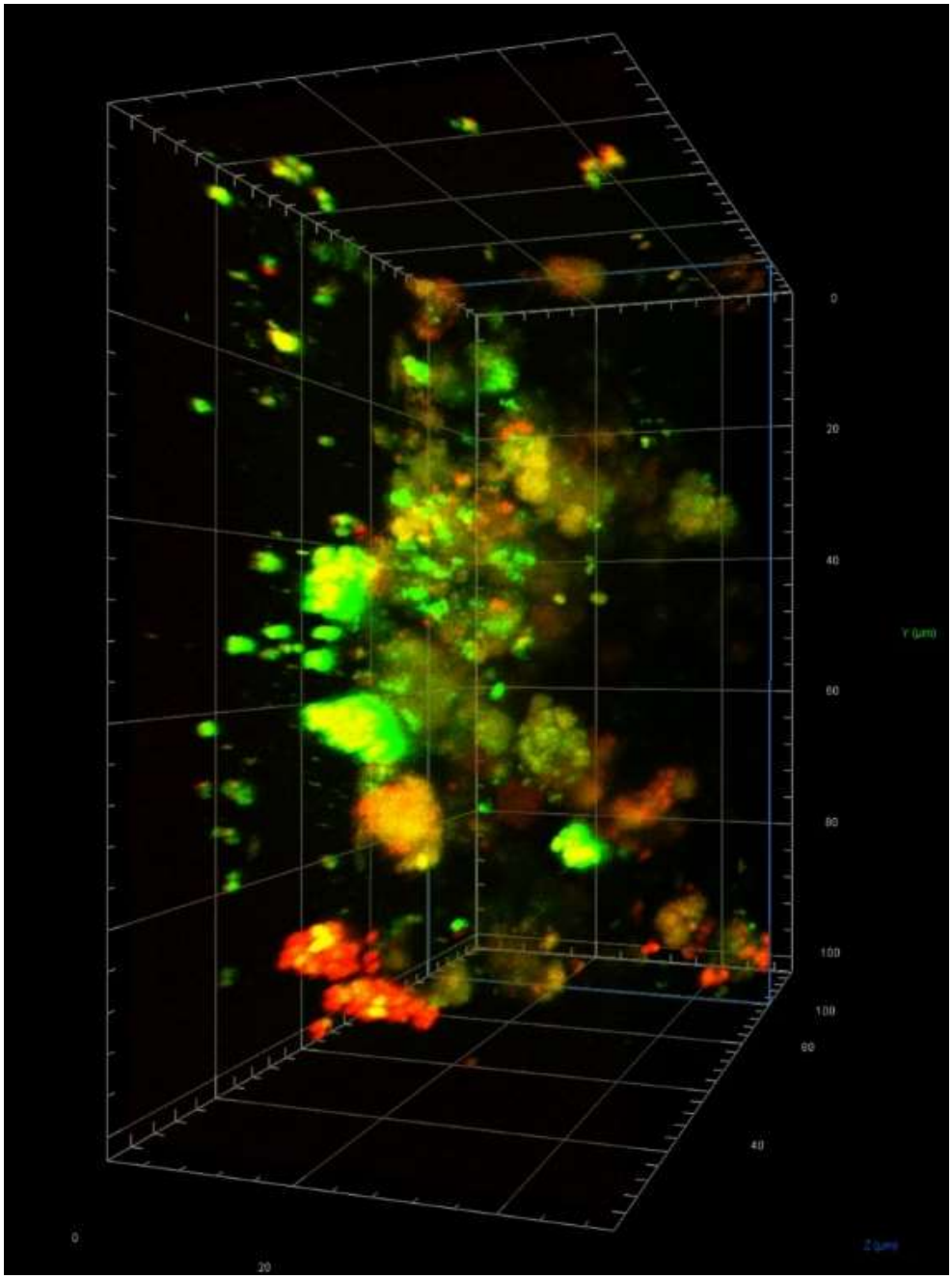

Figure 5.16 3D projection of lesion expressing *nuc* within Nacre embryo 26 hpi

3D reconstruction of Nacre WT (no labelled phagocytes) embryo infected with JE2-mCherry pCM20 (*nuc*::*GFP*) (constitutive expression of mCherry, GFP *nuc* reporter), 26 hpi with lesion within circulation. *S. aureus* is constitutively expressing mCherry with differential expression of *nuc* (GFP).

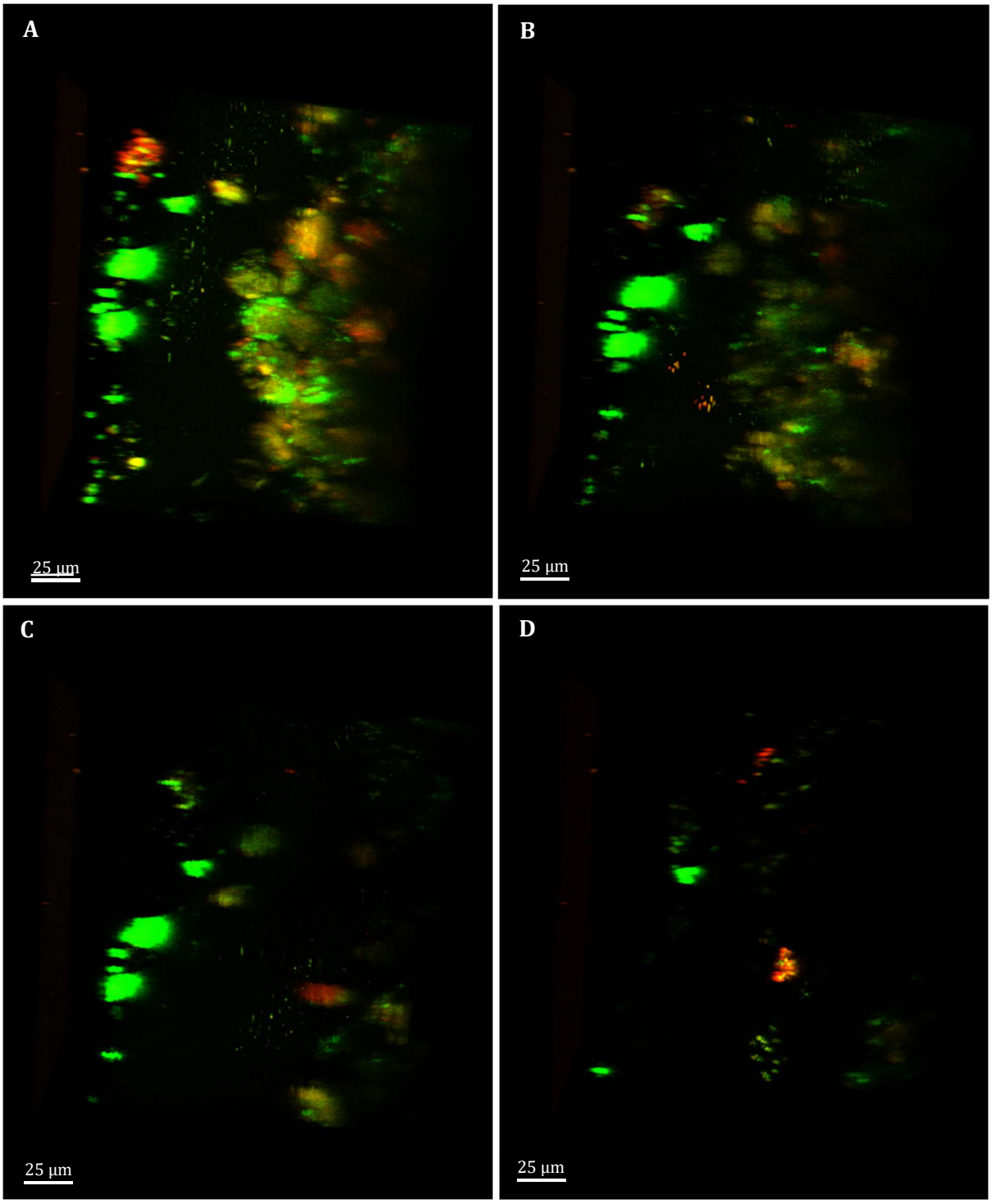

Figure 5.17 Timelapse of *nuc* expression within a lesion

3D reconstruction of Nacre WT (no labelled phagocytes) embryo infected with JE2-mCherry pCM20 (constitutive expression of mCherry, GFP *nuc* reporter), imaged every 20 minutes from 26 hpi onwards. Bacteria are constitutively expressing mCherry, with differential expression of *nuc*. **A)** 26.33 hpi **B)** 26.66 hpi **C)** 27 hpi **D)** 27.33 hpi repeated imaging of the same stack shows bleaching of the fluorescent proteins produced by the bacteria over a short time scale.

To avoid missing *nuc* expression within the embryo, FOV 6 was reconstructed in Arrivis 4D, macrophages were identified by segmentation analysis (diameter >10µm, mCherry) and *S. aureus* expressing *nuc* were identified by segmentation analysis (diameter >1.5µm, GFP) and colocalization analysis (objects identified by second segmentation analysis (GFP) completely covered by first segmentation analysis (mCherry)). This analysis can only identify *S. aureus* expressing *nuc* within the neutrophil if there is a large volume of *S. aureus* (diameter >10µm) within the neutrophil, but all *nuc* expressing *S. aureus* within macrophages will be identified. This analysis is more sensitive then manually examining individual slices within the volume, from 8 FOV over 65 timepoints, (21.66 h) and removes human error. This lower FOV was picked for analysis as it is further away from the heart, and there is less movement in the stack caused by the heartbeat. This analysis identified expression of *nuc* within the macrophage from 5.6 hpi, earlier than was detected when images were examined manually. Only a small proportion of the macrophages identified contained bacteria that were expressing *nuc*. Often only a few bacteria within the phagocyte will be expressing *nuc*, although the phagocyte can contain a large number of bacteria (this occurs in both neutrophils and macrophages). Reconstruction of the timecourse with co-localisation can be seen in **'Video 29 - Colocalisation analysis of *S. aureus* expressing *nuc* within phagocytes'** with pink 'centroids' marking areas of expression of Nuc within the phagocyte (volume of centroids is not proportional to Nuc expression).

The number of voxels occupied by *nuc* expressing *S. aureus* over time is shown in Figure 5.22, not only does the number of co-localised segments increase over time, but the volume (voxel count) of the co-localisation increases over time. This suggests that as time spent within the phagocyte increases *S. aureus* responds to an environmental queue which induces expression of *nuc*. Since the volume of voxels increases over time it is possible that *nuc* expression by an individual bacterium within the phagocyte, stimulates expression of *nuc* by other cells within the phagocyte similar to the way expression of *nuc* spreads within a lesion. The expression of *nuc* at this stage of the infectious process, when *S. aureus* is within the phagocyte, is potentially controlled by SaeRS, a known regulator of *nuc* (Olson et al., 2013). SaeS of the two-component systems SarRS, is located in the membrane *of S. aureus* and responds to phagocytosis related effector molecules, alpha defensins (found in both neutrophils and some macrophages), hydrogen peroxide and human neutrophil peptide (HNPs)(Geiger et al., 2008). In the zebrafish model of systemic *S. aureus* infection, ROS has been quantified in both neutrophils and macrophages, with more ROS in neutrophils than macrophages (Serba, 2015). Therefore both labelled host cell types in my experiment provide an environment that would activate SaeRS and its ensuing upregulation of *nuc*.

Interestingly macrophages containing *nuc* expressing bacteria appear to remain in the same region of the circulation over many time points. An example of this can be viewed in **'Video 30 - 3D**

rotation *nuc* expression within macrophage, timelapse subset FOV 6, t35-37' it is possible that the expression of nuclease is specific to a subpopulation of macrophages. This observation is suggestive of the instances when bacteria have expanded in number and escaped the macrophage, proceeding to overwhelm the host (see section 4.9). It could be that a type of 'resident' subset of the macrophage population is targeted by *S. aureus* factors specific to this cell type.

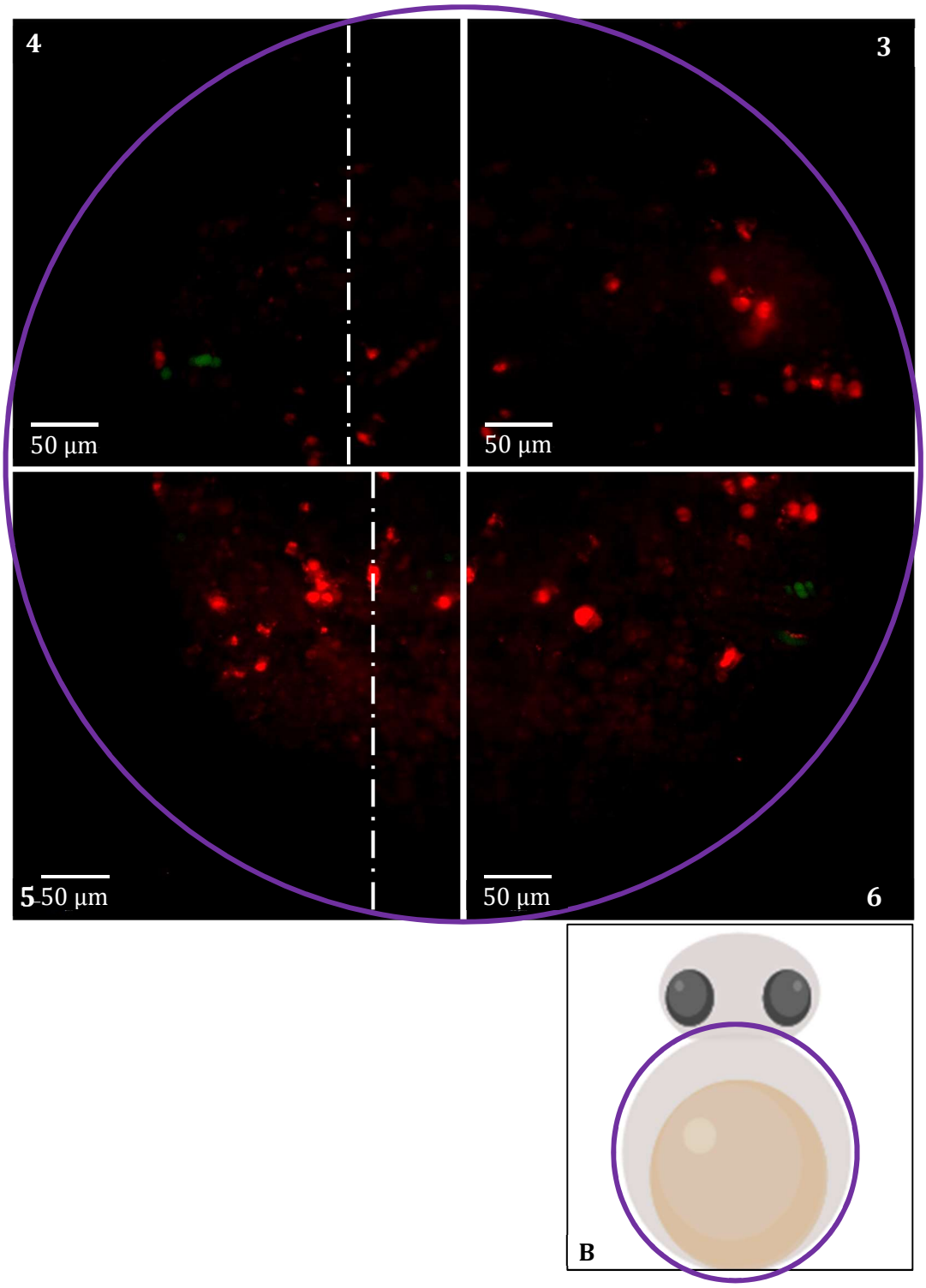

Figure 5.18 MaxIP of embryo with labelled macrophages and neutrophils infected with *S. aureus* reporter for *nuc* expression 1 hpi

A) MaxIP of *Tg*(*mpx*:GFP, *mpeg*:mCherry xCAAX)$^{I114, SH378}$ embryo (with GFP neutrophils and mCherry macrophages) infected with JE2-mCherry pCM20 (*nuc*::*GFP*) (constitutive expression of mCherry, GFP *nuc* reporter), imaged by LSFM at 1 hpi. FOV were acquired at the same imaging angle to cover circulation valley (ROI circled in purple). Dashed line shows regions of overlap with adjacent FOV, order of FOV acquisition numbered in outer corner of each image. **B)** schematic of embryo in ventral orientation, purple circle for approximation of FOV

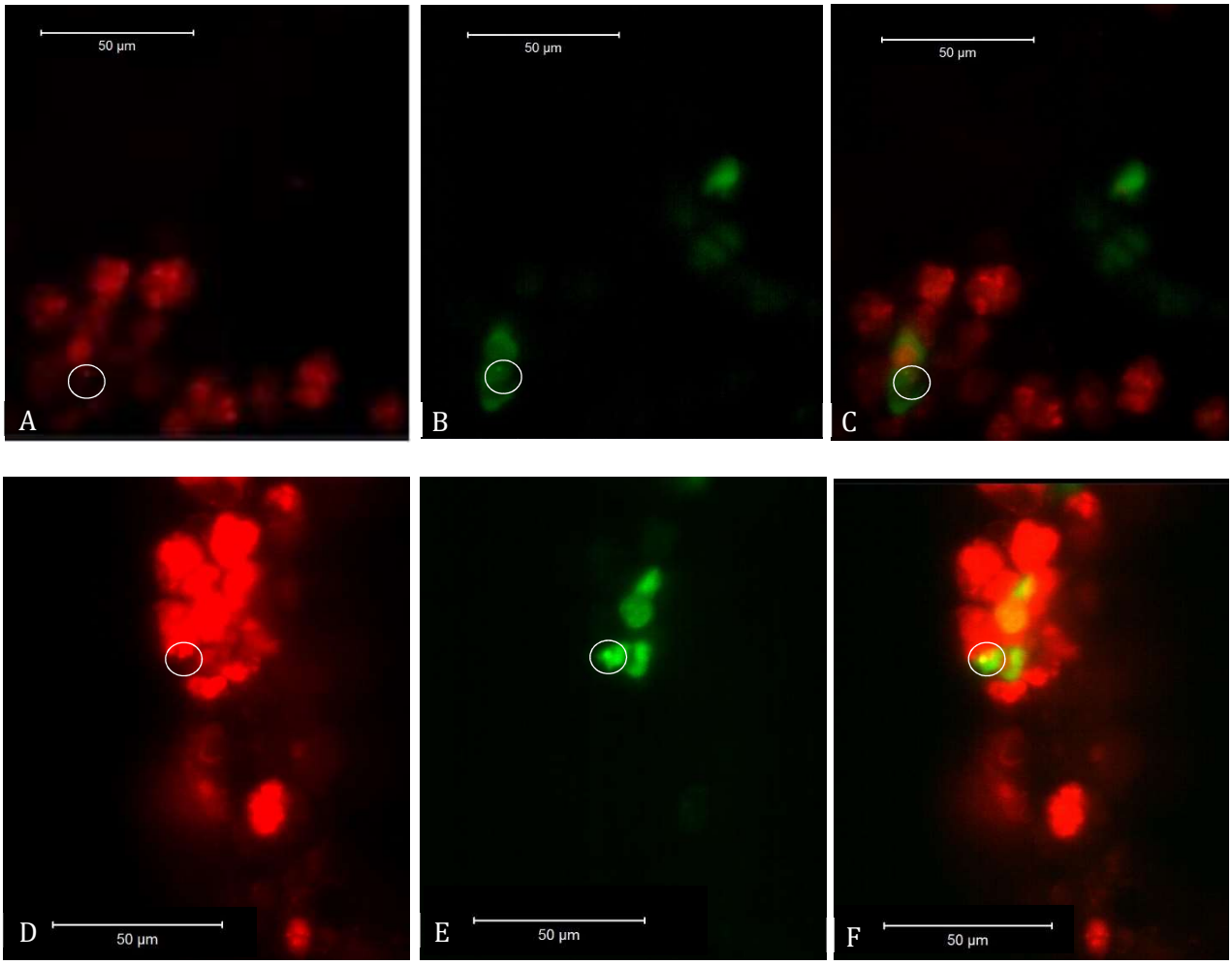

Figure 5.19 Expression of *nuc* by *S. aureus* within a neutrophil

Tg(*mpx*:*GFP*, *mpeg*:mCherry x CAAX)^{I114,SH260} embryo (GFP neutrophils, mCherry macrophages) infected with JE2 mCherry pCM20 pCM20 (*nuc*::*GFP*) (constitutive expression of mCherry, GFP *nuc* reporter), imaged by LSFM, 9hpi. **A)**, **B),** and **C)** are the same MaxIP (8 µm) of 16 slices (0.5µm) showing **A)** mCherry **B)** GFP **C)** merge. **D)**, **E),** and **F)** are the same MaxIP (6 µm) of 12 slices (0.5µm) showing **D)** mCherry **E)** GFP **F)** merge. White circles indicate *S. aureus* expressing *nuc.*

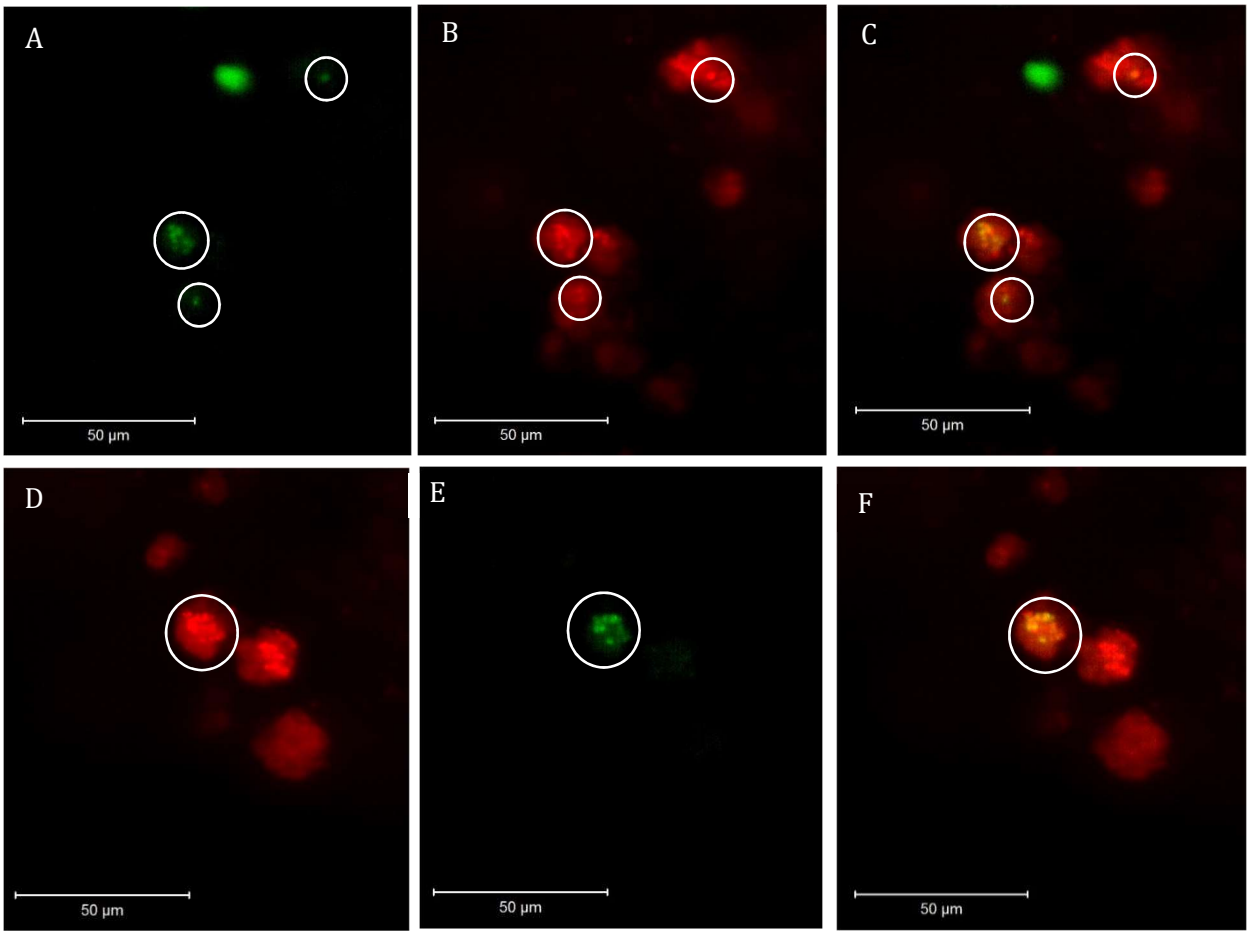

Figure 5.20 Expression of *nuc* by *S. aureus* within a macrophage

Tg(*mpx*:gfp, *mpeg*:mCherry x CAAX)^{I114,SH260} embryo (GFP neutrophils, mCherry macrophages) infected with JE2 mCherry pCM20 (*nuc*::*GFP*) (constitutive expression of mCherry, GFP *nuc* reporter), imaged by LSFM, 9hpi. **A),** **B),** and **C)** are the same MaxIP (7.5 µm) of 15 slices (0.5µm) showing **A)** mCherry **B)** GFP **C)** merge. **D)**, **E),** and **F)** are the same MaxIP (6 µm) of 8 slices showing **D)** mCherry **E)** GFP **F)** merge. White circles indicate *S. aureus* expressing *nuc*.

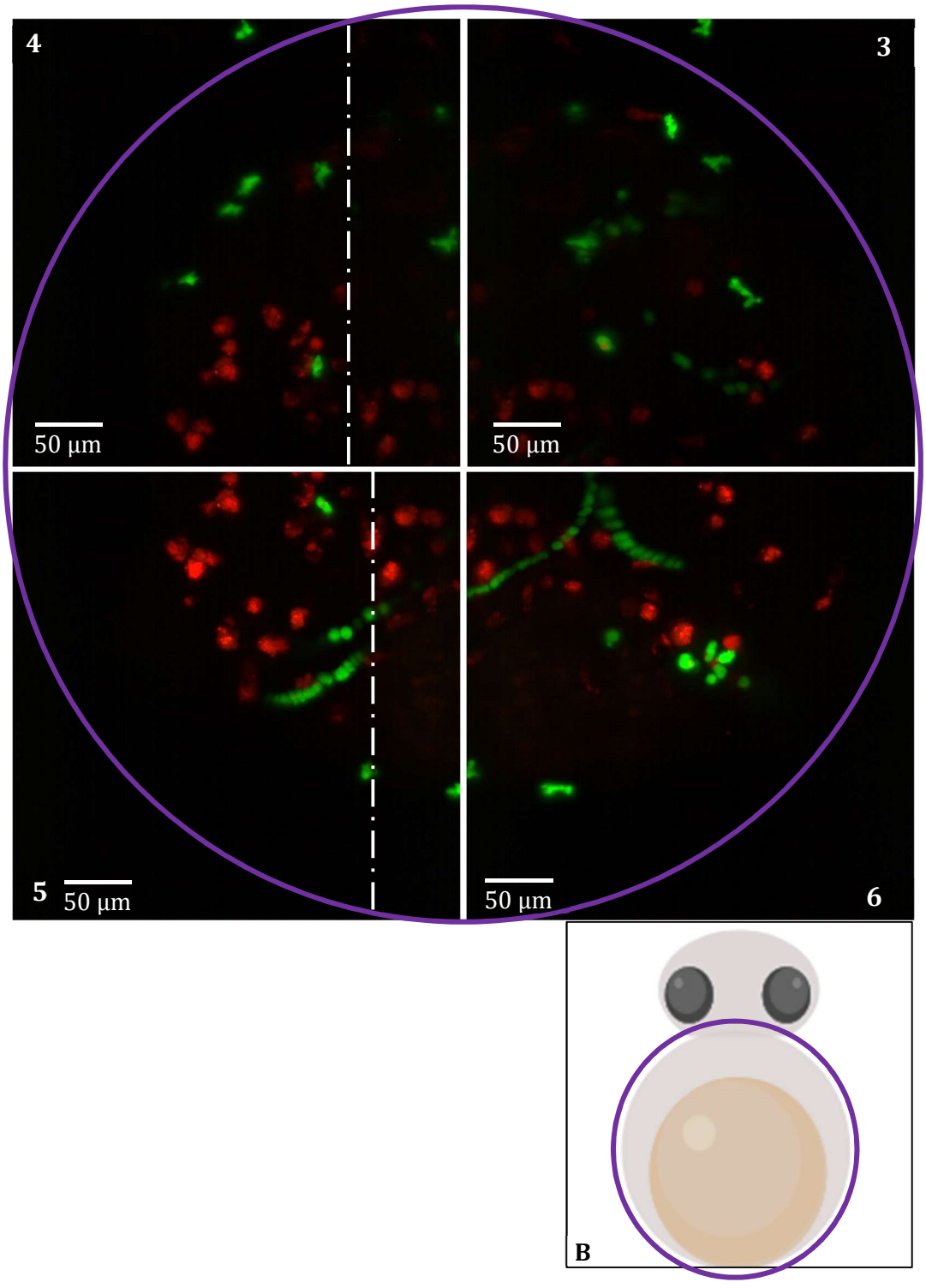

Figure 5.21 MaxIP of embryo with labelled macrophages and neutrophils infected with *S. aureus* reporter for *nuc* expression 23 hpi

A) MaxIP of *Tg*(*mpx*:GFP, *mpeg*:mCherry xCAAX)^{I114,SH260} embryo (with GFP neutrophils and mCherry macrophages) infected with JE2-mCherry pCM20 (*nuc*::*GFP*) (constitutive expression of mCherry, GFP *nuc* reporter) imaged by LSFM at 23 hpi. FOV were acquired at the same imaging angle to cover circulation valley (ROI circled in purple). Dashed line shows regions of overlap with adjacent FOV, order of FOV acquisition numbered in outer corner of each image. **B)** schematic of embryo in ventral orientation, purple circle for approximation of FOV

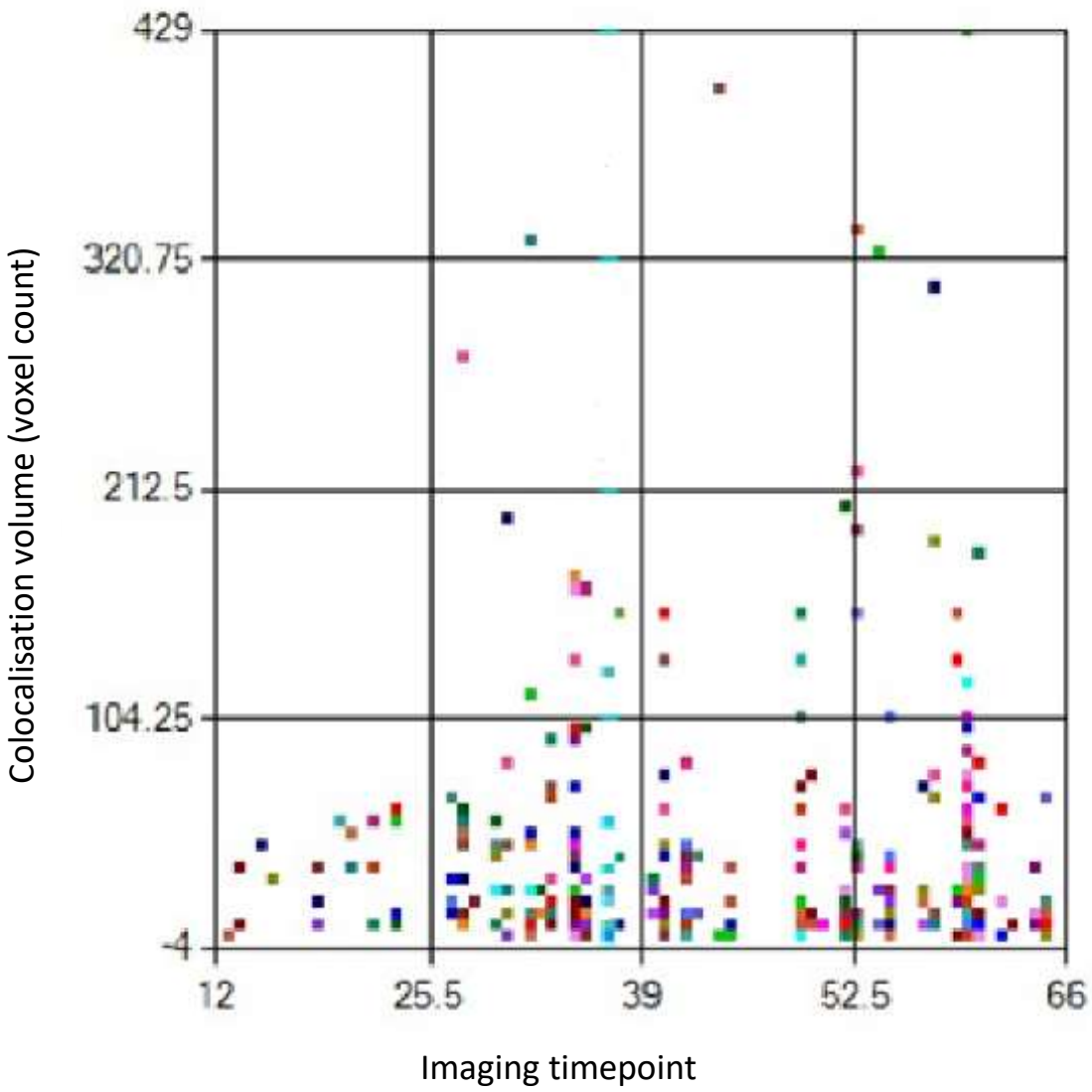

Figure 5.22 Volumetric analysis of *nuc* expression within phagocytes

Results of colocalization analysis of FOV 6 from timelapse imaging of *Tg*(*mpx*:GFP, *mpeg*:mCherry xCAAX)^{I114,SH260} embryo (GFP neutrophils, mCherry macrophages) infected with JE2-mCherry pCM20 (*nuc*::*GFP*) (constitutive expression of mCherry, GFP *nuc* reporter). The number of colocalization events (GFP >1µm within mCherry >10 µm) and the respective volume (in voxels) of each colocalization event plotted against timepoints during the experiment -timepoints every 20 min. T, 12 = 5 hpi T, 66 = 23 hpi.

5.8 *Discussion*

Reporters for the expression of *cid* and *lrg*, involved in the regulation of biofilm maturation through their modulation of murein hydrolase activity, were investigated *in vivo* to determine whether the lesions exhibit biofilm like expression. With interesting initial results from infection with a dual Cid and Lrg reporter strain, single reporters in constitutively fluorescent backgrounds were made. Initially these were made in a background with fluorescence from the pMV158-mCherry plasmid, as this multi-copy plasmid is brighter than the strains with fluorescence encoded on the chromosome so could be used in conjunction with microscopy techniques that are less sensitive than the LSFM but have higher throughput. After these strains were produced, plasmid incompatibility was experienced despite the promoters and resistance cassettes not being listed in any published incompatibility tables (Lozano et al., 2012; McCarthy and Lindsay, 2012; Novick and Brodsky, 1972; Udo and Grubb, 1991) and the reporter plasmids were moved into the chromosomal background.

Although time constraints meant the reporters for *cid* and *lrg* expression were not followed in real-time during infection progression, stable reporter strains for these experiments have now been created to enable LSFM imaging of the *cid* and *lrg* system *in vivo*. Expression of *cid* inside phagocytes is likely due to the acidic environment, as *cidR* has been shown to be activated by low oxygen environment (Moormeier et al., 2014). Furthermore, a recent study has shown that the TCS SrrAB, also regulates *cidABC* transcription (Windham et al., 2016), senses H_2O_2 and modulates H_2O_2 resistance factors. The *srrAB* mutant has decreased survival in stationary phase culture due to increased sensitivity to ROS (Mashruwala et al., 2017). Inactivation of *cidB* in an *srrAB* mutant rescues the phenotype of increased stationary phase and has implicated the CidB protein as a direct mediator of PCD in response to ROS (Windham et al., 2016).

The expression of the *cid* and *lrg* system can now be explored within transgenic embryos with labelled immune components, to elucidate the environments within the host which stimulate production of these proteins. Mutations in the individual *cidA, cidB, cidC lrgA & lrgB* are now available and the effect of these protein on *S. aureus* pathogenesis within a zebrafish host can be explored.

This study has determined that the *nuc* mutant is attenuated in the zebrafish model of systemic *S. aureus* infection, suggesting that the protein is important in pathogenesis. Production of the Nuc protein has been identified in both early and late stages of systemic *S. aureus* infection. If the temporal regulation of *nuc* expression follows the expression pattern *in vitro*, expression of *nuc* in the terminal stages of infection, throughout lesions, is regulated by Agr. Previous work (Prajsnar, 2009) determined that an *agr* mutant is not attenuated in the zebrafish embryo systemic infection model. This is unsurprising as *agr* disfunction is frequently reported in clinical isolates (Altman et

al., 2018; Ferreira et al., 2013; Traber et al., 2008) and has been implicated in persistence (Chong et al., 2013; Xu et al., 2017). It has also been observed that host mortality is negatively correlated with the proportion of *agr* mutants recovered from a bacterial population (Pollitt et al., 2013). Previous experiments with the *agr* mutant in the zebrafish infection model were conducted with a higher initial infection dose and McVicker et al., 2014 showed that clonal lesions do not occur in embryos infected with higher CFUs. It would be interesting to investigate the *agr* mutant infection phenotype and whether lesions form during infection progression, and if lesions do form whether there is *nuc* expression in lesions formed, as with WT *nuc* reporter strains.

Nuc expression has been observed in intracellular bacteria inside both macrophages and neutrophils. This expression will be in response to the intracellular environment, as the bacterial population are not expressing Nuc when initially injected into the embryo. Whilst expression has been followed during the timecourse of infection, overwhelming infection did not occur, so it is not possible to determine whether Nuc production contributes to phagocyte escape leading to lesion formation.

With recent developments in the Arrivis 4D processing software it would be possible to quantify the proportion of intracellular bacteria that express *nuc* during the timecourse of infection. This would be made simpler by transferring the *nuc* reporter to the newly constructed strain which constitutively expresses smURFP (section 4.10.2). By tracking bacteria from initial injection to overwhelming infection using this reporter strain, it could be determined whether expression of *nuc* within a phagocyte is responsible for escape of extracellular bacteria which proceed to overwhelm the host. It is also possible that attenuation of the *nuc* mutant in this model is due to the role of *nuc* expression in the evasion of NETs. A new transgenic zebrafish line has been produced, *Tg(lyz:histone2a.mCherry, mpx:GFP)* with mCherry labelled histones, as a reporter for NET formation (Isles, 2018). Infection of these embryos with *S. aureus* containing the *nuc* reporter or the *nuc* mutant with constitutive fluorescence plasmid could show NET formation and evasion by *S. aureus* for the first time *in vivo*.

6 Discussion

6.1 *Introduction*

Even though the pathogen *S. aureus* has been characterised for over a hundred years, it still poses a great threat to human health, with the continuing spread of antibiotic resistance and no successful vaccine. Much research has determined the role of bacterial and host factors in disease interactions, but mostly measured at a fixed endpoint (mortality, bacterial number in organs, host chemokine levels etc.).

There is still little known about disease dynamics within a host between initial infection and the outcome, be that resolution or the host succumbing. Intra-vital imaging is beginning to provide valuable insight into real-time infection dynamics both temporally and spatially.

The use of zebrafish embryos as a model for vertebrate infection is not only attractive from an ethical standpoint but has a high throughput and good genetic tractability. The transparent nature of the zebrafish embryos and ability to fluorescently labelled specific host cells and organelles lends this model to microscopic evaluation. It is for these reasons that it is being used to study host-pathogen interactions for a ever increasing number of pathogens (Ogryzko et al., 2019; Phelps and Neely, 2007; Prajsnar et al., 2013; Sar et al., 2003; Willis et al., 2018).

Our lab has pioneered the use of the zebrafish model for *S. aureus* infection (Prajsnar et al., 2008) and has primarily been used to identified factors important in pathogenesis (McVicker et al., 2014; Prajsnar, 2009; Prajsnar et al., 2008). The survival assays are a valuable tool when investigating bacterial components, not just as classical virulence determinants but proteins involved metabolism, biosynthesis and antibiotic resistance. This model has identified that the virulence regulator *saeR*, the peroxidase regulon repressor (*perR*) and phenylalanine permease (*pheP*) as important virulence determinants (Prajsnar, 2009). The *S. aureus* mutants with disruption of *purA* and *purB* genes, involved in the purine biosynthesis pathway, has revealed the mutants to be unable to replicate *in vivo* (Connolly et al., 2017). More interestingly *pabA* (involved tetrahydrofolate biosynthesis) mutants are also attenuated in the systemic embryo infection model, but do replicate in vivo, highlighting the pyrimidine salvage pathway as a potential therapeutic target (Connolly et al., 2017). The model has also identified the augmentation of *S. aureus* pathogenesis by human skin commensals (Boldock et al., 2018).

From the host side the model has also shown that both neutrophils and macrophages are essential for combatting *S. aureus* infection (Prajsnar et al., 2008; Serba, 2015). During the initial stages of infection there is an immune bottleneck, with phagocytes providing a niche for bacterial expansion, resulting in a clonal, overwhelming infection (McVicker et al., 2014; Serba, 2015).

Our previous imaging methods have been limited to a small FOV, with a limited depth of imaging and have only been able to focus on a small number of host cells. Any imaging of samples that has been performed at multiple timepoints was done on embryos that were not maintained in the standard conditions (incubated at 28.3 °C in E3 in the absence of anesthetic).

The work in my study has built upon our background knowledge, utilising novel microscopy methods to follow infection progression, in more physiologically relevant conditions throughout disease development. The imaging parameters in my study enable imaging of larger areas of the embryo and are able to track most bacteria within the host.

6.2 *Host-pathogen dynamics*

In order to track infection progression over extended time periods, LSFM was chosen as this type of microscopy can be performed in physiologically relevant conditions. The Zeiss Z1 was specifically designed for imaging of zebrafish (Reynaud et al., 2014b). A method was developed building on established LSFM protocols to mount infected embryos, incubation conditions and imaging parameters in order to image living samples *in toto* for up to 44 hpi. A proposed model of the dynamics of *S. aureus* infection within zebrafish embryos is depicted in Figure 6.1.

From previous results it was originally hypothesised that neutrophils were the 'weak link' in the host response, where bacterial population expansion and subsequent escape would occur (Prajsnar et al., 2012). In my work, escape of *S. aureus* from fluorescently labelled neutrophils during long-term imaging experiments was never observed. In my model neutrophils do not appear to be phagocytosing many bacteria early on during infection. This could be due to the naivety of neutrophils at 30 hpf when embryos are injected. Conversely, when long-term imaging of macrophages was performed phagocytosis was observed from 1 hpi.

Also, there were macrophages recruited to the infection site and many of these had high bacterial burden, to the extent that it was not possible to count individual bacteria within the macrophage. An example of the relative number of neutrophils and macrophages and their bacterial burden at 2.5 hpi is shown in Figure 6.2. Furthermore, there were often infection foci with extracellular bacteria and macrophages with a high bacterial load.

It was thus hypothesised that macrophages are the initial nexus for infection. Using clodronate to deplete macrophages within the embryos, and infection with a mixed inoculum of strains with different antibiotic resistance markers, macrophages were found to be the niche for clonal bacterial population expansion within the host. It is the failure of the macrophages to contain the bacteria in this model which leads to overwhelming infection; a model for this is depicted in Figure 6.3. This concurs with our recent work, which has identified macrophages, specifically Kupffer cells in the

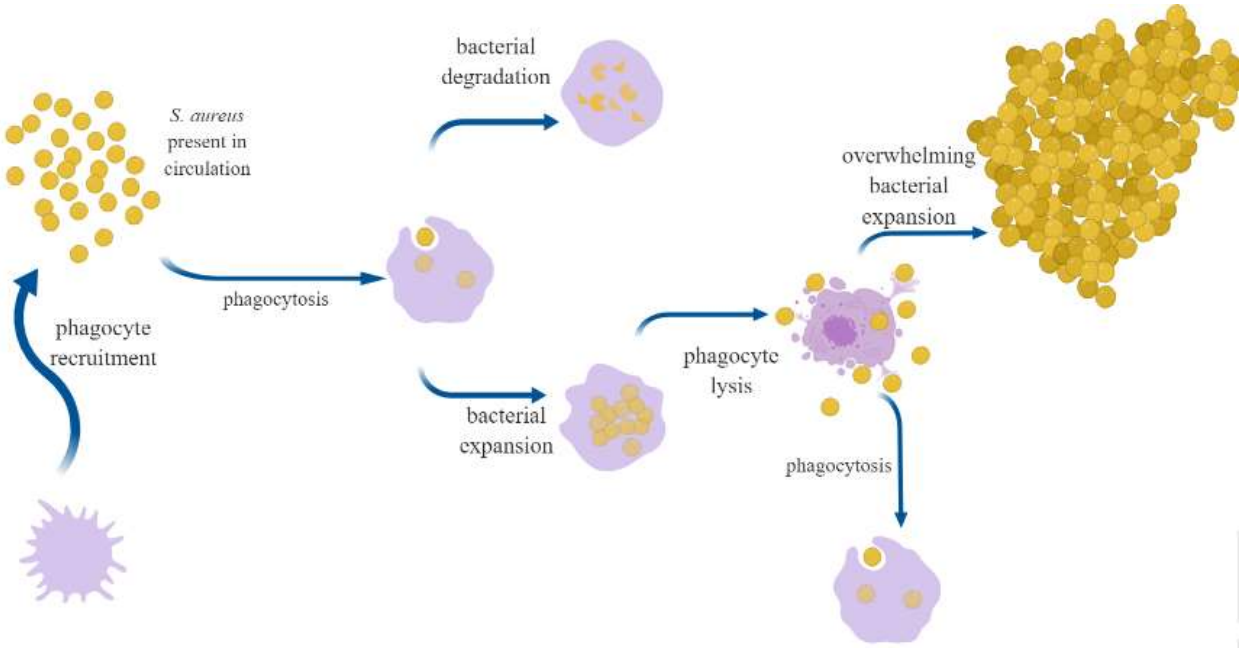

Figure 6.1 Dynamics of systemic infection of *S. aureus* within a zebrafish embryo host

Schematic to show infection progression within the zebrafish embryo host. After infection of the circulation with *S. aureus*, phagocytes are recruited. The bacteria are phagocytosed, subsequently bacteria are either killed within the phagocyte or survive within the host cell and replicate. This eventually leads to phagocyte lysis upon which the bacteria are either phagocytosed by more immune cells or continue to divide, forming large aggregates and overwhelm the host.

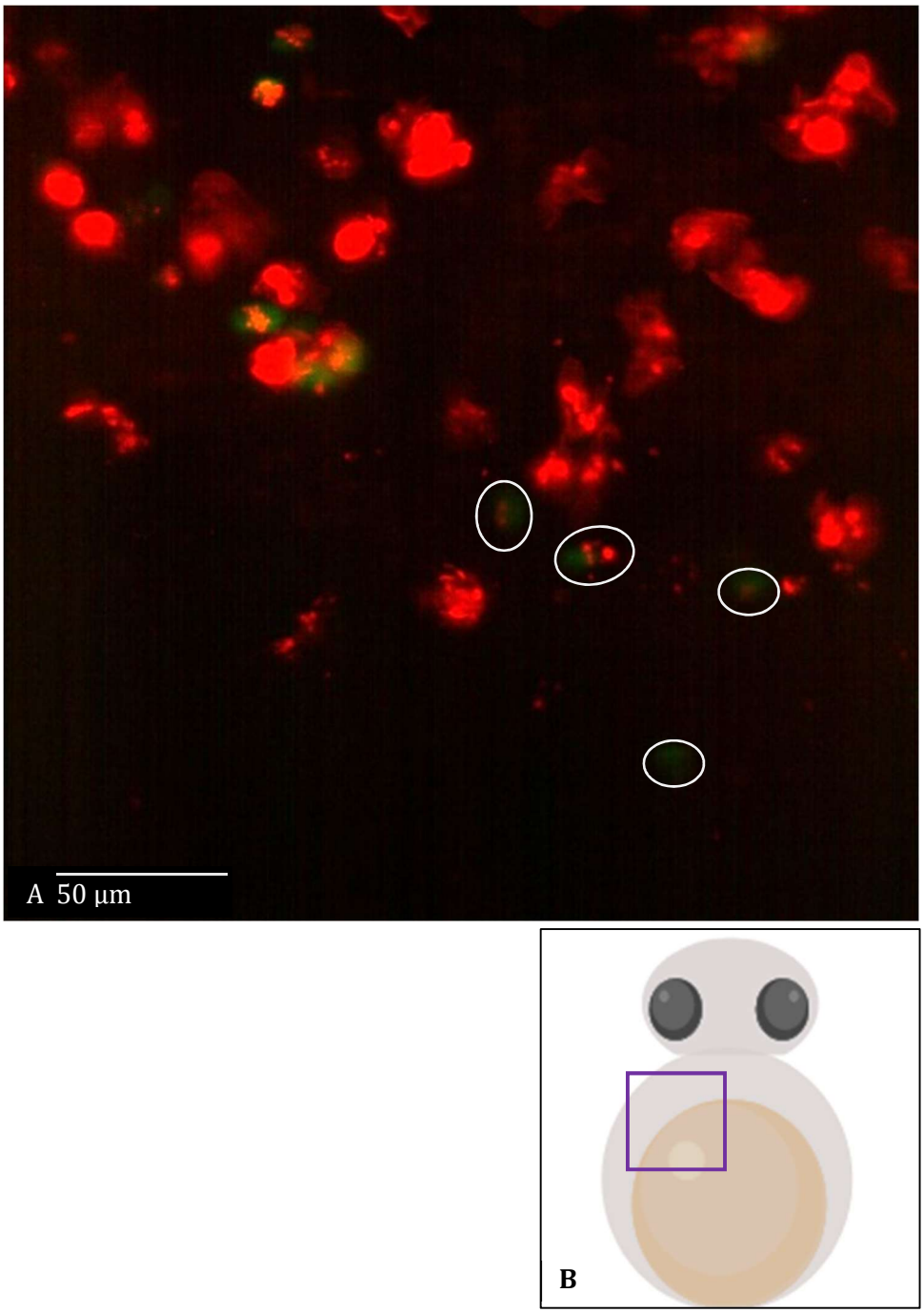

Figure 6.2 MaxIP of embryo with labelled neutrophils and macrophages infected with mCherry *S. aureus*

A) MaxIP of *Tg*(*mpx*:GFP, *mpeg*:mCherry xCAAX)^{I114,SH260} embryo (with GFP neutrophils and mCherry macrophages) infected with JE2-mCherry imaged by LSFM at 2.5 hpi. White ovals highlight faint neutrophils which contain 0-4 bacteria. At this timepoint, there are more macrophages than neutrophils within the circulation (~20 and ~8 respectively in this FOV). The macrophages present have high bacterial burden compared with neutrophils which have only phagocytosed a few bacteria. **B)** Schematic of embryo in ventral orientation with purple square for approximation of FOV

liver, as the niche for bacterial expansion in a systemic murine model of *S. aureus* infection (Pollitt et al., 2018). Loss of clonal expansion after infection with a mixed inoculum occurred when mice are treated with clodronate (Pollitt et al., 2018).

Often in LSFM experiments, after recruitment, macrophages with a high bacterial burden remain in the same region over many timepoints and this is true in the instances of phagocyte escape. *S. aureus* infection results in up-regulation of genes active in the innate immune response: TNF, IL-6, IL-12, IL-1β, CXCL8, CCL2 and CCL5, typically associated with associated with polarisation of macrophages to the M-1 subtype (Benoit et al., 2008). The integrin $\alpha_D\beta_2$ (CD11d/CD18) is a hallmark of M-1 polarised macrophages and increased expression of the α_D subunit results in increased adherence to inflammatory ECM (which typically contains fibronectin, thrombospondin, fibrinogen) and retention of M-1 macropahges (Cui et al., 2018).

Clonal expansion was identified in Kupffer cells, resident macrophages of the liver (Pollitt et al., 2018) and it is possible that *S. aureus* is targeting an immune component that is associated with the retention of macrophages to the tissue.

6.3 *Reporters of virulence determinants*

Differential expression of virulence factors is the response of the pathogen to its environment and this plasticity enables the pathogen to acquire nutrients and adapt to the host. During the initial stages of infection, expression of adhesins and immune evasion proteins occur (Geiger et al., 2008) ,many of which are regulated by the *sae*RS TCS (Nygaard et al., 2010). The ability to track expression of virulence factors within the host, within different biological niches, in real time provides insight to their role during infection progression.

In this study, expression of the *saeRS* regulated *nuc* within a living host was examined and it was found that *nuc* mutants are attenuated in the systemic embryo infection model. This work has also demonstrated differential expression within a population of genetically identical bacteria *in vivo*, particularly within phagocytes. It was found that there was increasing signal from the reporter for *nuc* expression as infection progresses and *nuc* was expressed by a subset of bacteria within phagocytes (both neutrophils and macrophages). Interestingly expression of *nuc* within macrophages was identified and followed over time, with an increasing number of intracellular bacteria expressing *nuc* as infection progresses. Other studies investigating nuc expression have mainly focused on neutrophils and the extravasion of NETS (Berends et al., 2010; Kiedrowski et al., 2014; Olson et al., 2013) and have not shown a role for *nuc* expression in macrophage escape or killing.

Expression of *nuc* in the lesions which form within embryos has also been identified, likely due to activation by Agr. This is analogous to expression of *nuc* in mature biofilms and probably leads to

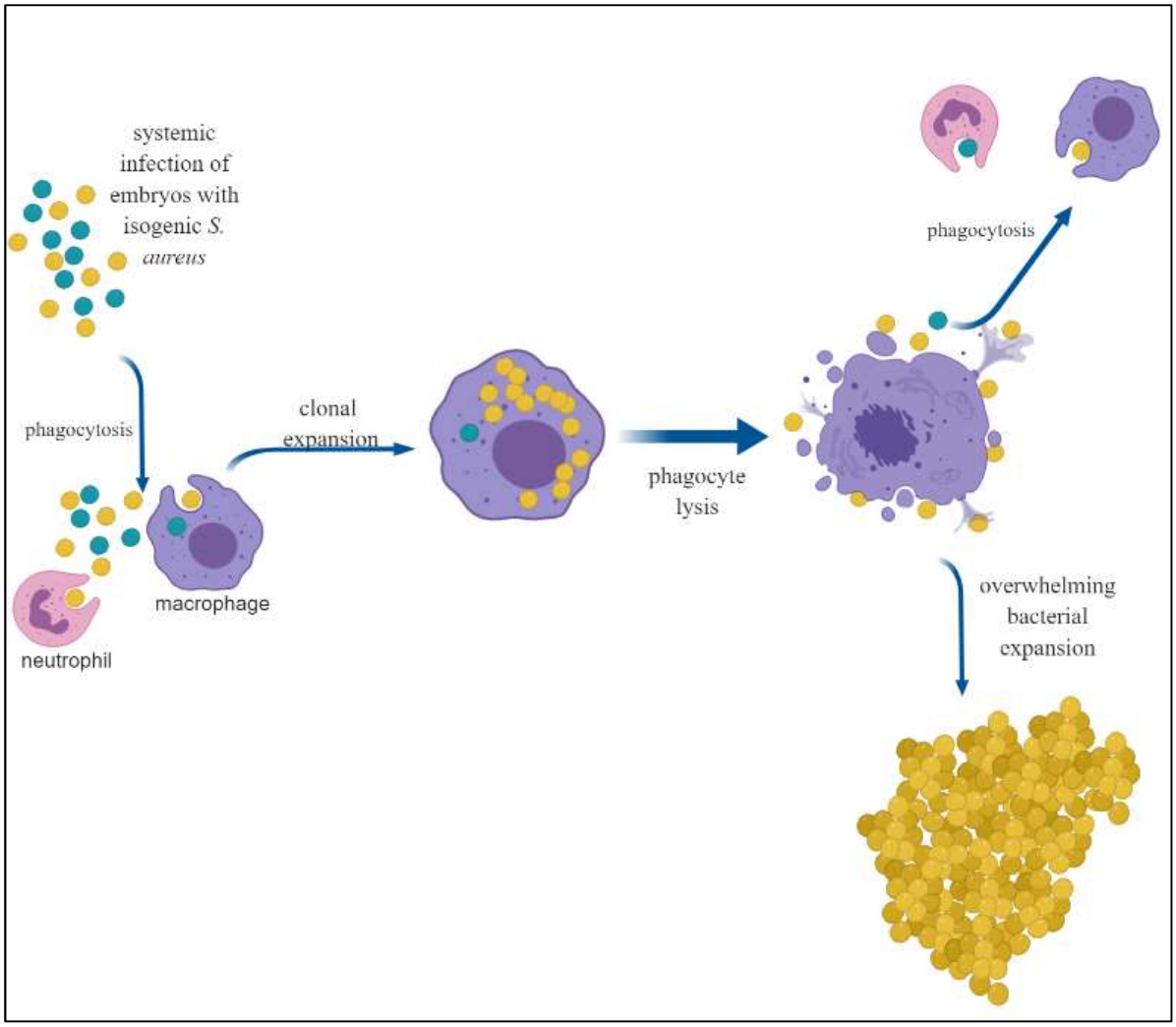

Figure 6.3 Clonal expansion of *S. aureus* leading to overwhelming infection

Upon systemic infection of embryos with isogenic strains, bacteria are initially phagocytosed. Once within macrophages a subset of bacteria replicates leading to the eventual cause of phagocyte lysis. After *S. aureus* has escaped the phagocyte, these bacteria go on to form lesions and cause overwhelming infection of the embryo. The lesion are derived from only a small number of the initial bacterial inoculum.

dissemination of bacteria from the aggregate to other niches within the host. Individual extracellular bacteria within the circulation both expressing and not expressing *nuc* has been found concomitantly with *nuc* expression in large aggregates.

The *nuc* reporter used in this study is an indirect indicator of *saeRS* activity and it is likely that alongside the expression of *nuc* within macrophages and neutrophils, other *saeRS* regulated virulence factors are being expressed. The expression of *nuc*-GFP within macrophages from pCM20 could be concomitant with activation of macrophage specific virulence factors also regulated by *sae* such as LukAB and PVL. In a macrophage culture model, there was no evidence for activation of *sae* within a macrophage, with the same level of *sae* expression in the inoculum as inside infected macrophages (Geiger et al., 2008). However, in my work extracellular bacteria were not expressing *nuc* directly after injection and *nuc* expression was not detected until 6 hpi, which is evidence of activation of *sae*. Shompole et al., (2003) have observed expression of AgrP3 within macrophages; it is possible that *nuc* expression within the phagocyte is due to the downstream activation of *sae* by *agr* and that in this instance the density of *S. aureus* within the phagocyte is responsible for the expression of *nuc*.

In the later stages of infection, the expression of the *nuc* reporter in lesions may be indicative of production of virulence factors involved in the further perturbation of phagocytes. One study has exemplified this by treating isolated macrophages with bacterial culture supernatant where the *sae* regulated production LukAB was identified as a cause of macrophage dysfunction (Scherr et al., 2015).

A proposed model of virulence expression during systemic infection of embryos with *S. aureus* is depicted in Figure 6.4. Briefly, upon infection bacteria are phagocytosed and respond to environmental cues from the intracellular environment. This leads to the production of virulence determinants, such a toxins and enzymes, which aid escape from phagocytes by causing host cell lysis. The escaped bacteria are either subsequently phagocytosed or expand within the host. Upon formation of lesions within the circulation of embryos there is expression of proteins which have roles in biofilm maturation and also expression of virulence determinants which further perturb the immune response.

6.4 *Limitations of this study*

The main limitation with the methodology used in this study to follow infection dynamics within a living host over extended time periods by LSFM, is throughput. The ability to only image one or two fish simultaneously limits the amount of quantitative analysis that can be performed on these data sets, but it remains a strong tool for gaining better insight to a hypothesis that can also be examined with survival and bacterial number assays. Whilst the vast size of the microscopy data makes it

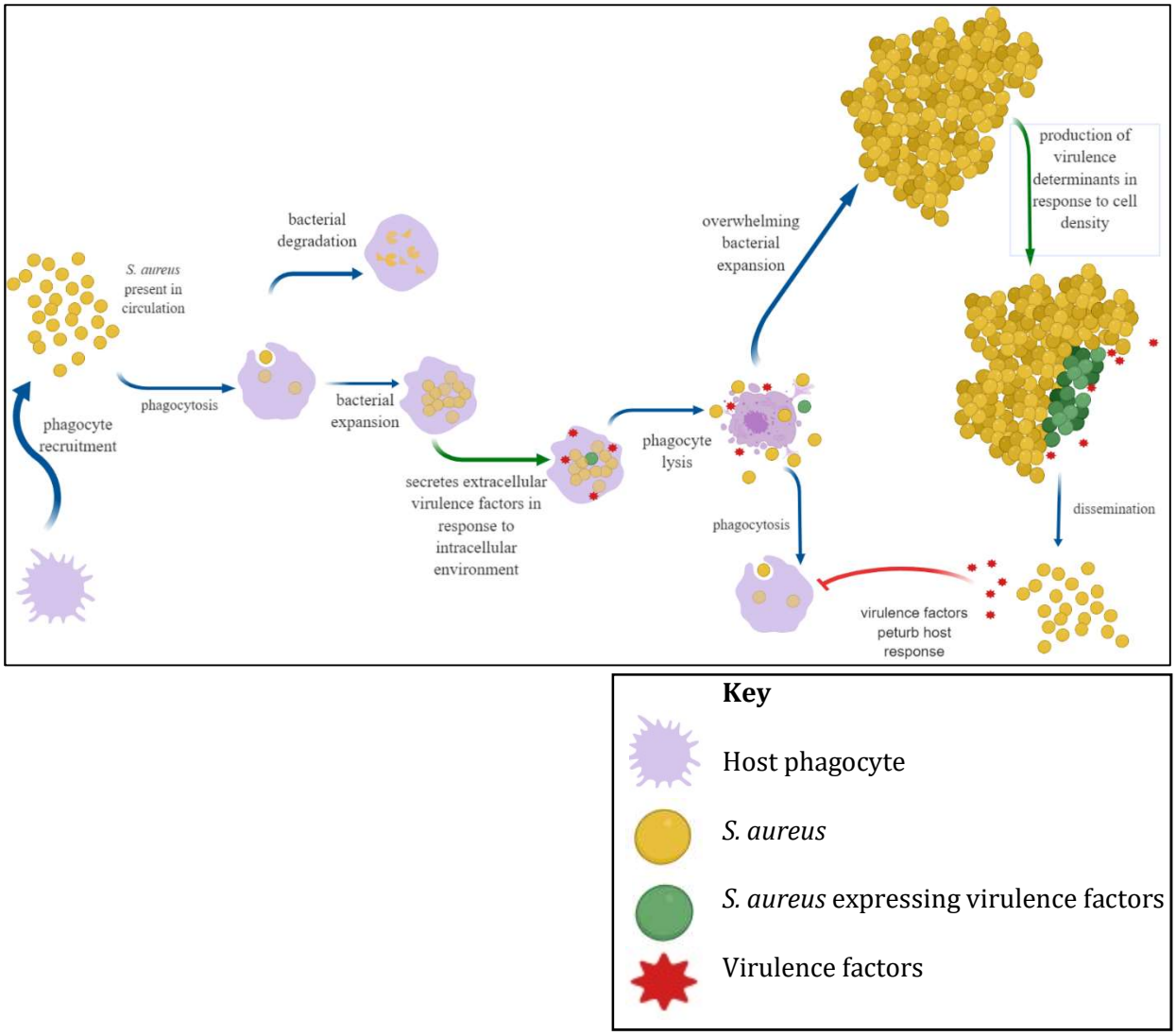

Figure 6.4 A model for virulence factor expression during infection

Schematic depicting possible temporal expression of virulence factors during systemic infection of a zebrafish embryo that succumbs to infection. Bacteria are initially phagocytosed, and a subset respond to the intracellular environment by producing virulence factors which target host components and aid escape from the phagocyte. Bacteria then undergo expansion within the circulation and form lesions. In response to cell density in these aggregates bacteria begin to express virulence factors which leads to dissemination of bacteria to other niches within the host and also perturb further phagocytosis.

difficult to handle, the ability to image an entire bacterial population, within the host over time by LSFM is unparalleled. Another limitation was the lack of a third fluorescent label that could be used for long-term imaging of host pathogen interactions and as such the strains with constitutive smURFP production were developed.

6.5 *Future directions*

6.5.1 Technical

Recently, some researchers in the LSFM community have begun to inject α-bungarotoxin (a small immobilising protein from snake venom) or mRNA encoding the toxin. This works by irreversibly binding and inactivating acetylcholine receptors and has been found to impact development less than immersion in anesthetic (such as tricaine) (Swinburne et al., 2015). This method could be used to further improve the development of embryos during imaging and better mimic infection observed in the survival assay.

6.5.2 Clonal expansion of *S. aureus*

Creating a chromosomally encoded, constitutively expressed smURFP background would provide more tangible imaging of *S. aureus* within embryos with both neutrophils and macrophages labelled. It would also enable the ability to infect fish with a mixed inoculum and track the process of clonality after phagocytosis. The use of this background in combination with expression reporter could provide data that could be more rigorously analysed to dissect spatial and temporal expression of bacterial factors within phagocytes and/or lesions.

To elucidate whether *S. aureus* are escaping from a subset of macrophages within the embryo, experiments following fluorescent bacteria in transgenic zebrafish lines which are currently being developed for labelled M-1 and M-2 macrophages, could be performed.

6.5.3 Virulence factors

The *sae* mutant is attenuated, but not completely, in the systemic model for *S. aureus* infection within zebrafish embryos (Prajsnar, 2009) probably due to the inability of the pathogen to produce pore-forming toxins required for phagocyte escape. Although this mutant might not go on to overwhelm the embryo, if *nuc* expression within the phagocyte from 6 hpi is from *sae* activity then transducing this reporter into a Δ*sae* background and examining intra phagocyte expression would confirm this. Furthermore, to determine whether the increase in volume of *nuc* expressing bacteria within macrophages over time is due to quorum sensing by *S. aureus* within the phagocyte from constitutive AIP production, the pCM20 plasmid could be transduced into an *agr* mutant background and intra-phagocyte expression of *nuc* followed over time by LSFM and subsequently quantified.

Since finishing this study, a novel transgenic fish line developed by Isles, 2018 has reached maturity and can now be used for infection with *S. aureus*. This line, *Tg(lyz:histone2a.mCherry, mpx:GFP)* has mCherry labelled histones in the *Tg*(*mpx:*GFP)^{i114,} background (GFP labelled neutrophils). In preliminary experiments NETs have been observed in this transgenic line after tail infection with *Candida albicans* (H. Isles, personal communication). Infection of *Tg(lyz:histone2a.mCherry, mpx:GFP)* embryos with JE2-smURFP pCM20 (constitutively expressing smURFP, GFP Nuc reporter) in combination with real-time LSFM during the initial stages of infection could be used to identify *nuc* expression by *S. aureus* to escape NETs. If this phenomenon occurs, escape could be compared with a fluorescent *nuc* mutant.

It would be interesting to investigate the expression of virulence factors known to be involved in macrophage escape *in vitro*, using fluorescent reporters like the ones used in Chapter 5, starting with *sae* regulated pore-forming toxins such as LukAB, which has been shown to target the CD11b (α) subunit of $\alpha_M\beta_2$, Mac-1 (DuMont et al., 2013) or PVL which targets the C5aR and C5aL receptors. Such reporters could also be used to look at the interaction of phagocytes with formed lesions, as expression of LukAB and α-toxin from biofilm culture supernatant causes macrophage disfunction in macrophages *in vitro* (Scherr et al., 2015).

6.5.4 Differential expression of genes implicated in biofilm maturation.

An *agr* deficient strain could also be used to determine whether biofilm-like lesions form during infection with an *agr* mutant and if so confirm that expression of *nuc* in these large aggregates is controlled by *agr*. The reagent SYTOX© nucleic acid stain could be used *in vivo* in combination with live imaging to stain lesions for the extracellular DNA characteristic of biofilm.

6.6 *Concluding remarks*

My study has developed a new approach to characterise the complex interaction between host and pathogen *in vivo*, in real time and at the cellular to whole organism level. This paves the way for future work to unravel the mechanisms that constitute the life or death struggle between a host and its invading pathogen.

7 References

Almirón, M.A., Goldschmidt, E., Bertelli, A.M., Gomez, M.I., Argibay, P., and Sanjuan, N.A. (2015). In Vitro infection of human dura-mater fibroblasts with Staphylococcus aureus: colonization and reactive production of IL-1beta. Neurological Research *37*, 867–873.

Altincicek, B., Stötzel, S., Wygrecka, M., Preissner, K.T., and Vilcinskas, A. (2008). Host-derived extracellular nucleic acids enhance innate immune responses, induce coagulation, and prolong survival upon infection in insects. J. Immunol. *181*, 2705–2712.

Altman, D.R., Sullivan, M.J., Chacko, K.I., Balasubramanian, D., Pak, T.R., Sause, W.E., Kumar, K., Sebra, R., Deikus, G., Attie, O., et al. (2018). Genome Plasticity of agr-Defective Staphylococcus aureus during Clinical Infection. Infect Immun *86*, e00331-18.

Amako, K., and Umeda, A. (1979). Mode of Cell Separation and Arrangement of *Staphylococcus*. Microbiology and Immunology *23*, 329–338.

Amat, F., Lemon, W., Mossing, D.P., McDole, K., Wan, Y., Branson, K., Myers, E.W., and Keller, P.J. (2014). Fast, accurate reconstruction of cell lineages from large-scale fluorescence microscopy data. Nature Methods *11*, 951–958.

Amdahl, H., Jongerius, I., Meri, T., Pasanen, T., Hyvärinen, S., Haapasalo, K., Strijp, J.A. van, Rooijakkers, S.H., and Jokiranta, T.S. (2013). Staphylococcal Ecb Protein and Host Complement Regulator Factor H Enhance Functions of Each Other in Bacterial Immune Evasion. The Journal of Immunology *191*, 1775–1784.

Anderson, A.S., Miller, A.A., Donald, R.G.K., Scully, I.L., Nanra, J.S., Cooper, D., and Jansen, K.U. (2012). Development of a multicomponent Staphylococcus aureus vaccine designed to counter multiple bacterial virulence factors. Hum Vaccin Immunother *8*, 1585–1594.

Archer, G.L. (1998). *Staphylococcus aureus* : A Well–Armed Pathogen. Clinical Infectious Diseases *26*, 1179–1181.

Archer, N.K., Mazaitis, M.J., Costerton, J.W., Leid, J.G., Powers, M.E., and Shirtliff, M.E. (2011). Staphylococcus aureus biofilms. Virulence *2*, 445–459.

Arrecubieta, C., Matsunaga, I., Asai, T., Naka, Y., Deng, M.C., and Lowy, F.D. (2008). Vaccination with Clumping Factor A and Fibronectin Binding Protein A to Prevent Staphylococcus aureus Infection of an Aortic Patch in Mice. J Infect Dis *198*, 571–575.

Barber, M. (1961). Methicillin-resistant staphylococci. Journal of Clinical Pathology *14*, 385–393.

Bardoel, B.W., Vos, R., Bouman, T., Aerts, P.C., Bestebroer, J., Huizinga, E.G., Brondijk, T.H.C., van Strijp, J.A.G., and de Haas, C.J.C. (2012). Evasion of Toll-like receptor 2 activation by staphylococcal superantigen-like protein 3. Journal of Molecular Medicine *90*, 1109–1120.

Barrett, L., and Atkins, B. (2014). The clinical presentation of prosthetic joint infection. J Antimicrob Chemother *69*, i25–i27.

Becker, K., Heilmann, C., and Peters, G. (2014). Coagulase-Negative Staphylococci. Clinical Microbiology Reviews *27*, 870–926.

Beenken, K.E., Mrak, L.N., Griffin, L.M., Zielinska, A.K., Shaw, L.N., Rice, K.C., Horswill, A.R., Bayles, K.W., and Smeltzer, M.S. (2010). Epistatic Relationships between sarA and agr in Staphylococcus aureus Biofilm Formation. PLoS One *5*, e10790.

Benoit, M., Desnues, B., and Mege, J.-L. (2008). Macrophage Polarization in Bacterial Infections. The Journal of Immunology *181*, 3733–3739.

Bera, A., Herbert, S., Jakob, A., Vollmer, W., and Götz, F. (2005). Why are pathogenic staphylococci so lysozyme resistant? The peptidoglycan O-acetyltransferase OatA is the major determinant for lysozyme resistance of Staphylococcus aureus. Molecular Microbiology *55*, 778–787.

Berends, E.T.M., Horswill, A.R., Haste, N.M., Monestier, M., Nizet, V., and von Köckritz-Blickwede, M. (2010). Nuclease Expression by Staphylococcus aureus Facilitates Escape from Neutrophil Extracellular Traps. J Innate Immun *2*, 576–586.

Bhattacharya, M., Wozniak, D.J., Stoodley, P., and Hall-Stoodley, L. (2015). Prevention and treatment of Staphylococcus aureus biofilms. Expert Rev Anti Infect Ther *13*, 1499–1516.

Bojarczuk, A., Miller, K.A., Hotham, R., Lewis, A., Ogryzko, N.V., Kamuyango, A.A., Frost, H., Gibson, R.H., Stillman, E., May, R.C., et al. (2016). *Cryptococcus neoformans* Intracellular Proliferation and Capsule Size Determines Early Macrophage Control of Infection. Scientific Reports *6*, 21489.

Boldock, E., Surewaard, B.G.J., Shamarina, D., Na, M., Fei, Y., Ali, A., Williams, A., Pollitt, E.J.G., Szkuta, P., Morris, P., et al. (2018). Human skin commensals augment Staphylococcus aureus pathogenesis. Nature Microbiology *3*, 881.

Boles, B.R., and Horswill, A.R. (2008). agr-Mediated Dispersal of Staphylococcus aureus Biofilms. PLOS Pathogens *4*, e1000052.

Boshra, H., Li, J., and Sunyer, J.O. (2006). Recent advances on the complement system of teleost fish. Fish & Shellfish Immunology *20*, 239–262.

Bottomley, A.L., Kabli, A.F., Hurd, A.F., Turner, R.D., Garcia-Lara, J., and Foster, S.J. (2014). Staphylococcus aureus DivIB is a peptidoglycan-binding protein that is required for a morphological checkpoint in cell division. Molecular Microbiology *94*, 1041–1064.

Bronner, S., Monteil, H., and Prévost, G. (2004a). Regulation of virulence determinants in Staphylococcus aureus: complexity and applications. FEMS Microbiology Reviews *28*, 183–200.

Bronner, S., Monteil, H., and Prévost, G. (2004b). Regulation of virulence determinants in Staphylococcus aureus: complexity and applications. FEMS Microbiol. Rev. *28*, 183–200.

Brothers, K.M., Gratacap, R.L., Barker, S.E., Newman, Z.R., Norum, A., and Wheeler, R.T. (2013). NADPH Oxidase-Driven Phagocyte Recruitment Controls Candida albicans Filamentous Growth and Prevents Mortality. PLOS Pathogens *9*, e1003634.

Brunskill, E.W., and Bayles, K.W. (1996a). Identification of LytSR-regulated genes from Staphylococcus aureus. Journal of Bacteriology *178*, 5810–5812.

Brunskill, E.W., and Bayles, K.W. (1996b). Identification and molecular characterization of a putative regulatory locus that affects autolysis in Staphylococcus aureus. Journal of Bacteriology *178*, 611–618.

Buchan, K.D., Foster, S.J., and Renshaw, S.A. (2019). Staphylococcus aureus: setting its sights on the human innate immune system. Microbiology *165*, 367–385.

Buchan, Kyle David (2018). Building Humanised Models of Staphylococcus aureus Infection.

Bunce, C., Wheeler, L., Reed, G., Musser, J., and Barg, N. (1992). Murine model of cutaneous infection with gram-positive cocci. Infect Immun *60*, 2636–2640.

Chain, E., Florey, H.W., Gardner, A.D., Heatley, N.G., Jennings, M.A., Orr-Ewing, J., Sanders, A.G., and Peltier, L.F. (2005). THE CLASSIC: Penicillin as a Chemotherapeutic Agent. Clinical Orthopaedics and Related Research® *439*, 23.

Chang, N., Sun, C., Gao, L., Zhu, D., Xu, X., Zhu, X., Xiong, J.-W., and Xi, J.J. (2013). Genome editing with RNA-guided Cas9 nuclease in Zebrafish embryos. Cell Research *23*, 465–472.

Charpentier, E., Anton, A.I., Barry, P., Alfonso, B., Fang, Y., and Novick, R.P. (2004). Novel Cassette-Based Shuttle Vector System for Gram-Positive Bacteria. Appl Environ Microbiol *70*, 6076–6085.

Chatterjee, S., Maiti, P., Dey, R., Kundu, A., and Dey, R. (2014). Biofilms on Indwelling Urologic Devices: Microbes and Antimicrobial Management Prospect. Ann Med Health Sci Res *4*, 100–104.

Cheng, A.G., Kim, H.K., Burts, M.L., Krausz, T., Schneewind, O., and Missiakas, D.M. (2009). Genetic requirements for Staphylococcus aureus abscess formation and persistence in host tissues. FASEB J. *23*, 3393–3404.

Cheung, G.Y.C., Wang, R., Khan, B.A., Sturdevant, D.E., and Otto, M. (2011). Role of the Accessory Gene Regulator agr in Community-Associated Methicillin-Resistant Staphylococcus aureus Pathogenesis. Infect. Immun. *79*, 1927–1935.

Cheung, G.Y.C., Duong, A.C., and Otto, M. (2012). Direct and synergistic hemolysis caused by Staphylococcus phenol-soluble modulins: implications for diagnosis and pathogenesis. Microbes and Infection *14*, 380–386.

Cho, H., Jeong, D.-W., Liu, Q., Yeo, W.-S., Vogl, T., Skaar, E.P., Chazin, W.J., and Bae, T. (2015). Calprotectin Increases the Activity of the SaeRS Two Component System and Murine Mortality during Staphylococcus aureus Infections. PLOS Pathogens *11*, e1005026.

Chong, Y.P., Kim, E.S., Park, S.-J., Park, K.-H., Kim, T., Kim, M.-N., Kim, S.-H., Lee, S.-O., Choi, S.-H., Woo, J.H., et al. (2013). Accessory Gene Regulator (agr) Dysfunction in Staphylococcus aureus Bloodstream Isolates from South Korean Patients. Antimicrob Agents Chemother *57*, 1509–1512.

Chu, J., Haynes, R.D., Corbel, S.Y., Li, P., González-González, E., Burg, J.S., Ataie, N.J., Lam, A.J., Cranfill, P.J., Baird, M.A., et al. (2014). Non-invasive intravital imaging of cellular differentiation with a bright red-excitable fluorescent protein. Nature Methods *11*, 572–578.

Clarke, S.R., Brummell, K.J., Horsburgh, M.J., McDowell, P.W., Mohamad, S.A.S., Stapleton, M.R., Acevedo, J., Read, R.C., Day, N.P.J., Peacock, S.J., et al. (2006). Identification of In Vivo–Expressed Antigens of Staphylococcus aureus and Their Use in Vaccinations for Protection against Nasal Carriage. J Infect Dis *193*, 1098–1108.

Clatworthy, A.E., Lee, J.S.-W., Leibman, M., Kostun, Z., Davidson, A.J., and Hung, D.T. (2009). Pseudomonas aeruginosa Infection of Zebrafish Involves both Host and Pathogen Determinants. Infection and Immunity *77*, 1293–1303.

Clauditz, A., Resch, A., Wieland, K.-P., Peschel, A., and Gotz, F. (2006). Staphyloxanthin Plays a Role in the Fitness of Staphylococcus aureus and Its Ability To Cope with Oxidative Stress. Infection and Immunity *74*, 4950–4953.

Connolly, J., Boldock, E., Prince, L.R., Renshaw, S.A., Whyte, M.K., and Foster, S.J. (2017). Identification of Staphylococcus aureus Factors Required for Pathogenicity and Growth in Human Blood. Infect Immun *85*, e00337-17.

Connolly, J (2015). Doctoral Thesis : Analysis of Staphylococcal Virulence Determinants.

Corrigan, R.M., Rigby, D., Handley, P., and Foster, T.J. (2007). The role of Staphylococcus aureus surface protein SasG in adherence and biofilm formation. Microbiology *153*, 2435–2446.

Cuatrecasas, P., Fuchs, S., and Anfinsen, C.B. (1967). Catalytic Properties and Specificity of the Extracellular Nuclease of Staphylococcus aureus. J. Biol. Chem. *242*, 1541–1547.

Cui, K., Ardell, C.L., Podolnikova, N.P., and Yakubenko, V.P. (2018). Distinct Migratory Properties of M1, M2, and Resident Macrophages Are Regulated by αDβ2 and αMβ2 Integrin-Mediated Adhesion. Front Immunol *9*, e2650.

Cunningham, L., Catlin, B.W., and de Garilhe, M.P. (1956). A Deoxyribonuclease of Micrococcus pyogenes1. J. Am. Chem. Soc. *78*, 4642–4645.

Curado, S., Stainier, D.Y.R., and Anderson, R.M. (2008). Nitroreductase-mediated cell/tissue ablation in zebrafish: a spatially and temporally controlled ablation method with applications in developmental and regeneration studies. Nat Protoc *3*, 948–954.

Dalla Serra, M., Coraiola, M., Viero, G., Comai, M., Potrich, C., Ferreras, M., Baba-Moussa, L., Colin, D.A., Menestrina, G., Bhakdi, S., et al. (2005). Staphylococcus aureus Bicomponent γ-Hemolysins, HlgA, HlgB, and HlgC, Can Form Mixed Pores Containing All Components. J. Chem. Inf. Model. *45*, 1539–1545.

Darouiche, R.O. (2004). Treatment of Infections Associated with Surgical Implants. N Engl j Med *350*, 1422–1429.

David, M.Z., and Daum, R.S. (2010). Community-Associated Methicillin-Resistant Staphylococcus aureus: Epidemiology and Clinical Consequences of an Emerging Epidemic. Clinical Microbiology Reviews *23*, 616–687.

Davis, J.M., Clay, H., Lewis, J.L., Ghori, N., Herbomel, P., and Ramakrishnan, L. (2002). Real-Time Visualization of Mycobacterium-Macrophage Interactions Leading to Initiation of Granuloma Formation in Zebrafish Embryos. Immunity *17*, 693–702.

Davis, J.P., Chesney, P.J., Wand, P.J., and LaVenture, M. (1980). Toxic-Shock Syndrome. New England Journal of Medicine *303*, 1429–1435.

Dee, C.T., Nagaraju, R.T., Athanasiadis, E.I., Gray, C., Fernandez del Ama, L., Johnston, S.A., Secombes, C.J., Cvejic, A., and Hurlstone, A.F.L. (2016). CD4-Transgenic Zebrafish Reveal Tissue-Resident Th2- and Regulatory T Cell–like Populations and Diverse Mononuclear Phagocytes. J Immunol *197*, 3520–3530.

Deivanayagam, C.C.S., Wann, E.R., Chen, W., Carson, M., Rajashankar, K.R., Höök, M., and Narayana, S.V.L. (2002). A novel variant of the immunoglobulin fold in surface adhesins of Staphylococcus aureus: crystal structure of the fibrinogen-binding MSCRAMM, clumping factor A. The EMBO Journal *21*, 6660–6672.

DeLeo, F.R., Otto, M., Kreiswirth, B.N., and Chambers, H.F. (2010). Community-associated meticillin-resistant Staphylococcus aureus. The Lancet *375*, 1557–1568.

Dinges, M.M., Orwin, P.M., and Schlievert, P.M. (2000). Exotoxins of Staphylococcus aureus. Clin Microbiol Rev *13*, 16–34.

DUMITRAŞCU, D.I., and GEORGESCU, A.V. (2013). The management of biofilm formation after hyaluronic acid gel filler injections: a review. Clujul Med *86*, 192–195.

DuMont, A.L., Nygaard, T.K., Watkins, R.L., Smith, A., Kozhaya, L., Kreiswirth, B.N., Shopsin, B., Unutmaz, D., Voyich, J.M., and Torres, V.J. (2011). Characterization of a new cytotoxin that contributes to Staphylococcus aureus pathogenesis. Molecular Microbiology *79*, 814–825.

DuMont, A.L., Yoong, P., Day, C.J., Alonzo, F., McDonald, W.H., Jennings, M.P., and Torres, V.J. (2013). Staphylococcus aureus LukAB cytotoxin kills human neutrophils by targeting the CD11b subunit of the integrin Mac-1. PNAS *110*, 10794–10799.

Dunman, P.M., Murphy, E., Haney, S., Palacios, D., Tucker-Kellogg, G., Wu, S., Brown, E.L., Zagursky, R.J., Shlaes, D., and Projan, S.J. (2001). Transcription Profiling-Based Identification ofStaphylococcus aureus Genes Regulated by the agrand/or sarA Loci. Journal of Bacteriology *183*, 7341–7353.

Dunyach-Remy, C., Ngba Essebe, C., Sotto, A., and Lavigne, J.-P. (2016). Staphylococcus aureus Toxins and Diabetic Foot Ulcers: Role in Pathogenesis and Interest in Diagnosis. Toxins (Basel) *8*, 209.

Dziarski, R., and Gupta, D. (2005). Staphylococcus aureus Peptidoglycan Is a Toll-Like Receptor 2 Activator: a Reevaluation. Infect Immun *73*, 5212–5216.

Edwards, A.M., Potter, U., Meenan, N.A.G., Potts, J.R., and Massey, R.C. (2011). Staphylococcus aureus Keratinocyte Invasion Is Dependent upon Multiple High-Affinity Fibronectin-Binding Repeats within FnBPA. PLOS ONE *6*, e18899.

Eliceiri, K.W., Berthold, M.R., Goldberg, I.G., Ibáñez, L., Manjunath, B.S., Martone, M.E., Murphy, R.F., Peng, H., Plant, A.L., Roysam, B., et al. (2012). Biological imaging software tools. Nature Methods *9*, 697–710.

Elks, P.M., Eeden, F.J. van, Dixon, G., Wang, X., Reyes-Aldasoro, C.C., Ingham, P.W., Whyte, M.K.B., Walmsley, S.R., and Renshaw, S.A. (2011). Activation of hypoxia-inducible factor-1α (Hif-1α) delays inflammation resolution by reducing neutrophil apoptosis and reverse migration in a zebrafish inflammation model. Blood *118*, 712–722.

Ellett, F., Pase, L., Hayman, J.W., Andrianopoulos, A., and Lieschke, G.J. (2011). mpeg1 promoter transgenes direct macrophage-lineage expression in zebrafish. Blood *117*, e49–e56.

Entenza, J.-M., Moreillon, P., Senn, M.M., Kormanec, J., Dunman, P.M., Berger-Bächi, B., Projan, S., and Bischoff, M. (2005). Role of σB in the Expression of Staphylococcus aureus Cell Wall Adhesins ClfA and FnbA and Contribution to Infectivity in a Rat Model of Experimental Endocarditis. Infection and Immunity *73*, 990–998.

Federspiel, J.J., Stearns, S.C., Peppercorn, A.F., Chu, V.H., and Fowler, V.G. (2012). Endocarditis Trends in the United States Demonstrate Increasing Rates of Staphylococcus aureus: 1999–2008. Arch Intern Med *172*, 363–365.

Ferreira, F.A., Souza, R.R., de Sousa Moraes, B., de Amorim Ferreira, A.M., Américo, M.A., Fracalanzza, S.E.L., dos Santos Silva Couceiro, J.N., and Sá Figueiredo, A.M. (2013). Impact of agr dysfunction on virulence profiles and infections associated with a novel methicillin-resistant Staphylococcus aureus (MRSA) variant of the lineage ST1-SCCmec IV. BMC Microbiol *13*, 93.

Fey, P.D., Endres, J.L., Yajjala, V.K., Widhelm, T.J., Boissy, R.J., Bose, J.L., and Bayles, K.W. (2013). A genetic resource for rapid and comprehensive phenotype screening of nonessential Staphylococcus aureus genes. MBio *4*, e00537-00512.

Flick, M.J., Du, X., Prasad, J.M., Raghu, H., Palumbo, J.S., Smeds, E., Höök, M., and Degen, J.L. (2013). Genetic elimination of the binding motif on fibrinogen for the S. aureus virulence factor ClfA improves host survival in septicemia. Blood *121*, 1783–1794.

Foster, T.J. (2005). Immune evasion by staphylococci. Nature Reviews. Microbiology *3*, 948–958.

Foster, T.J., Geoghegan, J.A., Ganesh, V.K., and Höök, M. (2014). Adhesion, invasion and evasion: the many functions of the surface proteins of Staphylococcus aureus. Nat Rev Microbiol *12*, 49–62.

Franchi, L., Warner, N., Viani, K., and Nuñez, G. (2009). Function of Nod-like Receptors in Microbial Recognition and Host Defense. Immunol Rev *227*, 106–128.

Fuchs, T.A., Abed, U., Goosmann, C., Hurwitz, R., Schulze, I., Wahn, V., Weinrauch, Y., Brinkmann, V., and Zychlinsky, A. (2007). Novel cell death program leads to neutrophil extracellular traps. J Cell Biol *176*, 231–241.

de la Fuente-Núñez, C., Reffuveille, F., Fernández, L., and Hancock, R.E. (2013). Bacterial biofilm development as a multicellular adaptation: antibiotic resistance and new therapeutic strategies. Current Opinion in Microbiology *16*, 580–589.

García-Lara, J., Needham, A.J., and Foster, S.J. (2005). Invertebrates as animal models for Staphylococcus aureus pathogenesis: a window into host–pathogen interaction. FEMS Immunol Med Microbiol *43*, 311–323.

Garrison, P.K., and Freedman, L.R. (1970). Experimental endocarditis I. Staphylococcal endocarditis in rabbits resulting from placement of a polyethylene catheter in the right side of the heart. Yale J Biol Med *42*, 394–410.

Garsin, D.A., Sifri, C.D., Mylonakis, E., Qin, X., Singh, K.V., Murray, B.E., Calderwood, S.B., and Ausubel, F.M. (2001). A simple model host for identifying Gram-positive virulence factors. PNAS *98*, 10892–10897.

Geiger, T., Goerke, C., Mainiero, M., Kraus, D., and Wolz, C. (2008). The virulence regulator Sae of Staphylococcus aureus: promoter activities and response to phagocytosis-related signals. J. Bacteriol. *190*, 3419–3428.

Geiger, T., Francois, P., Liebeke, M., Fraunholz, M., Goerke, C., Krismer, B., Schrenzel, J., Lalk, M., and Wolz, C. (2012). The Stringent Response of Staphylococcus aureus and Its Impact on Survival after Phagocytosis through the Induction of Intracellular PSMs Expression. PLOS Pathogens *8*, e1003016.

Geoghegan, J.A., Ganesh, V.K., Smeds, E., Liang, X., Höök, M., and Foster, T.J. (2010). Molecular Characterization of the Interaction of Staphylococcal Microbial Surface Components Recognizing Adhesive Matrix Molecules (MSCRAMM) ClfA and Fbl with Fibrinogen. J. Biol. Chem. *285*, 6208–6216.

Ghasemian, A., Najar Peerayeh, S., Bakhshi, B., and Mirzaee, M. (2015). The Microbial Surface Components Recognizing Adhesive Matrix Molecules (MSCRAMMs) Genes among Clinical Isolates of Staphylococcus aureus from Hospitalized Children. Iran J Pathol *10*, 258–264.

Gibson, G.W., Kreuser, S.C., Riley, J.M., Rosebury-Smith, W.S., Courtney, C.L., Juneau, P.L., Hollembaek, J.M., Zhu, T., Huband, M.D., Brammer, D.W., et al. (2007). Development of a mouse model of induced Staphylococcus aureus infective endocarditis. Comp. Med. *57*, 563–569.

Gibson, J., Evans, R., Bojarczuk, A., Hotham, R., Lagendijk, A., Hogan, B., Ingham, P., Renshaw, S., and Johnston, S. (2017). Dissemination of Cryptococcus neoformans via localised proliferation and blockage of blood vessels. BioRxiv 184200.

Giersing, B.K., Dastgheyb, S.S., Modjarrad, K., and Moorthy, V. (2016). Status of vaccine research and development of vaccines for Staphylococcus aureus. Vaccine *34*, 2962–2966.

Gómez, M.I., Lee, A., Reddy, B., Muir, A., Soong, G., Pitt, A., Cheung, A., and Prince, A. (2004). *Staphylococcus aureus* protein A induces airway epithelial inflammatory responses by activating TNFR1. Nature Medicine *10*, 842–848.

Grant, A.J., Restif, O., McKinley, T.J., Sheppard, M., Maskell, D.J., and Mastroeni, P. (2008). Modelling within-Host Spatiotemporal Dynamics of Invasive Bacterial Disease. PLoS Biol *6*.

Gray, C., Loynes, C.A., Whyte, M.K.B., Crossman, D.C., Renshaw, S.A., and Chico, T.J.A. (2011). Simultaneous intravital imaging of macrophage and neutrophil behaviour during inflammation using a novel transgenic zebrafish. Thromb Haemost *105*, 811–819.

Gresham, H.D., Lowrance, J.H., Caver, T.E., Wilson, B.S., Cheung, A.L., and Lindberg, F.P. (2000). Survival of Staphylococcus aureus Inside Neutrophils Contributes to Infection. The Journal of Immunology *164*, 3713–3722.

Groicher, K.H., Firek, B.A., Fujimoto, D.F., and Bayles, K.W. (2000). The Staphylococcus aureus lrgAB Operon Modulates Murein Hydrolase Activity and Penicillin Tolerance. J Bacteriol *182*, 1794–1801.

Haas, P.-J., Haas, C.J.C. de, Kleibeuker, W., Poppelier, M.J.J.G., Kessel, K.P.M. van, Kruijtzer, J.A.W., Liskamp, R.M.J., and Strijp, J.A.G. van (2004). N-Terminal Residues of the Chemotaxis Inhibitory Protein of Staphylococcus aureus Are Essential for Blocking Formylated Peptide Receptor but Not C5a Receptor. The Journal of Immunology *173*, 5704–5711.

Haggar, A., Hussain, M., Lönnies, H., Herrmann, M., Norrby-Teglund, A., and Flock, J.-I. (2003). Extracellular Adherence Protein from Staphylococcus aureus Enhances Internalization into Eukaryotic Cells. Infection and Immunity *71*, 2310–2317.

Haggar, A., Ehrnfelt, C., Holgersson, J., and Flock, J.-I. (2004). The Extracellular Adherence Protein from Staphylococcus aureus Inhibits Neutrophil Binding to Endothelial Cells. Infect Immun *72*, 6164–6167.

Hanzelmann, D., Joo, H.-S., Franz-Wachtel, M., Hertlein, T., Stevanovic, S., Macek, B., Wolz, C., Götz, F., Otto, M., Kretschmer, D., et al. (2016). Toll-like receptor 2 activation depends on lipopeptide shedding by bacterial surfactants. Nature Communications *7*, 12304.

Hartleib, J., Köhler, N., Dickinson, R.B., Chhatwal, G.S., Sixma, J.J., Hartford, O.M., Foster, T.J., Peters, G., Kehrel, B.E., and Herrmann, M. (2000). Protein A is the von Willebrand factor binding protein onStaphylococcus aureus. Blood *96*, 2149–2156.

Hartman, B.J., and Tomasz, A. (1984). Low-affinity penicillin-binding protein associated with beta-lactam resistance in Staphylococcus aureus. Journal of Bacteriology *158*, 513–516.

Hato, T., and Dagher, P.C. (2015). How the Innate Immune System Senses Trouble and Causes Trouble. Clin J Am Soc Nephrol *10*, 1459–1469.

Heintzmann, R., and Ficz, G. (2006). Breaking the resolution limit in light microscopy. Briefings in Functional Genomics and Proteomics *5*, 289–301.

Holtfreter, S., Radcliff, F.J., Grumann, D., Read, H., Johnson, S., Monecke, S., Ritchie, S., Clow, F., Goerke, C., Bröker, B.M., et al. (2013). Characterization of a Mouse-Adapted Staphylococcus aureus Strain. PLOS ONE *8*, e71142.

Howe, K., Clark, M.D., Torroja, C.F., Torrance, J., Berthelot, C., Muffato, M., Collins, J.E., Humphray, S., McLaren, K., Matthews, L., et al. (2013). The zebrafish reference genome sequence and its relationship to the human genome. Nature *496*, 498–503.

Huang, S.S., and Platt, R. (2003). Risk of Methicillin-Resistant Staphylococcus aureus Infection after Previous Infection or Colonization. Clin Infect Dis *36*, 281–285.

Huff, J. (2015). The Airyscan detector from ZEISS: confocal imaging with improved signal-to-noise ratio and super-resolution.

Huisken, J., Swoger, J., Bene, F.D., Wittbrodt, J., and Stelzer, E.H.K. (2004). Optical Sectioning Deep Inside Live Embryos by Selective Plane Illumination Microscopy. Science *305*, 1007–1009.

International Human Genome Sequencing Consortium (2004). Finishing the euchromatic sequence of the human genome. Nature *431*, 931–945.

Ishikawa, F., Yasukawa, M., Lyons, B., Yoshida, S., Miyamoto, T., Yoshimoto, G., Watanabe, T., Akashi, K., Shultz, L.D., and Harada, M. (2005). Development of functional human blood and immune systems in NOD/SCID/IL2 receptor γ chainnull mice. Blood *106*, 1565–1573.

Isles (2018). Doctoral thesis : Regulation of inflammation by differential migration patterns in zebrafish (University of Sheffield).

Jeong, D.-W., Cho, H., Lee, H., Li, C., Garza, J., Fried, M., and Bae, T. (2011). Identification of the P3 Promoter and Distinct Roles of the Two Promoters of the SaeRS Two-Component System in Staphylococcus aureus. Journal of Bacteriology *193*, 4672–4684.

Jin, T., Bokarewa, M., Foster, T., Mitchell, J., Higgins, J., and Tarkowski, A. (2004). Staphylococcus aureus Resists Human Defensins by Production of Staphylokinase, a Novel Bacterial Evasion Mechanism. The Journal of Immunology *172*, 1169–1176.

Jong, N.W.M. de, Ramyar, K.X., Guerra, F.E., Nijland, R., Fevre, C., Voyich, J.M., McCarthy, A.J., Garcia, B.L., Kessel, K.P.M. van, Strijp, J.A.G. van, et al. (2017). Immune evasion by a staphylococcal inhibitor of myeloperoxidase. PNAS *114*, 9439–9444.

Josefsson, E., Hartford, O., O'Brien, L., Patti, J.M., and Foster, T. (2001). Protection against Experimental *Staphylococcus aureus* Arthritis by Vaccination with Clumping Factor A, a Novel Virulence Determinant. The Journal of Infectious Diseases *184*, 1572–1580.

Jun, Y.W., Kim, H.R., Reo, Y.J., Dai, M., and Ahn, K.H. (2017). Addressing the autofluorescence issue in deep tissue imaging by two-photon microscopy: the significance of far-red emitting dyes †Electronic supplementary information (ESI) available: Materials and procedures regarding the synthesis of all of the dyes, photophysical properties and tissue and cell imaging. See DOI: 10.1039/c7sc03362a. Chem Sci *8*, 7696–7704.

Kanangat, S., Postlethwaite, A., Hasty, K., Kang, A., Smeltzer, M., Appling, W., and Schaberg, D. (2006). Induction of multiple matrix metalloproteinases in human dermal and synovial fibroblasts by Staphylococcus aureus: implications in the pathogenesis of septic arthritis and other soft tissue infections. Arthritis Research & Therapy *8*, R176.

Kaneko, J., Ozawa, T., Tomita, T., and Kamio, Y. (1997). Sequential Binding of Staphylococcal y-Hemolysin to Human Erythrocytes and Complex Formation of the Hemolysin on the Cell Surface†. Bioscience, Biotechnology, and Biochemistry *61*, 846–851.

Kasahara, M., Suzuki, T., and Pasquier, L.D. (2004). On the origins of the adaptive immune system: novel insights from invertebrates and cold-blooded vertebrates. Trends in Immunology *25*, 105–111.

Katayama, Y., Ito, T., and Hiramatsu, K. (2000). A New Class of Genetic Element, Staphylococcus Cassette Chromosome mec, Encodes Methicillin Resistance in Staphylococcus aureus. Antimicrobial Agents and Chemotherapy *44*, 1549–1555.

Kaufmann, A., Mickoleit, M., Weber, M., and Huisken, J. (2012). Multilayer mounting enables long-term imaging of zebrafish development in a light sheet microscope. Development *139*, 3242–3247.

Kawai, T., and Akira, S. (2010). The role of pattern-recognition receptors in innate immunity: update on Toll-like receptors. Nature Immunology *11*, 373–384.

Kiedrowski, M.R., and Horswill, A.R. (2011). New approaches for treating staphylococcal biofilm infections. Annals of the New York Academy of Sciences *1241*, 104–121.

Kiedrowski, M.R., Kavanaugh, J.S., Malone, C.L., Mootz, J.M., Voyich, J.M., Smeltzer, M.S., Bayles, K.W., and Horswill, A.R. (2011). Nuclease Modulates Biofilm Formation in Community-Associated Methicillin-Resistant Staphylococcus aureus. PLOS ONE *6*, e26714.

Kiedrowski, M.R., Crosby, H.A., Hernandez, F.J., Malone, C.L., Ii, J.O.M., and Horswill, A.R. (2014). Staphylococcus aureus Nuc2 Is a Functional, Surface-Attached Extracellular Nuclease. PLOS ONE *9*, e95574.

Kim, H.K., Missiakas, D., and Schneewind, O. (2014). Mouse models for infectious diseases caused by Staphylococcus aureus. J Immunol Methods *410*, 88–99.

Kisich, K.O., Howell, M.D., Boguniewicz, M., Heizer, H.R., Watson, N.U., and Leung, D.Y.M. (2007). The Constitutive Capacity of Human Keratinocytes to Kill Staphylococcus aureus Is Dependent on β-Defensin 3. J Invest Dermatol *127*, 2368–2380.

Klebanoff, S.J., Kettle, A.J., Rosen, H., Winterbourn, C.C., and Nauseef, W.M. (2013). Myeloperoxidase: a front-line defender against phagocytosed microorganisms. Journal of Leukocyte Biology *93*, 185–198.

Kloos, W.E., and Bannerman, T.L. (1994). Update on clinical significance of coagulase-negative staphylococci. Clinical Microbiology Reviews *7*, 117–140.

Kluytmans, J., Belkum, A. van, and Verbrugh, H. (1997). Nasal carriage of Staphylococcus aureus: epidemiology, underlying mechanisms, and associated risks. Clinical Microbiology Reviews *10*, 505–520.

Knop, J., Hanses, F., Leist, T., Archin, N.M., Buchholz, S., Gläsner, J., Gessner, A., and Wege, A.K. (2015). Staphylococcus aureus Infection in Humanized Mice: A New Model to Study Pathogenicity Associated With Human Immune Response. J Infect Dis *212*, 435–444.

Kobayashi, S.D., and DeLeo, F.R. (2009). An update on community-associated MRSA virulence. Current Opinion in Pharmacology *9*, 545–551.

Kobayashi, S.D., and DeLeo, F.R. (2013). Staphylococcus aureus Protein A Promotes Immune Suppression. MBio *4*, e00764-13.

von Köckritz-Blickwede, M., and Nizet, V. (2009). Innate immunity turned inside-out: antimicrobial defense by phagocyte extracellular traps. J Mol Med *87*, 775–783.

Kolaczkowska, E., and Kubes, P. (2013). Neutrophil recruitment and function in health and inflammation. Nature Reviews Immunology *13*, 159–175.

Kreiswirth, B.N., Löfdahl, S., Betley, M.J., O'Reilly, M., Schlievert, P.M., Bergdoll, M.S., and Novick, R.P. (1983). The toxic shock syndrome exotoxin structural gene is not detectably transmitted by a prophage. Nature *305*, 709–712.

Kupper, T.S., and Fuhlbrigge, R.C. (2004). Immune surveillance in the skin: mechanisms and clinical consequences. Nature Reviews Immunology *4*, 211–222.

Laarman, A.J., Mijnheer, G., Mootz, J.M., Rooijen, W.J.M. van, Ruyken, M., Malone, C.L., Heezius, E.C., Ward, R., Milligan, G., Strijp, J.A.G. van, et al. (2012). Staphylococcus aureus Staphopain A inhibits CXCR2-dependent neutrophil activation and chemotaxis. The EMBO Journal *31*, 3607–3619.

Lagacé-Wiens, P.R.S., Alfa, M.J., Manickam, K., and Karlowsky, J.A. (2007). Thermostable DNase Is Superior to Tube Coagulase for Direct Detection of Staphylococcus aureus in Positive Blood Cultures. J. Clin. Microbiol. *45*, 3478–3479.

Lambris, J.D., Ricklin, D., and Geisbrecht, B.V. (2008). Complement evasion by human pathogens. Nature Reviews Microbiology *6*, 132–142.

Lan, P., Tonomura, N., Shimizu, A., Wang, S., and Yang, Y.-G. (2006). Reconstitution of a functional human immune system in immunodeficient mice through combined human fetal thymus/liver and CD34+ cell transplantation. Blood *108*, 487–492.

Leclerc, V., and Reichhart, J.-M. (2004). The immune response of Drosophila melanogaster. Immunol. Rev. *198*, 59–71.

Lee, L.Y.L., Höök, M., Haviland, D., Wetsel, R.A., Yonter, E.O., Syribeys, P., Vernachio, J., and Brown, E.L. (2004). Inhibition of Complement Activation by a Secreted Staphylococcus aureus Protein. J Infect Dis *190*, 571–579.

Lehman, M.K., Bose, J.L., Sharma-Kuinkel, B.K., Moormeier, D.E., Endres, J.L., Sadykov, M.R., Biswas, I., and Bayles, K.W. (2015). Identification of the amino acids essential for LytSR-mediated signal transduction in Staphylococcus aureus and their roles in biofilm-specific gene expression. Molecular Microbiology *95*, 723–737.

Leulier, F., Parquet, C., Pili-Floury, S., Ryu, J.-H., Caroff, M., Lee, W.-J., Mengin-Lecreulx, D., and Lemaitre, B. (2003). The *Drosophila* immune system detects bacteria through specific peptidoglycan recognition. Nature Immunology *4*, 478–484.

Lewis, K. (2010). Persister Cells. Annu. Rev. Microbiol. *64*, 357–372.

Lieschke, G.J., Oates, A.C., Crowhurst, M.O., Ward, A.C., and Layton, J.E. (2001). Morphologic and functional characterization of granulocytes and macrophages in embryonic and adult zebrafish. Blood *98*, 3087–3096.

Lister, J.L., and Horswill, A.R. (2014). Staphylococcus aureus biofilms: recent developments in biofilm dispersal. Front Cell Infect Microbiol *4*, 178.

Liu, G.Y. (2009). Molecular Pathogenesis of Staphylococcus aureus Infection. Pediatr Res *65*, 71–77.

Liu, C., and Chambers, H.F. (2003). Staphylococcus aureus with Heterogeneous Resistance to Vancomycin: Epidemiology, Clinical Significance, and Critical Assessment of Diagnostic Methods. Antimicrobial Agents and Chemotherapy *47*, 3040–3045.

Liu, J., Zhou, Y., Qi, X., Chen, J., Chen, W., Qiu, G., Wu, Z., and Wu, N. (2017). CRISPR/Cas9 in zebrafish: an efficient combination for human genetic diseases modeling. Hum Genet *136*, 1–12.

Liu, Q., Yeo, W.-S., and Bae, T. (2016). The SaeRS Two-Component System of Staphylococcus aureus. Genes (Basel) *7*, 204.

Lowy, F. (2003). Antimicrobial resistance: the example of *Staphylococcus aureus*. Journal of Clinical Investigation *111*, 1265–1273.

Lowy, F.D. (1998). Staphylococcus aureus Infections. New England Journal of Medicine *339*, 520–532.

Lozano, C., García-Migura, L., Aspiroz, C., Zarazaga, M., Torres, C., and Aarestrup, F.M. (2012). Expansion of a Plasmid Classification System for Gram-Positive Bacteria and Determination of the Diversity of Plasmids in Staphylococcus aureus Strains of Human, Animal, and Food Origins. Appl. Environ. Microbiol. *78*, 5948–5955.

Luker, K.E., Pata, P., Shemiakina, I.I., Pereverzeva, A., Stacer, A.C., Shcherbo, D.S., Pletnev, V.Z., Skolnaja, M., Lukyanov, K.A., Luker, G.D., et al. (2015). Comparative study reveals better far-red fluorescent protein for whole body imaging. Scientific Reports *5*, 10332.

Malachowa, N., Kobayashi, S.D., Braughton, K.R., and DeLeo, F.R. (2013). Mouse Model of Staphylococcus aureus Skin Infection. In Mouse Models of Innate Immunity: Methods and Protocols, I.C. Allen, ed. (Totowa, NJ: Humana Press), pp. 109–116.

Mann, E.E., Rice, K.C., Boles, B.R., Endres, J.L., Ranjit, D., Chandramohan, L., Tsang, L.H., Smeltzer, M.S., Horswill, A.R., and Bayles, K.W. (2009). Modulation of eDNA Release and Degradation Affects Staphylococcus aureus Biofilm Maturation. PLOS ONE *4*, e5822.

Manso, A.S., Chai, M.H., Atack, J.M., Furi, L., Croix, M.D.S., Haigh, R., Trappetti, C., Ogunniyi, A.D., Shewell, L.K., Boitano, M., et al. (2014). A random six-phase switch regulates pneumococcal virulence via global epigenetic changes. Nature Communications *5*, 5055.

Mashruwala, A.A., Guchte, A. van de, and Boyd, J.M. (2017). Impaired respiration elicits SrrAB-dependent programmed cell lysis and biofilm formation in Staphylococcus aureus. ELife Sciences *6*, e23845.

Massey, R.C., Kantzanou, M.N., Fowler, T., Day, N.P.J., Schofield, K., Wann, E.R., Berendt, A.R., Höök, M., and Peacock, S.J. (2001). Fibronectin-binding protein A of Staphylococcus aureus has multiple, substituting, binding regions that mediate adherence to fibronectin and invasion of endothelial cells. Cellular Microbiology *3*, 839–851.

Mazon-Moya, M.J., Willis, A.R., Torraca, V., Boucontet, L., Shenoy, A.R., Colucci-Guyon, E., and Mostowy, S. (2017). Septins restrict inflammation and protect zebrafish larvae from Shigella infection. PLOS Pathogens *13*, e1006467.

McAdow, M., Kim, H.K., DeDent, A.C., Hendrickx, A.P.A., Schneewind, O., and Missiakas, D.M. (2011). Preventing Staphylococcus aureus Sepsis through the Inhibition of Its Agglutination in Blood. PLOS Pathogens *7*, e1002307.

McCarthy, A.J., and Lindsay, J.A. (2012). The distribution of plasmids that carry virulence and resistance genes in Staphylococcus aureus is lineage associated. BMC Microbiology *12*, 104.

McCarthy, H., Rudkin, J.K., Black, N.S., Gallagher, L., O'Neill, E., and O'Gara, J.P. (2015). Methicillin resistance and the biofilm phenotype in Staphylococcus aureus. Frontiers in Cellular and Infection Microbiology *5*, 1–9.

McCarthy, R.R., Mazon-Moya, M.J., Moscoso, J.A., Hao, Y., Lam, J.S., Bordi, C., Mostowy, S., and Filloux, A. (2017). Cyclic-di-GMP regulates lipopolysaccharide modification and contributes to *Pseudomonas aeruginosa* immune evasion. Nature Microbiology *2*, 17027.

McGuinness, W.A., Malachowa, N., and DeLeo, F.R. (2017). Vancomycin Resistance in Staphylococcus aureus. Yale J Biol Med *90*, 269–281.

McLoughlin, R.M., Solinga, R.M., Rich, J., Zaleski, K.J., Cocchiaro, J.L., Risley, A., Tzianabos, A.O., and Lee, J.C. (2006). CD4+ T cells and CXC chemokines modulate the pathogenesis of Staphylococcus aureus wound infections. PNAS *103*, 10408–10413.

McVicker, G., Prajsnar, T.K., Williams, A., Wagner, N.L., Boots, M., Renshaw, S.A., and Foster, S.J. (2014). Clonal Expansion during Staphylococcus aureus Infection Dynamics Reveals the Effect of Antibiotic Intervention. PLoS Pathogens *10*, e1003959.

Meijer, A.H., and Spaink, H.P. (2011). Host-Pathogen Interactions Made Transparent with the Zebrafish Model. Curr Drug Targets *12*, 1000–1017.

Meijer, A.H., Gabby Krens, S.F., Medina Rodriguez, I. a., He, S., Bitter, W., Snaar-Jagalska, B.E., and Spaink, H.P. (2004). Expression analysis of the Toll-like receptor and TIR domain adaptor families of zebrafish. Molecular Immunology *40*, 773–783.

Merino, N., Toledo-Arana, A., Vergara-Irigaray, M., Valle, J., Solano, C., Calvo, E., Lopez, J.A., Foster, T.J., Penadés, J.R., and Lasa, I. (2009). Protein A-Mediated Multicellular Behavior in Staphylococcus aureus. J Bacteriol *191*, 832–843.

Mesquita, F.S., Brito, C., Moya, M.J.M., Pinheiro, J.C., Mostowy, S., Cabanes, D., and Sousa, S. (2017). Endoplasmic reticulum chaperone Gp96 controls actomyosin dynamics and protects against pore-forming toxins. EMBO Reports *18*, 303–318.

Moormeier, D.E., and Bayles, K.W. (2017a). Staphylococcus aureus biofilm: a complex developmental organism. Molecular Microbiology *104*, 365–376.

Moormeier, D.E., and Bayles, K.W. (2017b). Staphylococcus aureus biofilm: a complex developmental organism. Molecular Microbiology *104*, 365–376.

Moormeier, D.E., Endres, J.L., Mann, E.E., Sadykov, M.R., Horswill, A.R., Rice, K.C., Fey, P.D., and Bayles, K.W. (2013). Use of Microfluidic Technology To Analyze Gene Expression during Staphylococcus aureus Biofilm Formation Reveals Distinct Physiological Niches. Appl. Environ. Microbiol. *79*, 3413–3424.

Moormeier, D.E., Bose, J.L., Horswill, A.R., and Bayles, K.W. (2014). Temporal and Stochastic Control of Staphylococcus aureus Biofilm Development. MBio *5*, e01341-14.

Mostowy, S., Boucontet, L., Moya, M.J.M., Sirianni, A., Boudinot, P., Hollinshead, M., Cossart, P., Herbomel, P., Levraud, J.-P., and Colucci-Guyon, E. (2013). The Zebrafish as a New Model for the In Vivo Study of Shigella flexneri Interaction with Phagocytes and Bacterial Autophagy. PLOS Pathogens *9*, e1003588.

Murphy, A.G., O'Keeffe, K.M., Lalor, S.J., Maher, B.M., Mills, K.H.G., and McLoughlin, R.M. (2014). Staphylococcus aureus infection of mice expands a population of memory γδ T cells that are protective against subsequent infection. J Immunol *192*, 3697–3708.

Needham, A.J., Kibart, M., Crossley, H., Ingham, P.W., and Foster, S.J. (2004). Drosophila melanogaster as a model host for Staphylococcus aureus infection. Microbiology *150*, 2347–2355.

Nguyen, M.-T., Uebele, J., Kumari, N., Nakayama, H., Peter, L., Ticha, O., Woischnig, A.-K., Schmaler, M., Khanna, N., Dohmae, N., et al. (2017). Lipid moieties on lipoproteins of commensal and non-commensal staphylococci induce differential immune responses. Nature Communications *8*, 2246.

Nieto, C., and Espinosa, M. (2003). Construction of the mobilizable plasmid pMV158GFP, a derivative of pMV158 that carries the gene encoding the green fluorescent protein. Plasmid *49*, 281–285.

Novick, R.P., and Brodsky, R. (1972). Studies on plasmid replication: I. Plasmid incompatibility and establishment in Staphylococcus aureus. Journal of Molecular Biology *68*, 285–302.

Nusslein-Volhard, C., and Dahm, R. (2002). Zebrafish. A practical approach. (Oxford University Press).

Nygaard, T.K., Pallister, K.B., Ruzevich, P., Griffith, S., Vuong, C., and Voyich, J.M. (2010). SaeR Binds a Consensus Sequence within Virulence Gene Promoters to Advance USA300 Pathogenesis. The Journal of Infectious Diseases *201*, 241–254.

O'Connell, D.P., Nanavaty, T., McDevitt, D., Gurusiddappa, S., Höök, M., and Foster, T.J. (1998). The Fibrinogen-binding MSCRAMM (Clumping Factor) ofStaphylococcus aureus Has a Ca2+-dependent Inhibitory Site. J. Biol. Chem. *273*, 6821–6829.

Ogryzko, N.V., Lewis, A., Wilson, H.L., Meijer, A.H., Renshaw, S.A., and Elks, P.M. (2019). Hif-1α–Induced Expression of Il-1β Protects against Mycobacterial Infection in Zebrafish. The Journal of Immunology *202*, 494–502.

Olson, M.E., Nygaard, T.K., Ackermann, L., Watkins, R.L., Zurek, O.W., Pallister, K.B., Griffith, S., Kiedrowski, M.R., Flack, C.E., Kavanaugh, J.S., et al. (2013). Staphylococcus aureus Nuclease Is an SaeRS-Dependent Virulence Factor. Infect. Immun. *81*, 1316–1324.

O'Neill, E., Pozzi, C., Houston, P., Humphreys, H., Robinson, D.A., Loughman, A., Foster, T.J., and O'Gara, J.P. (2008). A Novel Staphylococcus aureus Biofilm Phenotype Mediated by the Fibronectin-Binding Proteins, FnBPA and FnBPB. J Bacteriol *190*, 3835–3850.

Otto, M. (2013). Staphylococcal Infections: Mechanisms of Biofilm Maturation and Detachment as Critical Determinants of Pathogenicity. Annu. Rev. Med. *64*, 175–188.

Palmqvist, N., Foster, T., Fitzgerald, J.R., Josefsson, E., and Tarkowski, A. (2005). Fibronectin-Binding Proteins and Fibrinogen-Binding Clumping Factors Play Distinct Roles in Staphylococcal Arthritis and Systemic Inflammation. J Infect Dis *191*, 791–798.

Park, S.A., Choe, Y.H., Lee, S.H., and Hyun, Y.-M. (2018). Two-photon Intravital Imaging of Leukocytes During the Immune Response in Lipopolysaccharide-treated Mouse Liver. JoVE (Journal of Visualized Experiments) e57191.

Patton, T.G., Rice, K.C., and Bayles, K.W. The Staphylococcus aureus cidC gene encodes a pyruvate oxidase that affects acetate metabolism and cell death in stationary phase - Patton - 2005 - Molecular Microbiology - Wiley Online Library.

Pearson, A., Chronias, A., and Murray, M. (2009). Voluntary and mandatory surveillance for methicillin-resistant Staphylococcus aureus (MRSA) and methicillin-susceptible S. aureus (MSSA) bacteraemia in England. J Antimicrob Chemother *64*, i11–i17.

Pelz, A., Wieland, K.-P., Putzbach, K., Hentschel, P., Albert, K., and Götz, F. (2005). Structure and biosynthesis of staphyloxanthin from Staphylococcus aureus. J. Biol. Chem. *280*, 32493–32498.

Peng, H.L., Novick, R.P., Kreiswirth, B., Kornblum, J., and Schlievert, P. (1988). Cloning, characterization, and sequencing of an accessory gene regulator (agr) in Staphylococcus aureus. J Bacteriol *170*, 4365–4372.

Periasamy, S., Joo, H.-S., Duong, A.C., Bach, T.-H.L., Tan, V.Y., Chatterjee, S.S., Cheung, G.Y.C., and Otto, M. (2012). How Staphylococcus aureus biofilms develop their characteristic structure. Proceedings of the National Academy of Sciences *109*, 1281–1286.

Peschel, A., and Otto, M. (2013). Phenol-soluble modulins and staphylococcal infection. Nat Rev Microbiol *11*, 667–673.

Phelps, H.A., and Neely, M.N. (2007). SalY of the Streptococcus pyogenes Lantibiotic Locus Is Required for Full Virulence and Intracellular Survival in Macrophages. Infect Immun *75*, 4541–4551.

Pitrone, P.G., Schindelin, J., Stuyvenberg, L., Preibisch, S., Weber, M., Eliceiri, K.W., Huisken, J., and Tomancak, P. (2013). OpenSPIM: an open-access light-sheet microscopy platform. Nature Methods *10*, 598–599.

Pöhlmann-Dietze, P., Ulrich, M., Kiser, K.B., Döring, G., Lee, J.C., Fournier, J.-M., Botzenhart, K., and Wolz, C. (2000). Adherence of Staphylococcus aureus to Endothelial Cells: Influence of Capsular Polysaccharide, Global Regulator agr, and Bacterial Growth Phase. Infect Immun *68*, 4865–4871.

Pollitt, E.J.G., West, S.A., Cruzs, S.A., Burton-Chellew, M.N., and Diggle, S.P. (2013). Cooperation, Quorum Sensing, and Evolution of Virulence in Staphylococcus aureus | Infection and Immunity. ASM *82*, 1045–1051.

Pollitt, E.J.G., Szkuta, P.T., Burns, N., and Foster, S.J. (2018). Staphylococcus aureus infection dynamics. PLOS Pathogens *14*, e1007112.

Ponnuraj, K., Bowden, M.G., Davis, S., Gurusiddappa, S., Moore, D., Choe, D., Xu, Y., Hook, M., and Narayana, S.V.L. (2003). A "dock, lock, and latch" Structural Model for a Staphylococcal Adhesin Binding to Fibrinogen. Cell *115*, 217–228.

Poon, K.L., Wang, X., Ng, A.S., Goh, W.H., McGinnis, C., Fowler, S., Carney, T.J., Wang, H., and Ingham, P.W. (2017). Humanizing the zebrafish liver shifts drug metabolic profiles and improves pharmacokinetics of CYP3A4 substrates. Arch Toxicol *91*, 1187–1197.

Popov, L., Kovalski, J., Grandi, G., Bagnoli, F., and Amieva, M.R. (2014). Three-Dimensional Human Skin Models to Understand Staphylococcus aureus Skin Colonization and Infection. Front Immunol *5*, 41.

Postma, B., Kleibeuker, W., Poppelier, M.J.J.G., Boonstra, M., Kessel, K.P.M.V., Strijp, J.A.G.V., and Haas, C.J.C. de (2005). Residues 10–18 within the C5a Receptor N Terminus Compose a Binding Domain for Chemotaxis Inhibitory Protein of Staphylococcus aureus. J. Biol. Chem. *280*, 2020–2027.

Prajsnar, T.K. (2009). Doctoral Thesis: Development, characterisation and validation of a novel model of Staphylococcus aureus infection in zebrafish embryos (University of Sheffield).

Prajsnar, T.K., Cunliffe, V.T., Foster, S.J., and Renshaw, S.A. (2008). A novel vertebrate model of Staphylococcus aureus infection reveals phagocyte-dependent resistance of zebrafish to non-host specialized pathogens. Cellular Microbiology *10*, 2312–2325.

Prajsnar, T.K., Hamilton, R., Garcia-Lara, J., McVicker, G., Williams, A., Boots, M., Foster, S.J., and Renshaw, S.A. (2012). A privileged intraphagocyte niche is responsible for disseminated infection of Staphylococcus aureus in a zebrafish model. Cell Microbiol *14*, 1600–1619.

Prajsnar, T.K., Renshaw, S.A., Ogryzko, N.V., Foster, S.J., Serror, P., and Mesnage, S. (2013). Zebrafish as a Novel Vertebrate Model To Dissect Enterococcal Pathogenesis. Infect Immun *81*, 4271–4279.

Preibisch, S., Saalfeld, S., Schindelin, J., and Tomancak, P. (2010). Software for bead-based registration of selective plane illumination microscopy data. Nature Methods *7*, 418–419.

Prince, A., Wang, H., Kitur, K., and Parker, D. (2017). Humanized Mice Exhibit Increased Susceptibility to Staphylococcus aureus Pneumonia. J Infect Dis *215*, 1386–1395.

Rajan, V., Melong, N., Campbell, C.J., Dellaire, G., and Berman, J.N. (2015). A Humanized Zebrafish Transplant Model Expressing CXCL12 Provides an Enhanced In Vivo Therapeutic Screening Platform for T-ALL. Blood *126*, 4273–4273.

Ranjit, D.K., Endres, J.L., and Bayles, K.W. (2011). Staphylococcus aureus CidA and LrgA Proteins Exhibit Holin-Like Properties ▿. J Bacteriol *193*, 2468–2476.

Rauch, S., DeDent, A.C., Kim, H.K., Wardenburg, J.B., Missiakas, D.M., and Schneewind, O. (2012). Abscess Formation and Alpha-Hemolysin Induced Toxicity in a Mouse Model of Staphylococcus aureus Peritoneal Infection. Infection and Immunity *80*, 3721–3732.

Recsei, P., Kreiswirth, B., O'Reilly, M., Schlievert, P., Gruss, A., and Novick, R.P. (1986). Regulation of exoprotein gene expression in Staphylococcus aureus by agr. Mol Gen Genet *202*, 58–61.

Reizner, W., Hunter, J.G., O'Malley, N.T., Southgate, R.D., Schwarz, E.M., and Kates, S.L. (2014). A systematic review of animal models for Staphylococcus aureus osteomyelitis. Eur Cell Mater *27*, 196–212.

Renshaw, S.A., Loynes, C.A., Trushell, D.M.I., Elworthy, S., Ingham, P.W., and Whyte, M.K.B. (2006). A transgenic zebrafish model of neutrophilic inflammation. Blood *108*, 3976–3978.

Reyes-Robles, T., Alonzo, F., Kozhaya, L., Lacy, D.B., Unutmaz, D., and Torres, V.J. (2013). Staphylococcus aureus Leukotoxin ED Targets The Chemokine Receptors CXCR1 and CXCR2 to Kill Leukocytes and Promote Infection. Cell Host Microbe *14*, 453–459.

Reynaud, E.G., Kržič, U., Greger, K., and Stelzer, E.H.K. (2008a). Light sheet-based fluorescence microscopy: more dimensions, more photons, and less photodamage. HFSP J *2*, 266–275.

Reynaud, E.G., Kržič, U., Greger, K., and Stelzer, E.H.K. (2008b). Light sheet-based fluorescence microscopy: more dimensions, more photons, and less photodamage. HFSP J *2*, 266–275.

Reynaud, E.G., Peychl, J., Huisken, J., and Tomancak, P. (2014a). Guide to light-sheet microscopy for adventurous biologists. Nature Methods *12*, 30.

Reynaud, E.G., Peychl, J., Huisken, J., and Tomancak, P. (2014b). Guide to light-sheet microscopy for adventurous biologists.

Rhem, M.N., Lech, E.M., Patti, J.M., McDevitt, D., Höök, M., Jones, D.B., and Wilhelmus, K.R. (2000). The Collagen-Binding Adhesin Is a Virulence Factor in Staphylococcus aureus Keratitis. Infection and Immunity *68*, 3776–3779.

Rice, K.C., Bayles, K.W., Yang, S.-J., and Patton, T.G. (2003). The Staphylococcus aureus cidAB Operon: Evaluation of Its Role in Regulation of Murein Hydrolase Activity and Penicillin Tolerance. *185*, 2635–2643.

Rice, K.C., Nelson, J.B., Patton, T.G., Yang, S.-J., and Bayles, K.W. (2005). Acetic Acid Induces Expression of the Staphylococcus aureus cidABC and lrgAB Murein Hydrolase Regulator Operons. Journal of Bacteriology *187*, 813–821.

Richardson, E.J., Bacigalupe, R., Harrison, E.M., Weinert, L.A., Lycett, S., Vrieling, M., Robb, K., Hoskisson, P.A., Holden, M.T.G., Feil, E.J., et al. (2018). Gene exchange drives the ecological success of a multi-host bacterial pathogen. Nature Ecology & Evolution *2*, 1468.

Ricklin, D., Ricklin-Lichtsteiner, S.K., Markiewski, M.M., Geisbrecht, B.V., and Lambris, J.D. (2008). Cutting Edge: Members of the Staphylococcus aureus Extracellular Fibrinogen-Binding Protein Family Inhibit the Interaction of C3d with Complement Receptor 2. J Immunol *181*, 7463–7467.

Rodriguez, E.A., Tran, G.N., Gross, L.A., Crisp, J.L., Shu, X., Lin, J.Y., and Tsien, R.Y. (2016). A far-red fluorescent protein evolved from a cyanobacterial phycobiliprotein. Nature Methods *13*, 763–769.

Rooijakkers, S.H.M., Ruyken, M., Roos, A., Daha, M.R., Presanis, J.S., Sim, R.B., van Wamel, W.J.B., van Kessel, K.P.M., and van Strijp, J.A.G. (2005). Immune evasion by a staphylococcal complement inhibitor that acts on C3 convertases. Nature Immunology *6*, 920–927.

Rutherford, S.T., and Bassler, B.L. (2012). Bacterial Quorum Sensing: Its Role in Virulence and Possibilities for Its Control. Cold Spring Harb Perspect Med *2*.

Sadykov, M.R., and Bayles, K.W. (2012). The control of death and lysis in staphylococcal biofilms: a coordination of physiological signals. Curr Opin Microbiol *15*, 211–215.

Salamaga, B., Prajsnar, T.K., Jareño-Martinez, A., Willemse, J., Bewley, M.A., Chau, F., Belkacem, T.B., Meijer, A.H., Dockrell, D.H., Renshaw, S.A., et al. (2017). Bacterial size matters: Multiple mechanisms controlling septum cleavage and diplococcus formation are critical for the virulence of the opportunistic pathogen Enterococcus faecalis. PLOS Pathogens *13*, e1006526.

Sar, A.M.V.D., Musters, R.J.P., Eeden, F.J.M.V., Appelmelk, B.J., Vandenbroucke-Grauls, C.M.J.E., and Bitter, W. (2003). Zebrafish embryos as a model host for the real time analysis of Salmonella typhimurium infections. Cellular Microbiology *5*, 601–611.

Schaffer, A.C., and Lee, J.C. (2008). Vaccination and passive immunisation against Staphylococcus aureus. International Journal of Antimicrobial Agents *32*, S71–S78.

Scherr, T.D., Heim, C.E., Morrison, J.M., and Kielian, T. (2014). Hiding in Plain Sight: Interplay between Staphylococcal Biofilms and Host Immunity. Front Immunol *5*.

Scherr, T.D., Hanke, M.L., Huang, O., James, D.B.A., Horswill, A.R., Bayles, K.W., Fey, P.D., Torres, V.J., and Kielian, T. (2015). Staphylococcus aureus Biofilms Induce Macrophage Dysfunction Through Leukocidin AB and Alpha-Toxin. MBio *6*, e01021-15.

Schindelin, J., Arganda-Carreras, I., Frise, E., Kaynig, V., Longair, M., Pietzsch, T., Preibisch, S., Rueden, C., Saalfeld, S., Schmid, B., et al. (2012). Fiji: an open-source platform for biological-image analysis. Nature Methods *9*, 676–682.

Schwartz, K., Ganesan, M., Payne, D.E., Solomon, M.J., and Boles, B.R. (2015). Extracellular DNA facilitates the formation of functional amyloids in Staphylococcus aureus biofilms. Molecular Microbiology *99*, 123–134.

Scully, I.L., Liberator, P.A., Jansen, K.U., and Anderson, A.S. (2014). Covering all the Bases: Preclinical Development of an Effective Staphylococcus aureus Vaccine. Front. Immunol. *5*.

Selchow, O., and Huisken, J. (2013). Light sheet fluorescence microscopy and revolutionary 3D analyses of live specimens. Photonik 4.

Selchow, O., and Huisken, J. Light sheet fluorescence microscopy and revolutionary 3D analyses of live specimens. 4.

Serba, J. (2015). Doctoral Thesis: In vivo imaging of host-pathogen interactions in Staphylococcus aureus infection.

Serruto, D., Rappuoli, R., Scarselli, M., Gros, P., and van Strijp, J.A.G. (2010). Molecular mechanisms of complement evasion: learning from staphylococci and meningococci. Nature Reviews Microbiology *8*, 393.

Shompole, S., Henon, K.T., Liou, L.E., Dziewanowska, K., Bohach, G.A., and Bayles, K.W. (2003). Biphasic intracellular expression of Staphylococcus aureus virulence factors and evidence for Agr-mediated diffusion sensing. Molecular Microbiology *49*, 919–927.

Shukla, S.K., Karow, M.E., Brady, J.M., Stemper, M.E., Kislow, J., Moore, N., Wroblewski, K., Chyou, P.-H., Warshauer, D.M., Reed, K.D., et al. (2010). Virulence Genes and Genotypic Associations in Nasal Carriage, Community-Associated Methicillin-Susceptible and Methicillin-Resistant USA400 Staphylococcus aureus Isolates. Journal of Clinical Microbiology *48*, 3582–3592.

Siboo, I.R., Cheung, A.L., Bayer, A.S., and Sullam, P.M. (2001). Clumping Factor A Mediates Binding ofStaphylococcus aureus to Human Platelets. Infection and Immunity *69*, 3120–3127.

Sifri, C.D., Begun, J., Ausubel, F.M., and Calderwood, S.B. (2003). Caenorhabditis elegans as a model host for Staphylococcus aureus pathogenesis. Infect. Immun. *71*, 2208–2217.

Simor, A.E. (2011). Staphylococcal decolonisation: an effective strategy for prevention of infection? The Lancet Infectious Diseases *11*, 952–962.

Skerrett, S.J., Braff, M.H., Liggitt, H.D., and Rubens, C.E. (2017). Toll-like receptor 2 has a prominent but nonessential role in innate immunity to Staphylococcus aureus pneumonia. Physiol Rep *5*, e13491.

Spaulding, A.R., Satterwhite, E.A., Lin, Y.-C., Chuang-Smith, O.N., Frank, K.L., Merriman, J.A., Schaefers, M.M., Yarwood, J.M., Peterson, M.L., and Schlievert, P.M. (2012a). Comparison of Staphylococcus aureus strains for ability to cause infective endocarditis and lethal sepsis in rabbits. Front Cell Infect Microbiol *2*.

Spaulding, A.R., Lin, Y.-C., Merriman, J.A., Brosnahan, A.J., Peterson, M.L., and Schlievert, P.M. (2012b). Immunity to Staphylococcus aureus secreted proteins protects rabbits from serious illnesses. Vaccine *30*, 5099–5109.

Stainier, D.Y.R., Raz, E., Lawson, N.D., Ekker, S.C., Burdine, R.D., Eisen, J.S., Ingham, P.W., Schulte-Merker, S., Yelon, D., Weinstein, B.M., et al. (2017). Guidelines for morpholino use in zebrafish. PLOS Genetics *13*, e1007000.

Stapels, D.A.C., Ramyar, K.X., Bischoff, M., Köckritz-Blickwede, M. von, Milder, F.J., Ruyken, M., Eisenbeis, J., McWhorter, W.J., Herrmann, M., Kessel, K.P.M. van, et al. (2014). Staphylococcus aureus secretes a unique class of neutrophil serine protease inhibitors. PNAS *111*, 13187–13192.

Strandberg, K.L., Rotschafer, J.H., Vetter, S.M., Buonpane, R.A., Kranz, D.M., and Schlievert, P.M. (2010). Staphylococcal Superantigens Cause Lethal Pulmonary Disease in Rabbits. J Infect Dis *202*, 1690–1697.

Sullam, P.M., Bayer, A.S., Foss, W.M., and Cheung, A.L. (1996). Diminished platelet binding in vitro by Staphylococcus aureus is associated with reduced virulence in a rabbit model of infective endocarditis. Infection and Immunity *64*, 4915–4921.

Surewaard, B.G.J., Haas, C.J.C. de, Vervoort, F., Rigby, K.M., DeLeo, F.R., Otto, M., Strijp, J.A.G. van, and Nijland, R. (2013). Staphylococcal alpha-phenol soluble modulins contribute to neutrophil lysis after phagocytosis. Cellular Microbiology *15*, 1427–1437.

Surewaard, B.G.J., Deniset, J.F., Zemp, F.J., Amrein, M., Otto, M., Conly, J., Omri, A., Yates, R.M., and Kubes, P. (2016). Identification and treatment of the Staphylococcus aureus reservoir in vivo. Journal of Experimental Medicine *213*, 1141–1151.

Swinburne, I.A., Mosaliganti, K.R., Green, A.A., and Megason, S.G. (2015). Improved Long-Term Imaging of Embryos with Genetically Encoded α-Bungarotoxin. PLoS One *10*, e0134005.

Tarkowski, A., Collins, L.V., Gjertsson, I., Hultgren, O.H., Jonsson, I.-M., Sakiniene, E., and Verdrengh, M. (2001). Model systems: Modeling human staphylococcal arthritis and sepsis in the mouse. Trends in Microbiology *9*, 321–326.

Thwaites, G.E., and Gant, V. (2011). Are bloodstream leukocytes Trojan Horses for the metastasis of *Staphylococcus aureus*? Nature Reviews Microbiology *9*, 215–222.

Timme-Laragy, A.R., Karchner, S.I., and Hahn, M.E. (2012). Gene knockdown by morpholino-modified oligonucleotides in the zebrafish model: applications for developmental toxicology. Methods Mol Biol *889*, 51–71.

Tkaczyk, C., Kasturirangan, S., Minola, A., Jones-Nelson, O., Gunter, V., Shi, Y.Y., Rosenthal, K., Aleti, V., Semenova, E., Warrener, P., et al. (2017). Multimechanistic Monoclonal Antibodies (MAbs) Targeting Staphylococcus aureus Alpha-Toxin and Clumping Factor A: Activity and Efficacy Comparisons of a MAb Combination and an Engineered Bispecific Antibody Approach. Antimicrobial Agents and Chemotherapy *61*, e00629-17.

Tobin, D.M., May, R.C., and Wheeler, R.T. (2012). Zebrafish: A See-Through Host and a Fluorescent Toolbox to Probe Host–Pathogen Interaction. PLOS Pathogens *8*, e1002349.

Traber, K.E., Lee, E., Benson, S., Corrigan, R., Cantera, M., Shopsin, B., and Novick, R.P. (2008). agr function in clinical Staphylococcus aureus isolates. Microbiology *154*, 2265–2274.

Tsai, C.J.-Y., Loh, J.M.S., and Proft, T. (2016). Galleria mellonella infection models for the study of bacterial diseases and for antimicrobial drug testing. Virulence *7*, 214–229.

Tseng, C.W., Biancotti, J.C., Berg, B.L., Gate, D., Kolar, S.L., Müller, S., Rodriguez, M.D., Rezai-Zadeh, K., Fan, X., Beenhouwer, D.O., et al. (2015). Increased Susceptibility of Humanized NSG Mice to Panton-Valentine Leukocidin and Staphylococcus aureus Skin Infection. PLOS Pathogens *11*, e1005292.

Udo, E.E., and Grubb, W.B. (1991). A new incompatibility group plasmid in Staphylococcus aureus. FEMS Microbiology Letters *78*, 33–36.

van der Vaart, M., Spaink, H.P., and Meijer, A.H. (2012). Pathogen Recognition and Activation of the Innate Immune Response in Zebrafish. Adv Hematol *2012*, 159807.

Valle, J., Toledo-Arana, A., Berasain, C., Ghigo, J.-M., Amorena, B., Penadés, J.R., and Lasa, I. (2003). SarA and not σB is essential for biofilm development by Staphylococcus aureus. Molecular Microbiology *48*, 1075–1087.

Vandenesch, F., Naimi, T., Enright, M.C., Lina, G., Nimmo, G.R., Heffernan, H., Liassine, N., Bes, M., Greenland, T., Reverdy, M.-E., et al. (2003). Community-Acquired Methicillin-Resistant

Staphylococcus aureus Carrying Panton-Valentine Leukocidin Genes: Worldwide Emergence. Emerg Infect Dis *9*, 978–984.

van der Vaart, M., Korbee, C.J., Lamers, G.E.M., Tengeler, A.C., Hosseini, R., Haks, M.C., Ottenhoff, T.H.M., Spaink, H.P., and Meijer, A.H. (2014). The DNA Damage-Regulated Autophagy Modulator DRAM1 Links Mycobacterial Recognition via TLR-MYD88 to Autophagic Defense. Cell Host & Microbe *16*, 141.

Wacnik, K. (2016). Doctoral Thesis: Dissecting cell division in the human pathogen Staphylococcus aureus (University of Sheffield).

Walport, M.J. (2001a). Complement. N Engl J Med *344*, 1058–1066.

Walport, M.J. (2001b). Complement. N Engl J Med *344*, 1140–1144.

Wang, M., Zhang, Y., Fan, M., Guo, Y., Ren, W., and Luo, E. (2013). A rabbit model of right-sided Staphylococcus aureus endocarditis created with echocardiographic guidance. Cardiovasc Ultrasound *11*, 3.

Wang, R., Braughton, K.R., Kretschmer, D., Bach, T.-H.L., Queck, S.Y., Li, M., Kennedy, A.D., Dorward, D.W., Klebanoff, S.J., Peschel, A., et al. (2007). Identification of novel cytolytic peptides as key virulence determinants for community-associated MRSA. Nature Medicine *13*, 1510–1514.

Ward, A.C., and Lieschke, G.J. The Zebrafish as a model system for Human disease. *7*, 827-833,.

Wardenburg, J.B., Patel, R.J., and Schneewind, O. (2007). Surface Proteins and Exotoxins Are Required for the Pathogenesis of Staphylococcus aureus Pneumonia. Infection and Immunity *75*, 1040–1044.

Weber, M., Mickoleit, M., and Huisken, J. (2014). Multilayer Mounting for Long-term Light Sheet Microscopy of Zebrafish. Journal of Visualized Experiments e51119.

Willis, A.R., Torraca, V., Gomes, M.C., Shelley, J., Mazon-Moya, M., Filloux, A., Celso, C.L., and Mostowy, S. (2018). Shigella-Induced Emergency Granulopoiesis Protects Zebrafish Larvae from Secondary Infection. MBio *9*, e00933-18.

Wilson, R., and Cockcroft, W.H. (1952). Penicillin Resistant Staphylococcal Infection. Can Med Assoc J *66*, 548–551.

Windham, I.H., Chaudhari, S.S., Bose, J.L., Thomas, V.C., and Bayles, K.W. (2016). SrrAB Modulates Staphylococcus aureus Cell Death through Regulation of cidABC Transcription. J Bacteriol *198*, 1114–1122.

Wolf, A.J., and Underhill, D.M. (2018). Peptidoglycan recognition by the innate immune system. Nature Reviews Immunology *18*, 243–254.

Wong, C.H.Y., Jenne, C.N., Lee, W.-Y., Léger, C., and Kubes, P. (2011). Functional Innervation of Hepatic iNKT Cells Is Immunosuppressive Following Stroke. Science *334*, 101–105.

Wyllie, D.H., Walker, A.S., Miller, R., Moore, C., Williamson, S.R., Schlackow, I., Finney, J.M., O'Connor, L., Peto, T.E.A., and Crook, D.W. (2011). Decline of meticillin-resistant Staphylococcus aureus in Oxfordshire hospitals is strain-specific and preceded infection-control intensification. BMJ Open *1*, e000160.

Xu, T., Wang, X.-Y., Cui, P., Zhang, Y.-M., Zhang, W.-H., and Zhang, Y. (2017). The Agr Quorum Sensing System Represses Persister Formation through Regulation of Phenol Soluble Modulins in Staphylococcus aureus. Front Microbiol *8*, e2189.

Xu, Y., Rivas, J.M., Brown, E.L., Liang, X., and Höök, M. (2004). Virulence Potential of the Staphylococcal Adhesin CNA in Experimental Arthritis Is Determined by Its Affinity for Collagen. J Infect Dis *189*, 2323–2333.

Yang, S.-J., Rice, K.C., Brown, R.J., Patton, T.G., Liou, L.E., Park, Y.H., and Bayles, K.W. (2005). A LysR-Type Regulator, CidR, Is Required for Induction of the Staphylococcus aureus cidABC Operon. Journal of Bacteriology *187*, 5893–5900.

Yarwood, J.M., Bartels, D.J., Volper, E.M., and Greenberg, E.P. (2004). Quorum Sensing in Staphylococcus aureus Biofilms. Journal of Bacteriology *186*, 1838–1850.

Zaghloul, M.Z. (2015). Staphylococcus aureus Toxic Shock Syndrome. Tropical Medicine & Surgery *3*, 1–2.

Zapotoczna, M., Jevnikar, Z., Miajlovic, H., Kos, J., and Foster, T.J. (2013). Iron-regulated surface determinant B (IsdB) promotes Staphylococcus aureus adherence to and internalization by non-phagocytic human cells. Cellular Microbiology *15*, 1026–1041.

Zhang, L., Gray, L., Novick, R.P., and Ji, G. (2002). Transmembrane Topology of AgrB, the Protein Involved in the Post-translational Modification of AgrD in Staphylococcus aureus. J. Biol. Chem. *277*, 34736–34742.

Zong, Y., Xu, Y., Liang, X., Keene, D.R., Höök, A., Gurusiddappa, S., Höök, M., and Narayana, S.V.L. (2005). A 'Collagen Hug' Model for Staphylococcus aureus CNA binding to collagen. The EMBO Journal *24*, 4224–4236.

Zurek, O.W., Nygaard, T.K., Watkins, R.L., Pallister, K.B., Torres, V.J., Horswill, A.R., and Voyich, J.M. (2014). The Role of Innate Immunity in Promoting SaeR/S-Mediated Virulence in Staphylococcus aureus. JIN *6*, 21–30.

8 Appendix

8.1 *Codon optimised smURFP sequence*

The following sequence is the smURFP sequence codon optimised for expression in *S. aureus*. Optimisation was carried out by Mark Cooke and synthetic DNA was ordered from EuroFins.

ATGGCGAAAACATCAGAGCAGCGAGTTAATATAGCAACGTTATTGACAGAAAACAAAAAAAAAGATAGTGG
ATAAAGCAAGTCAAGACTTGTGGCGTCGACACCCTGACTTAATCGCACCGGGCGGAATTGCGTTTTCACAA
AGAGACAGAGCATTGTGTTTGAGAGATTATGGTTGGTTTTTGCACTTGATAACATTTTGTTTATTGGCGG
GAGACAAGGGTCCGATTGAATCTATCGGATTGATTAGTATAAGAGAAATGTATAACTCTTTGGGTGTGCC
GGTCCCAGCGATGATGGAGTCTATCCGATGTTTGAAAGAGGCGTCTTTATCATTGTTAGATGAAGAGGAT
GCTAACGAGACAGCTCCTTACTTTGACTATATCATAAAGGCTATGTCT